Analecta Technica Szegedinensia
Vol. 16, No. 01 ISSN 2064-7964 2022

SENSOR FUSION-BASED LOCALIZATION METHODS FOR MOBILE ROBOTS: A CASE STUDY FOR WHEELED ROBOTS

[1]Ákos Odry, [1]Dominik Csík, [2]Massimo Stefanoni, [1]Peter Sarcevic

[1]Department of Mechatronics and Automation, Faculty of Engineering, University of Szeged, Moszkvai krt. 9. 6725 Szeged, Hungary
[2]Istituto di Istruzione Superiore "A. Cesaris", Viale Cadorna, 26841 Casalpusterlengo LO, Italy
e-mail: odrya@mk.u-szeged.hu

ABSTRACT

Localization aims to provide the best estimate of the robot pose. It is a crucial algorithm in every robotics application, since its output directly determines the inputs of the robot to be controlled in its configuration space. In real world of engineering, the robot dynamics related measurements are subject to both uncertainties and disturbances. These error sources yield unreliable inferences of the robot state, which inherently result in wrong consensus about the appropriate control strategy to be applied. This outcome may drive the system out of stability and damage both the physical system and its environment. The localization algorithm captures the uncertainties with probabilistic approaches. Namely, the measurement processes are modelled along with their unreliability, moreover, the synergy of multiple information sources is formulated with the aim to calculate the most probable estimate of the robot pose. In essence, this algorithm is composed of two main parts, i.e., first the dynamics of the system is derived, and the corresponding uncertainties are initially predicted, next the additional sensor information is incorporated in the algorithm to refine the posterior estimate. This approach provides the state-of-the-art solution for the derivation of mobile robot poses in real applications.

Keywords: localization, pose estimation, sensor fusion, mobile robot, Kalman filter

1. INTRODUCTION

Mobile robots have a wide application spectrum from industrial applications, over domestic solutions in everyday life, to education platforms at universities [1]. Their popularity is based on the simple mechanical structure, small footprint, easily realizable and agile maneuvers. One of the main purposes of the software architecture, which operates the mobile robot, is the calculation of the suitable control inputs that contribute to successful robot motions. Successful control means that the robot is able to realize the motion between two desired points in its configuration space.

The control structure of mobile robots can be seen in Fig. 1. This control problem is solved in multiple steps. First, the sensors supply measurements of the instantaneous system dynamics. Next, the task of the localization is to obtain the most probable robot pose (position and orientation); i.e., this is a state estimation task. Then, the path planner designs the desired trajectory (series of feasible maneuvers) between the desired points based on both the obtained robot pose and information about its environment (i.e., occupancy grid that characterizes both the free space and obstacles around the robot). Finally, the control algorithm is responsible to track the trajectories, thus it calculates suitable inputs that are supplied to the actuators of the physical system.

In this work, the performance of the extended Kalman filter (EKF) for mobile robot pose estimation is evaluated for two test scenarios based on an experimental setup.

DOI: https://doi.org/10.14232/analecta.2022.1.1-7

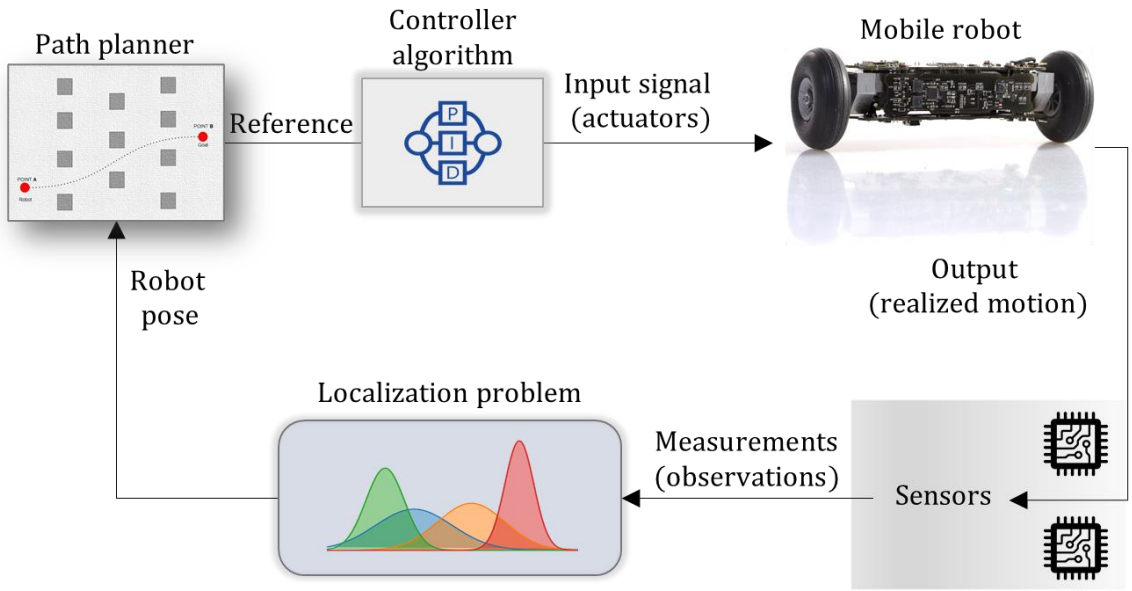

Figure 1: The control structure of mobile robots

2. MATERIALS AND METHODS

The localization problem is solved via fusing multiple independent sensors [2]. It is a recursive algorithm, which first incorporates the uncertainties of each sensor, then formulates the synergy of the applied sensors in a probabilistic framework:

$$p(x_t|map, z_t, u_t) = \eta \cdot p(z_t|x_t, map) \int_C p(x_t|u_t, x_{t-1}) p(x_{t-1}|map, z_{t-1}, u_{t-1})\, dx_{t-1} \quad (1)$$

where η is the normalization factor, C denotes the configuration space of the robot, $p(z_t|x_t, map)$ characterizes the observation, $p(x_t|u_t, x_{t-1})$ describes the motion dynamics, and $p(x_{t-1}|map, z_{t-1}, u_{t-1})$ denotes the probability density function of the system state in the previous epoch.

The problem is addressed in detail in the case of wheeled mobile robots as follows. The relative motion of the system is measured by wheel encoders [3] and/or inertial measurement units (IMU) [3-6]. Wheel encoders measure how many times has the motor rotated, which can be used to calculate distance based on the wheel diameter. IMUs consist of a three-axis accelerometer and a three-axis gyroscope. Accelerometers measure linear acceleration, while gyroscopes provide angular velocity measurements. The orientation can be computed by the integration of the gyroscope signals. By integrating once, the acceleration, the velocity can be given, and the position can be calculated by one further integration.

By the probabilistic characterization of the aforementioned sensors, the motion model of the system is obtained. The motion model describes the system evolution based on the input signals over time. However, the incorporated sensors are imperfect, namely, the inherent noise (e.g., random measurement noise and temperature dependent bias) yields to imprecise motion-model based pose results. On one hand, drift is generated during data processing, on the other hand, the uncertain parameters of the physical system, moreover, the uncertainties induced by the environment of the robot (e.g., uneven, and slippery terrain [3, 7]) significantly reduce the estimation performance and thus the reliability of the so-called a priori estimate.

DOI: https://doi.org/10.14232/analecta.2022.1.1-7

The a priori belief $\overline{\text{bel}}(x_t)$ of the robot pose x_t is obtained as follows.

$$\overline{\text{bel}}(x_t) = \int_C p(x_t|u_t, x_{t-1})\text{bel}(x_{t-1})dx_{t-1} \tag{2}$$

The localization algorithm handles the aforementioned problems and compensates for the generated errors in its update phase. The update phase incorporates additional sensors, which provide information of the robot pose in its inertial coordinate system. Namely, the absolute pose data is obtained based on vision sensors, signal strength measurements or global positioning system (GPS). Vision sensors are used in both indoor and outdoor environments, and they include cameras and LiDAR sensors [5-6, 8]. The GPS is a widely used technology for determining absolute position in outdoor environment, but it does not provide reliable measurements in indoor environment [9]. Signal strength measurements are widely used for absolute position estimation in indoor environments [9]. These methods utilize the received signal strength indicator (RSSI), which can be read from the wireless transceiver modules and can be used to estimate distances. The RSSI measurements collected during the communication between the mobile object and so-called anchor nodes, which have known position, can be used to estimate the position of the mobile object. The a posteriori belief $\text{bel}(x_t)$ of the robot pose x_t is given as follows.

$$\text{bel}(x_t) = \eta \cdot p(z_t|x_t)\overline{\text{bel}}(x_t) \tag{3}$$

It should be noted that these measurements are also characterized by anomalies (e.g., noise, low resolution, and low sampling rate). The characterization of these anomalies yields the observation model. In a recursive fashion, the localization algorithm predicts the state of the system with the a priori estimate (via the motion model), while the observation model evaluates this prediction and obtains the refined a posteriori robot pose in a Bayesian estimation framework. This framework is the basis for many popular state-of-the-art algorithms such as the Kalman filter, particle filter, information filter and histogram filter.
In the case of nonlinear systems, the EKF needs to be used, which linearizes about an estimate of the current mean and covariance.

3. RESULTS AND DISCUSSION

3.1. Kalman filter for localization

The Kalman filter is a recursive Bayes filter, which provides the optimal state estimate with minimized error variance [2]. It incorporates linear models for motion $p(x_t|u_t, x_{t-1})$ and observation $p(z_t|x_t, map)$, moreover, it significantly reduces the complexity of estimation by the utilization of normal distributions. The extension of the algorithm enables the usage of nonlinear models, however suboptimal performance is obtained in these cases. Prediction and update phases are given as follows.
Prediction:

$$x_- = f(x_t, u_t) \tag{4}$$
$$P_- = J_F P_t J_F^T + Q \tag{5}$$

Correction:

$$K = P_- J_H^T (J_H P_- J_H^T + R)^{-1} \tag{6}$$
$$x_{t+1} = x_- + K\big(z - h(x_-)\big) \tag{7}$$
$$P_{t+1} = (I - K J_H) P_- \tag{8}$$

DOI: https://doi.org/10.14232/analecta.2022.1.1-7

The algorithm obtains the predicted state along with its covariance ($x\_$ and $P\_$) based on the system dynamics $f(x_t, u_t)$, Jacobian of the system dynamics (J_F), and covariance matrix of this motion model Q. Then, the Kalman gain is calculated with the help of both the Jacobian J_H of the observation model $h(x\_)$ and covariance matrix of measurement R. This gain determines the importance of instantaneous measurement z and updates the predicted state estimation accordingly.

3.2. Experimental setup

The pose of the mobile robot which performs planar motion is characterized by the position x, y and orientation ϕ. The wheel encoders are used by low level controllers to maintain the instantaneous linear and angular speed values. Thus, the input of the motion model is formulated as:

$$u_t = (v_t, \omega_t)^T. \tag{9}$$

Since the encoders are sensitive to uneven and slippery terrains, therefore it is expected that the input signal-based prediction ensures only short-term accuracy. Complementary measurements are provided by the GPS receiver, which provides observations for the position of the robot:

$$z_t = (x_t, y_t)^T. \tag{10}$$

The motion model is characterized with the state vector x, as given in (11).

$$x = (x, y, \phi, v)^T \tag{11}$$

The motion equations are described in discrete time nonlinear state space. The coordinates of the robot are obtained in the t+1 epoch based on simple discrete time integration as follows.

$$x_{t+1} = x_t + v_t \cos\phi \tag{12}$$
$$y_{t+1} = y_t + v_t \sin\phi \tag{13}$$
$$\phi_{t+1} = \phi_t + \omega_t\, dt \tag{14}$$
$$v_{t+1} = v_t \tag{15}$$

The state estimation performance is influenced by the process and measurement covariance matrices (Q and R). It can be assumed that the state variables are uncorrelated, thus diagonal matrices are defined as in (16) and (17).

$$Q = \mathrm{diag}\left(\sigma_x^2, \sigma_y^2, \sigma_\phi^2, \sigma_v^2\right) \tag{16}$$
$$R = \mathrm{diag}\left(\sigma_{gps,x}^2, \sigma_{gps,y}^2\right) \tag{17}$$

3.3. Simulation results

The performance of the Kalman filter for robot pose estimation based on the described experimental setup is evaluated for two scenarios. The algorithm was implemented in MATLAB/Simulink framework. The robot executed piece wise constant control speeds. The covariance matrices were set up as: $Q = \mathrm{diag}(0.01, 0.01, 0.0003, 1)$ and $R = \mathrm{diag}(1,1)$. The simulations lasted for 60 s and the sampling time was 0.1 s. Fig. 2 and Fig. 3 highlight the simulation results, where the blue line shows the true state of the robot, the red line indicates the state prediction results based on encoder measurements, the yellow dots show the GPS updates, while the purple line indicates the performance of the EKF algorithm, i.e., the state

DOI: https://doi.org/10.14232/analecta.2022.1.1-7

estimation results. Tab. 1 and Tab. 2 present the root mean square (RMS) and the standard deviation (STD) of the errors for the two scenarios, which can be calculated using (18) and (19).

$$\mathrm{RMS} = \sqrt{\frac{1}{N}\sum_{i=1}^{N} e_i^2} \tag{18}$$

$$\mathrm{STD} = \sqrt{\frac{\sum_{i=1}^{N}(e_i - \bar{e})^2}{N-1}} \tag{19}$$

where N is the number of measurement points, e_i is the error at the ith point, and $\bar{e}$ is the mean error.
It can be seen from the results that the encoder-based state determination does not provide reliable results. This outcome was expected, since the encoder is sensitive to parasitic accelerations, uneven terrain, and slippage, therefore the inevitable noise generates drift during the integration process. However, the EKF successfully combines the short-term accurate encoder results with the GPS updates, thus providing reliable state estimation results for the high-level controllers.

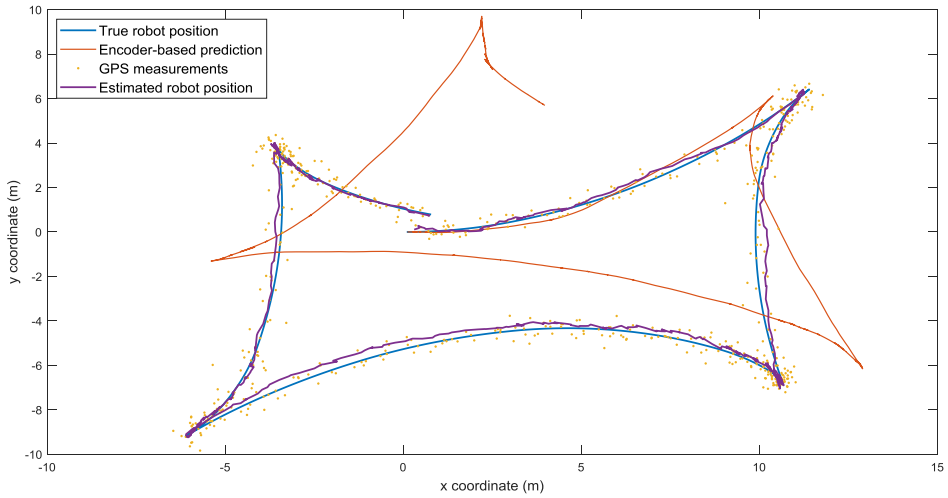

Figure 2: Simulation results in the first scenario

Table 1. Errors (m) in the first scenario

	X axis		Y axis	
Method	RMS	STD	RMS	STD
Encoder	2.7038	2.0510	4.0825	2.7861
EKF	0.1218	0.1218	0.1656	0.1491

DOI: https://doi.org/10.14232/analecta.2022.1.1-7

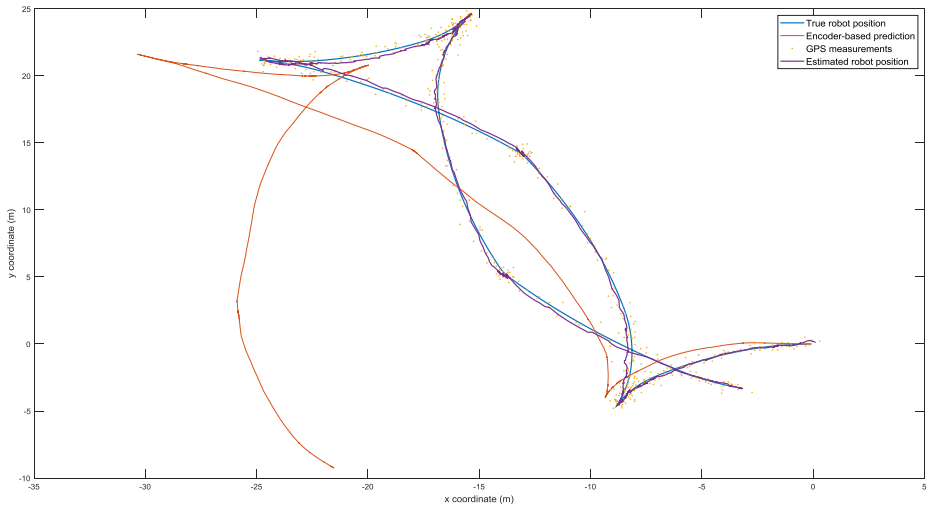

Figure 3: Simulation results in the second scenario

Table 2. Errors (m) in the second scenario

	X axis		Y axis	
Method	RMS	STD	RMS	STD
Encoder	7.2668	4.6859	7.2668	1.9872
EKF	0.1227	0.1226	0.1650	0.1647

4. CONCLUSIONS

The Kalman filter is one of the most popular choices for solving the localization problem of mobile robots. If the system is characterized by uncertainties, then the estimation of robot pose cannot be performed with deterministic approaches. The Kalman filter offers an effective way to address the vagueness of the system; it fuses the information provided by different sources and derives the optimal state estimate with suppressed noise and uncertainty components. Mobile robots operate in environments, where the terrain conditions often change. Variable environment is effectively handled by adaptive strategies, which measure the external disturbance magnitudes and vary the filter parameters during real time operation.
In this paper, the performance of the EKF was evaluated for pose estimation of a mobile robot. Two scenarios were tested based on the experimental setup. The obtained results showed that the encoder-based state determination does not provide reliable results, while the EKF successfully combines the short-term accurate encoder results with the GPS updates and provides reliable state estimation results.

DOI: https://doi.org/10.14232/analecta.2022.1.1-7

REFERENCES

[1] M. B. Alatise, G. P. Hancke, A Review on Challenges of Autonomous Mobile Robot and Sensor Fusion Methods, IEEE Access, 8 (2020), pp. 39830-39846. DOI: 10.1109/ACCESS.2020.2975643
[2] S. Thrun, W. Burgard, D. Fox, Probabilistic Robotics, 1st Edition, MIT Press, Cambridge, MA, USA, 2005.
[3] J. Yi, J. Zhang, D. Song, S. Jayasuriya, IMU-based Localization and Slip Estimation for Skid-Steered Mobile Robots, Proceedings of the 2007 IEEE/RSJ International Conference on Intelligent Robots and Systems (IROS), San Diego, CA, USA, October 29 - November 2, 2007, pp. 2845-2850. DOI: 10.1109/IROS.2007.4399477
[4] A. Benini, A. Mancini, A. Marinelli, S. Longhi, A Biased Extended Kalman Filter for Indoor Localization of a Mobile Agent using Low-Cost IMU and UWB Wireless Sensor Network, 10th IFAC Symposium on Robot Control International Federation of Automatic Control, Dubrovnik, Croatia, September 5-7, 2012, pp. 735-740. DOI: 10.3182/20120905-3-HR-2030.00144
[5] M. B. Alatise, G. P. Hancke, Pose Estimation of a Mobile Robot Based on Fusion of IMU Data and Vision Data Using an Extended Kalman Filter, Sensors, 17 (2017), 2164. DOI: 10.3390/s17102164
[6] P. Jiang, L. Chen, H. Guo, M. Yu, J. Xiong, Novel indoor positioning algorithm based on Lidar/inertial measurement unit integrated system, International Journal of Advanced Robotic Systems, 18 (2) (2021), pp. 1-11. DOI: 10.1177/1729881421999923
[7] D. Csík, Á. Odry, J. Sárosi, P. Sarcevic, Inertial sensor-based outdoor terrain classification for wheeled mobile robots, 2021 IEEE 19th International Symposium on Intelligent Systems and Informatics (SISY), Subotica, Serbia, September 16-18, 2021, pp. 159-164. DOI: 10.1109/SISY52375.2021.9582504
[8] P. Kolar, P. Benavidez, M. Jamshidi, Survey of Datafusion Techniques for Laser and Vision Based Sensor Integration for Autonomous Navigation, Sensors, 20 (2020), 2180. DOI: 10.3390/s20082180
[9] T. Yang, A. Cabani, H. Chafouk, A Survey of Recent Indoor Localization Scenarios and Methodologies, Sensors, 21 (2021), 8086. DOI: 10.3390/s21238086

Analecta Technica Szegedinensia
Vol. 16, No. 01 ISSN 2064-7964 2022

SOFT ROBOTICS: STATE OF ART AND OUTLOOK

[1]Attila Mészáros, [1]József Sárosi

[1]Department of Mechatronics and Automation, Faculty of Engineering, University of Szeged, Moszkvai krt. 9., 6725 Szeged, Hungary
e-mail: m-attila@mk.u-szeged.hu

ABSTRACT

Widely used robot systems have a rigid base structure that limits the interaction with their environment. Due to the inflexible attachment points, conventional robotic structures can only manipulate objects with their special gripping system. It can be difficult for these systems to grasp objects with different shapes, handle complex surfaces or navigating in a heavily crowded environment. Many of the species observed in nature, like octopuses are able to perform complex sequences of movements using their soft-structured limbs, which are made up entirely of muscle and connective tissue. Researchers have been inspired to design and build robots based on these soft biological systems. Thanks to the soft structure and high degree of freedom, these soft robots can be used for tasks that would be extremely difficult to perform with traditional robot manipulators. This article discusses the capabilities and usability of soft robots, reviews the state of the art, and outlines the challenges in designing, modelling, manufacturing, and controlling.

Keywords: soft robotics, soft actuators, bio-inspired robots, pneu-net, flexible robots

1. INTRODUCTION

Engineers have been studying the mechanics of biological systems for a long time and that always been a great source of inspiration for them. Softness and adaptability are outstanding properties of the biological systems, tend to strive for simplicity and show reduced complexity in their interactions with the environment. Based on these biological systems, a new class of machines was defined as soft robots [1][2]. These systems contain soft elements instead of a rigid structure, allowing them to perform tasks that conventional robotic systems would not be able to perform. Conventional, rigid robots are widely used in manufacturing today and can be used with high efficiency to efficiently perform a single well-defined task. However, their adaptability is very limited as they consist of rigid bonds and joints, so their use in a changing environment poses many problems. Soft robotics allows to design systems that adapt to the environment and unspecified events with great efficiency. These features open new opportunities for machine-human collaboration and the development of autonomous systems

2. COMPONENTS OF SOFT ACTUATION

2.1. Materials and power sources

Soft materials are key to creating a soft robot. The elasticity of the materials is described by the Young's modulus, but it is only defined for homogeneous prismatic bars subjected to axial loading and small deformations. Nevertheless, it is a useful measure of stiffness for materials used in the manufacture of robotic systems. Materials used in robotics (e.g., metals, hard plastics) have a modulus of the order of 10^9-10^{12} Pa, while natural organisms often consist of materials (e.g., skin, muscle tissue) with a modulus of the order of 10^4-10^9 Pa [2]. Soft robotics defines systems that consist primarily of materials whose modulus falls within the modulus of soft biological materials.
The power supply systems required for their operation are a major challenge for soft robots. These systems are usually able to operate using 2 types of energy: pneumatic and electrical. For pneumatic actuators, the existing power sources are not soft and are usually large. Pressure sources available from the current shelf are usually limited to compressors or pumps [3]. Compressors convert electrical energy into mechanical

DOI: https://doi.org/10.14232/analecta.2022.1.8-13

energy, and compressed gas cylinders store a certain volume of pressurized fluid so that it can be discharged when needed.
Electrically driven actuators require a soft, flexible, lightweight power source [4]. Soft electronics, like soft robotics, are one of the most active research area.

2.2. Actuation

The easiest way to create a homogeneous load on a deformable piece of material is to increase the applied pressure with the aid of a liquid medium. This concept is the core of many soft actuators and their various implementations. The simplest soft actuators include blisters that can be rapidly inflated with compressed air to generate the mechanical effect that creates displacement. If a specific spatial architecture is developed for the bladder, one direction of expansion may be preferred over the others and as a result, different types of motion can create (see Figure 1.). In addition, folds can be added to the design, allowing movement to follow prescribed paths [5][6].

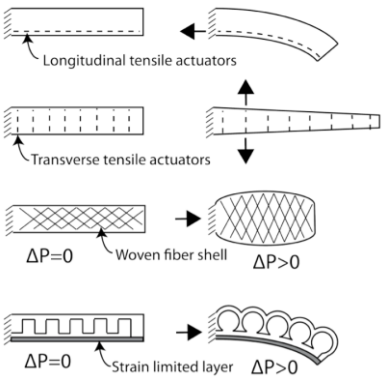

Figure 1: Common approaches to actuation of soft robot bodies in resting (left) and actuated (right) states [2]

Soft robot segments are generally operated by inflate channels in soft material and this achieve the desired deformation. Pneumatic artificial muscles (PAMs), also known as McKibben actuators, are examples of suitable linear soft actuators consisting of elastomeric tubes in fibrous sheaths [7].
Fluid elastomer actuators (FEAs) are a new type of highly extensible and adaptable low-power soft actuators. FEAs are synthetic elastomers operated by dilating embedded channels using pressure. The FEAs can be operated pneumatically [8] or hydraulically [9].
While most soft robots use pneumatic or hydraulic actuation, researchers are also focused on the development of electrically operated soft actuators, which used electro-active polymers (EAPs). These actuators include dielectric EAPs, electrostrictive graft polymers, and stimulus-responsive gels [10].

3. FABRICATION OF SOFT ROBOTIC STRUCTURES

3.1 Molding

The vast majority of soft structures are made of a catalysed polymer, such as silicone rubber, which is prepared by mixing two components prior to casting operations. However, the homogenization steps add air bubbles to the mixture and these bubbles can cause weaknesses in the final structure. These should be removed, usually by vacuum degassing of the mixture or alternatively by rotating the mold and using centrifugal forces [11].

DOI: https://doi.org/10.14232/analecta.2022.1.8-13

The most difficult part of making a mold is that cavities have to be left in the internal structure, so the usual manufacturing methods are out of the question. The simplest solution to the problem is to cast the part from several parts, which can then be sealed together by gluing or dipping the parts into an unbound material [12]. However, the seam obtained by this method may be structurally weak.

3.2 Additive manufacturing

In contrast to classical machining methods, also called extraction manufacturing, where the tool removes material from a workpiece to produce the desired shapes, additive manufacturing (AM) is based on the local deposition of a small amount of material to form the shape. The available technologies have been constantly improving since the early 1990s [13], so it is now possible to create components from polymers and elastomers, metals, ceramics, and in some cases even to combine or mix two or more building materials.
The most commonly used method for AM is the fused deposition modelling (FDM) procedure. In this case, the 3D shape is formed by sweeping each layer with a thermoplastic extrusion nozzle to form a thin polymer fiber [14].

4. APPLICATIONS

4.1. Location changing

In soft robotics, there is a great opportunity to design systems that are able to change their own location. Most of the research is based on the movement of animals whose muscles and tissues can be modelled with soft robotic elements such as e.g., caterpillar [15] [16], octopus [17], fish [18]. These systems can diversify depending on the number of the soft actuators and their design (see Figure 2.). Various forms of movement can be produced with soft elements such as: four-legged movement [19], rolling [8], snake-like waving [20] and jumping movement [21].

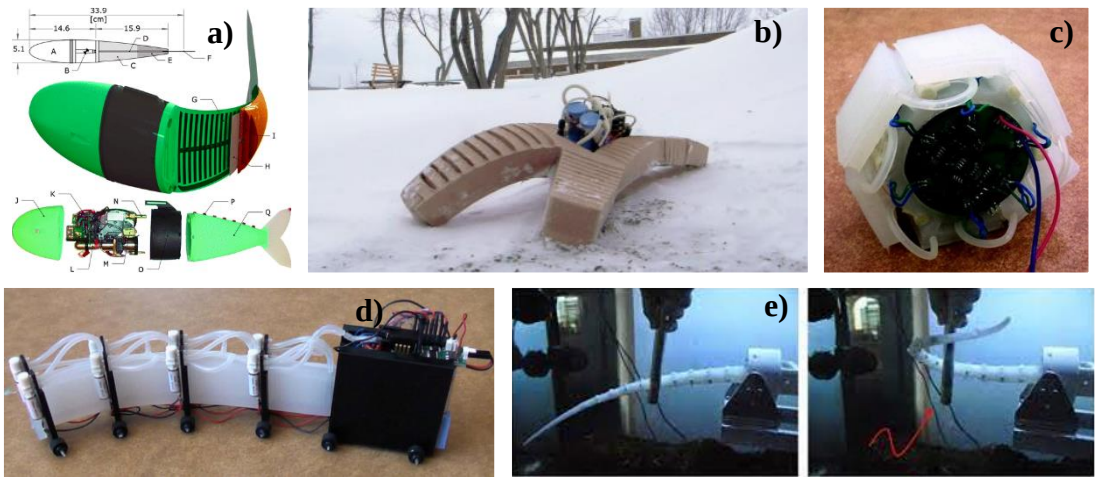

Figure 2: Soft robot systems of different designs. a) hydraulically operated soft robot [18], b) four-legged autonomous soft robot[19], c) rolling soft system [8], d) meandering soft unit [20], e) octopus arm like soft actuator [17]

The typical operating power sources (e.g., air compressors, batteries) are relatively heavy, so this greatly simplify the system design by significantly reducing load capacity. One approach to implementing mobile systems is to connect a soft robot to a mobile rigid robot with higher load capacity [22] and the other

DOI: https://doi.org/10.14232/analecta.2022.1.8-13

approach has developed materials and designs that are designed to operate at high pressures to transport payloads [19].

4.2. Manipulation

Manipulation is one of the most exciting challenges in robotics. Soft systems have a natural advantage over rigid robots in manipulating unknown objects (see Figure 3.). Due to the soft grippers, it is possible to adapt to different objects with simple control schemes [23]. Grippers used in isothermal systems can take of this advantage over conventional rigid manipulators [24] and this silicone elastomers demonstrate impressive adaptability thanks to embedded pneumatic channels [25][26].

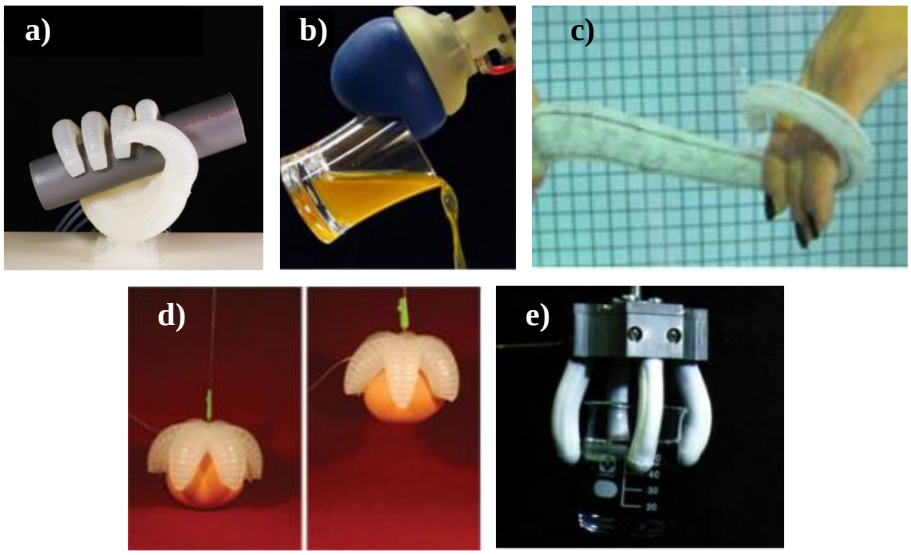

Figure 3: Soft grippers of different designs. a) hand shape gripper [25], b) jamming based manipulation [24], c) octopus arm like soft gripper [17], d) 6 segment gripper [23], e) microactuation manipulation [26]

4.3. Wearable applications

One of the natural advantages of soft robotic systems is that their wear does not restrict limb movement due to the flexibility of their modules. For rigid medical devices or orthoses
there is a risk that wearing it uncomfortably may damage human tissue. One option is integrating a degree of fitness into wearable devices such as orthopedic rehabilitation. Recently, researchers have begun to study soft wearable medical applications (see Figure .4), including soft orthodes for human ankle-foot rehabilitation [27], hand rehabilitation [28] and soft sensing suits for measuring lower extremities [29].

DOI: https://doi.org/10.14232/analecta.2022.1.8-13

Figure 4: Wearable soft robotic devices. a) ankle rehabilitation with soft actuator [27], b) soft robotic glove [28], c) soft sensing suit [29]

5. CONCLUSIONS AND PERSPECTIVES

Soft robotics is a relatively new area of research. A wide range of systems have already been developed with a number of applications but there is still plenty of scope in many disciplines. The development of technology is closely linked to the development of new manufacturing techniques, enabling the production of increasingly complex devices that can facilitate the production of soft systems. The introduction of new innovative materials such as self-healing polymers or biocompatible elastomers will also lead to a further expansion of soft robotics in medical and biomechanical applications. Current manufacturing technologies already allow for the widespread use of soft robotics and these opportunities will evolve with the development of many scientific communities approaching soft robotics.

REFERENCES

[1] Trivedi, D., Rahn, C. D., Kier, W. M. & Walker, I. D. (2008): Soft robotics: Biological inspiration, state of the art, and future research. Applied Bionics and Biomechanics 5, 99–117. https://doi.org/10.1080/11762320802557865
[2] Rus, D., and Tolley, M. T. (2015): Design, fabrication and control of soft robots. Nature 521, 467–475. http://dx.doi.org/10.1038/nature14543
[3] Wehner, M. et al. (2014): Pneumatic energy sources for autonomous and wearable soft robotics. Soft Robotics 1, 263–274. https://doi.org/10.1089/soro.2014.0018
[4] Xu, S. et al. (2013): Stretchable batteries with self-similar serpentine interconnects and integrated wireless recharging systems. Nature communications 4, 1543. https://doi.org/10.1038/ncomms2553
[5] Nishioka, Y., Uesu, M., Tsuboi, H., Kawamura, S., Masuda, W., Yasuda, T., et al. (2017): Development of a pneumatic soft actuator with pleated inflatable structures. Adv. Robot. 31, 753–762. https://doi.org/10.1080/01691864.2017.1345323
[6] Robertson, M. A., Sadeghi, H., Florez, J. M., and Paik, J. (2016): Soft pneumatic actuator fascicles for high force and reliability. Soft Robot. 4, 23–32. https://doi.org/10.1089/soro.2016.0029
[7] Chou, C.-P., Hannaford, B. (1996): Measurement and modeling of McKibben pneumatic artificial muscles. Robotics and Automation, IEEE Transactions on 12, 90–102. http://dx.doi.org/10.1109/70.481753
[8] Onal, C. D., Chen, X., Whitesides, G. M., Rus, D. (2011): Soft mobile robots with on-board chemical pressure generation. In International Symposium on Robotics Research (ISRR), 1–16. https://doi.org/10.1007/978-3-319-29363-9_30
[9] Katzschmann, R. K., Marchese, A. D., Rus, D. (2014): Hydraulic Autonomous Soft Robotic Fish for 3D Swimming. In International Symposium on Experimental Robotics (ISER), 1122374. http://doi.org/10.1007/978-3-319-23778-7_27

DOI: https://doi.org/10.14232/analecta.2022.1.8-13

[10] Bar-Cohen, Y. (2004): Electroactive Polymer (EAP) Actuators as Artificial Muscles: Reality, Potential, and Challenges (SPIE Press) http://dx.doi.org/10.2514/6.2001-1492
[11] Mazzeo, A. D., and Hardt, D. E. (2013): Centrifugal casting of microfluidic components with PDMS. J. Micro Nano Manufactur. https://doi.org/10.1115/1.4023754
[12] Tolley, M. T., Shepherd, R. F., Mosadegh, B., Galloway, K. C., Wehner, M., Karpelson, M., et al. (2014): A resilient, untethered soft robot. Soft Robot. 1, 213–223. https://doi.org/10.1089/soro.2014.0008
[13] Kruth, J.-P. (1991): Material incress manufacturing by rapid prototyping techniques. CIRP Ann. 40, 603–614. https://doi.org/10.1016/S0007-8506(07)61136-6
[14] Zolfagharian, A. et al. (2016): Evolution of 3D printed soft actuators. Sensors and Actuators A: Physical. 250. 258-272. https://doi.org/10.1016/j.sna.2016.09.028
[15] Laschi, C. et al. (2012): Soft robot arm inspired by the octopus. Advanced Robotics 26, 709–727. https://doi.org/10.1163/156855312X626343
[16] Lin, H.-T., Leisk, G. G., Trimmer, B. (2011): GoQBot: a caterpillar-inspired soft-bodied rolling robot. Bioinspiration & biomimetics 6, 026007. doi: 10.1088/1748-3182/6/2/026007
[17] Mazzolai, B., Margheri, L., Cianchetti, M., Dario, P., Laschi, C. (2012): Soft-robotic arm inspired by the octopus: from artificial requirements to innovative technological solutions. Bioinspiration & biomimetics 7, 025005. https://doi.org/10.1088/1748-3182/7/2/025005
[18] Marchese, A. D., Onal, C. D., Rus, D. (2014): Autonomous soft robotic fish capable of escape maneuvers using fluidic elastomer actuators. Soft Robotics 1, 75–87. https://doi.org/10.1089/soro.2013.0009
[19] Tolley, M. T. et al. (2014): A resilient, untethered soft robot. Soft Robotics 1, 213–223 https://doi.org/10.1089/soro.2014.0008
[20] Onal, C. D., Rus, D. (2013) Autonomous undulatory serpentine locomotion utilizing body dynamics of a fluidic soft robot. Bioinspiration & biomimetics 8, 026003.
doi: 10.1088/1748-3182/8/2/026003
[21] Tolley, M. T. et al. (2014): An untethered jumping soft robot. In Intelligent Robots and Systems (IROS). IEEE/RSJ International Conference on, 561–566 https://doi.org/10.1089/soro.2014.0008
[22] Stokes, A. A., Shepherd, R. F., Morin, S. A., Ilievski, F., Whitesides, G. M. (2013): A hybrid combining hard and soft robots. Soft Robotics 1, 70–74. https://doi.org/10.1089/soro.2013.0002
[23] Ilievski, F., Mazzeo, A. D., Shepherd, R. F., Chen, X. & Whitesides, G. M. (2011): Soft robotics for chemists. Angewandte Chemie 123, 1930–1935 https://doi.org/10.1002/anie.201006464
[24] Brown, E. et al. (2010): Universal robotic gripper based on the jamming of granular material. Proceedings of the National Academy of Sciences 107, 18809–18814. https://doi.org/10.1073/pnas.1003250107
[25] Deimel, R., Brock, O. (2014): A novel type of compliant, underactuated robotic hand for dexterous grasping. Robotics: Science and Systems, Berkeley, CA 1687–1692 https://doi.org/10.1177/0278364915592961
[26] Suzumori, K., Iikura, S., Tanaka, H. (1992): Applying a flexible microactuator to robotic mechanisms. Control Systems, IEEE 12, 21–27 doi: 10.1109/37.120448
[27] Park, Y.-L. et al. (2014): Design and control of a bio-inspired soft wearable robotic device for ankle–foot rehabilitation. Bioinspiration & biomimetics 9, 016007 doi: 10.1088/1748-3182/9/1/016007
[28] Polygerinos, P., Wang, Z., Galloway, K. C., Wood, R. J., Walsh, C. J. (2014): Soft robotic glove for combined assistance and at-home rehabilitation. Robotics and Autonomous Systems inpress https://doi.org/10.1016/j.robot.2014.08.014
[29] Mengüç, Y. et al. (2014): Wearable soft sensing suit for human gait measurement. TheInternational Journal of Robotics Research 33,1748-1764 https://doi.org/10.1177/0278364914543793

DOI: https://doi.org/10.14232/analecta.2022.1.8-13

Analecta Technica Szegedinensia
Vol. 16, No. 01 ISSN 2064-7964 2022

A REVIEW: THE PROTECTIVE EFFECTS OF DIETARY POLYPHENOLS ON ALZHEIMER'S DISEASE

[1]Ünkan Urganci,[1]Fatma Işık

[1]: Pamukkale University, Faculty of Engineering, Department of Food Engineering, 20020, Denizli/Turkey
e-mail: unkanurganci@gmail.com

ABSTRACT

Alzheimer's disease (AD) is a progressive irreversible neurodegenerative disease in the hippocampus and cortex regions of the brain and is the most common cause of dementia in the elderly population among 40 million cases worldwide today, it is thought that this number will exceed up to 100 million by 2050. The disease is characterized by symptoms of memory loss, difficulty in speaking, decision making, learning, problem solving, and impaired perception of time and orientation. In its pathogenesis, the amyloid beta (Aβ) senile plaques accumulation in the extracellular synaptic spaces of the neurocortex, the formation of intracellular hyperphosphorylated tau protein deposition and neurofibrillary tangles (NFY) are important and triggered neurodegeneration mainly affects cognitive behavior and memory. Phenolic compounds are organic compounds containing a benzene ring to which one or more hydroxyl groups are attached. Studies have shown that regular consumption of polyphenols reduces the risk of developing neurodegenerative diseases. Studies have reported that polyphenols inhibit Aβ production and accumulation processes by interacting with different forms of amyloid structure. In this study, polyphenols and their therapeutic properties against AD will be discussed extensively.

Keywords: Alzheimer's Disease, Amyloid Beta, Neurodegeneration, Polyphenols

1. INTRODUCTION

Alzheimer's Disease (AD), characterized by Alois Alzheimer in 1907, is the main form of dementia and is a fatal neurodegenerative disease that develops and progresses under the influence of multiple factors including genetic, environmental and infectious mechanisms [1,2]. Dementia is the seventh most common reason of death today. The latest Alzheimer report shows 50 million people suffer from dementia and 1 trillion US dollars was spent on the treatment of dementia in the World [3]. It is predicted that this figure will increase and there will be 132 million dementia patients in 2050, and it is calculated that the expenditures for dementia treatment will double then [3]. AD affects more than 20 million people worldwide and this number will increase significantly in the future with the increase in the number of elderly people in the total population. Its prevalence is 10% around the age of 65 and 50% around the age of 85 [1]. AD affects large areas of the cerebral cortex and hippocampus. The abnormalities are usually first detected in brain tissue including the frontal and temporal lobes and then slowly progress to other areas of the neocortex at rates that are highly variable between individuals. AD is a chronic neurodegenerative disease that is the most common cause of dementia (60-80%). The most common causes of dementia in patients over the age of 65 are AD, vascular dementia and coexistence of vascular dementia and AD [3].

Approximately 10% of clinical dementia incidences are due to reversible causes such as metabolic anomalies (eg, hypothyroidism), nutritional disorders (eg, vitamin B12 deficiency, folate deficiency) or depression. It is estimated that 4.6 million new cases of AD develop every year all over the world. In molecular level, Alzheimer's disease is characterized by a wide variety of events such as errors in protein sequence and aggregation, oxidative stress, mitochondrial abnormalities and neuroinflammatory pathway [4]. Extracellular amyloid beta (Aβ) accumulation and intercellular hyperphosphorylated tau protein are accepted as the main pathological findings of AD [5]. Fibril tangles that are another neuropathological sign

DOI: https://doi.org/10.14232/analecta.2022.1.14-26

of AD, consist of abnormally hyperphosphorylated tau proteins [6]. In addition, the intracellular formation of extracellular accumulations and neurofibrillary tangles of Aβ plays an important role in oxidative stress, excitotoxicity, neuroinflammation and neurotransmitter deficiencies [7,8].
As a consequence of many mechanisms exist in the pathogenesis of AD, there is no approach that can prevent, completely treat or slow the progression of the disease, but drugs that delay the progression of the symptoms of the disease continue to be developed [9]. The developed treatment strategies are based on the approaches that constitute the pathogenesis of AD, especially acetylcholinesterase (AChE) and secretase inhibitors and tau therapies [10]. Acetylcholinesterase inhibitors (AChEIs) such as donepezil, galantamine and rivastigmine, and N-methyl D aspartate (NMDA) receptor antagonists such as memantine are approved by the US Food and Drug Administration (FDA) to improve the symptoms of Alzheimer's disease [11]. Donepezil, galantamine and rivastigmine are recommended for mild to moderate AD patients; and memantine is recommended for moderate to severe AD patients [12].
In addition to existing treatments, some herbal medicines, extracts and some active compounds can provide a therapeutic benefit against AD, thanks to their neuroprotective effect with cholinesterase inhibition activity, anti-tau, antioxidant, antiapoptosis, anti-inflammatory properties, and their ability to act as β-secretase inhibitors by affecting Aβ production [11,13]. It is considered that polyphenols found in plants can regulate Aβ production and aggregation by inhibiting amyloid self-assembly by stimulating α-secretase pathway or inhibiting β- and γ-secretase pathways [14]. Also, mitochondrial dysfunction, inflammation, hyperphosphorylated tau and Aβ accumulation in AD are associated with reactive oxygen species (ROS) [15]. ROS can occur through different mechanisms and has complex roles in accelerating AD development [16]. Further studies are needed to determine these complex roles of ROS in AD and to develop antioxidant-based therapeutic targets [16,17]. Here, the therapeutic properties of different polyphenols and their derivatives will be highlighted.

POLYPHENOLS

Polyphenols are secondary metabolites found in high amounts in fruits, vegetables, seeds and oils. Today, more than 10,000 natural polyphenols have been identified, and they are categorized into various groups according to the number of phenolic rings and the number of structural elements bonding these rings. These are mainly, phenolic acids and their derivatives, lignans, stilbenes, flavonoids which are also categorized into various subgroups [18,19].
The main common feature of all polyphenols is the presence of hydroxyl groups in the -ortho or -para positions required for redox reactions and that they contain more than one phenolic ring. These natural compounds have strong antioxidant properties that protect against oxidative damage due to their scavenging and metal chelating properties of free radicals produced by reactive oxygen species [18,20].
It was proven that polyphenols can have a neuroprotective effect in neurodegenerative diseases such as AD, prevent Aβ formation, and suppress the vicious circle between Aβ production and oxidative stress, with their anti-aging, cardiovascular protection and anti-inflammatory properties [20,21]. Previous findings show that all polyphenols have different effects on amyloid structure by interacting with different amyloid forms such as monomeric, oligomeric or fibril forms. It was stated that these compounds prevent the accumulation process by entering between the aromatic rings in the amyloidogenic protein structure [22,23]. Furthermore, it was discussed that polyphenols have the ability to stimulate the α-secretase pathway and inhibit the β- and γ-secretase pathway, and thus have the capacity to modulate Aβ production [24-26]. I was identified in AD studies that some polyphenols perform strong enzymatic inhibition in the Aβ production pathway, while some others prevent amyloid aggregation and fibril formation significantly [20-27]. E.g; quercetin and myricetin, which are some of the most known natural polyphenols exert significant effects by inhibiting the β-secretase enzymes. On the other hand, it was stated that epigallocatechin-3 gallate (EGCG), resveratrol, and curcumin, which are well-known polyphenols, form a

DOI: https://doi.org/10.14232/analecta.2022.1.14-26

non-covalent complex with the Aβ peptide and inhibit amyloid aggregation and also interact with the secretases or cyclooxygenase pathway [24]. It was emphasized that hydrophobic forces, aromatic stacking, electrostatic and aromatic interactions play an important role in the formation of Aβ, and the mechanism of polyphenolic compounds should be studied as predicting that they can be conjugated to Aβ formed in this way [28,29].

Phenolic Acids and AD

Phenolic or phenolcarboxylic acids are one of the main classes of plant phenolic compounds and are found in high concentrations in seeds, colored fruits such as berries and pomegranate, fruit skins, vegetables including onions and vegetable leaves as free or soluble conjugates. Phenolic acids are basically categorized into two subgroups as hydroxybenzoic and hydroxycinnamic acids [30,31]. Phenolic acids are phytochemicals commonly used in daily food intake, containing an aromatic ring bearing an acidic group and one or more hydroxyl groups. Phenolic acids are secondary metabolites that can often be found in plant-derived foods and form an important part of our daily diet [32-34]. These phenolic acids additionally form a group of secondary metabolites with redox and metal chelating properties that act as reducing agents [35]. Considering its potential health benefits such as antioxidant [36], antiviral [37], anticarcinogenic activities [38-40] and neuroprotective properties [41-51], it has attracted the attention of researchers due to these effects. It has therefore been demonstrated that phenolic acids can be used as health-promoting ingredients in functional foods and other products [52].
Chang et al. [41] have determined the protective effect of caffeic acid against AD that including caffeic acid in diet modulated Aβ accumulation, decreased the p-tau expression in the hippocampus and attenuated the APP expression as well as β-site APP cleaving enzyme in rat model of hyperinsulinemia. Mori et al. [42] and Yu et al. [43] have demonstrated that using gallic acid in the diet of transgenic mice with AD improved cognition, rescued learning and memory deficits and reduced Aβ aggregation. Also, Ogunlade et al. [44] have suggested that gallic acid was effective on ameliorating hippocampal neurodegeneration and cognitive stress in $AlCl_3$ induced rat model of AD. Shan et al. [45] have shown that implicating rosmarinic acid in diet of mice decreased tau phosphorylation and insoluble phosphorylated tau formation in the brain. Mori et al. [46] have determined that orally administrated tannic acid in transgenic mice with AD prevented cognitive impairment, decreased the cleavage of the β-carboxyl-terminal APP fragment and soluble APP-β production, as well as reduced β-site APP cleaving enzyme and diminished neuroinflammation. Hornedo-Ortega et al. [47] have found that protocatechuic acid inhibited Aβ aggregation and its preformed fibrils, also prevented the cell death triggered by Aβ toxicity in PC12 cell line model of AD. Guven et al. [48] have suggested that consumption of p-coumaric acid in rat model caused reduction of Aβ protein accumulation and decrease in neuroinflammation. Lee et al. [49] have demonstrated that sinapic acid application rescued neuronal cell death in hippocampus, attenuated memory impairment and oxidative stress as well as glial cell activation in Aβ-induced mice. Jha et al. [50] have shown that ellagic acid reduced neuroinflammation and oxidative stress, attenuated Aβ plaque and AChE levels and improved synaptic connectivity in rat model of sporadic AD. Ogut et al. [51] have determined that syringic acid decreased neuroinflammation and oxidative stress and improved neurobehavioral impairments in $AlCl_3$ induced rat model of AD.

Lignans and AD

Lignans are natural polyphenol compounds containing 2,3-dibenzyl butane skeleton that are attracting due to their strong antioxidant capacity and other biological and therapeutic properties on human health. Lignans are natural constituents known as the oxidative coupling product of β-hydroxyphenylpropane and are widely found as minor constituents in the plant kingdom [52]. Lignans are commonly available in

DOI: https://doi.org/10.14232/analecta.2022.1.14-26

edible plants, where they are synthesized via the phenylpropanoid pathway and following the biosynthesis of lignin [53]. Today, the amount and characterisation of lignans in various foods been evaluated [54]. It was reported that some lignans are known for their antitumor [55], antiviral [56], antibacterial [57] and immunosuppressive properties [58] as well as lignans have protective effect on cardiovascular diseases and diabetes [59]. Some studies [60-65] have proven the anti-neurodegenerative properties of lignans and neolignans.

Kantham et al. [60] have demonstrated the neuroprotective activity of biphenyl neolignane honokiol against AD in transgenic *Caenorhabditis elegans* by inhibiting Aβ aggregation and AChE, also scavenging DPPH radicals and chelating iron (II). Qi et al. [61] have determined that the use of arctigenin inhibited the hyperphosphorylated tau protein expression in hippocampus and provided protection against learning and memory deficits in Aβ-induced mice model of AD. Somani et al. [62] have shown that cubebin application prevented learning and memory deficits, also attenuated the AChE activity and oxidative stress level in scopolamine-induced mice model. Gu et al. [63] have determined that justicidin inhibited hyperphosphorylation of tau in AD; and enhanced activity of AMP-activated protein kinase, which is the key molecule for hyperphosphorylation of tau and elevated cell viability in Aβ-induced SH-SY5Y cell line. Huang et al. [64] have demonstrated that lignans, especially isolariciresinol and lyoniside showed a strong Aβ inhibition activity. Yang et al. [65] have suggested that two new dibenzocyclooctadiene lignans (L6-14, NL5-10) isolated from *Schisandra chinensis* exhibited protective effect against neurotoxicity in Aβ-induced PC12 cell line, and also increased the cell viability.

Stilbenes and AD

Stilbenes constitutes an important group of polyphenols that are quite common in plants. The most known compound is resveratrol (3,5,4'-trihydroxystilbene) which is found in large amounts in red wine and also in the grape skin [66]. Stilbenes are produced by plants in response to infections due to pathogens or various stress conditions. It has been detected in more 400 natural stilbenes in over 70 plant species, especially in grape, strawberry and peanut [67,68]. Some stilbenes have a great antioxidant activity and radical scavenging activity, and it was also reported that they prevent lipid peroxidation [69]. Also, stilbenes are associated with a wide range of pharmacological properties including antimicrobial and antifungal activity [70,71] and protective activity neurodegenerative pathologies such as AD [72-77].

Porquet et al. [72] have demonstrated that administration of *trans*-resveratrol in diet showed neuroprotective activity by reducing Aβ aggregation and tau hyperphosphorylation, attenuating cognitive impairment and increasing the lifetime in SAMP8 mice. Also, Karuppagounder et al. [73] have determined that oral supplementation of *trans*-resveratrol decreased Aβ plaque accumulation in Tg199589 transgenic mice model of AD. Caillaud et al. [74] have proven that use trans ε-viniferin decreased the Aβ aggregation and prevented neuroinflammation in the brain of transgenic APPswe/PS1dE9 mice. Hu et al. [75] have shown that miyabenol C reduced sAPPβ and soluble Aβ levels in the cortex and hippocampus of transgenic APP/PS1 mice. Chang et al. [76] and Hou et al. [77] have demonstrated that daily supplementation of pterostilbene in diet improved cognitive status and decreased neuroinflammation, cellular stress and AD markers in SAMP8 mice and C57BL/6 mice, relatively.

Flavonoids and AD

Flavonoids are one of the largest classes of phenolic compounds having a group of benzo-γ-pyrone derivatives [78]. They are synthesized by all vascular plants and are found in the composition of fruits, vegetables, seeds, herbs, whole grains and tea [79]. It is estimated that over 6500 flavonoids were identified in this group [80]. Flavonoids are divided into 6 subgroups: flavonols, flavones, flavanones, flavan-3-ols (catechins), isoflavones and anthocyanidins [81]. It was emphasized that flavonoids have

DOI: https://doi.org/10.14232/analecta.2022.1.14-26

many biological benefits including antioxidant [82], anti-inflammatory [83], antiatherogenic [84,85] and anticarcinogenic activities [86,87]. More recently, dietary intake of flavonoids has been associated to early proof that the onset of some neurodegenerative disorders such as dementia and AD may be postponed [88-96].

Jimenez-Aliaga et al. [88] have demonstrated that quercetin and rutin inhibited the Aβ formation and disaggregated Aβ fibrils, reduced the β-secretase enzyme activity and ROS generation in H_2O_2-treated APPswe cells. Ho et al. [89] have shown that dietary quercetin-3-O-glucuronide extracted from Cabernet Sauvignon red wine reduced the generation of Aβ peptides in transgenic Tg2576 mice. DeToma et al. [90] have proven that myricetin was effective against metal associated Aβ generation and modulated Aβ aggregation as well as neurotoxicity in human neuroblastoma cells and in vitro. Sharoar et al. [91] have determined that kaempferol-3-O-rhamnoside inhibited fibrilogenesis of Aβ in SH-SY5Y cell line, but as a consequence of this inhibition caused an oligomeric species accumulation, yet these aggregates were smaller, soluble, non-β-sheet formed and non-toxic. Ahmad et al. [92] have demonstrated that the use of fisetin decreased the accumulation of Aβ peptides, β-secretase enzyme expression and hyperphosphorylation of tau protein, and prevented the neuroinflammation, also improved the cognitive activity by increasing the presynaptic and postsynaptic proteins in C57BL/6N mice. Tarozzi et al. [93] have shown that cyanidin 3-O-glucoside inhibited the spontaneous aggregation of Aβ into oligomers, also prevented the neuronal loss and synaptic dysfunction in SH-SY5Y cell line. Wang et al. [94] have proven that dietary supplementation of naringin improved cognitive and locomotor activities, reduced scattered senile plaques and moderated disturbances in brain energy metabolism of APPswe/PSdE9 transgenic mice. Balez et al. [95] have suggested that apigenin showed anti-inflammatory effect as protecting neurites and preventing cellular death by promoting nitric oxide and cytokine release in inflammatory cells in human induced pluripotent stem cells. Bieschke et al. [96] have determined that epigallocatechin gallate (EGCG) inhibited the fibrilogenesis of Aβ and α-synuclein, which is associated with cognitive impairment, and converted these fibrils into smaller aggregates in HEK-293 cell line. Table 1 indicates the summarized results of studies of each polyphenol groups that were highlighted in this review.

Table1. The effect of polyphenols on AD

Polyphenols	***Sample***	***Intervention***	***Summary of Findings***	***Ref.***
Apigenin	Stem cell model of AD	Inoculated into stem cells (10 μM)	• Performed anti-inflammatory effect via protecting neurites • Prevented neuronal loss	95
Arctigenin	Mouse model of AD (ICR)	Orally administrated (150 mg/kg b.w./day)	• Attenuated behavioral impairments • Inhibited tau phosphorylation in the hippocampus	61
Caffeic acid	Rat model of hyperinsulinemia	Orally administrated (30 mg/kg b.w./day)	• Ameliorated memory and learning impairments • Decreased the p-tau expression in the hippocampus • Attenuated APP expression and β-site APP cleaving enzyme	41
Cubebin	Mouse model of AD	Orally administrated (50 mg/kg b.w./day)	• Prevented scopolamine-induced cognitive impairment • Inhibited AChE activity and decreased oxidative stress	62
Cyanidin 3-O-glucoside	SH-SY5Y cell line	Inoculated into the cell line (25, 50 and 100 μM)	• Inhibited spontaneous Aβ aggregation • Prevented neuronal loss and synaptic dysfunction	93
Ellagic acid	Rat model of sporadic AD	Orally administrated (50 mg/kg b.w./day)	• Diminished oxidative stress, neuroinflammation, AchE and Aβ level • Normalized abnormal behavioral	50

DOI: https://doi.org/10.14232/analecta.2022.1.14-26

			representations	
(-)-epi-gallo-catechine gallate	HEK-293 cell line	Inoculated into the cell line (50 μM)	• Inhibited Aβ and α-synuclein fibrilogenesis • Converted large Aβ and α-synuclein fibrils into smaller	96
Fisetin	Mouse model of AD (C57BL/6N)	Intraperitoneal injection (20 mg/kg b.w./day)	• Decreased Aβ accumulation, BACE-1 expression and tau phosphorylation • Prevented neuroinflammation • Improved memory	92
Gallic acid	Transgenic mouse model of AD (APP/PS1)	Orally administrated (20 mg/kg b.w./day)	• Reversed learning and memory impairment • Decreased Aβ deposits, reduced β-secretase activity, inhibited neuroinflammation	42
Gallic acid	Transgenic mouse model of AD (APP/PS1)	Orally administrated (30 mg/kg b.w./day)	• Improved memory and learning • Reduced Aβ aggregation	43

Table1. (Continued)

Polyphenols	***Sample***	***Intervention***	***Summary of Findings***	***Ref.***
Gallic acid	Rat model of AD ($AlCl_3$ induced)	Orally administrated (100 mg/kg b.w./day)	• Ameliorated memory impairment and learning deficit • Restored stress markers	44
Honokiol	Transgenic *Caenorhabditis elegans* model of AD	Inoculated (10, 100 and 1000 μM)	• Inhibited AChE and Aβ aggregation • Performed DPPH scavenging and chelating iron (II) activity	60
Justicidin	SH-SY5Y cell line	Inoculated into the cell line (62.5, 125, 250, and 500 nM)	• Inhibited tau phosphorylation • Induced autophagy by regulating GSK-3β and AMP-activated protein kinase	63
Kaempferol-3-O-rhamnoside	SH-SY5Y cell line	Inoculated into the cell line (10, 20, 30, 40 and 50 μM)	• Reduced Aβ mediated cytotoxicity • Inhibited fibrilogenesis and accumulation	91
Miyabenol C	Transgenic mouse model of AD (APP/PS1)	Intracerebroventricular injection (0.6μg/g)	• Reduced Aβ and sAPPβ levels in the brain • Inhibited of β-secretase activity	75
Myricetin	SK-N-BE(2)-M17 cell line	Inoculated into the cell line (20 μM)	• Diminished metal induced Aβ generation • Modulated Aβ aggregation	90
Naringin	Transgenic mouse model of AD ($APP^{swe}/PS^{\Delta E9}$)	Orally administrated (100 mg/kg b.w./day)	• Attenuated plaque burden • Improved cognitive functioning	94
p-coumaric acid	Sprague-Dawley rats	Orally administrated (100 mg/kg b.w./day)	• Reduced Aβ aggregation • Decreased neuroinflammation	48
Pterostilbene	Mouse model of AD (SAMP8)	Orally administrated (120 mg/kg b.w./day)	• Reduced cellular stress, inflammation and AD pathology	76
Pterostilbene	Mouse model of AD (C57BL/6)	Orally administrated (400 mg/kg b.w./day)	• Attenuated cognitive impairment • Inhibited microglia activation	77
Protocatechuic acid	PC12 cell line	Inoculated into the cell line (2, 5, 10, 20, 50 and 100 μM)	• Inhibited Aβ and α-synuclein aggregation and fibrillation • Prevented cell death triggered by their toxicity	47
Quercetin *Rutin*	APPswe cell line	Inoculated into the cell line (25, 50 and 100 nM each)	• Both inhibited Aβ formation and disaggregated Aβ fibrils • Both decreased ROS generation • Rutin inhibited β-secretase enzyme activity	88
Rosmarinic acid	Mouse model of AD (C57BL/6)	Orally administrated (2 mg/kg b.w./day)	• Decreased tau phosphorylation and insoluble phosphorylated tau in the brain	45
Sinapic acid	Mouse model of AD (ICR)	Orally administrated (10 mg/kg b.w./day)	• Rescued neuronal cell death • Attenuated memory impairment	49
Syringic acid	Rat model of AD ($AlCl_3$ induced)	Orally administrated (25 mg/kg b.w./day)	• Reduced neuroinflammation and oxidative stress • Diminished neurobehavioral impairments	51
Tannic acid	Transgenic mouse model of AD (APP/PS1)	Orally administrated (30 mg/kg b.w./day)	• Prevented behavioral impairment • Mitigated Aβ deposition	46
Trans ε-viniferin	Transgenic mouse model of AD (APP/PS1)	Orally administrated (10 mg/kg b.w./day)	• Reduced size and density of Aβ deposits • Decreased reactivity of astrocytes and	74

DOI: https://doi.org/10.14232/analecta.2022.1.14-26

			microglia	
Trans-Resveratrol	Mouse model of AD (SAMP8)	Orally administrated (1 g/kg b.w./day)	• Reduced cognitive impairment • Diminished Aβ burden and tau phosphorylation	72
Trans-Resveratrol	Transgenic mouse model of AD (Tg19959)	Orally administrated (300 mg/kg b.w./day)	• Diminished Aβ plaque formation	73

2. CONCLUSIONS

In conclusion, some dietary polyphenols described and discussed in this review have demonstrated many important therapeutic properties against AD. From the worldwide public health viewpoint, the daily consumption of plant-based aliments and their derivates including berries, citrus fruits, pomegranate, grape, herbs, nuts, coffee, tea, and wine have become the main tool for prevention of AD. This has encouraged studies through the comprehending of the mechanisms at the principle of such precautions. The aforesaid initiatives have led to the recognition of such mechanisms including antioxidant capacities, reducing ROS content, capability to prevent the fibrilogenesis of Aβ and its accumulation, inhibition the AChE activity. Taking everything into account, these findings confirm the potential of dietary polyphenols as active agents against AD as well as other neurodegenerative disorders and should inspire scientists to use the data for the design of potential therapies for the mentioned disorders.

REFERENCES

[1] Colombres M., Sagal J. P., Inestrosa N. C. (2004): An overview of the current and novel drugs for Alzheimer's disease with particular reference to anti-cholinesterase compounds, *Current pharmaceutical design* 10(25), 3121-3130. https://doi.org/10.2174/1381612043383359
[2] Tyas S. L., Manfreda J., Strain L. A., Montgomery P. R. (2001): Risk factors for Alzheimer's disease: a population-based, longitudinal study in Manitoba, Canada, *International journal of epidemiology* 30(3), 590-597. https://doi.org/10.1093/ije/30.3.590
[3] Patterson, C. (2018): World alzheimer report 2018.
[4] Singh M., Kaur M., Kukreja H., Chugh R., Silakari O., Singh D. (2013): Acetylcholinesterase inhibitors as Alzheimer therapy: from nerve toxins to neuroprotection, *European journal of medicinal chemistry* 70, 165-188. https://doi.org/10.1016/j.ejmech.2013.09.050
[5] Lansdall C. J. (2014): An effective treatment for Alzheimer's disease must consider both amyloid and tau, *Bioscience Horizons: The International Journal of Student Research* 7, 1-11. https://doi.org/10.1093/biohorizons/hzu002
[6] Minati L., Edginton T., Grazia Bruzzone M., Giaccone G. (2009): Reviews: current concepts in Alzheimer's disease: a multidisciplinary review, *American Journal of Alzheimer's Disease & Other Dementias®* 24(2), 95-121. https://doi.org/10.1177/1533317508328602
[7] Kumar K., Kumar A., Keegan R. M., Deshmukh R. (2018): Recent advances in the neurobiology and neuropharmacology of Alzheimer's disease, *Biomedicine & pharmacotherapy* 98, 297-307. https://doi.org/10.1016/j.biopha.2017.12.053
[8] Tramutola A., Lanzillotta C., Perluigi M., Butterfield D. A. (2017): Oxidative stress, protein modification and Alzheimer disease, *Brain research bulletin* 133, 88-96. https://doi.org/10.1016/j.brainresbull.2016.06.005
[9] Hane F. T., Robinson M., Lee B. Y., Bai O., Leonenko Z., Albert M. S. (2017): Recent progress in Alzheimer's disease research, part 3: diagnosis and treatment, *Journal of Alzheimer's Disease* 57(3), 645-665. https://doi.org/10.3233/JAD-160907

DOI: https://doi.org/10.14232/analecta.2022.1.14-26

[10] Kamat P. K., Kalani A., Rai S., Swarnkar S., Tota S., Nath C., Tyagi N. (2016): Mechanism of oxidative stress and synapse dysfunction in the pathogenesis of Alzheimer's disease: understanding the therapeutics strategies, *Molecular neurobiology* 53(1), 648-661. https://doi.org/10.1007/s12035-014-9053-6
[11] Kumar A., Singh A., Aggarwal A. (2017): Therapeutic potentials of herbal drugs for Alzheimer's disease—An overview, *Indian Journal of Experimental Biology* 55(2), 63-73.
[12] Hansen R. A., Gartlehner G., Webb A. P., Morgan L. C., Moore C. G., Jonas D. E. (2008): Efficacy and safety of donepezil, galantamine, and rivastigmine for the treatment of Alzheimer's disease: a systematic review and meta-analysis, *Clinical interventions in aging* 3(2), 211.
[13] Zeng Q., Siu W., Li L., Jin Y. U., Liang S., Cao M., Wu Z. (2019): Autophagy in Alzheimer's disease and promising modulatory effects of herbal medicine, *Experimental Gerontology* 119, 100-110. https://doi.org/10.1016/j.exger.2019.01.027
[14] Mattioli R., Francioso A., d'Erme M., Trovato M., Mancini P., Piacentini L., Mosca L. (2019): Anti-inflammatory activity of a polyphenolic extract from Arabidopsis thaliana in in vitro and in vivo models of Alzheimer's disease, *International journal of molecular sciences* 20(3), 708. https://doi.org/10.3390/ijms20030708
[15] Chen Z., Zhong C. (2014): Oxidative stress in Alzheimer's disease, *Neuroscience bulletin* 30(2), 271-281. https://doi.org/10.1007/s12264-013-1423-y
[16] Liu Z., Zhou T., Ziegler A. C., Dimitrion P., Zuo, L. (2017): Oxidative stress in neurodegenerative diseases: from molecular mechanisms to clinical applications, *Oxidative medicine and cellular longevity* 2017. https://doi.org/10.1155/2017/2525967
[17] Butterfield D. A., Halliwell B. (2019): Oxidative stress, dysfunctional glucose metabolism and Alzheimer disease, *Nature Reviews Neuroscience* 20(3), 148-160. https://doi.org/10.1038/s41583-019-0132-6
[18] Pandey K. B., Rizvi S. I. (2009): Plant polyphenols as dietary antioxidants in human health and disease, *Oxidative medicine and cellular longevity* 2(5), 270-278. https://doi.org/10.4161/oxim.2.5.9498
[19] Shahidi F., Ambigaipalan P. (2015): Phenolics and polyphenolics in foods, beverages and spices: Antioxidant activity and health effects–A review, *Journal of functional foods* 18, 820-897. https://doi.org/10.1016/j.jff.2015.06.018
[20] Phan H. T., Samarat K., Takamura Y., Azo-Oussou A. F., Nakazono Y., Vestergaard M. D. C. (2019): Polyphenols modulate alzheimer's amyloid beta aggregation in a structure-dependent manner, *Nutrients* 11(4), 756. https://doi.org/10.3390/nu11040756
[21] Ebrahimi A., Schluesener H. (2012): Natural polyphenols against neurodegenerative disorders: potentials and pitfalls, *Ageing research reviews* 11(2), 329-345. https://doi.org/10.1016/j.arr.2012.01.006
[22] Bastianetto S., Krantic S., Quirion R. (2008): Polyphenols as potential inhibitors of amyloid aggregation and toxicity: possible significance to Alzheimer's disease, *Mini reviews in medicinal chemistry* 8(5), 429-435. https://doi.org/10.2174/138955708784223512
[23] Bhullar K. S., Rupasinghe H. P. (2013): Polyphenols: multipotent therapeutic agents in neurodegenerative diseases, *Oxidative medicine and cellular longevity* 2013. https://doi.org/10.1155/2013/891748
[24] Zhang H. Y. (2007): Can food-derived multipotent agents reduce the risk of Alzheimer's disease, *Trends in food science & technology* 18(9), 492-495. https://doi.org/10.1016/j.tifs.2007.04.008
[25] Lee J. W., Lee Y. K., Ban J. O., Ha T. Y., Yun Y. P., Han S. B., ..., Hong J. T. (2009): Green tea (-)-epigallocatechin-3-gallate inhibits β-amyloid-induced cognitive dysfunction through modification of secretase activity via inhibition of ERK and NF-κ B pathways in mice, *The Journal of nutrition* 139(10), 1987-1993. https://doi.org/10.3945/jn.109.109785

DOI: https://doi.org/10.14232/analecta.2022.1.14-26

[26] Kim J., Lee H. J., Lee K. W. (2010): Naturally occurring phytochemicals for the prevention of Alzheimer's disease, *Journal of neurochemistry* 112(6), 1415-1430. https://doi.org/10.1111/j.1471-4159.2009.06562.x
[27] Zheng Q., Kebede M. T., Kemeh M. M., Islam S., Lee B., Bleck S. D., ..., Lazo N. D. (2019): Inhibition of the self-assembly of Aβ and of tau by polyphenols: Mechanistic studies, *Molecules* 24(12), 2316. https://doi.org/10.3390/molecules24122316
[28] Porat Y., Mazor Y., Efrat S., Gazit E. (2004): Inhibition of islet amyloid polypeptide fibril formation: a potential role for heteroaromatic interactions, *Biochemistry* 43(45), 14454-14462. https://doi.org/10.1021/bi048582a
[29] Hills Jr R. D., Brooks III C. L. (2007): Hydrophobic cooperativity as a mechanism for amyloid nucleation, *Journal of molecular biology* 368(3), 894-901. https://doi.org/10.1016/j.jmb.2007.02.043
[30] Kumar N., Goel N. (2019): Phenolic acids: Natural versatile molecules with promising therapeutic applications, *Biotechnology Reports* 24, e00370. https://doi.org/10.1016/j.btre.2019.e00370
[31] Tsao R., Deng Z. (2004): Separation procedures for naturally occurring antioxidant phytochemicals, *Journal of chromatography B* 812(1-2), 85-99. https://doi.org/10.1016/j.jchromb.2004.09.028
[32] Zhang L., Li Y., Liang Y., Liang K., Zhang F., Xu T., ..., Lu B. (2019): Determination of phenolic acid profiles by HPLC-MS in vegetables commonly consumed in China, *Food chemistry* 276, 538-546. https://doi.org/10.1016/j.foodchem.2018.10.074
[33] Heleno S. A., Martins A., Queiroz M. J. R., Ferreira I. C. (2015): Bioactivity of phenolic acids: Metabolites versus parent compounds: A review, *Food chemistry* 173, 501-513. https://doi.org/10.1016/j.foodchem.2014.10.057
[34] Sevgi K., Tepe B., Sarikurkcu C. (2015): Antioxidant and DNA damage protection potentials of selected phenolic acids, *Food and Chemical Toxicology* 77, 12-21. https://doi.org/10.1016/j.fct.2014.12.006
[35] Rao Y., Zhao X., Li Z., Huang J. (2018): Phenolic acids induced growth of 3D ordered gold nanoshell composite array as sensitive SERS nanosensor for antioxidant capacity assay, *Talanta* 190, 174-181. https://doi.org/10.1016/j.talanta.2018.07.069
[36] Spiegel M., Kapusta K., Kołodziejczyk W., Saloni J., Żbikowska B., Hill G. A., Sroka Z. (2020): Antioxidant activity of selected phenolic acids–ferric reducing antioxidant power assay and QSAR analysis of the structural features, *Molecules* 25(13), 3088. https://doi.org/10.3390/molecules25133088
[37] Ozcelik B., Kartal M., Orhan I. (2011): Cytotoxicity, antiviral and antimicrobial activities of alkaloids, flavonoids, and phenolic acids, *Pharmaceutical biology* 49(4), 396-402. https://doi.org/10.3109/13880209.2010.519390
[38] Verma S., Singh A., Mishra A. (2013): Gallic acid: molecular rival of cancer, *Environmental toxicology and pharmacology* 35(3), 473-485. https://doi.org/10.1016/j.etap.2013.02.011
[39] Gomes C. A., Girão da Cruz T., Andrade J. L., Milhazes N., Borges F., Marques M. P. M. (2003): Anticancer activity of phenolic acids of natural or synthetic origin: a structure− activity study, *Journal of medicinal chemistry* 46(25), 5395-5401. https://doi.org/10.1021/jm030956v
[40] Yi W., Fischer J., Akoh, C. C. (2005): Study of anticancer activities of muscadine grape phenolics in vitro, *Journal of agricultural and food chemistry* 53(22), 8804-8812. https://doi.org/10.1021/jf0515328
[41] Chang W., Huang D., Lo Y. M., Tee Q., Kuo P., Wu J. S., ..., Shen S. (2019): Protective effect of caffeic acid against Alzheimer's disease pathogenesis via modulating cerebral insulin signaling, β-amyloid accumulation, and synaptic plasticity in hyperinsulinemic rats, *Journal of agricultural and food chemistry* 67(27), 7684-7693. https://doi.org/10.1021/acs.jafc.9b02078

DOI: https://doi.org/10.14232/analecta.2022.1.14-26

[42] Mori T., Koyama N., Yokoo T., Segawa T., Maeda M., Sawmiller D., ..., Town T. (2020): Gallic acid is a dual α/β-secretase modulator that reverses cognitive impairment and remediates pathology in Alzheimer mice, *Journal of Biological Chemistry* 295(48), 16251-16266. ps://doi.org/10.1074/jbc.RA119.012330
[43] Yu M., Chen X., Liu J., Ma Q., Zhuo Z., Chen H., ..., Hou S. T. (2019): Gallic acid disruption of Aβ1–42 aggregation rescues cognitive decline of APP/PS1 double transgenic mouse, *Neurobiology of Disease* 124, 67-80. https://doi.org/10.1016/j.nbd.2018.11.009
[44] Ogunlade B., Adelakun S. A., Agie J. A. (2020): Nutritional supplementation of gallic acid ameliorates Alzheimer-type hippocampal neurodegeneration and cognitive impairment induced by aluminum chloride exposure in adult Wistar rats, *Drug and chemical toxicology* 1-12. https://doi.org/10.1080/01480545.2020.1754849
[45] Shan Y., Wang D. D., Xu Y. X., Wang C., Cao L., Liu Y. S., Zhu C. Q. (2016): Aging as a precipitating factor in chronic restraint stress-induced tau aggregation pathology, and the protective effects of rosmarinic acid, *Journal of Alzheimer's Disease* 49(3), 829-844. https://doi.org/10.3233/JAD-150486
[46] Mori T., Rezai-Zadeh K., Koyama N., Arendash G. W., Yamaguchi H., Kakuda N., ..., Town T. (2012): Tannic acid is a natural β-secretase inhibitor that prevents cognitive impairment and mitigates Alzheimer-like pathology in transgenic mice, *Journal of Biological chemistry* 287(9), 6912-6927. https://doi.org/10.1074/jbc.M111.294025
[47] Hornedo-Ortega R., Alvarez-Fernandez M. A., Cerezo A. B., Richard T., Troncoso A. M., Garcia-Parrilla M. C. (2016): Protocatechuic acid: inhibition of fibril formation, destabilization of preformed fibrils of amyloid-β and α-synuclein, and neuroprotection, *Journal of agricultural and food chemistry* 64(41), 7722-7732. https://doi.org/10.1021/acs.jafc.6b03217
[48] Guven M., Sehitoglu M. H., Yuksel Y., Tokmak M., Aras A. B., Akman T., ..., Cosar M. (2015): The neuroprotective effect of coumaric acid on spinal cord ischemia/reperfusion injury in rats, *Inflammation* 38(5), 1986-1995. https://doi.org/10.1007/s10753-015-0179-0
[49] Lee H. E., Kim D. H., Park S. J., Kim J. M., Lee Y. W., Jung J. M., ..., Ryu J. H. (2012): Neuroprotective effect of sinapic acid in a mouse model of amyloid β1–42 protein-induced Alzheimer's disease, *Pharmacology Biochemistry and Behavior* 103(2), 260-266. https://doi.org/10.1016/j.pbb.2012.08.015
[50] Jha A. B., Panchal S. S., Shah A. (2018): Ellagic acid: insights into its neuroprotective and cognitive enhancement effects in sporadic Alzheimer's disease, *Pharmacology Biochemistry and Behavior* 175, 33-46. https://doi.org/10.1016/j.pbb.2018.08.007
[51] Ogut E., Akcay G., Yildirim F. B., Derin N., Aslan M. (2020): The influence of syringic acid treatment on total dopamine levels of the hippocampus and on cognitive behavioral skills, *International Journal of Neuroscience* 1-9. https://doi.org/10.1080/00207454.2020.1849191
[52] Cui Q., Du R., Liu M., Rong L. (2020): Lignans and their derivatives from plants as antivirals, *Molecules* 25(1), 183. https://doi.org/10.3390/molecules25010183
[53] Umezawa T. (2003): Diversity in lignan biosynthesis, *Phytochemistry Reviews* 2(3), 371-390. https://doi.org/10.1023/B:PHYT.0000045487.02836.32
[54] Durazzo A., Lucarini M., Camilli E., Marconi S., Gabrielli P., Lisciani S., ..., Marletta L. (2018): Dietary lignans: definition, description and research trends in databases development, *Molecules* 23(12), 3251. https://doi.org/10.3390/molecules23123251
[55] Kim K. H., Moon E., Kim S. Y., Choi S. U., Lee K. R. (2012): Lignan constituents of Tilia amurensis and their biological evaluation on antitumor and anti-inflammatory activities, *Food and Chemical Toxicology* 50(10), 3680-3686. https://doi.org/10.1016/j.fct.2012.07.014

DOI: https://doi.org/10.14232/analecta.2022.1.14-26

[56] Huh J., Song J. H., Kim S. R., Cho H. M., Ko H. J., Yang H., Sung S. H. (2019): Lignan dimers from forsythia viridissima roots and their antiviral effects, *Journal of natural products*, 82(2), 232-238. https://doi.org/10.1021/acs.jnatprod.8b00590
[57] Favela- Hernández J. M. J., García A., Garza- Gonzalez E., Rivas- Galindo V. M., Camacho- Corona M. D. R. (2012): Antibacterial and antimycobacterial lignans and flavonoids from Larrea tridentata, *Phytotherapy research* 26(12), 1957-1960. https://doi.org/10.1002/ptr.4660
[58] Park S. Y., Lee S. H., Choi W. H., Koh E. M., Seo J. H., Ryu S. Y., ..., Koh W. S. (2007): Immunosuppressive lignans isolated from Saururus chinensis, *Planta medica* 73(07), 674-678. https://doi.org/10.1055/s-2007-981525
[59] Hyvärinen H. K., Pihlava J. M., Hiidenhovi J. A., Hietaniemi V., Korhonen, H. J., Ryhänen, E. L. (2006): Effect of processing and storage on the stability of flaxseed lignan added to dairy products, *Journal of Agricultural and Food Chemistry* 54(23), 8788-8792. https://doi.org/10.1021/jf061285n
[60] Kantham S., Chan S., McColl G., Miles J. A., Veliyath S. K., Deora G. S., ..., Ross B. P. (2017): Effect of the biphenyl neolignan honokiol on Aβ42-induced toxicity in Caenorhabditis elegans, Aβ42 fibrillation, cholinesterase activity, DPPH radicals, and iron (II) chelation, *ACS Chemical Neuroscience* 8(9), 1901-1912. https://doi.org/10.1021/acschemneuro.7b00071
[61] Qi Y., Dou D. Q., Jiang H., Zhang B. B., Qin W. Y., Kang K., ..., Jia D. (2017): Arctigenin attenuates learning and memory deficits through PI3k/Akt/GSK-3β pathway reducing tau hyperphosphorylation in Aβ-induced AD mice, *Planta Medica* 83(01/02), 51-56. https://doi.org/10.1055/s-0042-107471
[62] Somani G. S., Nahire M. S., Parikh A. D., Mulik M. B., Ghumatkar P. J., Laddha K. S., Sathaye S. (2017): Neuroprotective effect of Cubebin: A dibenzylbutyrolactone lignan on scopolamine-induced amnesia in mice, *The Indian journal of medical research* 146(2), 255. https://doi.org/10.4103/ijmr.IJMR_156_14
[63] Gu M. Y., Kim J., Yang, H. O. (2016): The neuroprotective effects of justicidin A on amyloid beta25–35-induced neuronal cell death through inhibition of Tau hyperphosphorylation and induction of autophagy in SH-SY5Y cells, *Neurochemical research* 41(6), 1458-1467. https://doi.org/10.1007/s11064-016-1857-5
[64] Huang X. X., Xu Y., Bai M., Zhou L., Song S. J., Wang X. B. (2018): Lignans from the seeds of Chinese hawthorn (Crataegus pinnatifida var. major NE Br.) against β-amyloid aggregation, *Natural product research* 32(14), 1706-1713. https://doi.org/10.1080/14786419.2017.1399378
[65] Yang B. Y., Guo J. T., Li Z. Y., Wang C. F., Wang Z. B., Wang Q. H., Kuang H. X. (2016): New thymoquinol glycosides and neuroprotective dibenzocyclooctane lignans from the rattan stems of Schisandra chinensis, *Chemistry & Biodiversity* 13(9), 1118-1125. https://doi.org/10.1002/cbdv.201500311
[66] Espín J. C., García-Conesa M. T., Tomás-Barberán F. A. (2007): Nutraceuticals: facts and fiction, *Phytochemistry* 68(22-24), 2986-3008. https://doi.org/10.1016/j.phytochem.2007.09.014
[67] Shen T., Wang X. N., Lou H. X. (2009): Natural stilbenes: an overview, *Natural product reports* 26(7), 916-935. https://doi.org/10.1039/B905960A
[68] Skowyra M., Falguera V., Gallego G., Peiró S., Almajano M. P. (2014): Antioxidant properties of aqueous and ethanolic extracts of tara (Caesalpinia spinosa) pods in vitro and in model food emulsions, *Journal of the Science of Food and Agriculture* 94(5), 911-918. https://doi.org/10.1002/jsfa.6335
[69] Vincenzi S., Tomasi D., Gaiotti F., Lovat L., Giacosa S., Torchio F., ..., Rolle L. (2013): Comparative study of the resveratrol content of twenty-one Italian red grape varieties, *South African Journal of Enology and Viticulture* 34(1), 30-35. https://doi.org/10.21548/34-1-1078
[70] Aslam S. N., Stevenson P. C., Kokubun T., Hall D. R. (2009): Antibacterial and antifungal activity of cicerfuran and related 2-arylbenzofurans and stilbenes, *Microbiological Research* 164(2), 191-195. https://doi.org/10.1016/j.micres.2006.11.012

DOI: https://doi.org/10.14232/analecta.2022.1.14-26

[71] Tellone E., Galtieri A., Russo A., Giardina B., Ficarra S. (2015): Resveratrol: a focus on several neurodegenerative diseases, *Oxidative medicine and cellular longevity* 2015. https://doi.org/10.1155/2015/392169
[72] Porquet D., Casadesús G., Bayod S., Vicente A., Canudas A. M., Vilaplana J., ..., Del Valle J. (2013): Dietary resveratrol prevents Alzheimer's markers and increases life span in SAMP8, *Age* 35(5), 1851-1865. https://doi.org/10.1007/s11357-012-9489-4
[73] Karuppagounder S. S., Pinto J. T., Xu H., Chen H. L., Beal M. F., Gibson G. E. (2009): Dietary supplementation with resveratrol reduces plaque pathology in a transgenic model of Alzheimer's disease, *Neurochemistry international* 54(2), 111-118. https://doi.org/10.1016/j.neuint.2008.10.008
[74] Caillaud M., Guillard J., Richard D., Milin S., Chassaing D., Paccalin M., ..., Rioux Bilan A. (2019): Trans ε viniferin decreases amyloid deposits and inflammation in a mouse transgenic Alzheimer model, *PLoS One* 14(2), e0212663. https://doi.org/10.1371/journal.pone.0212663
[75] Hu J., Lin T., Gao Y., Xu J., Jiang C., Wang G., ..., Zhang Y. W. (2015): The resveratrol trimer miyabenol C inhibits β-secretase activity and β-amyloid generation, *PLoS One* 10(1), e0115973. https://doi.org/10.1371/journal.pone.0115973
[76] Chang J., Rimando A., Pallas M., Camins A., Porquet D., Reeves J., ..., Casadesus, G. (2012): Low-dose pterostilbene, but not resveratrol, is a potent neuromodulator in aging and Alzheimer's disease, *Neurobiology of aging* 33(9), 2062-2071. https://doi.org/10.1016/j.neurobiolaging.2011.08.015
[77] Hou Y., Xie G., Miao F., Ding L., Mou Y., Wang L., ..., Wu C. (2014): Pterostilbene attenuates lipopolysaccharide-induced learning and memory impairment possibly via inhibiting microglia activation and protecting neuronal injury in mice, *Progress in Neuro-Psychopharmacology and Biological Psychiatry* 54, 92-102. https://doi.org/10.1016/j.pnpbp.2014.03.015
[78] Boušová I., Skálová L. (2012): Inhibition and induction of glutathione S-transferases by flavonoids: possible pharmacological and toxicological consequences, *Drug metabolism reviews* 44(4), 267-286. https://doi.org/10.3109/03602532.2012.713969
[79] Wildman R. E., Wildman R., Wallace T. C. (2016): Handbook of nutraceuticals and functional foods, *CRC press*. https://doi.org/10.1201/9781420006186
[80] Corradini E., Foglia P., Giansanti P., Gubbiotti R., Samperi R., Lagana A. (2011): Flavonoids: chemical properties and analytical methodologies of identification and quantitation in foods and plants, *Natural product research* 25(5), 469-495. https://doi.org/10.1080/14786419.2010.482054
[81] Crozier A., Jaganath I. B., Clifford M. N. (2009): Dietary phenolics: chemistry, bioavailability and effects on health, *Natural product reports* 26(8), 1001-1043. https://doi.org/10.1039/B802662A
[82] Zeng Y., Song J., Zhang M., Wang H., Zhang Y., Suo H. (2020): Comparison of in vitro and in vivo antioxidant activities of six flavonoids with similar structures, *Antioxidants* 9(8), 732. https://doi.org/10.3390/antiox9080732
[83] Ginwala R., Bhavsar R., Chigbu D. G. I., Jain P., Khan Z. K. (2019): Potential role of flavonoids in treating chronic inflammatory diseases with a special focus on the anti-inflammatory activity of apigenin, *Antioxidants* 8(2), 35. https://doi.org/10.3390/antiox8020035
[84] Ciumărnean L., Milaciu M. V., Runcan O., Vesa Ș. C., Răchișan A. L., Negrean V., ... Dogaru G. (2020): The effects of flavonoids in cardiovascular diseases, *Molecules* 25(18), 4320. https://doi.org/10.3390/molecules25184320
[85] Perez-Vizcaino F., Duarte J. (2010): Flavonols and cardiovascular disease, *Molecular aspects of medicine* 31(6), 478-494. https://doi.org/10.1016/j.mam.2010.09.002
[86] Montané X., Kowalczyk O., Reig-Vano B., Bajek A., Roszkowski K., Tomczyk R., ..., Tylkowski B. (2020): Current perspectives of the applications of polyphenols and flavonoids in cancer therapy, *Molecules* 25(15), 3342. https://doi.org/10.3390/molecules25153342

DOI: https://doi.org/10.14232/analecta.2022.1.14-26

[87] Russo M., Spagnuolo C., Tedesco I., Bilotto S., Russo G. L. (2012): The flavonoid quercetin in disease prevention and therapy: facts and fancies, *Biochemical pharmacology* 83(1), 6-15. https://doi.org/10.1016/j.bcp.2011.08.010

[88] Jiménez-Aliaga K., Bermejo-Bescós P., Benedí J., Martín-Aragón S. (2011): Quercetin and rutin exhibit antiamyloidogenic and fibril-disaggregating effects in vitro and potent antioxidant activity in APPswe cells, *Life sciences* 89(25-26), 939-945. https://doi.org/10.1016/j.lfs.2011.09.023

[89] Ho L., Ferruzzi M. G., Janle E. M., Wang J., Gong B., Chen T. Y., ..., Pasinetti G. M. (2013): Identification of brain- targeted bioactive dietary quercetin- 3- O- glucuronide as a novel intervention for Alzheimer's disease, *The FASEB Journal* 27(2), 769-781. https://doi.org/10.1096/fj.12-212118

[90] DeToma A. S., Choi J. S., Braymer J. J., Lim M. H. (2011): Myricetin: a naturally occurring regulator of metal- induced amyloid- β aggregation and neurotoxicity, *ChemBioChem* 12(8), 1198-1201. https://doi.org/10.1002/cbic.201000790

[91] Sharoar M. G., Thapa A., Shahnawaz M., Ramasamy V. S., Woo E. R., Shin S. Y., Park I. S. (2012): Keampferol-3-O-rhamnoside abrogates amyloid beta toxicity by modulating monomers and remodeling oligomers and fibrils to non-toxic aggregates, *Journal of biomedical science* 19(1), 1-13. https://doi.org/10.1186/1423-0127-19-104

[92] Ahmad A., Ali T., Park H. Y., Badshah H., Rehman S. U., Kim M. O. (2017): Neuroprotective effect of fisetin against amyloid-beta-induced cognitive/synaptic dysfunction, neuroinflammation, and neurodegeneration in adult mice, *Molecular neurobiology* 54(3), 2269-2285. https://doi.org/10.1007/s12035-016-9795-4

[93] Tarozzi A., Morroni F., Merlicco A., Bolondi C., Teti G., Falconi M., ..., Hrelia P. (2010): Neuroprotective effects of cyanidin 3-O-glucopyranoside on amyloid beta (25–35) oligomer-induced toxicity, *Neuroscience Letters* 473(2), 72-76. https://doi.org/10.1016/j.neulet.2010.02.006

[94] Wang D., Gao K., Li X., Shen X., Zhang X., Ma C., ..., Zhang L. (2012): Long-term naringin consumption reverses a glucose uptake defect and improves cognitive deficits in a mouse model of Alzheimer's disease, *Pharmacology Biochemistry and Behavior* 102(1), 13-20. https://doi.org/10.1016/j.pbb.2012.03.013

[95] Balez R., Steiner N., Engel M., Muñoz S. S., Lum J. S., Wu Y., ..., Ooi L. (2016): Neuroprotective effects of apigenin against inflammation, neuronal excitability and apoptosis in an induced pluripotent stem cell model of Alzheimer's disease, *Scientific reports* 6(1), 1-16. https://doi.org/10.1038/srep31450

[96] Bieschke J., Russ J., Friedrich R. P., Ehrnhoefer D. E., Wobst H., Neugebauer K., Wanker E. E. (2010): EGCG remodels mature α-synuclein and amyloid-β fibrils and reduces cellular toxicity, *Proceedings of the National Academy of Sciences* 107(17), 7710-7715. https://doi.org/10.1073/pnas.0910723107

DOI: https://doi.org/10.14232/analecta.2022.1.14-26

Analecta Technica Szegedinensia
Vol. 16, No. 01 ISSN 2064-7964 2022

KINEMATIC AND DYNAMIC INVESTIGATION OF A NOVEL INERTIAL PROPULSION DRIVE

[1]Stelica Timofte, [1]Zoltan I. Korka, [2]Attila Gerőcs, [2]Elena S. Wisznovszky (Muncut)[2], [1]Camelia R. Sfetcu

[1] Babeş-Bolyai University, Doctoral School of Engineering, P-ta Traian Vuia no. 1-4, 320085 Resita, Romania
[2] "Aurel Vlaicu" University of Arad, Automation, Industrial Engineering, Textiles and Transportation Department, B-dul Revoluției no. 77, Arad 310032, Romania,
e-mail: zoltan.korka@ubbcluj.ro

ABSTRACT

Today there is a great deal of controversy over the operation of inertial propulsion drives (IPD), as they challenge the laws of Newtonian mechanics. Starting with the last decades of the previous century, many devices that use the centrifugal force to generate linear propulsion were patented. Regrettably, whether we are talking about the initial, or the most recent attempts, only a few of these systems passed the patent stage and were involved for practical applications. The aim of this paper is to present an IPD, developed by the authors, which uses for generating linear motion the kinetic energy of several masses, placed in the articulation points of the links of a chain drive. The masses placed equidistantly along the half-length of the chain perform a complex movement, consisting of the specific displacement of the chain elements and a rotation around an axis, that is parallel to the line which joins the centres of the chain wheels. After deducting the equations of the geometric coordinates of the masses, the total propulsion force was computed. The obtained results are supporting the ability of the IPD to generate propulsive force and linear motion.

Keywords: dynamics, inertial force, kinematic, propulsion drive

1. INTRODUCTION

In the last decades, countless enthusiastic researchers and inventors have invested a lot of time and efforts to imagine devices able to confront Newtonian mechanics and to develop linear motion by using centrifugal forces. Thus, Allan Jr. [1] asked rhetorically, "Why does classical mechanics forbid inertial propulsion devices when they evidently exist?" Thus, in his book, this author presents some of the functional inertial propulsion drives.
These drives are multi-body systems, their displacement being provided by a propulsive force generated as a reaction to the variable centrifugal force acting on a rotating mass.
Starting from the general equation of the centrifugal force F_c acting on a rotating body:

$$F_c = m \cdot \omega^2 \cdot R \tag{1}$$

where, *m*- the mass of the body, *ω*- the angular speed and *R*- the radius of the trajectory, it can be concluded that a time- fluctuating centrifugal force $F_c(t)$ can be obtained by varying one of the terms on the right-hand side of (1): $m(t)$, $\omega(t)$ or $R(t)$.
Most of the proposed inertial propulsion drives are based on the rotation of several masses on an eccentric trajectory of variable radius. Thus, the "thrust generating device and moving body" proposed by Komora [2] uses two gears to impart a Limaçon-type trajectory (of variable radius) to a mass. Thus, the variable centrifugal force acting on this mass generates a thrust force of the device.
A similar principle is used for the „device for providing propulsion force" developed by Helavuo [3]. As presented in Fig. 1, the device comprises of a mass element (6) and gear for moving the center of gravity of mass (6) around the axis of rotation of an inner gear (2) in such a path (8) in which the centrifugal force provided by mass (6) is higher on the portion (16) of the path (8) than at the second portion (17). In this way, the device generates an asymmetric centrifugal force, which attempts to pull the system.

DOI: https://doi.org/10.14232/analecta.2022.1.27-33

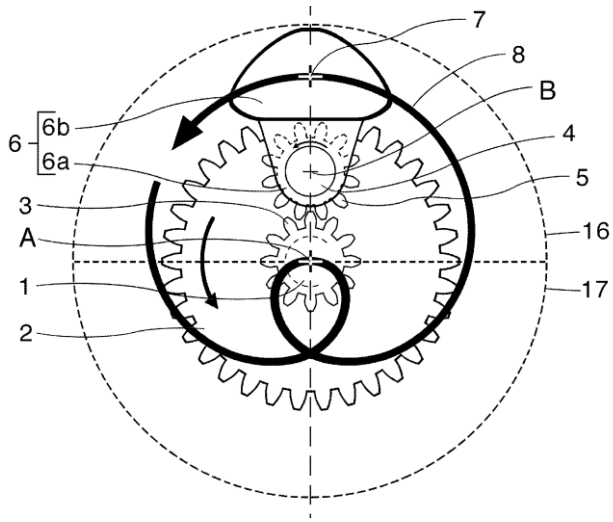

Figure 1. Principle of device for providing propulsion force [2]

Gerocs et al. [4, 5, 6] propose an IPS which generates variable centrifugal force by rotating 8 steel balls along different pseudo- circular trajectories. By means of analytical approach and motion simulation performed in SolidWorks, they conclude that the most advantageous version of the IPS, in terms of velocities, displacements and power consumption, is the version of the retaining disk with cylindrical bore placed eccentric.

The present paper presents a novel propulsion drive developed by the authors, which uses the kinetic energy of equidistant disposed masses, placed in the articulation points of the links of a chain drive, along the half-length of the chain. The masses perform a complex movement, consisting of the specific displacement of the chain elements and a rotation around an axis parallel to the line that joins the centers of the chain wheels.

2. PROPOSED INERTIAL PROPULSION DRIVE

The operating principle of the IPD is based on obtaining a variable resultant centrifugal force, which generates an opposite reaction force for the propulsion of the system.

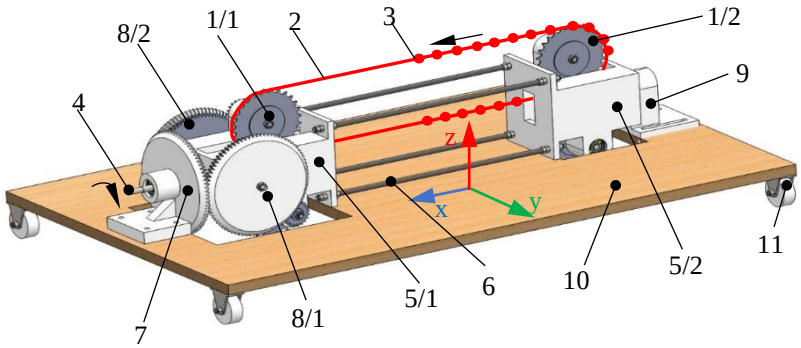

Figure 2. Overview of the IPD

For this purpose, cylindrical steel weights (3) of the same mass are placed on the bolts of a chain (2), on half of its length, on either side of the links. In the same time, the chain drive, having identical wheels (1/1

DOI: https://doi.org/10.14232/analecta.2022.1.27-33

and 1/2) with z= 28 teeth, is rotating, together with the housings (5/1 and 5/2), around the axis of the driving shaft (4), that is parallel to the line which joins the centres of the chain wheels. The centre distance of the chain drive is a= 42·p, where p is the pitch of the chain. These constructive details ensure a complex movement of the weights which have the peculiarity that, at a complete (pendular) rotation around the axis of the drive shaft, the first two weights placed on the chain reach the starting position. In the same time, the chain wheels are doing four complete rotations. This kinematic connection is ensured by the conical transmission, consisting of a fixed wheel (7), respective two satellite wheels (8/1 and 8/2), and a pair of cylindrical wheels placed inside the housing (8/1) for driving the chain wheel (1/1).The weights of the housings are supported by bearings placed inside the fixed wheel (7) and the support (9), while the centre distance between the chain wheels is maintained constant by 4 threaded rods (6) and hexagon nuts, respectively. The whole assembly is mounted on a rectangular plate (10), supported by four wheels (11). To have a better understanding of the proposed system, Figure 2 provides an overview of the IPD.

3. KINEMATIC AND DYNAMIC ANALYSIS OF THE PROPULSION DRIVE

In order to calculate the propulsion force developed by the system, due to the centrifugal forces acting on the masses equal disposed along the half-length of the chain, the kinematic of these masses is investigated. For this purpose, a Cartesian system (xOyz) was attached to the plate (10). In addition, it was considered that, in the starting position, the first and last masses are placed in the middle of the centre distance of the chain drive (position A and D in Fig. 3).

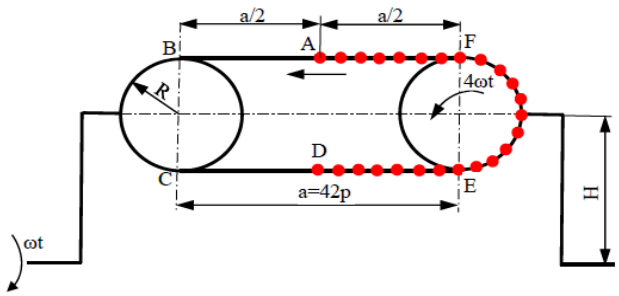

Figure 3. Schematic representation of mass movement

Let's consider M the total mass of the weights placed in the chain joints. M can be decomposed into 3 elements (M1, M2 and M3), which change their shape (linear, respectively arc), value and position of gravity centre, during travelling the route A-B-C-D-E-F-A. The inertial force along the y axis, generated by the complex movement of the masses attached to the chain can be written as:

$$F_y = \int_0^t \sum_{i=1}^{3} M_i(t) \cdot a_{y_i}(t) dt \tag{2}$$

where t is the time for a complete rotation of the housings around the input shaft axis, $M_i(t)$ the mases of the $i=3$ elements and $a_{yi}(t)$ the accelerations in y direction of the M_i masses.
The first two masses attached to the chain pass through the points A to F, while the driving shaft and the chain wheels rotate with the angles $\alpha = \omega \cdot t$ and $\beta = 4 \cdot \omega \cdot t$ respectively (ω- angular velocity of the driving shaft), whose values are indicated in Tab. 1.
For the computation of the propulsion force with (2), the masses $M_1(t)$, $M_2(t)$ and $M_3(t)$, respectively the coordinates $y_1(t)$, $y_2(t)$ and $y_3(t)$ of the gravity centres of these masses, were determined for each of the 6 characteristic intervals of the angle α (see Tab. 1).

DOI: https://doi.org/10.14232/analecta.2022.1.27-33

Table 1. Characteristic angles of the IPD

Point	*A*	*B*	*C*	*D*	*E*	*F*	*A*
α [rad]	0	3π/8	5π/8	π	11π/8	13π/8	2π
β [rad]	0	3π/2	5π/2	4π	11π/2	13π/2	8π

The calculation for the first domain - α∈ (0, 3π/8]) - was done based on the notations shown in Fig. 4, being presented below, while the calculation results for the other domains are summarized in Tabs. 2 and 3.

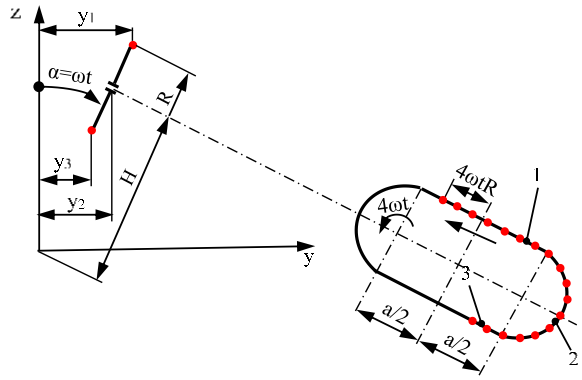

Figure 4. Calculus scheme for the domain α∈ (0, 3π/8]

The masses $M_1(t)$, $M_2(t)$ and $M_3(t)$ are calculated as follows:

$$M_i(t) = \bar{M} \cdot l_i(t) = \begin{cases} \bar{M} \cdot (a/2 + 4\omega t R), & i = 1 \\ \bar{M} \cdot 14p, & i = 2 \\ \bar{M} \cdot (a/2 - 4\omega t R), & i = 3 \end{cases} = \begin{cases} \bar{M} \cdot (21p + 4\omega t R), & i = 1 \\ \bar{M} \cdot 14p, & i = 2 \\ \bar{M} \cdot (21p - 4\omega t R), & i = 3 \end{cases} \quad (3)$$

where $\bar{M}$ [kg/m] is the linear mass of the weights and R the pitch radius of the chain wheel.
The coordinates $y_1(t)$, $y_2(t)$ and $y_3(t)$ of the gravity centres of the masses $M_1(t)$, $M_2(t)$ and $M_3(t)$ are calculated as follows:

$$y_i(t) = \begin{cases} (H + R) \cdot \sin(\omega t), & i = 1 \\ H \cdot \sin(\omega t), & i = 2 \\ (H - R) \cdot \sin(\omega t), & i = 3 \end{cases} \quad (4)$$

where H is the distance between the axis of the driving shaft and the axis which joins the centres of the chain wheels.

Table 2. Results of masses calculation

Range of α	$M_1(t)$	$M_2(t)$	$M_3(t)$
(0; 3π/8]	$\bar{M} \cdot (21p + 4\omega t R)$	$14\bar{M}p$	$\bar{M} \cdot (21p - 4\omega t R)$
(3π/8; 5π/8]	$\bar{M} \cdot R \cdot (4\omega t - 3\pi/2)$	$42\bar{M}p$	$\bar{M} \cdot [14p - (4\omega t - 3\pi/2)R]$
(5π/8; π]	$\bar{M} \cdot R \cdot (4\omega t - 5\pi/2)$	$14\bar{M}p$	$\bar{M} \cdot [42p - (4\omega t - 5\pi/2)R]$
(π; 11π/8]	$\bar{M} \cdot [21p + (4\omega t - 4\pi)R]$	$14\bar{M}p$	$\bar{M} \cdot [21p - (4\omega t - 4\pi)R]$
(11π/8;13π/8]	$\bar{M} \cdot R \cdot (4\omega t - 11\pi/2)$	$42\bar{M}p$	$\bar{M} \cdot [14p - (4\omega t - 11\pi/2)R]$
(13π/8; 2π]	$\bar{M} \cdot R \cdot (4\omega t - 13\pi/2)$	$14\bar{M}p$	$\bar{M} \cdot [42p - (4\omega t - 13\pi/2)R]$

DOI: https://doi.org/10.14232/analecta.2022.1.27-33

Table 3. Results of coordinate's calculation

Range of α	$y_1(t)$	$y_2(t)$	$y_3(t)$
(0; 3π/8]	$(H+R)sin\omega t$	$Hsin\omega t$	$(H-R)sin\omega t$
(3π/8; 5π/8]	Eq. (5)	$(H+R)sin\omega t$	Eq. (6)
(5π/8; π]	$(H-R)sin\omega t$	$Hsin\omega t$	$(H+R)sin\omega t$
(π; 11π/8]	$(H-R)sin\omega t$	$Hsin\omega t$	$(H+R)sin\omega t$
(11π/8;13π/8]	Eq. (7)	$(H+R)sin\omega t$	Eq. (8)
(13π/8; 2π]	$(H+R)sin\omega t$	$Hsin\omega t$	$(H-R)sin\omega t$

$$y_1 = \left[H + R\frac{sin\left(2\omega t-\frac{3\pi}{4}\right)}{2\omega t-\frac{3\pi}{4}}cos\left(2\omega t-\frac{3\pi}{4}\right)\right]sin\omega t \quad (5) \qquad y_3 = \left[H + R\frac{sin\left(\frac{5\pi}{4}-2\omega t\right)}{\frac{5\pi}{4}-2\omega t}cos\left(\frac{5\pi}{4}-2\omega t\right)\right]sin\omega t \quad (6)$$

$$y_1 = \left[H + R\frac{sin\left(2\omega t-\frac{11\pi}{4}\right)}{2\omega t-\frac{11\pi}{4}}cos\left(2\omega t-\frac{11\pi}{4}\right)\right]sin\omega t \quad (7) \qquad y_3 = \left[H + R\frac{sin\left(\frac{13\pi}{4}-2\omega t\right)}{\frac{13\pi}{4}-2\omega t}cos\left(\frac{13\pi}{4}-2\omega t\right)\right]sin\omega t \quad (8)$$

Calculating the second-order derivative of the coordinates $y_i(t)$, the accelerations $a_{yi}(t)$ of the $M_i(t)$ masses can be conveniently deducted. The results are summarized in Tab. 4.

Table 4. Results of acceleration calculation

Range of α	$a_1(t)$	$a_2(t)$	$a_3(t)$
(0; 3π/8]	$-\omega^2(H+R)sin\omega t$	$-\omega^2 Hsin\omega t$	$-\omega^2(H-R)sin\omega t$
(3π/8; 5π/8]	Eq. (9)	$-\omega^2(H+R)sin\omega t$	Eq. (9)
(5π/8; π]	$-\omega^2(H-R)sin\omega t$	$-\omega^2 Hsin\omega t$	$-\omega^2(H+R)sin\omega t$
(π; 11π/8]	$-\omega^2(H-R)sin\omega t$	$-\omega^2 Hsin\omega t$	$-\omega^2(H+R)sin\omega t$
(11π/8;13π/8]	Eq. (9)	$-\omega^2(H+R)sin\omega t$	Eq. (9)
(13π/8; 2π]	$-\omega^2(H+R)sin\omega t$	$-\omega^2 Hsin\omega t$	$-\omega^2(H-R)sin\omega t$

$$a_{1,3}(t) = -\left\{\omega^2\left[H + \frac{Rsin(2\theta_{1,3})}{2\theta_{1,3}}\right] + R\frac{\theta_{1,3}\left[\cos(2\theta_{1,3}) + 2\theta_{1,3}\sin(2\theta_{1,3}) + \dot{\theta}_{1,3}\cos(2\theta_{1,3})\right] + \dot{\theta_{1,3}}\sin(2\theta_{1,3})}{{\theta_{1,3}}^3}\right\}sin\omega t + \omega R\frac{2\theta_{1,3}\cos(2\theta_{1,3}) - \dot{\theta}_{1,3}\sin(2\theta_{1,3})}{{\theta_{1,3}}^2}cos\omega t \quad (9)$$

where θ_1 is used in the calculus of $a_1(t)$ and θ_3 for the calculus of $a_3(t)$. θ_1 and θ_3 have following values:

$$\theta_1 = \begin{cases} 2\omega t - \frac{3\pi}{4} & \alpha \in (3\pi/8;\ 5\pi/8] \\ 2\omega t - \frac{11\pi}{4} & \alpha \in (11\pi/8;\ 11\pi/8] \end{cases}, \quad \theta_3 = \begin{cases} \frac{5\pi}{4} - 2\omega t & \alpha \in (3\pi/8;\ 5\pi/8] \\ \frac{13\pi}{4} - 2\omega t & \alpha \in (11\pi/8;\ 11\pi/8] \end{cases} \quad (10)$$

Table 5. Geometrical characteristics of the IPD

H [mm]	p [mm]	R [mm]	$\bar{M}$ [kg/m]
70	12,7	56,718	1,003

Further, involving (2) and considering the geometrical characteristics of the IPD, which are described in Tab. 5, the resultant force generated by the system along the y axis where computed for an input speed n= *250 min*$^{-1}$ of the driving shaft, which is equivalent to an angular velocity ω= *26,18 rad/s.*
The variation of the propulsion force during a complete rotation of the driving shaft is presented in Fig. 5. As one can observe, during the rotation of the drive shaft with an angle of up to 180°, the system generates a positive force, while in the range of 180-360°, the resulting force changes its direction.

DOI: https://doi.org/10.14232/analecta.2022.1.27-33

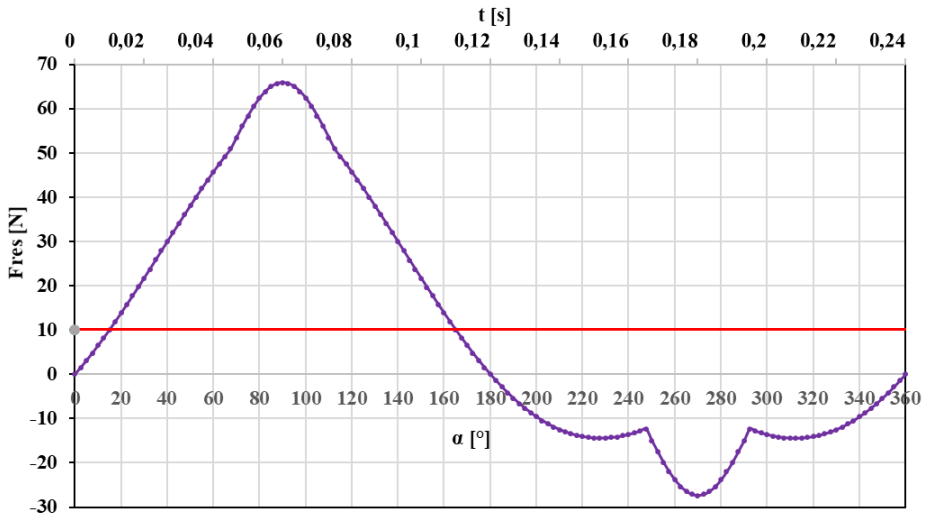

Figure 5. Variation of the propulsion force during a complete rotation of the driving shaft

Even if the resulting force has a fluctuating character, both in terms of size and sense, overall, the system is able to generate a propulsive force, which is plotted as a red line in Fig. 5. This confirms the capability of the IPD to generate linear motion.

4. CONCLUSIONS

The paper presents the structure of a novel inertial propulsion drive with masses, which are moving along a complex trajectory. Due to time varying of masses and accelerations of cylindrical weights attached to a chain transmission, the system is generating a one-way inertial force, as a response to the fluctuation of centrifugal force acting on these weights.

Analysing the trajectory of the rotating weights, their masses and coordinates of gravity centres were computed. Finally, the propulsive force generated by the system was deducted.

Based on the analytical approach presented in the paper, it can be concluded that the IPD developed by the authors is functional and capable to generate unidirectional linear movement, being a feasible solution in terms of propulsion on slippery grounds, such as ice or mud, or for spaces where the gravity is missing.

REFERENCES

[1] D. P. Allen Jr., Why Does Classical Mechanics Forbid Inertial Propulsion Devices When They Evidently Do Exist?: Is Newtonian Mechanics a Done Deal?, Createspace Independent Pub: Scotts Valley, California, US, 2018.
[2] M. Komora, Thrust generating device and moving body. Patent no. WO/2001/004491, 2001.
[3] K. U. Helavuo, Device for providing propulsion force. Patent no. WO/2013/087991, 2012.
[4] A. Gerocs, Z. I. Korka, I. Biro, V. Cojocaru, Analytical investigation of an inertial propulsion system using rotating masses. Journal of Physics: Conference Series 1426: 012031, 2020.
[5] A. Gerocs, G. R. Gillich, D. Nedelcu, Z. I. Korka, A multibody inertial propulsion drive with symmetrically placed balls rotating on eccentric trajectories. Symmetry, 2020 12 (9): 1422.
[6] A. Gerocs, Z. I. Korka, G. R. Gillich, Analytical investigations on the influence of the geometry of an inertial drive on the propulsion force. Annals of "Eftimie Murgu" University from Resita, 2019, 26 (1), pp. 76-85.

DOI: https://doi.org/10.14232/analecta.2022.1.27-33

Analecta Technica Szegedinensia
Vol. 16, No. 01 ISSN 2064-7964 2022

EVALUATION OF GEAR PITTING SEVERITY BY USING VARIOUS CONDITION MONITORING INDICATORS

[1]Camelia R. Sfetcu, [1]Zoltan I. Korka, [1]Alin V. Bloju, [1]Dalina E. Traistaru, [1]Corneliu Hrimiuc*

[1] Babeş-Bolyai University, Doctoral School of Engineering, P-ta Traian Vuia no. 1-4, 320085 Resita, Romania
*e-mail: zoltan.korka@ubbcluj.ro

ABSTRACT

Fault detection techniques based on vibration measurement are implemented to identify in an early stage failures appearing in gear transmissions. Condition monitoring indicators (CMI), like: Root Mean Square (RMS), Crest Factor, Kurtosis, FMO, FM4, Energy ratio, Energy operator, NA4 or NB4, are used to estimate the level of gear faults such as pitting, cracks, spalling, scuffing or scoring. However, in is multitude of indicators, the question that arises is: which CMI is the most sensitive in estimating the severity of defects? Thus, this paper presents an extensive comparison between the before mentioned indicators computed from vibration signals collected on four pinions with different pitting grades, created by artificial means. The pinions where incorporated in a single helical gearbox and the tests were performed on an open-energy test rig at three different input speeds. This comparative study assesses the receptivity of different condition monitoring indicators towards gear pitting failure. We concluded that all the involved indicators are responsive and sensitive to fault diagnosis, even in low speed operating conditions.

Keywords: condition monitoring indicators, fault diagnosis, gear pitting

1. INTRODUCTION

Gearboxes are widely used in different industrial applications, because, compared to other mechanical transmissions, they are capable to transmit, both speeds and high moments, in small volumes. When the gear teeth are loaded near to their maximum capacity, they are forced to endure high contact pressures, which are leading to various fatigue deteriorations, such as scoring, scuffing, spalling or pitting. These failures occur even under proper lubrication conditions of the gears and represent nearly 60% of the damages in the gearboxes components [1].

Pitting is the most common failure of the gear teeth surface, working under oil lubrication conditions [2], [3]. It is initiated in the inclusions from the gear material, which act as stress concentrators, spreading parallel and below the teeth surfaces. When these cracks are joining or are breaking through the tooth surface, material separation occurs forming the so-called pits.

In the last decades were developed different gear fault diagnosis methods and condition monitoring techniques [4], [5], [6]. Fundamentally, vibration signals acquired from gearboxes by means of accelerometers, are filtered, amplified, processed and analysed in time domain [7], frequency domain [8], or time-frequency domain [9].

With the fast development of artificial intelligence technologies, classification of gear faults using machine learning became a hot topic in the field of gear fault diagnosis methods. Thus, Liu et al. [10] proposed a personalized fault diagnosis method using finite element method simulation and extreme learning machine to detect faults in gears. Further, He et al. [11] introduce a deep transfer multi-wavelet auto-encoder for intelligent gear fault diagnosis with small training samples.

Statistical indicators, likewise known as condition monitoring indicators, are also extensively used to identify failures in gear transmissions appearing in an early stage [12]. However, in the bunch of indicators, the doubt that rises is: which of these CMI's is the most sensitive, being able to assess the gear fault severity. Therefore, this paper aims to analyse the responsiveness of different indicators towards gear pitting severity. Incorporating four pinions with various pitting grades, made by artificial means, in a single helical gearbox, vibration measurements were performed at three different input speeds, on an open-energy

DOI: https://doi.org/10.14232/analecta.2022.1.34-41

test rig. Finally, the research has concluded regarding the receptivity of the involved condition monitoring indicators to predict gear-pitting severity.

2. CONDITION MONITORING INDICATORS

Following CMI's were involved in the present research:

2.1. Root Mean Square

The root mean square (RMS) of a continuous-time waveform is the square root of the arithmetic mean of the squares of the values, or the square of the function that defines the continuous waveform. RMS was initially developed to characterize the heating of a resistor exposed to a sine wave varying current. In case of a set of *n* values $\{x_1, x_2, \ldots, x_n\}$ the RMS is:

$$RMS_x = \left(\frac{1}{n}\sum_{i=1}^{n} x_i^2\right)^{0.5} \tag{1}$$

2.2. Crest Factor

The Crest Factor (CF) is a parameter of a waveform showing the ratio of the maximum positive peak value to the RMS value:

$$CF = \frac{\max(x_1, x_2, \ldots, x_n)}{RMS_x} \tag{2}$$

Crest factor is a normalized parameter of the signal amplitude. A signal with a few high amplitude peaks are producing a bigger CF, as the numerator increases (high amplitude peaks), while the denominator decreases (few peaks means lower RMS).

2.3. Kurtosis

The shape of the amplitude disposal is regularly involved as a data descriptor. Kurtosis shows how peaked or flat a waveform signal is. When a vibration signal incorporates sharp peaks with higher value, then the distribution function will be sharper. We can presume that damaged gears produce these types of waves. Consequently, a damaged gear will have higher kurtosis value then a healthy gear. A mathematical expression of Kurtosis is given in (3):

$$K = \frac{n \cdot \sum_{i=1}^{n}(x_i - \bar{x})^4}{(\sum_{i=1}^{n}(x_i - \bar{x})^2)^2} \tag{3}$$

where $\bar{x}$ is the mean value of the signal.

2.4. Zero-order Figure of Merit (FM0)

The zero-order figure of merit (FM0) is an indicator of major faults in a gear mesh, being defined as the ratio between the peak-to-peak value of a signal and the energy of the mesh frequency and its harmonics. In contrast to CF, which compares the peak value of the synchronous averaged signal with the energy of the synchronous averaged signal, FMO compares the same peak value of the synchronous averaged signal, with the energy of the regular signal. Thus, FMO is deducted as:

DOI: https://doi.org/10.14232/analecta.2022.1.34-41

$$FM0 = \frac{x_{max} - x_{min}}{\sum_{i=1}^{n} A(i)} \tag{4}$$

where x_{max} is the maximum amplitude of the signal, x_{min} the minimum amplitude of the signal, *A(i)* is the amplitude of the *i-th* mesh frequency harmonics and *n* is the total number of harmonics in the frequency spectrum.

2.5. Fourth-order Figure of Merit FM4

Fourth-order figure of merit (FM4) was designed to improveFM0 in the detection of damages located only on a finite number of gear teeth. This can be done by removing the gear meshing frequency and its harmonics from the time synchronous average signal. The obtained result is the so-called differential signal *d*. FM4 is computed as:

$$FM4 = \frac{n \cdot \sum_{i=1}^{n} \left(d_i - \bar{d}\right)^4}{\left(\sum_{i=1}^{n} \left(d_i - \bar{d}\right)^2\right)^2} \tag{5}$$

where $\bar{d}$ is the mean of the differential signal, d_i the *i*-th point of the differential signal the time signal and *N* the total number of data points in the time signal.

2.6. Energy Ratio (ER)

Energy ratio (ER) is an indicator for uniform wear. It is computed as the ratio of the RMS of the difference signal *d* to the RMS of the signal containing only the regular meshing components x_d:

$$ER = \frac{RMS_d}{RMS_{x_d}} \tag{6}$$

As wear progresses, energy moves from the regular signal to the difference signal.

2.7. Energy Operator (EOP)

Is calculated as a normalized kurtosis of a so-called resultant signal (*re*), *re* being computed as a difference between the squared input signal for each point x_i ($i=1....n$) and the product of the point before and after ($x_{i-1} \cdot x_{i+1}$):

$$EOP = \frac{n \cdot \sum_{i=1}^{n} (re_i - \overline{re})^4}{\left(\sum_{i=1}^{n} (re_i - \overline{re})^2\right)^2}, \tag{7}$$

where $re_i = x_i^2 - x_{i-1} \cdot x_{i+1}$ is the i[th] measurement of the resulting signal *re* and $\overline{re}$ is the average of the resulting signal. In case of the endpoints, the signal is assumed to be a continuous loop, meaning that for calculating the first point is involved the last point and inversely.

2.8. NA4

The NA4 parameter was evolved to overcome the deficiency of FM4, which becomes less sensitive as the manifestation of faults grows in both number and severity. Two changes were done to develop NA4 to be more sensitive to the damage evolution: firstly, it is computed from the residual signal and secondly, trending was incorporated into the parameter. Thus, NA4 is calculated as the ratio of fourth moment of the residual signal to the square of its run time averaged variance:

DOI: https://doi.org/10.14232/analecta.2022.1.34-41

$$NA4 = \frac{n \cdot \sum_{i=1}^{n} \left(r_{i_M} - \overline{r_M}\right)^4}{\left\{\frac{1}{m}\sum_{j=1}^{m}\left[\sum_{i=1}^{n}\left(r_{ij} - \bar{r}_j\right)^2\right]\right\}^2}\ , \tag{8}$$

where $\bar{r}$ is the mean of the residual signal, *n* the total number of data points in the time signal, *j* the index of the time signal in the run ensemble, and *m* the number of the current time signal.

2.9. NB4

NB4 is computed as a time-averaged kurtosis of the envelope of the signal after it was band-pass filtered about the mesh frequency. The envelope *s(t)* is calculated involving the Hilbert Transform, being given by:

$$s(t) = |\{b(t) + iH[b(t)]\}|\ , \tag{9}$$

where, *b(t)* is band-pass filtered signal about the mesh frequency, *i* the number of samples and $H[b(t)]$ the Hilbert Transform of *b(t)*.

3. MATERIALS AND METHODS

For the evaluation of the gear pitting by involving the upper described CMI's, an open-energy test stand was used. The main components of the stand are shown in Fig. 1, these being: an electric motor with variable speed, the gearbox and a hydraulic pump, used as a brake.

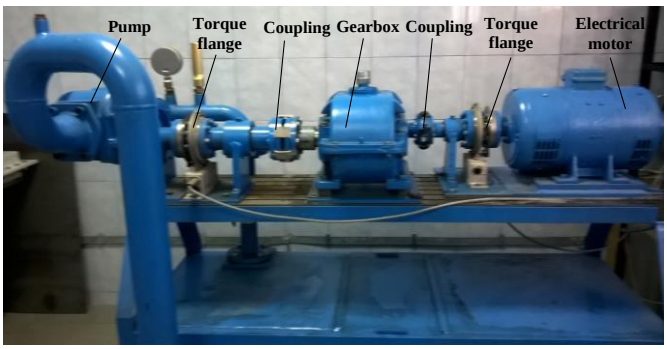

Figure 1. Main components of the test stand [13]

The connection between these components was made through two couplings with rubber strips, which ensure a good torsional vibration damping and allow a smooth assembling. For reading the input speed and the torques on the input shaft and output shaft respectively, two torque flanges of type T 10 FE, made by HBM- Germany, were used.

Table 1. Technical data of the test stand

Element	*Technical data*	
Electric motor	Power:	P_{max}= 2,5 kW
	Speed:	n= 0…1500 min^{-1}
Gearbox	Centre distance:	A= 125 mm
	Teeth number:	z_1/ z_2= 17/ 43
	Module	m_n= 4 mm
	Face width	b= 40 mm
	Helix angle	β= 11°
Break	KF 6/400 gear pump (KRACHT)	

DOI: https://doi.org/10.14232/analecta.2022.1.34-41

A Kistler made accelerometer of type 8772, placed on the top of the gearbox housing, above the high-speed shaft, was used for vibration measurements. The vibration signals were acquired via a 92234 National Instruments module, placed in a chassis cDAQ-9172.
For fine processing, the vibration signals were sent to a laptop programmed to run in LabView software a self-developed application. The main technical data of the test stand are described in Tab. 1.
The before mentioned CMI's were computed from vibration signals collected on four pinions with different pitting conditions, created by practicing artificial grooves with a diameter of 3 mm and a depth of about 0.5 mm, along the pitch line of the teeth. The pinions with different failure status (PC1- healthy teeth; PC2- teeth with slight pitting; PC3- teeth with mild pitting; PC4- teeth with acute pitting) are presented in Fig. 2.

PC1 PC2 PC3 PC4

Figure 2. Pinions with different failure status

The experimental procedure was conducted following the below mentioned steps:
- the healthy pinion (PC1- status) was assembled into the gearbox and the test stand was operated in turn, at following input speeds: 1000, 1250 and 1500 min^{-1};
- collection, storage and processing of the vibration signals;
- replacement of the pinion with PC1- status with the one having PC2- status, followed by the resumption of steps described above;
- continuation of experimental measurements, as before described, for the other two pinions.

4. RESULTS AND DISCUSSION

CMI's for pinions with different failure status operating at three different speeds have been evaluated. Values of the nine parameters described in Section 2 were computed, being organized in Tab. 2. To have a better image about how the nine condition parameters are influenced by the input speed of the gearbox and the pitting severity, Fig. 3 depicts the variation of the CMI's for the three operating speeds and the four pinion healthy conditions.

Table 2. Condition Monitoring Indicators

CMI	n_1= 1000 min^{-1}				n_1= 1250 min^{-1}				n_1= 1500 min^{-1}			
	PC1	PC2	PC3	PC4	PC1	PC2	PC3	PC4	PC1	PC2	PC3	PC4
RMS	1,005	1,234	1,896	2,314	1,055	1,750	2,514	3,088	1,075	2,254	3,756	6,988
CF	2,755	2,890	3,550	4,215	2,815	3,025	3,770	4,890	2,865	4,326	5,132	6,309
K	3,021	3,775	3,895	4,777	3,210	3,995	5,210	6,455	3,431	4,055	6,643	9,342
FM0	0,008	0,009	0,011	0,010	0,008	0,010	0,012	0,013	0,010	0,003	0,015	0,022
FM4	2,890	3,150	3,364	3,955	3,050	3,390	3,675	4,750	3,179	4,305	5,925	7,795
ER	0,555	0,690	0,712	0,798	0,595	0,722	0,756	0,912	0,605	1,765	2,095	2,849
EOP	2,987	7,855	10,025	11,250	3,025	5,677	8,875	15,554	3,519	11,207	19,764	38,733
NA4	3,015	3,187	3,247	3,998	3,010	3,022	3,225	4,205	3,035	4,115	4,435	4,878
NB4	2,225	2,220	2,415	3,895	2,195	2,945	4,895	6,473	2,218	4,068	6,218	10,764

DOI: https://doi.org/10.14232/analecta.2022.1.34-41

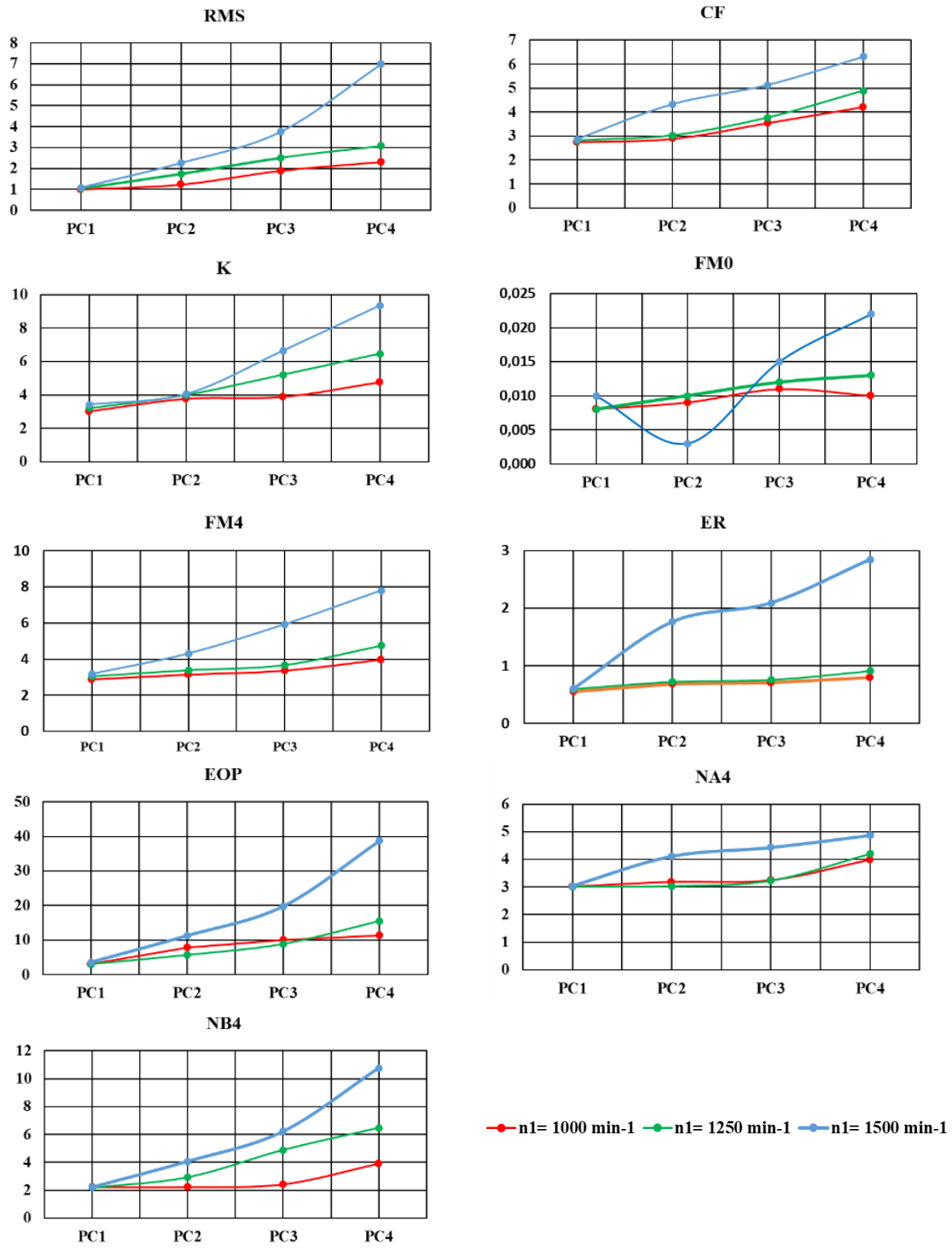

DOI: https://doi.org/10.14232/analecta.2022.1.34-41

Figure 3. Variation of CMI's for different input speeds and failure status

As one can observe, all the nine indicators are working well, displaying increased shapes with the growth of the speed, respectively of the severity of the pitting. If in the case of the input speeds of 1000 $min^{-1}$and 1250 min^{-1}, respectively, the increases of the nine investigated parameters are not spectacular, but still visible, with the aggravation of the pitting failure, this becomes obvious at the maximum speed (1500 min^{-1}) of the gearbox input shaft.

Regardless of speed, the most receptive parameters to gear failure were in descending order, EOP, RMS, NB4 and ER. In this sense, Fig. 4 provides a visual proof of this finding. At the minimum investigated speed, the least sensitive parameters proved to be FMO, NA4 and FM4, a characteristic that was maintained even at the maximum speed of the input shaft.

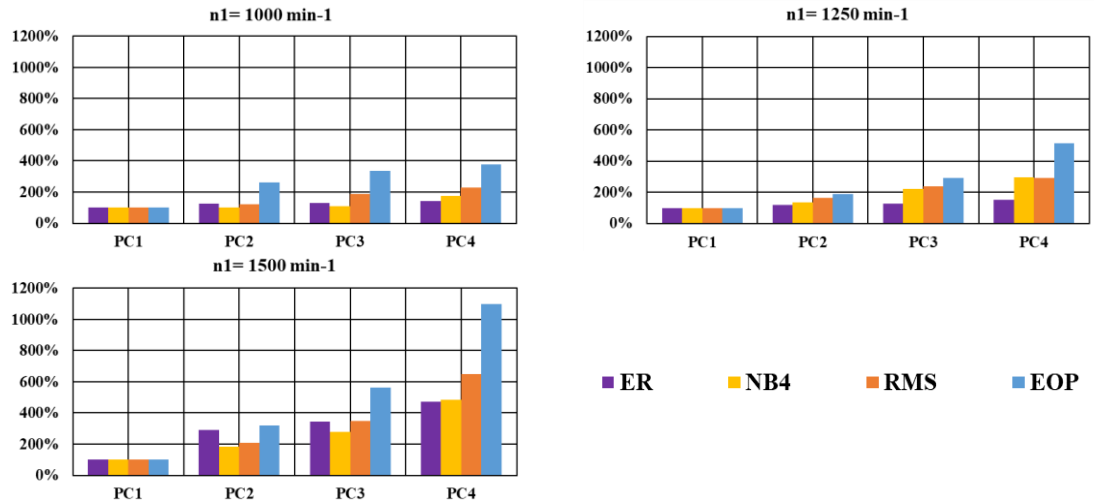

Figure 4. Percentage variation of the parameters with the highest sensitivity

Starting from these findings, we express the opinion that based on the previous analysed condition monitoring parameters extracted in time domain, it would be possible to classify the gear pitting stage, by involving machine-learning techniques. This capability will prove effective, especially in the case of fluctuating speed operating regimes, when frequency spectrum analysis is no longer applicable.

5. CONCLUSIONS

Gearboxes have wide application in different industries for speed and torque conversion. Inappropriate failure of the gearbox can be costly. Therefore, an early diagnosis of faults is very critical for their reliable operation.

In this study, experiments were performed for various gear pitting stages at three different input speeds. A comparative study of RMS, Crest Factor, Kurtosis, FM0, FM4, Energy ratio, Energy operator, NA4 and NB4 has been done for no, slight, mild and acute pitting of a pinion. This research highlights that all the indicators are responsive and sensitive to fault diagnosis, even at a low operating speed. Moreover, the experimental result indicates that CMI's describing the overall vibration level track the condition of the tested gearbox condition very well. Certain CMI provide not only information that something has happened in the gear transmission but they provide information about what has happened.

DOI: https://doi.org/10.14232/analecta.2022.1.34-41

Furthermore, the condition monitoring indicators may be involved, together with machine learning techniques, to classify the gear pitting status, in case of fluctuating speed operating regimes, where spectral analysis is more difficult to apply.
Additionally, these CMI's need to be also checked for fluctuating loading condition which is going to be the next goal in the area of non-stationary signals with non-constant operating circumstances. Our further research will be focussed on this topic.

REFERENCES

[1] Z. I. Korka, A. Bara, B. Clavac, L. Filip, Gear Pitting Assessment Using Vibration Signal Analysis, Romanian Journal of Acoustics and Vibration, 14 (1) (2017), pp. 44-49.
[2] K. Feng, W. A. Smith, R. B. Randall, H. Wu, Z. Peng, Vibration-based monitoring and prediction of surface profile change and pitting density in a spur gear wear process, Mechanical Systems and Signal Processing, 165 (2022), 108319.
[3] P. Kund, A. K. Darpe, M. S. Kulkarni, A correlation coefficient based vibration indicator for detecting natural pitting progression in spur gears, Mechanical Systems and Signal Processing, 129 (2019), pp. 741-763.
[4] S. Raadnui, Condition monitoring of worm gear wear and wear particle analysis of industrial worm gear sets, Wear, 476 (2021), 203687.
[5] R. B. Randall, W. A. Smith, P. Borghesani, Z. Peng, A new angle-domain cepstral method for generalised gear diagnostics under constant and variable speed operation, Mechanical Systems and Signal Processing, 178 (2022), 109313.
[6] P. Gandhi, N. Turk, R. Dahiya, Health monitoring of induction motors through embedded systems-simulation of broker rotor bar fault and abnormal gear teeth fault, Microprocessors and Microsystems, 76 (2020, 103077.
[7] H. Liu, S. D. Jaspreet, A time domain approach to diagnose gearbox fault based on measured vibration signals, Journal of Sound and Vibration, 333(7) (2014), pp. 2164-2180.
[8] V. Sharma, Gear fault detection based on instantaneous frequency estimation using variational mode decomposition and permutation entropy under real speed scenarios, Wind Energy, 24 (2021), pp. 246–259.
[9] J. Cai, X. Li, Gear fault diagnosis based on time–frequency domain de-noising using the generalized S transform, Journal of Vibration and Control, 24(15) (2018), pp. 3338-3347.
[10] X. Liu, H. Huang, J. Xiang, A personalized diagnosis method to detect faults in gears using numerical simulation and extreme learning machine, Knowledge-Based Systems, 195 (2020), 105653.
[11] Z. Y. He, H. D. Shao, X. Y. Zhang, J. S. Cheng, Y. Yang, Improved deep transfer auto-encoder for fault diagnosis of gearbox under variable working conditions with small training samples, IEEE Access 7 (2019), pp. 115368–115377.
[12] E. Bechhoefer, R. Li, D. He, Quantification of condition indicator performance on a split torque gearbox, Journal of Intelligent Manufacturing, 23 (2012), pp. 213-220.
[13] Z. I. Korka, Research on vibration reduction in operation of cylindrical gearboxes, PhD Thesis, "Eftimie Murgu" University of Resita, Romania, 2009.

DOI: https://doi.org/10.14232/analecta.2022.1.34-41

Analecta Technica Szegedinensia
Vol. 16, No. 01 ISSN 2064-7964 2022

EVALUATING THE SEVERITY OF TRANSVERSE CRACKS IN BEAM-LIKE STRUCTURES BY USING AN ENERGY LOSS METHOD

[1]Marius Pop, [1]Cristian Tufisi, [1]Gilbert-Rainer Gillich, [1] Daniela Georgiana Burtea

[1]Babeş-Bolyai University, Faculty of Engineering, Piața Traian Vuia nr. 1-4, 0320003, Reşiţa, România,
e-mail: cristian.tufisi@ubbcluj.ro

ABSTRACT

Over functioning time, structures can be affected by multiple types of damages caused by fatigue, improper production methods, or exceeding loads. The current paper describes a method for evaluating the severity of transverse cracks that are present in beam-like structures based on changes in the natural frequencies. Because the presence of damage has a negative impact on the energy that a beam can store in the affected section, it is possible to find the influence of the crack on any other position along the beam, considering the stored normalized energy in that location. The technique is based on a mathematical relationship that provides the exact solution to the frequency changes of the bending vibration modes, considering two terms. The first term is related to the tensile energy stored in the beam, and the second term considers the increase of flexibility due to cracks, for this reason, damage assessment is performed in two stages; first, the location of the crack is found and then an assessment of its severity is performed. In this study, the aim is to test the developed method for estimating the severity of transverse cracks for different sections and lengths of beams.

Keywords: damage detection, deflection, transverse crack, stiffness reduction, structural health monitoring

1. INTRODUCTION

The concept of Structural Health Monitoring (SHM) refers to diagnosing the integrity of structures with the purpose of estimating their remaining life while maintaining the designated performance. The integrity of a structure can be altered over time, due to several factors such as wear and tear due to material fatigue, the action of environmental factors as well as external or accidental events [1]. In the industrial sphere, the process of monitoring the integrity of structures can be applied both in the mechanical field as well as in civil engineering. A multitude of structures in the field can be monitored during their functioning time, such as wind turbines, rotative parts of machines and equipment, bridges and roads, buildings and stadiums, aircraft, marine vessels, and platforms [2].

The main scope of structure integrity evaluation is the detection of cracks in the incipient state before they can cause significant damage that may lead to functional failure and accidents. Damage occurrence reduces the structure's loading capacity resulting in the decrease of its energy storing capability and therefore, the dynamic behavior is also altered [3]. Dynamic identification methods have been developed in the past decades by analyzing the natural frequency changes that occur due to the stiffness reduction caused by cracks [7]. Comprehensive studies have been developed by several researchers [4, 5, 6], that consider the changes in modal parameters correlated with the presence of certain types of damages.

In recent research [8] direct and indirect natural frequency-based methods for identifying multiple cracks in beams are proposed. Direct methods include the simplified definition of natural frequency drops caused by cracks. The relationships between the natural frequencies obtained from the defective beams and the undamaged ones are determined by an approach that uses the local crack flexibility model [9, 10].

The current paper focuses on the accuracy of estimating the severity of transverse cracks that are present in beams by involving the finite element method, starting from the observation that if a crack is present, in a section that is subjected to a bending moment, it produces a decrease in natural frequencies, consequently, the change of frequency for a vibration mode i due to the damage depends on the energy stored in the affected section. In the current research, we demonstrate the advantages of considering the normalized stored energy in the affected section for estimating the influence of a certain crack on the modal parameters of beams. At first, we performed simulations to observe the changes in the static and dynamic behavior of

DOI: https://doi.org/10.14232/analecta.2022.1.42-49

the beam that occurs in the presence of damage using the Finite Element Method (FEM) with the help of the simulation software ANSYS.

2. MATERIALS AND METHODS

In the study presented in paper [11] the authors develop an algorithm for evaluating transverse cracks in composite structures based on natural frequency changes due to cracks. Damage assessment is performed in two stages; first, the location of the crack is found and then an assessment of its severity is performed. The technique is based on a mathematical Equation (1) that provides the exact solution to the frequency changes of the bending vibration modes, considering the tensile energy stored in the beam, and the second term considers the increase of flexibility due to cracks [12].

$$f_{i-D}(x,a) = f_{i-U}\left\{1-\gamma(a)\left[\bar{\phi}_i''(x)\right]^2\right\} \tag{1}$$

where f_{i-U} is the frequency for the beam without damage, $f_{i-D}(x, a)$ the frequency for the beam having a crack of depth a in position x, $\gamma(a)$ represents the severity of the crack and $\bar{\phi}_i''(x)$ the curvature of the normalized modal form, having values between -1 and 1.
The transverse crack severity is determined with the model presented in paper [11, 12], using the following Equation (2):

$$\gamma(a) = \frac{\sqrt{\delta_D(a)} - \sqrt{\delta_U}}{\sqrt{\delta_D(a)}} \tag{2}$$

where δ_U is the deflection at the free end of the intact beam, and $\delta_D(a)$ is the deflection at the free end of the beam with a crack of depth a. Because at the fixed end the deformation manifests just on one side of the crack, the severity achieved here is smaller as expected. To this aim, we simulate cracks at different positions near the fixed end and find the theoretical severity from the linear regression curve, as presented in the paper [11].
The method for determining the modal curvature and natural frequency caused by a crack, with a known position x, is given in papers [12, 13, 14, 15].
In the current paper, the analysis was performed for damages reducing the rigidity of a cantilever beam subjected to the highest bending moment. From this analysis, the evolution of the severity of the damage and the effect of the position of the crack was discovered, reflected by a decrease in frequency. The reliability of this relationship was tested with the results obtained by the finite element method.
The crack detection methodology has also validated the results show that the location reports and the depth of the transverse cracks are successfully anticipated by using the methods presented in the paper [11, 12].
This paper presents a numerical study designed to establish the dynamic response of cantilever beams with different transverse cracks, and different lengths to demonstrate that the use of the severity estimation method is reliable for detecting cracks by using the beam's natural frequencies.
For this study, console beams with transverse cracks were analysed using the finite element method. The damages considered are breathing cracks, which affect the entire width of the beam, have different levels of depth, and are in certain positions along the beam.
Modal and static analysis was performed in the Ansys program to extract the natural frequencies and deflection under own weight values for a steel cantilever beam of the constant section, both intact and damaged, with different lengths and thicknesses as shown in Tab.1 along with the material's physical-mechanical properties.

DOI: https://doi.org/10.14232/analecta.2022.1.42-49

Table 1. Physical-mechanical properties of the material and main dimensions of the test beams

Mechanical properties of the material						Main dimensions of the beam		
Density [kg/m3]	Young modulus [N/m2]	Poisson [-]	Fracture strength Rm [MPa]	Yield strength [MPa]	Elong. [%]	Length [mm]	Lăţime [mm]	Grosime [mm]
7850	$2 \cdot 10^{11}$	0.3	470-630	355	20	1000 1200 1400	50	4 5

For performing the FEM analysis, the considered beam geometries were modelled, the necessary end constraints were applied, a fine mesh of maximum edge size of 2 mm was developed, and static and modal studies were performed. The beam geometries were generated using the ANSYS design modeler both in an undamaged and damaged state as shown in Fig. 1.

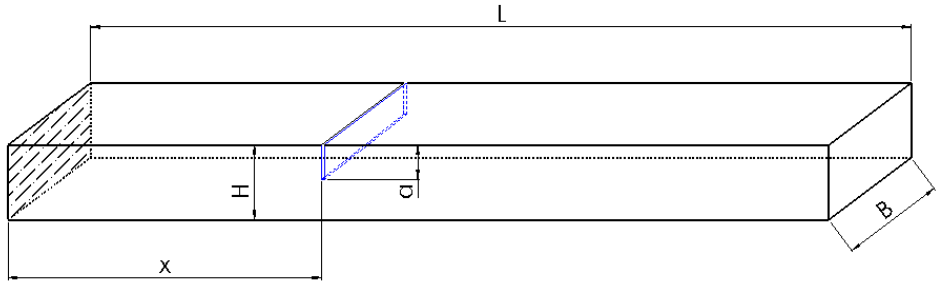

Figure 1. Main dimensions of the cantilever beam

The crack positions *x* are considered from 6 mm to 42 mm with a step of 6mm and depths *a* starting from 5% of the cross-section of the beam to a maximum of 40 %. The six test beam dimensions are shown in Tab.2. For all damage scenarios, the width of the crack is always 0.04 mm.

Table 2. Damage scenarios

Test beam dimensions			Crack location [mm]	Crack depth [mm]
L [mm]	*B* [mm]	*H* [mm]		
1000	20	4	6 - 42	0.2, 0.4, 0.6, 0.8, 1.0, 1.2, 1.4, 1.6
1200	20	4		
1400	20	4		
1000	20	5		0.25, 0.5, 0.75, 1.0, 1.25, 1.5, 1.75, 2.0
1200	20	5		
1400	20	5		

2.1. Static FEM simulations

We performed FEM simulations using the ANSYS software for all damage scenarios presented in the previous section, in Fig. 2 we illustrate the results obtained for static analysis.

DOI: https://doi.org/10.14232/analecta.2022.1.42-49

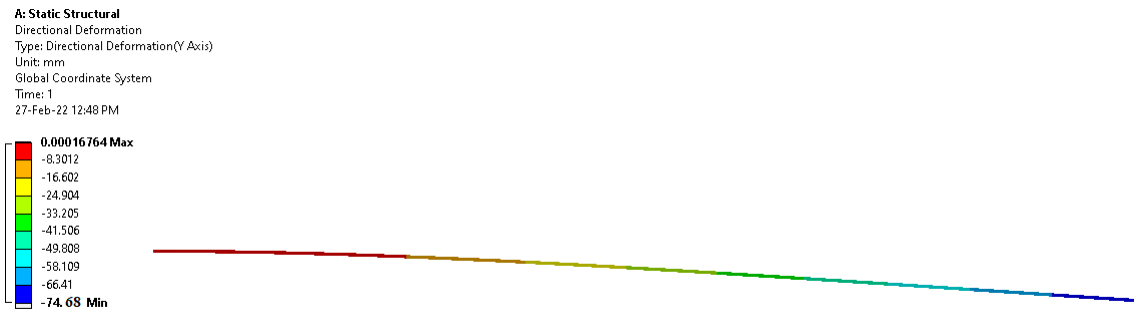

Figure 2. Deflection under own weight for the 1200x20x4 mm cantilever in

For the intact beam, we obtained the deflection δ_U shown in Tab. 3.

Table 3. Deflection values obtained for the intact beams

Test beam dimensions			Undamaged deflection
L [mm]	B [mm]	H [mm]	δ_U [mm]
1000	20	4	36.001
1200	20	4	74.68
1400	20	4	138.39
1000	20	5	23.045
1200	20	5	47.802
1400	20	5	88.582

To estimate the crack severity at the fixed end, we plot the trend lines for all damage scenarios. In Fig. 3, we present the plotted trend lines for the *1000x4x20* mm beam with all the considered damage scenarios.

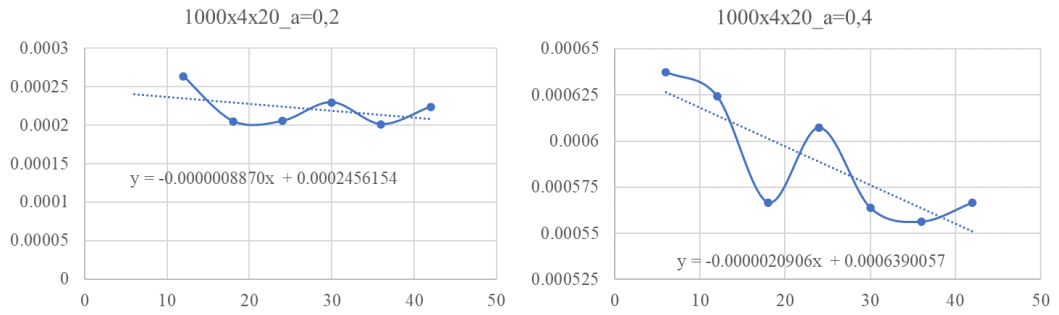

DOI: https://doi.org/10.14232/analecta.2022.1.42-49

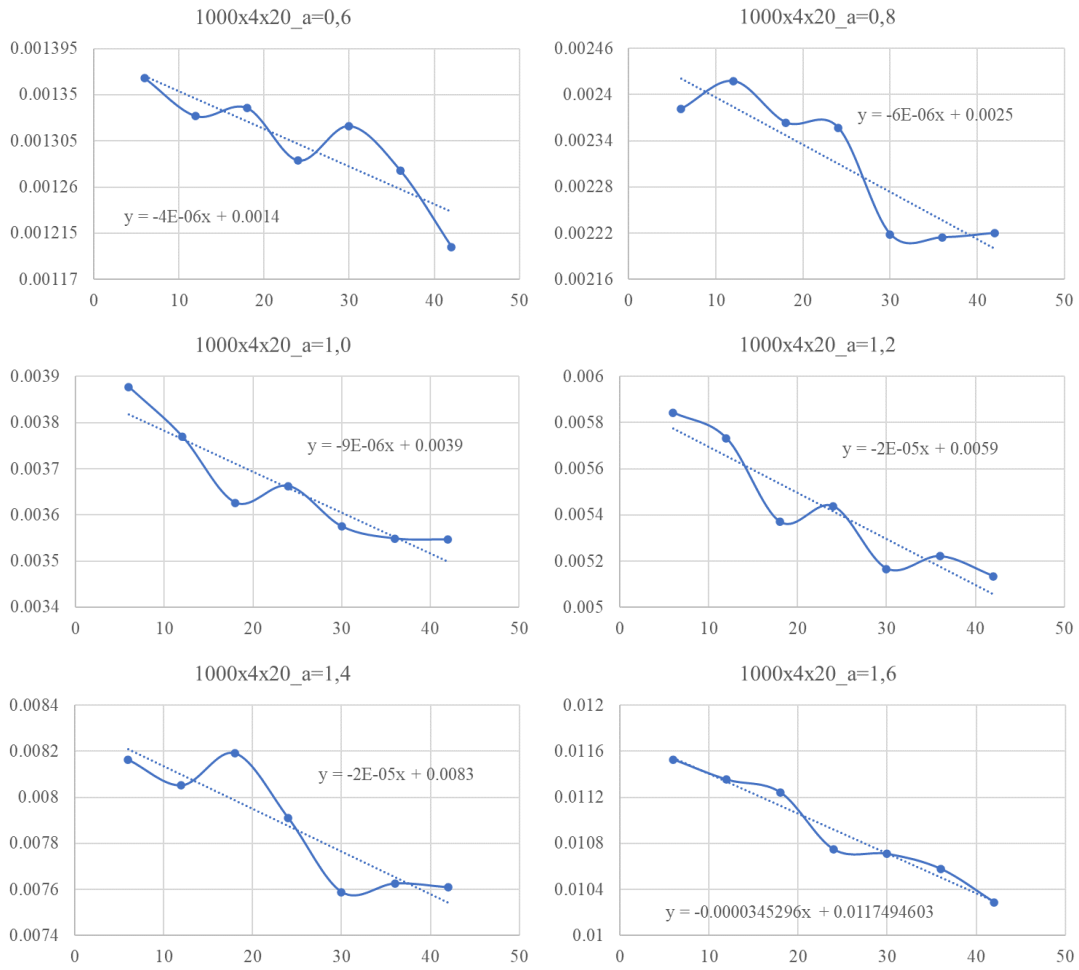

Figure 3. Regression curves for the beam 1000x4x20 in a damaged state

The deflections in these figures are found from the values of the trend line at the distance x=0 calculated with the corresponding mathematical relations.

3. RESULTS AND DISCUSSION

With the data obtained from applying the regression method, we calculate the severities for the different crack depths, and we also compare the corresponding severities for the different beam lengths. We plot a diagram, Fig. 4 for the beams with a thickness of H=4 mm and in Fig. 5 for the beams having a 5 mm thickness, which represents the evolution of the damage severity with the crack depth.

DOI: https://doi.org/10.14232/analecta.2022.1.42-49

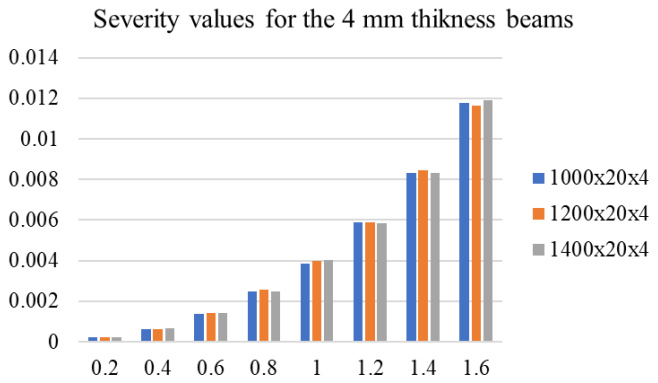

Figure 4. Obtained severity values for the beams having a thickness H=4 mm

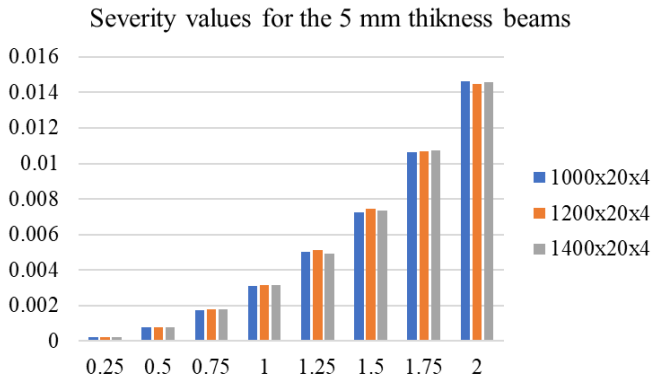

Figure 5. Obtained severity values for the beams having a thickness H=5 mm

Furthermore, we compare the calculated natural frequencies using Equation (1) for different damage scenarios with the ones obtained by performing modal FEM simulations in ANSYS. The considered damage scenarios for all the presented beam dimensions consist of transverse cracks of depth a=1 mm positioned at x=150m and afterward, at x=360 mm. The obtained results are shown in Tab. 4 for the damage position 150 mm respectively Tab. 5 for position 360 mm.

Table 4. Comparison between analytical and FEM determined frequencies for the damage position x=150 mm

Beam dim.:	1000x20x4		1200x20x4		1400x20x4		1000x20x5		1200x20x5		1400x20x5	
Mode no.	Calc.	FEM	Calc.	FEM	Calc.	FEM	Calc.	FEM	Calc.	FEM	Calc.	FEM
1	3.257	3.257	2.262	2.262	1.662	1.662	4.071	4.073	2.827	2.829	2.078	2.078
2	20.455	20.455	14.206	14.200	10.437	10.430	25.566	25.567	17.755	17.750	13.045	13.038
3	57.286	57.287	39.766	39.778	29.200	29.219	71.593	71.594	49.699	49.715	36.496	36.520
4	112.16	112.16	77.840	77.926	57.164	57.158	140.16	140.18	97.27	97.29	71.443	71.460
5	185.24	185.25	128.61	128.72	94.53	94.61	231.45	231.52	160.72	160.88	118.14	118.14
6	276.65	276.66	192.24	192.18	141.35	141.25	345.60	345.71	240.21	240.19	176.63	176.54

DOI: https://doi.org/10.14232/analecta.2022.1.42-49

Table 5. Comparison between analytical and FEM determined frequencies for the damage position x=360 mm

Beam dim.:	1000x20x4		1200x20x4		1400x20x4		1000x20x5		1200x20x5		1400x20x5	
Mode no.	Calc.	FEM	Calc.	FEM	Calc.	FEM	Calc.	FEM	Calc.	FEM	Calc.	FEM
1	3.262	3.262	2.265	2.265	1.664	1.663	4.077	4.078	2.831	2.831	2.080	2.080
2	20.442	20.443	14.193	14.203	10.427	10.436	25.550	25.555	17.740	17.753	13.033	13.044
3	57.210	57.210	39.724	39.722	29.182	29.193	71.498	71.518	49.647	49.661	36.473	36.494
4	112.25	112.25	77.94	77.90	57.26	57.20	140.26	140.27	97.40	97.36	71.56	71.50
5	185.22	185.22	128.61	128.81	94.49	94.63	231.42	231.51	160.72	160.97	118.08	118.27
6	276.80	276.80	192.22	192.14	141.22	141.32	345.79	345.87	240.17	240.16	176.46	176.61

4. CONCLUSIONS

The aim of the current research is to establish the precision of a known mathematical relation to calculate the severity of a crack with help of the deflection of the cantilever beam under dead load for several damage scenarios that consider different beam dimensions and also different crack depths.
The comparison between the frequencies calculated by applying the analytical described method which takes into consideration the normalized modal form as well as the determined severity at the fixed end of a certain crack with the ones obtained using FEM simulations illustrates the precision of the developed analytical method. In further research we propose to create a database that will be used in training an artificial neural network using the presented method for detecting transverse cracks in beamlike structures.

ACKNOWLEDGMENTS

This paper received financial support through the project "Entrepreneurship for innovation through doctoral and postdoctoral research": POCU/380/ 6/13/123866, a project co-financed by the European Social Fund through the Operational Program Human Capital 2014-2020.

REFERENCES

[1] D. Balageas, C. Fritzen, A. Güemes, Structual Health Monitoring; Wiley-ISTE: London, UK, 2006; ISBN 9781905209019.
[2] J. M. Ndambia, J. Vantommea, K. Harri, Damage assessment in reinforced concrete beams using eigenfrequencies and mode shape derivatives, Engineering Structures, Engineering Structures, 24, 2002, pp. 501–515.
[3] W.M. Ostachowicz, C. Krawczuk, Analysis of the effect of cracks on the natural frequencies of a cantilever beam, Journal of Sound and Vibration, 150(2), 1991, pp.191–201.
[4] T.J. Chondros, A.D. Dimarogonas, J. Yao, A continuous cracked beam vibration theory, J. Sound Vibration, 215 (1) (1998), pp. 17-34.
[5] Z.B. Yang, M. Radzienski, P. Kudela, W. Ostachowicz, Scalewavenumber domain filtering method for curvature modal damage detection, Composite Structures, 154, 2016, pp. 396– 409.
[6] J.K. Sinha, M.I. Friswell, S. Edwards, Simplified models for the location of cracks in beam structures using measured vibration data, Journal of Sound and Vibration, 251(1), 2002, pp. 13-38.
[7] S. W. Doebling, C. R. Farrar, M. B. Prime, D. W. Shevitz, Damage identification and health monitoring of structural and mechanical systems from changes in their vibration characteristics, A literature review, United States N. p., 1996.
[8] A. Bensalem, C. A. Fairfield, A. Sibbald, Non-destructive evaluation of the dynamic response of a brickwork arch. J Structures and Buildings, ICE, 122(1) (1997), pp. 69-82.

[9] V. Srinivas, K. Ramanjaneyulu, C.A. Jeyasehar, Multi-stage approach for structural damage identification using modal strain energy and evolutionary optimization techniques, Structural Health Monitoring, 10(2), 2010, pp. 219-230.
[10] Athanasios Chasalevris, Analytical evaluation of the static and dynamic characteristics of three-lobe journal bearings with finite length, ASME. J. Tribol, 137(4): 041701, 2015.
[11] M. V. Pop, G. R. Gillich, C. Tufisi, Z. I. Praisach, L. Păun, Estimation of the severity of damage produced by a transverse crack, Studia Engineering, Edition no.1, 2020.
[12] Z. I. Praisach, G. R. Gillich, O. Vasile, E. D. Birdeanu, C. Protocsil, Assessment of damages in sandwich panels based on the damage location indexes, Department of Mechanics, "Eftimie Murgu" University of Resita, 2013.
[13] G. R. Gillich, C. Tufisi, Z. I. Korka, C.O. Hamat, N. Gillich, Automatic detection of L and T shaped cracks in semifinished casting products, IOP Conference Series: Materials Science and Engineering 393(1):012016, 2018.
[14] C. Tufisi, G. R. Gillich, C. O. Hamat, T. Manescu, Study regarding the effect of crack branching on the eigenfrequencies of beams, Proceedings of the 13th International Conference on Damage Assessment of Structures, 2020, pp. 79-91.
[15] C. Tufisi, G. R. Gillich, D. Nedelcu, C. O. Hamat, Numerical study on complex shaped cracks in cantilever beams concerning frequency and stiffness changes, 19, 2018, pp. 253-258.

DOI: https://doi.org/10.14232/analecta.2022.1.42-49

Analecta Technica Szegedinensia
Vol. 16, No. 01 ISSN 2064-7964 2022

INFLUENCE OF SYNTHESIS ON COMPOSITE/LAMINATED STARCH-GELATINE BASED BIOPOLYMER FILM PROPERTIES

Danijela Šuput, Senka Popović, Jovana Ugarković, Nevena Hromiš*

Faculty of Technology Novi Sad, Bulevar cara Lazara 1, 21000 Novi Sad, Serbia
*e-mail: suput.danijela@gmail.com

ABSTRACT

Biopolymer films have an increasing share in the packaging material sector due to a number of advantages: availability, cheapness, easy processing, degradability, etc. On the other hand, numerous methods have been developed to optimize their unfavorable properties (weaker mechanical characteristics, hydrophilicity, etc.). This paper examines the influence of the synthesis method on starch-gelatin films properties. The starch-gelatin film was synthesized in a ratio 1:1 as a composite film (C). The second sample was obtained by gelatin film lamination on starch film (L). Plain starch film was used as a control (0). Mechanical, structural and physico-chemical properties of importance for the application of packaging materials were tested on the obtained samples. All the obtained biopolymer films were transparent and easy to handle. FTIR spectroscopy identified all characteristic groups and bonds formed in composite and laminated films. The results showed a significant contribution of gelatin in the developed biopolymer films compared to the control sample. Gelatin incorporated as a film component or as a separate layer improved mechanical properties and water solubility. Slight differences were observed between composite and laminated films because the effect of the method of added gelatin is minimal compared to the sample without the addition of gelatin.

Keywords: biopolymer films, starch, gelatin, synthesis, properties

1. INTRODUCTION

The Polymer packaging materials are the most popular in the international packaging market for a variety of reasons: strength, flexibility, workability, the ability to combine with other materials and low cost. However, two issues connected to the use of polymers in the packaging sector have emerged in recent years: the synthesis of polymers from non-renewable sources, as well as the environmental impact of their excessive usage and disposal [1]. Petroleum-based plastics are not biodegradable or compostable, resulting in a massive amount of plastic waste around the planet [2]. The food packaging business is a major contributor to plastic waste creation. In this segment, it appears that an alternative to synthetic polymer should be found. Biodegradable materials have been the subject of extensive research for the past decades: the prospect of employing renewable raw materials and agro-industrial waste as an alternative to synthetic polymers is being explored. There has been an increase in demand for packaging materials that are biodegradable, offer less environmental risk, and are made from sustainable and renewable resources [3]. Biopolymers fall into three broad categories [4]:

- Biopolymers extracted from biomass (agricultural, animal processing, forest, or ocean wastes)
- Polymers synthesized using the bio-originated or bio-derived monomeric units via classical polymer synthesis routes (polylactic acid, bio-based polyethylene terephthalate, and biopolyolefins)
- Polymers produced by genetically modified microorganisms (bacterial cellulose and polyhydroxyalkanoates).

The first group of biopolymers has received a lot of attention [5]. Biopolymer film is a free-standing sheet that can be deposited on or between food components, usually categorized according to the dominant building material. Polysaccharides (cellulose, chitin, pectin, starch, etc.), proteins (whey protein, casein, collagen, zein, soy protein, myofibrillar proteins of animal muscle), and lipids (free fatty acids, wax, paraffin, resin) derived from plants, marine, and domestic animals are the three main groups of biopolymer films sources [6,7]. Biopolymers must meet specific characteristics, regardless of their application,

DOI: https://doi.org/10.14232/analecta.2022.1.50-55

including good barrier properties (water, gas, and oil), mechanical properties (resistance, stress-resistance, flexibility), and aesthetic properties (translucence, lack of color) [8]. Because starch and gelatin are abundant, cheap, and biodegradable materials that are also edible and hence suitable for food contact [9], they have been extensively explored for the aim of designing packaging materials. Starch is one of the most widespread polysaccharides in nature, obtained from renewable sources, whose price is low, so the use of edible starch-based packaging in the field of food packaging is a potential direction for the development of packaging materials today. From starch, it is possible to easily form packaging films with good sensory properties (color, smell, taste), which do not adversely affect the packaged contents. Gelatin is a multipurpose substance utilized as a gelling agent, a stabilizer, a thickening, an emulsifier, and even as a microencapsulating agent in the culinary, pharmaceutical and cosmetic industries [10]. Because of its good film-formation capabilities and abundance in nature, it is one of the biomaterials of interest for the production of biodegradable films [11]. Gelatin–starch blends are also gaining popularity, as both are renewable resources with good film-forming qualities, resulting in films with unique attributes such as biodegradability and non-toxicity [12].
The aim of this paper was to produce starch-gelatin films by lamination and by making composite film. Further, the aim was to characterize the properties of synthesized biopolymer films based on starch and gelatin obtained by lamination of one layer of biopolymer on another (L) and composite films obtained by mixing filmogenic solutions (C). Starch film was used as a control (0) in order to compare obtained results and propose more suitable film preparation method.

2. MATERIALS AND METHODS

2.1. Materials

Modified corn starch (C*EmTex 12688), was provided by Palco (Serbia), while gelatin was procured from Barentz (Serbia). Glycerol (99,8%) was purchased from Laboratorija (Serbia).

2.2. Methods

Starch solution preparation: Aqueous modified corn starch solution (1.5 % (w/v)) was heated at 90 ˚C in a water bath for 60 min with the addition of glycerol (40% of the starch mass).
Gelatin solution preparation: Aqueous gelatin solution (7% (w/w)) was prepared and left for 30 minutes at room temperature to undergo gelation, and then dissolved in a water bath at 50°C for about 20 min. Afterwards, 0.2 g glycerol/g gelatin was added and stirred.
Control sample (0) preparation: 50 g of starch solution was poured on Petri dishes coated with Teflon and left to dry for 5 days at room temperature on a leveled area after which they were analyzed.
Laminated sample (L) preparation: after pouring 40 g of starch film solution in Petri dishes coated with Teflon, they were left to dry. After 5 days 20g of gelatin solution was poured on their surface and left to dry on leveled surface after which they were analyzed.
Composite film (C) preparation: after preparing starch film solution and gelatin film solution, both solutions were mixed in a ratio 1:1. Obtained solution was poured in Petri dishes coated with Teflon (50g) and left to dry for 5 days at room temperature on a leveled area after which they were analyzed.

2.3. Mechanical properties

Film thickness was surveyed with 1 μm sensitivity micrometer. Eight replicates were carried out on each sample.
Tensile strength (TS) and elongation to break (EB) were evaluated by utilizing Instron Universal Testing Instrument Model No 4301 (Instron Engineering, Canton, Massachusetts, USA), in accordance with EN ISO 527-3:2018. The grip separation was set at 50 mm, and crosshead speed was 50 mm/min.

DOI: https://doi.org/10.14232/analecta.2022.1.50-55

2.4. Physical properties

Moisture content was determined as a percentage of weight reduction during film drying, expressed on the total weight of the film:

$$MC\ (\%) = 100\ [(m2-m1) - (m3-m1)]/\ (m2-m1) \quad (1)$$

where: m1- mass of measuring vessel, m2- mass of film samples with measuring vessel prior drying, m3- mass of dried film samples with measuring vessel

Swelling capacity: Film samples (2x2 cm) were weighed (m1), and then dipped in 20 ml of deionized water at room temperature, for 2 min. After removing samples from the water, the excess water was removed by a filter paper and samples were reweighed (m2). Swelling degree was calculated:

$$Swelling\ (\%) = 100\ (m2 - m1) / m1 \quad (2)$$

where m1- mass of film samples prior to dipping in deionized water, m2- mass of film samples after dipping in deionized water

The film solubility: Dry film samples, after moisture content determination, were submerged in 20 ml of deionized water at room temperature for 30 min, with mixing. After 30 min, excess water was emptied and samples were dried in the oven, for 60 min, and reweighed (m4). The solubility was calculated:

$$Solubility\ (\%) = 100\ [(m3–m1) - (m4-m1)]/\ (m3–m1) \quad (3)$$

where, m1- mass of measuring vessel, m2- mass of film samples with measuring vessel prior drying, m3- mass of dried film samples with measuring vessel, m4- mass of dried film samples with measuring vessel after immersion and drying

2.5. Structural properties

Fourier transform spectroscopy (FTIR) analysis of the film samples was carried out using the IR spectrophotometer, Nicolet IS10, Thermo Scientific (Massachusetts, USA). Omnic 8.1. software was used to operate the FTIR spectrometer, collect and process all the data.

2.6. Statistical analysis

MicroSoft Excel was used to run statistical analysis for calculating the means and standard error (MicroSoft Office 2010).

3. RESULTS

Results related to mechanical properties are presented in Table 1.

Table 1. Mechanical properties of control film, laminated and composite film

Sample	Thickness (μm)	Tensile strength (N/15mm)	Elongation at break (%)
Control	100.11±5.00	13.94±1.24	30.88±7.58
Laminated film	163.67±6.30	102.72±17.12	2.06±0.70
Composite film	211.00±5.96	75.92±12.66	1.33±0.16

According to the obtained results it was concluded that gelatin addition improved mechanical properties. Tensile strength increased while elongation at break values decreased. The highest tensile strength was at laminated samples, which were the firmest, no matter composite film had highest thickness value.

DOI: https://doi.org/10.14232/analecta.2022.1.50-55

Results related to physical properties are presented in Table 2.

Table 2. Physical properties of control film, laminated and composite film

Sample	Moisture content (%)	Swelling (%)	Solubility (%)
Control	18.17±0.05	234.12±29.41	73.68±3.78
Laminated film	11.41±1.02	109.35±5.16	22.12±1.61
Composite film	12.36±0.44	127.62±11.17	20.76±0.98

The gelatin addition improved swelling and solubility, which are considered undesirable characteristics of packaging materials, since values were lower compared to control film. There was no difference regarding film synthesis route- - weather it was laminated or composite.

Results obtained via FTIR are presented at Figure 1.

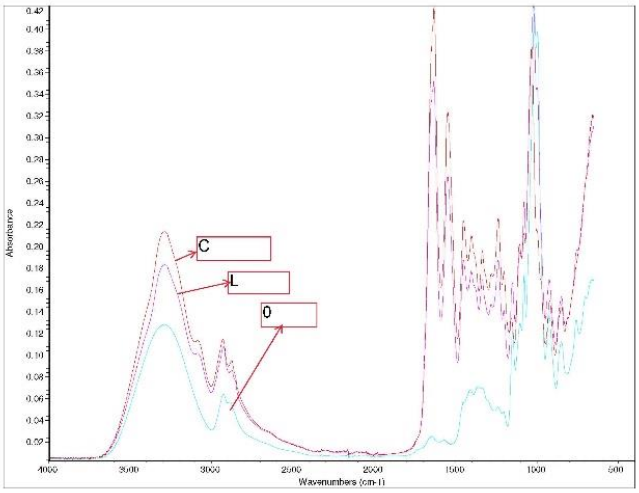

Figure 1. Control film, laminated and composite film spectra

Presence of absorption band at 3300-3600, 2900, 1640 and 1000-1100 cm-1 indicated that all samples contain starch with OH, C-H, C-O-C, and C-O functional group, respectively. C and L spectra contain both starch and gelatin and show almost similar peaks related to gelatin presence: four major peaks at wavenumbers 3500- 2300 cm-1, 1656-1644 cm-1, 1560-1335 cm-1 and 1240-670 cm-1 which correspond to Amide A, Amide I, Amide II, and Amide III regions, respectively.

4. DISCUSSION

When compared to their synthetic counterparts, biopolymers have inferior barrier, thermal, and mechanical qualities [13]. Polymer blending is a well-known method for developing new materials and optimizing polymer characteristics, resulting in composite polymers with superior properties to those generated from pure components [14]. The addition of hydrocolloids to the starch protects the granules from shearing during the manufacturing process. They retain moisture and diminish the blend's syneresis, water solubility, and water absorption [15]. The addition of starch to gelatin films increases the thickness, transparency, and mechanical strength of the films, decreases their solubility, and enhances their structure, all of which increase the films' application [16]. Various results were reported regarding starch-gelatin

DOI: https://doi.org/10.14232/analecta.2022.1.50-55

biopolymer films properties. According to the results of Silva et al. [17] the inclusion of gelatin increased films' mechanical strength and water solubility. On the other hand, according to results of Al-Hassan and Norziah [18] gelatin addition to starch films reduced tensile strength and water vapor permeability but increased the percentage of elongation at break. The same study proved interaction between polysaccharides and proteins, clearly visible using FTIR.
The obtained results in this study are in accordance with Fakhouri et al. [19] findings: gelatin incorporation improves water solubility, thickness, mechanical strength and clarity of starch-based films due to hydrogen bond formation between gelatin and starch as shown by Fourier transform infrared (FTIR) spectroscopy [16]. Fakhoury et al. [19] also found that higher gelatin concentrations increased water solubility, thickness and mechanical strength values, and reduce opacity. However, higher concentrations of starch increased the thickness and improve the mechanical properties. Gelatin incorporation resulted in tougher films with improved break resistance which was sustained with previous finding of Acosta et al. [20].

4. CONCLUSION

The goal of this paper was to evaluate the properties of biopolymer films based on starch and gelatin that were made by laminating one layer of biopolymer on top of another (L) and composite films made by mixing filmogenic solutions (C). In order to compare the results and suggest a better film preparation procedure, starch film was utilized as a control (0). The obtained results of this paper are in favor of the fact that starch films are improved by the addition of gelatin. The method of film preparation (lamination/composite films) did not affect the monitored physical characteristics of the films. The most pronounced differences between laminated and composite have been observed by monitoring the mechanical characteristics so the lamination is suggested as the optimal method of film preparation.

Acknowledgements: This paper is a result of the program of the Ministry of Education, Science and Technological Development, Republic of Serbia, number: 451-03-68/2022-14/200134.

REFERENCES

[1] T. Schwarzbock, E. Van Eygen, H. Rechberger, J. Fellner, Determining the amount of waste plastics in the feed of Austrian waste-to-energy facilities, Waste Management & Research, 35 (2016), pp. 207–216. https://doi.org/10.1177/0734242X16660372.
[2] A., Moeini, N., Germann, M., Malinconico, G., Santagata, Formulation of secondary compounds as additives of biopolymer-based food packaging: A review, Trends in Food Science & Technology, 114 (2021), pp. 342-354. https://doi.org/10.1016/j.tifs.2021.05.040.
[3] Y. Han, M., Yu, L., Wang, Physical and antimicrobial properties of sodium alginate/carboxymethyl cellulose films incorporated with cinnamon essential oil, Food Packaging and Shelf Life, 15 (2018), pp. 35–42. https://doi.org/10.1016/j.fpsl.2017.11.001.
[4] M.J., Fabra, A., López-Rubio, J.N., Lagaron, Biopolymers for food packaging applications. In: Smart Polymers and their Application. Elsevier, 2014, pp. 476–509. https://doi.org/10.1533/9780857097026.2.476.
[5] S., Popović, V., Lazić, N., Hromiš, D., Šuput, S., Bulut, Biopolymer packaging materials for food shelf-life prolongation. In: Biopolymers for food design, Academic Press, Elsevier, 2018, pp. 223-277 https://doi.org/10.1016/B978-0-12-811449-0.00008-6.
[6] D., Šuput, V., Lazić, S., Popović, N., Hromiš, Edible films and coatings – sources, properties and application, Food and Feed Research, 42 (2015), pp.11-22. https://doi.org/10.5937/FFR1501011S.

[7] D., Šuput, D. Sinteza, karakterizacija, optimizacija svojstava i primena jestivog, aktivnog ambalažnog materijala na bazi skroba. PhD Thesis, University of Novi Sad, Faculty of Technology Novi Sad, 2016.
[8] D. Kowalczyk M., Kordowska-Wiater J., Nowak, B., Baraniak, Characterization of films based on chitosan lactate and its blends with oxidized starch and gelatin, International Journal of Biological Macromolecules, 77 (2015), pp. 350–359. https://doi.org/10.1016/j.ijbiomac.2015.03.032.
[9] P., Cazón, G., Velazquez, J.A., Ramírez, M., Vázquez, Polysaccharide-based films and coatings for food packaging: A review, Food Hydrocolloids, 68 (2017), pp. 136–148. https://doi.org/10.1016/j.foodhyd.2016.09.009.
[10] L., Lin, J.M., Regenstein, S., Lv, J., Lu, S., Jiang, An overview of gelatin derived from aquatic animals: properties and modification, Trends in Food Science and Technology, 68 (2017), pp.102–112. https://doi.org/10.1016/j.tifs.2017.08.012
[11] N., Suderman, M.I.N., Isa, N.M., Sarbon, The effect of plasticizers on the functional properties of biodegradable gelatin-based film: a review, Food Bioscience, 24 (2018), pp. 111–119. https://doi.org/10.1016/j.fbio.2018.06.006.
[12] C. Shi, F., Tao, Y., Cui, New starch ester/gelatin-based films: developed and physicochemical characterization, International Journal of Biological Macromolecules, 109 (2018), pp. 863–887. https://doi.org/10.1016/j.ijbiomac.2017.11.073 .
[13] N., Jabeen, I., Majid, G.A., Nayik, Bioplastics and food packaging: A review, Cogent Food & Agriculture, 1 (2015), pp. 1117749. https://doi.org/10.1080/23311932.2015.1117749.
[14] B.A.L., Perez, E., Agama-Acevedo, E. Starch. In Starch-Based Materials in Food Packaging. Elsevier, (2017), pp. 1–18. https://doi.org/10.1016/b978-0-12-809439-6.00001-7.
[15] K., Mahmood, H., Kamilah, P.L., Shang, S., Sulaiman, F., Ariffin, A.K., Alias, A review: interaction of starch/non-starch hydrocolloid blending and the recent food applications, Food Bioscience, 19 (2017), pp.110–120. https://doi.org/10.1016/j.fbio.2017.05.006.
[16] K., Wang, W., Wang, R., Ye, J., Xiao, Y., Liu, J., Ding, J., et al., Mechanical and barrier properties of maize starch - gelatin composite films: Effects of amylose content, Journal of the Science of Food and Agriculture, 97 (2017), pp.3613–3622. https://doi.org/10.1002/jsfa.8220.
[17] N.M., Silva, F.M., Fakhouri R.L.L., Fialho, E.C.D.M.A., Albuquerque, Starch-recycled gelatin composite films produced by extrusion: physical and mechanical properties, Journal of Applied Polymer Science, 135 (2018), pp.46254. https://doi.org/10.1002/app.46254.
[18] A.A., Al-Hassan, M.H., Norziah, Effect of transglutaminase induced crosslinking on the properties of starch/gelatin films, Food Packaging and Shelf Life, 13 (2017), pp.15–19. https://doi.org/10.1016/j.fpsl.2017.04.006.
[19] F.M., Fakhoury, S.M., Martelli, L.C., Bertan, F., Yamashita, L.H.I., Mei, F.P.C., Queiroz, Edible films made from blends of manioc starch and gelatin – influence of different types of plasticizer and different levels of macromolecules on their properties, LWT 49 (2012), pp.149–154. https://doi.org/10.1016/j.lwt.2012.04.017.
[20] S., Acosta, A., Jiménez, M., Cháfer, C., González-Martínez, A., Chiralt, Physical properties and stability of starch–gelatin-based films as affected by the addition of esters of fatty acids, Food Hydrocolloids, 49 (2015), pp. 135–143. https://doi.org/10.1016/j.foodhyd.2015.03.015.

DOI: https://doi.org/10.14232/analecta.2022.1.50-55

Analecta Technica Szegedinensia
Vol. 16, No. 01 ISSN 2064-7964 2022

A NEW APPROACH FOR IMPERFECT BOUNDARY CONDITIONS ON THE DYNAMIC BEHAVIOR

[1]Zeno-Iosif Praisach, [1]Dorel Ardeljan, [1]Dan Alexandru Pîrșan, [1]Gilbert-Rainer Gillich

[1]Babeș-Bolyai University, Faculty of Engineering, Piața Traian Vuia, Nr. 1-4, 320085, Reșița, ROMÂNIA
zeno.praisach@ubbcluj.ro

ABSTRACT

Real beams have non-ideal boundary conditions and it is necessary to use new models to determine the real modal parameters. Models that use ideal conditions do not fully reflect reality and can lead to unsatisfactory description of the dynamic behavior. The hinged – hinged boundary conditions, which is in the focus of the paper, are not analyzed as a single beam, but as a continuous beam with three spans, free at the ends. The continuous beam with three spans is analyzed for cases in which the intermediate supports can occupy any position along the length of the beam, by an analytical solution of the problem, with the example of cases when the intermediate supports are located very close at the free ends of the continuous beam, thus simulating the real case for an hinged beam at both ends; the situation in which the intermediate supports are very close to one of the ends of the beam, thus simulating the real case of the clamped beam, with an imperfect clamped end; and the situation in which the intermediate supports are very close located anywhere on the beam length, thus simulating the hypothetic case with a continuous beam free at the ends and fix on the hinged supports. The analytic results are compared with numerical results by using finite elements method.

Keywords: natural frequency, boundary conditions, dynamic behavior

1. INTRODUCTION

Measuring natural frequencies requires the use of relatively inexpensive and very robust instruments [1, 2]. The determination of natural frequencies are easy to calculate both by using analytical models and by using numerical methods.
However, the precise calculation of the natural frequencies is significantly influenced by the correct positioning of the supports, respectively by the correct choice of the boundary conditions [3].
For example, the analytical calculation for a simple supported beam involves positioning the supports exactly at the ends of the beam, but in the real case, the positioning of these supports is very close to the ends of the beam, which requires treating the problem as a continuous beam with three openings.
Complex studies on the calculation of natural frequencies and modal shapes of continuous beams can be found in [4] and [5].
For this reason, the paper focuses on the analysis of natural frequencies and percentage deviations by applying the ideal boundary conditions and considering the imperfect boundary conditions, by moving the supports by 1%, 2% of the beam length.

2. MATERIALS AND METHODS

2.1. Analytical approach

It will be considered a continuous beam with three openings supported with two intermediate hinges and free at the ends.
The lengths of the spans are denoted (Fig. 1) with l_1, l_2 and l_3 and the sum of the lengths are equal to one, thus: $l_1 + l_2 + l_3 = 1$.
Using Euler-Bernoulli theory for each characteristic point on the beam (1, 2, 3, 4), the following boundary conditions can be written:

DOI: https://doi.org/10.14232/analecta.2022.1.56-61

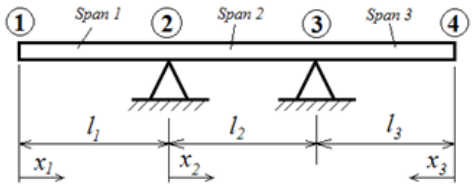

Figure 1. Continuous beam with three spans, free at the ends.

$$\langle 1\rangle \begin{cases} W_1''(0) = 0 \\ W_1'''(0) = 0 \end{cases} \qquad \langle 4\rangle \begin{cases} W_3''(0) = 0 \\ W_3'''(0) = 0 \end{cases}$$

$$\langle 2\rangle \begin{cases} W_1\ (l_1) = 0 \\ W_2\ (0) = 0 \\ W_1'(l_1) = W_2'(0) \\ W_1''(l_1) = W_2''(0) \end{cases} \qquad \langle 3\rangle \begin{cases} W_2\ (l_2) = 0 \\ W_3\ (l_3) = 0 \\ W_2'(l_2) = -W_3'(l_3) \\ W_2''(l_2) = W_3''(l_3) \end{cases} \tag{1}$$

where:
$W_i(x_i) = A_i sin(a_n x_i) + B_i cos(a_n x_i) + C_i sinh(a_n x_i) + D_i cosh(a_n x_i)$ is the normal mode shape of the span;
i = 1, 2, 3 represents the number of spans;
n is the nth vibration mode number;
A_i, B_i, C_i, D_i are the integration coefficients;
$x_1 \in [0, l_1]$, $x_2 \in [0, l_2]$, $x_3 \in [0, l_3]$;
a_n - the eigenvalues, obtained as solutions of the characteristic equation:

$$(Z_{12} \cdot Z_{21} + Z_{11} \cdot Z_{22}) \cdot Z_{32} + (Z_{12} \cdot Z_{22} + Z_{11} \cdot Z_{23}) \cdot Z_{31} = 0 \tag{2}$$

and,

$$\begin{cases} Z_{11} = 2\dfrac{1 + \cos(a_n l_1)\cosh(a_n l_1)}{\cos(a_n l_1) + \cosh(a_n l_1)} \\ Z_{12} = -2\dfrac{\cos(a_n l_1)\sinh(a_n l_1) - \sin(a_n l_1)\cosh(a_n l_1)}{\cos(a_n l_1) + \cosh(a_n l_1)} \end{cases}$$

$$\begin{cases} Z_{31} = 2\dfrac{1 + \cos(a_n l_3)\cosh(a_n l_3)}{\cos(a_n l_3) + \cosh(a_n l_3)} \\ Z_{32} = -2\dfrac{\cos(a_n l_3)\sinh(a_n l_3) - \sin(a_n l_3)\cosh(a_n l_3)}{\cos(a_n l_3) + \cosh(a_n l_3)} \end{cases} \tag{3}$$

$$\begin{cases} Z_{21} = 1 - \cos(a_n l_2)\cosh(a_n l_2) \\ Z_{22} = \cos(a_n l_2)\sinh(a_n l_3) - \sin(a_n l_2)\cosh(a_n l_2) \\ Z_{23} = 2\sin(a_n l_2)\sinh(a_n l_2) \end{cases}$$

By knowing the eigenvalues, the natural frequencies for the continuous beam with three openings can be calculated using the relation:

DOI: https://doi.org/10.14232/analecta.2022.1.56-61

$$f_n = \frac{a_n^2}{2\pi}\sqrt{\frac{E \cdot I}{m \cdot L^4}} \tag{4}$$

where:
f_n [Hz] is the natural frequency;
E [N/m^2] is the elasticity modulus;
I [m^4] is the moment of inertia;
m [kg] is the beam mass;
L [m] is the beam length.
In conclusion, in order to calculate the natural frequencies, we must obtain our own values with relation (2), to know the material from which the continuous beam is made and its geometry.
For this, it will be considered the beam made of steel with a density ρ = 7800 kg/m^3 and $E = 2.1 \cdot 10^{11}$ N/m^2, having length L =1 m.
The beam is considered to have a constant cross section, a rectangular shape with a width of b = 0,05 m and a thickness of h = 0,005 m.

2.2. Numerical approach

The validation of the results obtained by the analytical method was done using FEM analysis.
The beam described in the previous chapter was analyzed for different locations of the intermediate supports.
For the mesh of the 3D model, finite elements with an average size of 1 mm were used, and the intermediate supports are frictionless hinges located in the neutral axis of the beam.
For $l_1 = l_2 = l_3 = L/3$, the eigenvalues (a_n) obtained with relation (2) and the natural frequencies for the first $n = 6$ vibration modes calculated analytically (f_{n_a}) and obtained by FEM (f_{FEM}) are presented in Tab. 1.

Table 1. The first 6 natural frequencies calculated analytically and obtained by FEM

n	**1**	**2**	**3**	**4**	**5**	**6**
a_n	4.237	4.947	10.732	12.827	14.118	20.104
f_{n_a} [Hz]	21.401	29.168	137.295	196.111	237.594	481.771
f_{FEM} [Hz]	21.720	29.474	137.960	196.870	239.390	483.830
ε [%]	**1.492**	**1.050**	**0.484**	**0.387**	**0.756**	**0.427**

Comparing the results obtained for the natural frequencies, presented in table 1, it can be seen that the error ε [%] between the two methods is below 1.5% for vibration modes 1 and 2, respectively below 1% for the other vibration modes.

3. RESULTS

The first particular case considered is that in which the intermediate supports are located very close to the free ends of the continuous beam, thus simulating the real case of a simply supported beam, with hinges at the ends.
The analyzed cases took into account the values of natural frequencies calculated analytically, for $l_1 = l_3 =$ 0.02 m; l_1 = 0.01 m, l_3 = 0.02 m; $l_1 = l_3$ = 0.01 m and their comparison with the natural frequencies obtained for the case of the simply supported beam ($L = 1$) and percentage deviations from them.
The results are presented in Tab. 2
The percentage deviations are shown in Fig. 2.

DOI: https://doi.org/10.14232/analecta.2022.1.56-61

Table 2. Natural frequencies and percentage deviations for a simple supported beam with imperfect boundary conditions

	n	**1**	**2**	**3**	**4**	**5**	**6**
***L* = 1 m**	f_{n_a} **[Hz]**	**11.764**	**47.057**	**105.878**	**188.227**	**294.104**	**423.510**
l_1 = 0.02	f_{n_a} [Hz]	12.764	51.048	114.823	204.044	318.647	458.546
l_3 = 0.02	ε **[%]**	**8.500**	**8.481**	**8.449**	**8.403**	**8.345**	**8.273**
l_1 = 0.01	f_{n_a} [Hz]	12.503	50.006	112.495	199.946	312.323	449.582
l_3 = 0.02	ε **[%]**	**6.278**	**6.267**	**6.250**	**6.226**	**6.195**	**6.156**
l_1 = 0.01	f_{n_a} [Hz]	12.249	48.996	110.236	195.966	306.178	440.862
l_3 = 0.01	ε **[%]**	**4.123**	**4.120**	**4.117**	**4.112**	**4.105**	**4.097**

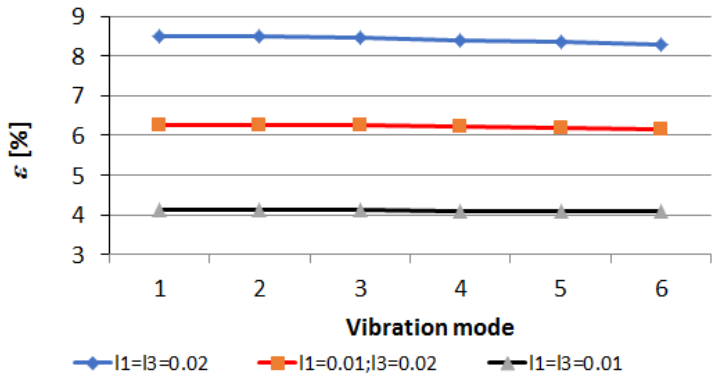

Figure 2. Percentage deviations for the case of the simply supported beam with imperfect boundary conditions.

The second particular case considered is that in which the intermediate supports are located very close to the left free end of the continuous beam, thus simulating the case of a imperfect clamped – free beam.
The analyzed cases took into account the values of natural frequencies calculated both analytically and obtained by FEM, for $l_1 = l_2 = 0.02$ m;$l_1 = 0.02$ m, $l_2 = 0.01$ m; $l_1 = 0.01$ m, $l_2 = 0.02$ m; $l_1 = l_2 = 0.01$ m and their comparison with the natural frequencies obtained for the ideal case ($L = 1$) of the clamped– free beam.
The results are presented in Table 3and the percentage deviations are shown in figure 3.

Table 3. Natural frequencies and percentage deviations for a clamped - free beam with imperfect boundary conditions

	n	**1**	**2**	**3**	**4**	**5**	**6**
***L* = 1 m**	f_{n_a} **[Hz]**	**4.191**	**26.264**	**73.541**	**144.110**	**238.225**	**355.866**
l_1 = 0.02	f_{n_a} [Hz]	4.486	28.119	78.757	154.374	255.258	381.408
l_2 = 0.02	ε **[%]**	**7.029**	**7.063**	**7.093**	**7.122**	**7.150**	**7.177**
l_1 = 0.02	f_{n_a} [Hz]	4.424	27.726	77.639	152.153	251.537	375.779
l_2 = 0.01	ε **[%]**	**5.558**	**5.566**	**5.574**	**5.581**	**5.588**	**5.595**
l_1 = 0.01	f_{n_a} [Hz]	4.394	27.546	77.151	151.226	250.052	373.628
l_2 = 0.02	ε **[%]**	**4.849**	**4.881**	**4.909**	**4.937**	**4.965**	**4.991**
l_1 = 0.01	f_{n_a} [Hz]	4.334	27.165	76.068	149.074	246.446	368.172
l_2 = 0.01	ε **[%]**	**3.422**	**3.430**	**3.437**	**3.444**	**3.451**	**3.458**

DOI: https://doi.org/10.14232/analecta.2022.1.56-61

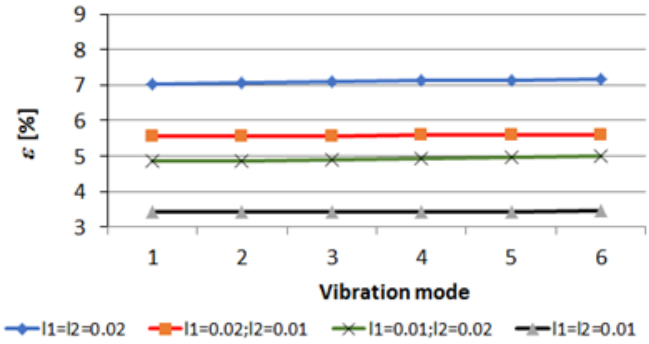

Figure 3. Percentage deviations for the case of the clamped-free beam with imperfect boundary conditions.

The third particular case considered is that in which the intermediate supports are located very close on the continuous beam, thus simulating the hypothetic case of a free – clamped – free continuous beam.
The analyzed cases took into account the values of natural frequencies calculated both analytically and obtained by FEM, for l_1 = 0.20 m and l_2 = 0.02 m.
The results are presented in Tab. 4.

Table 4. Natural frequencies and percentage deviations when the intermediate supports are very close on the continuous beam

	n	**1**	**2**	**3**	**4**	**5**	**6**
l_1 = 0.20 l_2 = 0.02	a_n	2.384	5.969	9.086	9.997	13.991	17.990
	f_{n_a} [Hz]	6.774	42.465	98.393	119.128	233.320	385.751
	f_{FEM} [Hz]	6.796	42.589	99.571	119.400	233.930	386.840
	ε [%]	**0.329**	**0.293**	**1.197**	**0.229**	**0.262**	**0.282**

A comparison of the vibration modes between the analytical method and the FEM method, for l_1= 0.20 m andl_2 = 0.02 m, is illustrated in Fig. 4.

4. CONCLUSIONS

In this paper we have applied three cases for which imperfect contour conditions generate errors in the calculation of natural frequencies for simple structures.
Tab. 1 and 4 show that, regardless of the method applied, the analytical method and the numerical method, respectively, when calculating the natural frequencies, approximately the same values are obtained for the continuous beam with three openings. The errors obtained by the two calculation methods are below 1%, except for modes 1 and 2 for the case when the intermediate supports are positioned equidistant from the ends of the bar, respectively for mode three (Tab 4) in case of simulating the imperfect stiffness, but for this, in this case, the shape of the vibration modes obtained by the two methods has the same shape.
In the case of simply supported beams, a displacement of the supports towards the ends of the beam by 2% produces deviations of the natural frequencies of more than 8% from the case when the supports are positioned at the ends of the beam,the precision deviation decreases to about 4% for the displacement of the supports by 1% with respect to the ends of the beam.
In the case of the imperfectly clamped-free beam (Tab. 3), the positioning of the intermediate supports with 2% - 4% produces deviations in the calculation of the own frequencies of 3% - 7%.
Regardless of the analyzed cases, for the first 6 analyzed vibration modes, the deviations have approximately the same value (Fig. 2 and 3).

DOI: https://doi.org/10.14232/analecta.2022.1.56-61

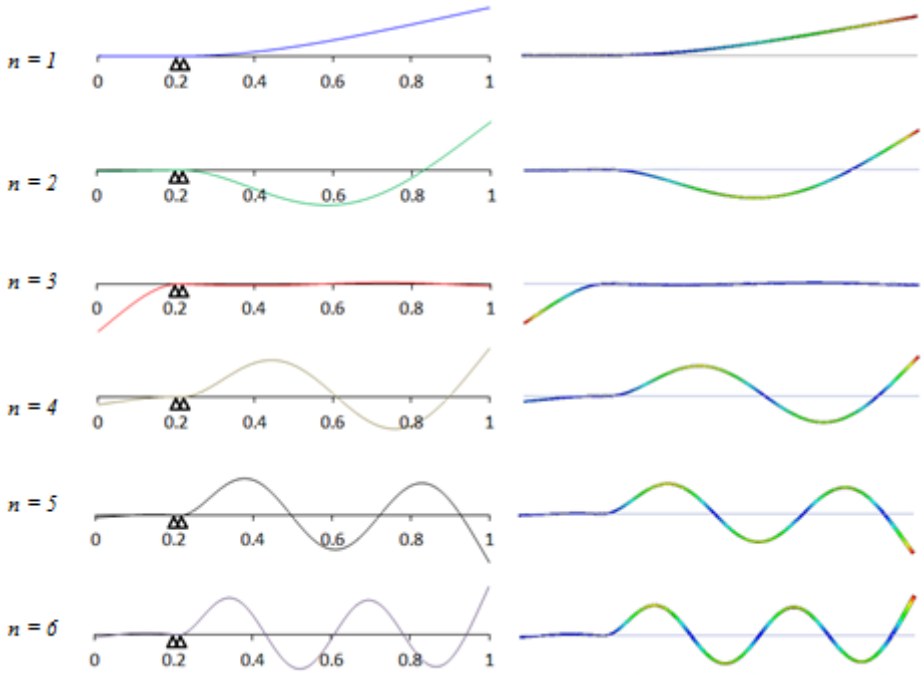

Figure 4. A comparison for the six vibration modes for $l_1 = 0.20$ and $l_2 = 0.02$ obtained by analytical (left) and numerical method (right).

In conclusion, for real cases, small deviations of the position of the beam supports from the ends, or an imperfect fixation of the beam lead to significant deviations of the natural frequencies. It is important that, when calculating the natural frequencies for real beams, we take into account the imperfections of the positioning of the supports.

REFERENCES

[1] N. Gillich, C. Tufisi, C. Sacarea, C.V. Rusu, G-R. Gillich, Z-I. Praisach, M. Ardeljan, Beam Damage Assesment Using Natural Frequency Shift and Machine Learning. Sensors 22: 1-23, (2022), ttps://doi.org/10.3390/s22031118.

[2] A. Mustafazade, M. Pandit, C. Zhao, G. Sobreviela, Z. Du, P. Steinmann, X. Zou, R.T. Howe, A.A. Seshia, A vibrating beam MEMS accelerometer for gravity and seismic measurements. Scientific Reports 10: 1-8, (2020), https://doi.org/10.1038/s41598-020-67046-x.

[3] C. Yanxia, Z. Kai, Y. Zhoujing, L. Chang, L. Kaiji, W. Linbing,Inluence of Temperature on the Natural Vibration Characteristics of Simply Supported Reinforced Concrete Beam. Sensors 21: 1-14, (2021), https://doi.org/10.3390/s21124242.

[4] Z-I. Praisach, N. Gillich, I. Negru, Natural frequency Changes of Euler-Bernoulli Continuous Beam with Two Spans due to Crack Occurrence. Romanian Journal of Acoustic and Vibrations 11, issue 2: 80-83, (2014), ISSN 1584-7284.

[5] K. Saeedi, B.R. Bhat,Clustered Natural Frequencies in Multi-Span Beams with Constrained Characteristic Functions. Shock and Vibrations 18: 697-707, (2011),. https://doi.org/10.3233/SAV-2010-0592.

Analecta Technica Szegedinensia
Vol. 16, No. 01 ISSN 2064-7964 2022

DESIGNING AN EXCEL VBA FUNCTION TO RECOGNIZE MORE IMPORTANT IRRATIONAL NUMBERS

Zoltán Fabulya

Faculty of Engineering, University of Szeged, Mars tér 7, 6724, Szeged, Hungary
e-mail: fabulya@mk.u-szeged.hu

ABSTRACT

Calculations typically performed on a calculator or computer show the result as a decimal fraction if it is not an integer. It would be easier to interpret the result if a value could be expressed with integers and operations, such as the root subtraction operation. This article shows how this can be done with a developed algorithm in Microsoft Excel, which recognizes the most famous irrational numbers and displays them in text form together with the character of the operation sign. For example, "5√3/2" is given for 4.330127019. It is also useful to display irrational numbers with integers because only an infinite number of decimal places in a decimal fraction could show the exact value, and that is not possible. So, the developed algorithm can display a more interpretable and accurate form of the irrational number. In addition to the results that can be written as square roots, the algorithm is capable of displaying irrational numbers that can be expressed as the number Pi, using the π character. The Excel algorithm which was implemented in Visual Basic for Applications shows all rational numbers as the quotient of two integers that are relative primes.

Keywords: irrational number, Excel VBA, programming, function, root recognition

1. INTRODUCTION

Irrational numbers appear in decimal form on the display of our electronic devices. The exact value will not be readable, because an infinite number of decimal digits make up the irrational numbers, in which there is no infinitely repeating section [1]. Such is the number Pi (π), but as a result of extracting the root, an irrational number is obtained even for integers if it is not a square number. An irrational number is shorter, more intelligible, and more accurate if appropriate symbols such as the root (√) or Pi (π) are used in their description. However, this type of display is not supported by our programs.
It is often necessary to enter the angles in radians. The decimal fraction form of a famous angle in radians is almost incomprehensible, as shown in (1).

$$30° = \frac{\pi}{6} = 0.523598775598299 \tag{1}$$

The values of the trigonometric functions in the case of famous angles are easier to interpret in radical form (2).

$$\cos 30° = \frac{\sqrt{3}}{2} = 0.866025403784439 \tag{2}$$

In the above formulas, the equation editor provided the appropriate display, but character mode can also be used (π/6, √3/2). This mode now allows us to read a decimal number obtained as a result of a calculation in a character-like, text-type manner in Excel. This article describes the development of an Excel worksheet function to display the most famous types of irrational numbers in character mode, where the essential element was the development of an algorithm for recognizing numbers in the Visual Basic for Applications (VBA) development environment. There are several research articles using the capabilities of Excel VBA [2] [3].

DOI: https://doi.org/10.14232/analecta.2022.1.62-70

2. MATERIALS AND METHODS

The theoretical background of the research is in the field of irrational numbers, while programming tasks require an overview of Excel VBA.
Since there are an infinite number of irrational numbers, including those that cannot be represented by special characters, the article deals only with the recognition of some of the more important types of irrational numbers, which have the following (3) and (4) forms.

$$\frac{m}{n} \times \pi \tag{3}$$

$$\frac{m}{n} \times \sqrt{a} \tag{4}$$

where:
$m =$ integer
$n =$ positive integer $(1 \leq n)$
$a =$ positive integer $(1 \leq a)$

So, the irrational number to be recognized is based on either the number Pi or the square root of an integer. An additional constraint is needed for numbers *n* and *a* since the recognition process cannot be extended to infinity [4]. During the tests, an upper limit of 100 proved to be sufficient. The numbers *m* and *n* should be integers so that the irrational value that causes the display problem can only be the result of Pi or square root subtraction.

2.1. Irrational numbers

Irrational numbers, by definition, are real numbers cannot be written as the quotient of two integers. It is easy to prove that the square root of a positive integer is also an irrational number, except for square numbers, where the square root is an integer [5].
Irrational numbers consist of an infinite number of decimal places without repeating sections. For this reason, their exact value cannot be described in decimal form, although any precision can be achieved by increasing the number of decimal places. That, in turn, will make the described number longer.
A famous group of irrational numbers are the ones that result from the square root of a rational number. Another group are the ones that denote an angle in radians which can be writen with rational numbers in degrees unit of measure [6]. These irrational numbers can be written in the form given by formula (3) or (4). Our goal was to develop an Excel VBA function that can display an irrational number, if possible, in this form.

2.2. Excel VBA

The typical purpose of using Excel spreadsheet program is to get calculated end results. This is achievable with built-in formulas and worksheet functions. In addition, user defined, custom functions can also be created [7]. To do that, some programming is necessary in Visual Basic for Applications (VBA). VBA is based on the Basic programming language. The functions have a name and give a result that depends on the variables in their argument [8]. The general format of the function is:

```
Public Function_name(arguments)
  statements
  function_name = value
```

DOI: https://doi.org/10.14232/analecta.2022.1.62-70

```
End Function
```
When using functions, the value of their argument needs to be specified. Executing the statement creates a value that will be the result of the function `function_name = value` statement.
By default, the instructions in the function are executed once in a row. This is called the sequence instruction structure and has the following form [9]:
```
…
statement1
statement2
statement3
…
```
A selection structure is needed when the execution of the instruction depends on a condition [9]:
```
If condition Then
  statement1
Else
  statement2
End If
```
When the condition is met, the statements in `statement1` block are executed. Otherwise, the `statement2` block is performed.
An iteration structure is necessary in the program when instructions must be repeated several times [9]. In the following conditional loop structure, the statements are performed again and again until the condition is met:
```
While condition
  statements
Wend
```
Any program can be written with the sequence, selection, and iteration structures described above.

2.3. Search algorithm

An essential pillar of this work is to recognize from a number whether it can be produced in the needed form. This problem can be solved with a search algorithm. The point is to find the item that meets the criteria from a list of available items in case there is one. This is achievable by examining the items one by one until items run out or a suitable item is found [10]. This can be accomplished with a conditional loop structure. At the end of the loop, another selection structure is used to check whether the loop ended with a successful search or the items in the list ran out. The pseudocode of the algorithm is as follows:
```
Let the examined item to be the first item on the list
While the examined item is not appropriate and_
                                there is another item not yet tested
  Let the examined item to be the next item on the list
Wend
If the examined item is appropriate Then
  The hit is the examined item
Else
  No hit
End If
```

3. RESULTS

Within the research, the conditions were checked whether a number can be written in the form (3) or (4). This was necessary in order not to limit the number of digits that can be displayed in the given form. The

DOI: https://doi.org/10.14232/analecta.2022.1.62-70

next task was to create a program containing the necessary algorithms, and the last phase was to create the function that can be used in the Excel worksheet, which displays the number in the given (3) or (4) format.

3.1. Irrational numbers that can be accurately displayed

An irrational number can only be short and accurate if it can be expressed as an irrational number of a known value that can be described by a finite sequence of symbols or by a finite sequence of functions. For form (3) or (4), the Pi or the root sign is needed.

We can write any angular value in form (3) that can be described with a rational number $\left(\frac{p}{q}\right)$ in degrees, as shown in (5).

$$\frac{p}{q}[°] = \frac{p}{q} \times \frac{\pi}{180}[rad] = \frac{p}{180 \times q} \times \pi[rad] = \frac{m}{n} \times \pi[rad] \tag{5}$$

where:
$p =$ integer
$q =$ positive integer $(1 \leq q)$
$m =$ integer $(m = p)$
$n =$ positive integer $(n = 180 \times q)$

From derivation (6), it is visible that the form (4) can be utilized to write down the square root of a non-negative integer and the square root of any non-negative rational number.

$$\sqrt{\frac{p}{q}} = \sqrt{\frac{p \times q}{q^2}} = \frac{\sqrt{p \times q}}{q} = \frac{1}{q} \times \sqrt{p \times q} = \frac{m}{n} \times \sqrt{a} \tag{6}$$

where:
$p =$ not negative integer
$q =$ positive integer $(1 \leq q)$
$m =$ integer $(m = 1)$
$n =$ positive integer $(n = q)$
$a =$ positive integer $(1 \leq n = p \cdot q)$

The following derivation (7) shows an example where the square root of an integer can be given in several forms (4) using the square root of a smaller integer.

$$\begin{gathered}\sqrt{32} = \sqrt{4 \times 8} = 2 \times \sqrt{8} \\ \sqrt{32} = \sqrt{16 \times 2} = 4 \times \sqrt{2}\end{gathered} \tag{7}$$

Within the research, a search algorithm was developed which provides the form (4) as the square root of the smallest positive integer.

3.2. The created functions

First, a universal search function was created we could use for both forms (3) and (4). This was possible because these forms can be generalized, as shown in formula (8).

DOI: https://doi.org/10.14232/analecta.2022.1.62-70

$$\frac{m}{n} \times \pi = \frac{m}{n} \times y, \frac{m}{n} \times \sqrt{a} = \frac{m}{n} \times y \tag{8}$$

where:
m = integer
n = positive integer ($1 \leq n$)
a = positive integer ($1 \leq a$)
y = generalized value ($y = \pi$ or $y = \sqrt{a}$)

The search algorithm should indicate a successful search if the recognizable number (x) can be generated in the form (8), i.e., the relation (9) is met.

$$\mathrm{x} = \frac{m}{n} \times y \tag{9}$$

where:
$x =$ the number to recognize
m = integer
n = positive integer ($1 \leq n$)
y = generalized value

A further interesting feature of this generalization is that for $y = 1$, the recognizable number we can be obtained as the quotient of two integers.
The created search function is a bivariate function of x and y that searches for an n positive integer for which equation (9) is fulfilled in the case of some integer m. The result of rearranging (9) to (10) shows that the value of m can be calculated for any value of n, but it cannot be guaranteed that m is an integer. This is exactly what the algorithm checks: to see if the counter (s) providing exact equality is an integer because only then can it be considered suitable ($m = s$).

$$\mathrm{x} = \frac{s}{n} \times y \implies s = \frac{n \times x}{y} \tag{10}$$

where:
$x =$ the number to recognize
$s =$ not necessarily integer
n = positive integer ($1 \leq n$)
y = generalized value

The name of the search function below is denominator because it searches for and returns the `denominator` value that provides the desired representation. If no suitable denominator can be found, the result will be 0.

```
Public Function denominator(x, y)
  Dim n As Integer
  n = 1
  s = Abs(n * x / y)
  d = Abs(WorksheetFunction.Round(s, 0) - s)
  While n < 100 And d > 0.000001
    n = n + 1
    s = Abs(n * x / y)
    d = Abs(WorksheetFunction.Round(s, 0) - s)
```

DOI: https://doi.org/10.14232/analecta.2022.1.62-70

```
  Wend
  If n < 100 Then
    denominator = n
  Else
    denominator = 0
  End If
End Function
```

The function checks whether the value *s* ensuring equality (9) is an integer by examining the absolute value of its deviation from its rounded value as a difference (*d*). Of course, this should be 0 if *s* is an integer, but due to the inaccuracy of number representation, a non-negative value we can be considered as a 0 if it is not greater than 0.000001. Rounding is done with the function `Round`. The function starts from 1 with increments of 1 up to 100, searching for a suitable denominator. So, if it finds one, it will be the smallest one.

The following function is named numerator because it determines the numerator (*m*) of the equation (9) if it exists, i. e. a suitable denominator is found. The numerator will be 0 if there is no such denominator.

```
Public Function numerator(x, y)
  Dim n, m As Integer
  n = denominator(x, y)
  If n = 0 Then
    numerator = 0
  Else
    m = n * x / y
    numerator = m
  End If
End Function
```

Functions are also necessary to find out whether the recognizable number (*x*) can be produced with one of the Pi or root characters, i.e., in the form (3) or (4). These functions are called `pi_base` and `root_base` which return 0 if the desired format is not possible. Generatability can be ascertained from the value of the function denominator from the suitability of $y = \pi$ or $y = \sqrt{a}$. In the case of generatability, the value of the functions will be the value that provides generation, that is, the value of *Pi* of the function `pi_base` and the value *a* of function `root_base`. However, the latter is also a search algorithm for the value *a*, to be examined starting from 1 with increments of 1. Thus, in the case of a hit, the lowest suitable value is acquired, even if more than one value would be suitable.

```
Public Function pi_base(x)
  Dim n As Integer
  y = WorksheetFunction.Pi
  n = denominator(x, y)
  If n = 0 Then
    pi_base = 0
  Else
    pi_base = y
  End If
End Function

Public Function root_base(x)
  Dim a, n As Integer
  a = 1
  n = denominator(x, a)
  While n = 0 And a < 100
```

DOI: https://doi.org/10.14232/analecta.2022.1.62-70

```
    a = a + 1
    n = denominator(x, a ^ (1 / 2))
  Wend
  If a < 100 Then
    root_base = a
  Else
    root_base = 0
  End If
End Function
```

The functions created so far were used for the final one called `txt_num` that gives the number to be recognized in the form (3) or (4). The result is the appropriate form in text data type if it exists, or otherwise the number with four decimal places.

```
Public Function txt_num(x)
  Dim s, n As Integer
  If x = 0 Then
    txt_num = "0"
    Exit Function
  End If
  st = ""
  p = WorksheetFunction.Pi
  If pi_base(x) > 0 Then
    s = numerator(x, p)
    n = deniminator(x, p)
    symb = ChrW(960)              ' character Pi
  ElseIf root_base(x) > 0 Then
    a = root_base(x)
    If a = 1 Then
      y = 1
      symb = ""
    Else
      y = a ^ (1 / 2)
      symb = ChrW(8730) & a     'character root
    End If
    s = numerator(x, y)
    n = deniminator(x, y)
  Else
    txt_num = "" & WorksheetFunction.Round(x, 4)
    Exit Function
  End If
  If s = -1 Then
    If symb = "" Then
      st = "-1"
    Else
      st = "-" & symb
    End If
  ElseIf s = 1 Then
    If symb = "" Then
      st = "1"
    Else
      st = symb
```

DOI: https://doi.org/10.14232/analecta.2022.1.62-70

```
    End If
  Else
    st = s & symb
  End If
  If n > 1 Then
    st = st & " / " & n
  End If
  txt_num = st
End Function
```

The format of the representation depends on several conditions:

- Can the number be generated, and if so, in which form?
- If the value of the numerator is 1, it is only necessary to display it if the recognized value is rational (for example, 1/4). Otherwise, if it is irrational, it is sufficient to display Pi or the square root value in the numerator without a value of 1 (for example, $\pi / 4$ or $\sqrt{3}/2$).
- The dominator does not need to be displayed if its value is 1, but in this case, the numerator is required if its value is 1 and has a rational value.
- When displaying a negative number, the negative sign should appear in front of the number. Otherwise, it is unnecessary.

Table 1 shows the representation of some numbers obtained with the function.

Table 1. Some recognized numbers and their representation

Value	Representation
1.13137085	$4\sqrt{2}/5$
12.12435565	$7\sqrt{3}$
4.188790205	$4\pi/3$
4.294117647	73/17

4. CONCLUSION

A worksheet function was developed for the Microsoft Excel spreadsheet program, that can display the value of the most important types of irrational numbers in a clear, short, and more accurate form than in the inaccurate and difficult-to-understand decimal format. The range of recognizable numbers can be expanded according to the needs, for example, with irrational numbers which can be displayed with the help of the third and fourth roots. The developed function can be used in Excel spreadsheets for easier interpretation of results whenever it is necessary.

REFERENCES

[1] J. Gy. Obádovics, Matematika. Középiskolai tanulók, főiskolai és egyetemi hallgatók, valamint műszaki és gazdasági szakemberek számára, gyakorlati alkalmazásokkal, Tizenkilencedik, bővített kiadás, Scolar Kiadó, Budapest, 2012

[2] Gy. Hampel, Excel VBA alkalmazása egy biometriai esettanulmány példáján bemutatva, Jelenkori társadalmi és gazdasági folyamatok, 12 (4) (2017), pp. 35-40.

[3] Gy. Hampel, Egymintás t-próba programozható kialakítása Excel VBA környezetben, Jelenkori társadalmi és gazdasági folyamatok, 13 (3-4) (2018), pp. 169-175.

[4] I. Niven, Irrational Numbers - The Carus Mathematical Monnographs, Number 11, The Mathematical Association of America, New Jersey, 1956

DOI: https://doi.org/10.14232/analecta.2022.1.62-70

[5] R. P., Agrawal, H. Agrawal, Origin of Irrational Numbers and Their Approximations. Computation, 9 (3) (2021), pp. 1-49.
[6] I. Georgiev, L. Kristiansen, F. Stephan, Computable irrational numbers with representations of surprising complexity, Annals of Pure and Applied Logic, 172 (2) (2021), pp. 1-30.
[7] G. Kovalcsik, Az Excel programozása, Computerbooks, Budapest, 2005
[8] B. L. Matteson, Microsoft Excel Visual Basic Programmer's Guide, MicrosoftPress, Washington, 1995
[9] M., Alexander, D. Kusleika, Excel 2019 Power Programming with VBA, Wiley & Sons, Indianapolis, Indiana, 2019
[10] J. Walkenbach, Excel VBA Programming for Dummies, 3rd edition, John Wiley & Sons Inc., New Jersey, 2013

DOI: https://doi.org/10.14232/analecta.2022.1.62-70

Analecta Technica Szegedinensia
Vol. 16, No. 01 ISSN 2064-7964 2022

ANTIBACTERIAL EFFECT OF EDIBLE COATINGS WITH ESSENTIAL OIL

Anita Vidács, Balázs Győri, Tamás Lázár*

Department of Food Engineering, Faculty of Engineering, University of Szeged, Mars square 7., 6724, Szeged,
email: vidacsa@mk.u-szeged.hu

ABSTRACT

Food preservation technologies are continuously renewed area because of industrial and customer needs, social transformation, environmentally friendly processing and climate change. The shelf life of perishable food products must be extended with different technologies, for example using green methods like the edible coating (EC). EC is made from different biopolymers (chitosan, alginate, gelatine, agar), the effect can increase using plant extracts. This study examined the effect of chitosan EC, chitosan EC+thyme essential oil (EO); effect of alginate EC, alginate EC+thyme EO on fresh chicken breast having artificial contamination with *Escherichia coli*; *Enterococcus faecalis*, that the EC can extend the shelf life. The organoleptic quality of baked treated chicken breast was also established. Based on the result both EC can decrease the cell number (with 1-3 log CFU/g) on treated chicken breast and this antimicrobial effect was enhanced with thyme essential oil (3.2 µl/ml concentration). There was significant differences ($p<0.05$) between the two edible coatings. Alginate had better preservation effect, than chitosan. However, the thyme EO could increase the antimicrobial activity of chitosan in higher values, than the effect of alginate EC. In this experiment, *E. faecalis* was more sensitive to treatment than *E. coli*. In conclusion, the edible coating can be used as an alternative preservation technique and combined with essential oils can extend the shelf life of chicken breast fillet.

Keywords: chicken breast, edible coating, preservation, thyme essential oil

1. INTRODUCTION

The prevention of food contamination has always been an important point in the food chain. The various food-borne diseases affect not only the food industry but also health and regulatory agencies too. The microbes can contaminate the different food products and one of the most significant source of bacterial contamination is the raw meat. For example, *Listeria* spp., *Escherichia* spp., Salmonella sp., *Staphylococcus* spp., *Pseudomonas* spp., *Enterococcus* spp. are the most common food-borne pathogens/spoilage bacteria [1-4]. There are different processing steps for preservation of food: chilling, freezing, heat processing, canning, drying, smoking, vacuum packaging, modified atmosphere packaging, fermentation, smoking, using different spices, adding preservatives and use other new technology (active packaging, high hydrostatic pressure, irradiation, edible coating) [5-6].

The edible coatings can be a potential approach to extend the shelf life of meat and these are bio-based packaging materials [7]. The edible coating is a thin layer of edible material, which coats the food, usually used in liquid form and with immersion method on food [8]. Chitosan is a polysaccharide, derived from chitin, nontoxic, biodegradable, having antimicrobial and film-forming properties. Chitosan film has selective permeability to oxygen and carbon dioxide. [5, 7, 9-12] Sodium-alginate is derived from seaweed, algae, or synthetized by microorganisms used as gel-forming and colloidal stabilizing agents in the food industry. Alginate solution can form gel with different ions (calcium, magnesium, iron, aluminium), gel is water-soluble, flexible, tasteless, odorless, low permeable to oxygen and oils. [13-15]

Plant extracts, including essential oils (EOs), show antibacterial and antifungal effect, suggesting that they can become novel antimicrobial compounds. Most of the EOs are generally recognized as safe (GRAS). [16-17]

Therefore, this study examined the shelf-life extension ability of chitosan and alginate edible coatings on chicken breast fillet having *Escherichia coli* and *Enterococcus faecalis* contamination. Beside this, the preservation effect of coating was enhanced with thyme essential oils.

DOI: https://doi.org/10.14232/analecta.2022.1.71-76

2. MATERIALS AND METHODS

2.1. Bacterial strains

One Gram-positive bacterium (*Enterococcus faecalis*) and one Gram-negative bacterium (*Escherichia coli*) were used during the research. For culturing and for determination of minimum bactericidal concentration, TGE (Tryptone-Glucose-Extract) broth and agar was used (10 g glucose - VWR, Hungary; 5 g tryptone - VWR, Hungary; 2.5 g yeast-extract – Merck, Hungary; 20 g agar-agar - VWR, Hungary). The incubation temperature was 37 °C.

2.2. Minimum bactericide concentration (MBC)

For determination of MBC values on bacteria, the thyme essential oil (tEO) (Aromax Natural Products Zrt., Hungary) was investigated with macrodilution method in different concentrations (in the range of 50 to 0.1 mg/ml). Tween 40 was used to disperse the EOs in the medium. The used cell suspension was 24-h old and the cell number was 10^6 CFU/ml. In previous tests 1% Tween 40 did not affect the growth of the investigated bacteria [18]. The inoculated broth without EO served as control. After 24 hours incubation at 37 °C MBCs were determined by the tracking plate method [19] transferring 10 µl from the microplate wells to TGE agar for the enumeration of living cells. After 24-h incubation at 37 °C, the number of colonies was counted. MBC was defined as the EO concentration where no colony growth was observed on TGE agar.

2.3. Coating preparation

Chitosan (CH) edible coatings: 2 % (wt/v) Chitosan (Sigma-Aldrich) was added to distillated water and acidified with 1 % acetic acid (v/v) (Sigma-Aldrich).
Alginate (AL) edible coatings: 1.5 % (wt/v) Sodium-alginate (Sigma-Aldrich) and 1.5 % (wt/v) $CaCl_2$ (wt/v) was used for the coating preparation. The food sample was immersed firstly in the alginate solution and after that in $CaCl_2$ liquid for crosslinking the alginate (egg-box model/gelation mechanism [20]).
The effect of edible coating was enhanced with tEO in MBC concentration. The tEO was mixed with chitosan, alginate solution (25 °C).

2.3. Antibacterial effect of edible coatings on chicken breast fillet

The chicken breast fillet was obtained from Spar market. The 10-10 g of fillet were prepared for the coatings: each of 10 g fillet was immersed in *E. coli* suspension (10^6 CFU/ml, 10 min) for homogenous dispersion of bacterium on surfaces. After that, the fillets were divided three parts: control-without edible coating; edible coating; edible coating +tEO. The control was placed in sterile plastic box. Second part of the contaminated sample was immersed in 2% CH solution for 10 minutes and place in sterile plastic box; the third part of fillet was immersed in 2% CH solution having tEO in MBC for 10 minutes and place in sterile plastic box. The experiments of alginate coatings were taken at the same way with having one extra step, after the immersion in 1.5 % AL solution/AL+tEO the sample was put in 1.5% $CaCl_2$ solution for 10 minutes. Control and the treated samples in triplicates were stored at 8°C in plastic box and the cell numbers were monitored at 0, 24, 120, 168 hours. 10-10 g of fillet sample were mashed up in 90 ml steril water, prepared 10-fold serial dilutions and surfaced 0.1 ml onto TGE agar and incubated 37°C and for 24 h. After the incubation the remained cell number was established with colony counting.
The study of *E. faecalis* was designed as *E. coli* experiments.

The statistical differences was established by using T-test, Microsoft Excel software.

DOI: https://doi.org/10.14232/analecta.2022.1.71-76

The sensory evaluation was made with scoring method (points were awarded from 1 to 5 point: 5 excellence; 1 not accepted), where the panelists were 12 non-trained people. The organoleptic properties were the taste, odour, texture and the acceptance. The results were the average points of each of properties. The chicken fillets were covered with edible coatings having thyme essential oils and baked in pan.

3. RESULTS AND DISCUSSION

3.1. Minimum bactericide concentration of thyme essential oil

The MBC was established where were not colony formation on the surfaces of agar. Both bacteria had 3.2 mg/ml MBC values, based on this study there was not difference in sensitivity against tEO between the *E. coli* and *E. faecalis*. In the further experiments, 3.2 mg/ml tEO was used.

3.2. Effect of coatings on chicken breast contaminated with E. coli

Based on the results, the chitosan and alginate coating had an inhibitory/antibacterial effect; the cell number was reduced with 0.5-3 log CFU/g on chicken breast fillet (Diagram 1.). The control cell number was increased from 5.66 log CFU/g (24 h: 7.26 log CFU/g; 120 h: 9.10 log CFU/g) to 10.01 log CFU/g for the 168 hours. Despite of that, the AL treated sample had a slow rising: 5.49 log CFU/g, 6.46 and 6.86 log CFU/g, respectively 24, 120 and 168 h; the coating could inhibit the growing of the bacterium. There was the same tendency by the CH, but the cell number was higher, 6.60, 6.91, 7.25 log CFU/g. The preservation effect was enhanced with added tEO, mainly the effect of CH was improved. After 24 hours, the EO could help in the preservation (there was a bactericide effect with the tEO), because there was significant difference between the edible coating and edible coating+ tEO treatment ($p<0.05$). At the 120-168h experiment, there was not differences between the treatments, perhaps the volatile components of EO had not effect on the bacterium and the tEO could only supported the inhibitory effect of CH coating. Sogut and Seydim [21] observed that, the edible chitosan film could decline the *E. coli* cell number by 1.0-1.5 log CFU/g in vitro. In other research, the cinnamon essential oil could improve the antibacterial effect of CH edible coating [10].

DOI: https://doi.org/10.14232/analecta.2022.1.71-76

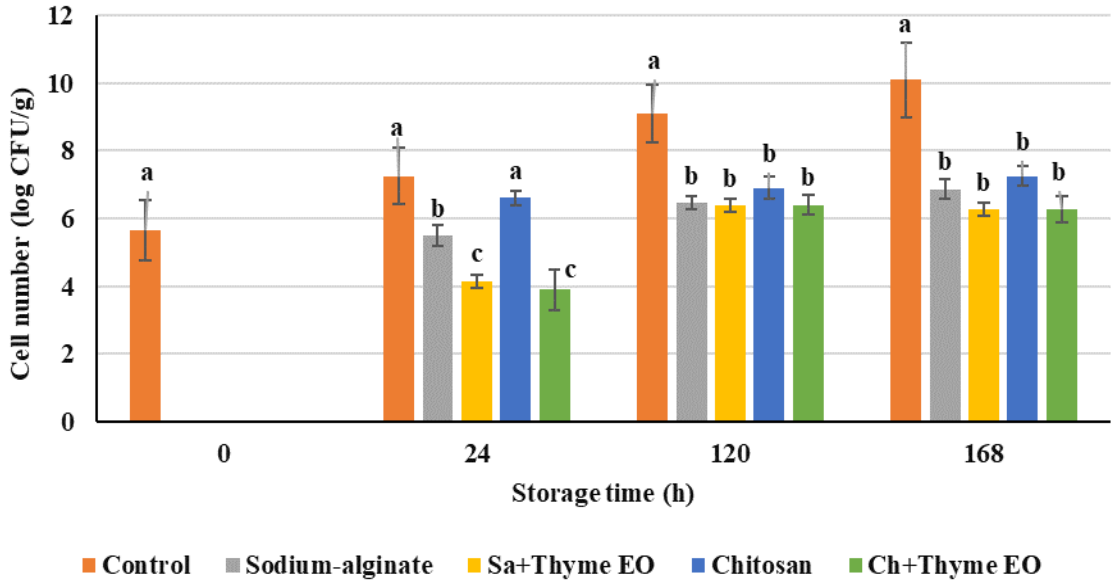

Diagram 1. Effect of edible coatings on E. coli (Different small letters indicate significant differences (p< 0.05))

The chitosan and alginate edible coating had a preservative effect on *E. faecalis* contaminated chicken breast fillet (Diagram 2.). There was same results as on *E. coli*, the AL could inhibit better cells in the first 24 hours, than CH. However, there were no significant differences between the CH and CH+tEO treatment, but the thyme EO raised the effect of AL edible coating, at the end, there was declining by 5 log CFU/g in the cell number. The *E. faecalis* was more sensitive to tEO in edible coating, than *E. coli* (Diagram 1-2.).

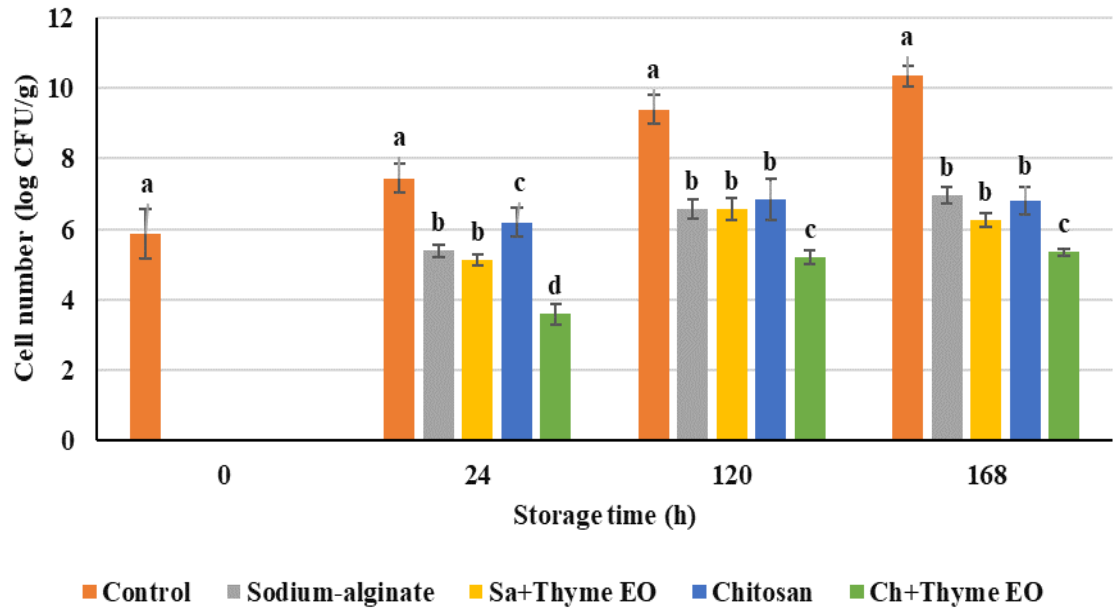

Diagram 2. Effect of edible coatings on E. faecalis (Different small letters indicate significant differences (p< 0.05))

DOI: https://doi.org/10.14232/analecta.2022.1.71-76

At the sensory evaluation, the taste of the prepared chicken fillet was around 3, and the chitosan+tEO got better points. In contrast, the odour of chitosan+tEO was scored down (2.3). In the background, perhaps, the gas permeability and water holding capacity of the two ECs were different, for this needs more examination. The overall acceptance was same, the panelists added 4.1-4.3 point (maximum point was 5).

Based on the results, the used edible coatings had a preservative effect on chicken breast fillet among 1 week, it could be an alternative way for extended the shelf life of raw meat. There is different sensitivity between the bacteria, there need more research for establishment the difference between the microbes, and how could be standardized the using of edible coating for preservation. Attention should also be attended to improving sensory properties in the future. It will be found that extracts, which match the best to the particular food.

4. CONCLUSIONS

Given today's global challenges (sustainability, environmentally friendly, renewable technology, customer demands), the need for new, green, alternative methods/technology for prolonging the shelf life of food with preserving or enhancing its impact on health is increasingly intensive. These biopolymer edible coatings in alone and combined with thyme EO were found to be effective against two investigated bacteria, can prolong the shelf life in refrigerated storage. Future studies are needed to establish the shelf-life extension effect of edible coatings on more different food, which have contaminated other microbes or multiple-species.

REFERENCES

[1] M. S. Fernandes, D. Y. Kabuki, A.Y. Kuaye. Behavior of Listeria Monocytogenes in a Multi-Species Biofilm with Enterococcus Faecalis and Enterococcus Feacium and Control Through Sanitation Procedures. Journal of Food Microbiology, 200 (2015), pp. 5-12. https://doi.org/10.1016/j.ijfoodmicro.2015.01.003

[2] E. Giaouris, E. Heir, M. Hébraud, N. Chorianopoulos, S. Langsrud, T. Møretrø, O. Habimana, M. Desvaux, S. Renier, G. J. Nychas, G. J. Attachment and Biofilm Formation by Foodborne Bacteria in Meat Processing Environments: Causes, Implications, Role of Bacterial Interactions and Control by Alternative Novel Methods. Meat Science, 97 (3) (2014), pp. 298-309. https://doi.org/10.1016/j.meatsci.2013.05.023

[3] O. Rendueles, J.M. Ghigo. Multi-Species Biofilms: How to Avoid Unfriendly Neighbors. FEMS Microbiology Reviews, 36 (2012), pp. 972-989. https://doi.org/10.1111/j.1574-6976.2012.00328.x

[4] M. Simões, L. C. Simões, M. J. Vieira. A Review of Current and Emergent Biofilm Control Strategies. LWT-Food Science and Technology, 43 (2010), pp. 573-583. https://doi.org/10.1016/j.lwt.2009.12.008

[5] B. Schumann, M. Schmid. Packaging Concepts for Fresh and Processed Meat – Recent Progresses. Innovative Food Science and Emerging Technologies, 47 (2018). https://doi.org/10.1016/j.ifset.2018.02.005

[6] G. H. Zhou, X. L. Xu, Y. Liu. Preservation Technologies for Fresh Meat – A Review. Meat Science, 86 (2010), pp. 119–128. https://doi.org/10.1016/j.meatsci.2010.04.033

[7] L. Motelica, D. Ficai, A. Ficai, O. Oprea, D. Kaya, E. Andronescu. Biodegradable Antimicrobial Food Packaging: Trends and Perspectives. Foods, 9 (2020), pp. 1438. https://doi.org/10.3390/foods9101438

[8] V. Falguera, J. P. Quintero, A. Jiménez, J. A. Muñoz, A. Ibarz. Edible Films and Coatings: Structures, Active Functions and Trends in Their Use. Trends in Food Science and Technology, 22 (6) (2011), pp. 292-303. https://doi.org/10.1016/j.tifs.2011.02.004

DOI: https://doi.org/10.14232/analecta.2022.1.71-76

[9] V. Coma, A. Martial-Gros, S. Garreau, A. Copinet, F. Salin, A. Deschamps. Edible Antimicrobial Films Based on Chitosan Matrix. Journal of Food Science, 67 (2002), pp. 1162-1169. https://doi.org/10.1111/j.1365-2621.2002.tb09470.x
[10] M. Z. Elsabee, E. S. Abdou. Chitosan Based Edible Films and Coatings: A Review. Materials Science and Engineering: C Biomaterials, 33 (4) (2013), pp. 1819-41. https://doi.org/10.1016/j.msec.2013.01.010
[11] D. H. Ngo, T. S. Vo, D. N. Ngo, K. H. Kang, J. Y. Je, H. N. D. Pham, H. G. Byun, S. K. Kim. Biological effects of chitosan and its derivatives. Food Hydrocolloids, 51 (2015), pp. 200-216. https://doi.org/10.1016/j.foodhyd.2015.05.023
[12] R. Ribeiro-Santos, M. Andrade, N. R. de Melo, A. Sanches-Silva. Use of Essential Oils in Active Food Packaging: Recent Advances and Future Trends. Trends in Food Science and Technology, 61 (2017), pp. 132-140. https://doi.org/10.1016/j.tifs.2016.11.021
[13] D. S. Cha, M. S. Chinnan. Biopolymer-Based Antimicrobial Packaging: A Review. Critical Reviews in Food Science and Nutrition, 44 (4) (2004), pp. 223-237. https://doi.org/10.1080/10408690490464276
[14] A. Kurucz, E. Gyimes. Edible Film Coatings for the Packaging of Pre-Cooked Poultry Meat Products (frankfurters). Journal of Food Investigation 62 (2016), pp. 952-955.
[15] E. Tavassoli-Kafrani, H. Shekarchizadeh, M. Masoudpour-Behabadi. Development of Edible Films and Coatings from Alginates and Carrageenans. Carbohydrate Polymers, 137 (2016), pp. 360-374. https://doi.org/10.1016/j.carbpol.2015.10.074
[16] S. Burt. Essential Oils: Their Antibacterial Properties and Potential Applications in Foods - A Review. International Journal of Food Microbiology, 94 (2004), pp. 223–253. https://doi.org/10.1016/j.ijfoodmicro.2004.03.022
[17] FDA.gov, Food Additive Status List [online] Available at:https://www.fda.gov/food/food-additives-petitions/food-additive-status-list#additives (Accessed 21.02.2022)
[18] E. B. Kerekes, A. Vidács, M. Takó, T. Petkovits, C. Vágvölgyi, G. Horváth, V. L. Balázs, J. Krisch. Anti-Biofilm Effect of Selected Essential Oils and Main Components on Mono- and Polymicrobic Bacterial Cultures. Microorganisms, 7 (2019), pp. 345. https://doi.org/10.3390/microorganisms7090345
[19] B. D. Jett, K. L. Hatter, M. M. Huycke, M. S. Gilmore. (1997): Simplified Agar Plate Method For Quantifying Viable Bacteria. BioTechniques, 23 (1997), pp. 648-650. https://doi.org/10.2144/97234bm22
[20] L. Cao, W. Lu, A. Mata, K. Nishinari, Y. Fang. Egg-Box Model-Based Gelation of Alginate and Pectin: A Review. Carbohydrate Polymers, 242 (2020), pp. 116389. https://doi.org/10.1016/j.carbpol.2020.116389
[21] E. Sogut, A. C. Seydim. The Effects of Chitosan and Grape Seed Extract-Based Edible Films on the Quality of Vacuum Packaged Chicken Breast Fillets. Food Packaging and Shelf Life, 18 (2018), pp. 13-20. https://doi.org/10.1016/j.fpsl.2018.07.006

DOI: https://doi.org/10.14232/analecta.2022.1.71-76

Analecta Technica Szegedinensia
Vol. 16, No. 01 ISSN 2064-7964 2022

ENRICHMENT OF RARE EARTH ELEMENTS FROM CONTAMINATED BIOMASS PRIOR TO EXTRACTION

[1]Truong Dinh, [1]Zsolt Dobó, [1]Helga Kovács*

[1]Institute of Energy and Quality, University of Miskolc, 3515 Miskolc, Hungary
email: truong.dinh@uni-miskolc.hu

ABSTRACT

Under the context of reserve depletion, recovering rare earth elements (REEs) from secondary resources is essential which assists to strengthen the circular economy. Contaminated biomass growing from brownfield lands is a potential material for REE recovery. However, prior to the extraction stage, polluted plants need to be lessened to a manageable volume. In this study, contaminated biomass gathered from an abandoned mining area was combusted in a pilot-scale boiler, while solid residuals from different positions in the burning system were collected and analyzed. Higher REE concentration in the ash samples compared to that in the woody biomass indicates the efficiency of the combustion process from the metal enrichment point of view. The significant metal concentration in the solid remains is an advantage for the following step of extraction to reclaim REEs. It was concluded that the concentration of REEs in bottom ash is greater than in the other solid residuals. That indicates that the volatility of rare earth minerals is limited during biomass incineration.

Keywords: rare earth metals, contaminated biomass, combustion, recovery

1. INTRODUCTION

Rare earth elements (REEs) are a group of 17 chemically similar metallic elements comprising Y (yttrium), Sc (scandium), and 15 "lanthanides" elements [1]. The term “rare” refers to they are not commonly found in commercially viable concentrations. REEs are vital in green modern technologies such as wind turbines, batteries, electric cars, hybrid cars, etc [2]. These valuable elements are deemed as critical strategic materials due to their importance and vulnerable supply [3], [4]. The demand for rare earths has surged noticeably which could lead to reserve depletion. While recycling rate of REEs from end-products reportedly is only 1% [2]. Therefore, reclaiming rare earth minerals from secondary resources is essential to strengthening the circular economy.

Phytomining is an innovative approach for recovering REEs in brownfield lands where conventional mining techniques are neither effective nor profitable [5]. In the initial stage of the entire phytomining pathway, plants accumulate REEs from soils and store them into their roots and shoots referred to as the phytoextraction process [6]. Following that, rare earth minerals accumulated in plants could be reclaimed via extraction technologies [7]–[9]. However, before the extraction process, contaminated biomass needs to be reduced, and REEs would be enriched in solid residuals called bio-ores [10]. Several enrichment manners including composting, compaction, thermal conversion (ashing, pyrolysis, gasification, combustion) have been mentioned [11], [12]. To date, only a few studies about heightening REEs from biomass have been conducted so far. C. Liu et al. incinerated *Dicranopteris linearis* fern at 500 °C to remove organic matter and elevate rare earths in ash [13]. It was observed that 2032 mg kg^{-1} REEs in the plant was enhanced to 15956 mg kg^{-1} in the solid remain; and 93% of rare earth metal input from the biomass was converted into the ash sample. Likewise, incineration of the collected fern *Dicranopteris linearis* at 550 °C resulted in 92.3% mass reduction [10]. The concentration of REEs in the ash (30000 mg kg^{-1}) is over eleven times greater than in the plant (2700 mg kg^{-1}). In another study, an ecologically friendly pathway of vacuum-pyrolysis-condensation was proposed for elevating rare earth minerals [14]. The results unveiled that the pyrolytic product derived from harvested fern *Dicranopteris linearis* contenting 1948.67 mg kg^{-1} rare earths could reach a level of 6160 mg kg^{-1} REEs.

DOI: https://doi.org/10.14232/analecta.2022.1.77-82

Enrichment is a crucial stage in the whole concept of phytomining to recover rare earth metals. The available information pertained to that is scanty and sparse. This research investigates the heightening of REEs from contaminated biomass via the combustion process and the behavior of these metals in the burning system.

2. MATERIALS AND METHODS

The resource of biomass utilized in this research is a brownfield land located in Gyöngyösoroszi, Hungary. In fact, it is an abandoned mining area where industrial lead and zinc production was operating until 1986. The common ligneous plant species living there are oak, pine, wattle, walnut, birch, poplar, bushes, etc. From the contaminated land, bulk biomass collection was done including the necessary sample preparation steps such as drying, grinding, and pelletizing to the required dimensions for the boiler operation. The polluted woody pellet is a mixture of 75:16:9 % of trunk, branches, leaf respectively, corresponding to the mass ratio of a real tree. The general properties of the contaminated biomass are given in Table 1.

Table 1. Properties of the contaminated biomass

Pellet's diameter mm	Pellet's height mm	Element (m/m %)				Moisture content m/m %	Ash content m/m %
		N	C	H	S		
6	10–30	0.395	46.747	6.050	0.0143	5.62	2.30

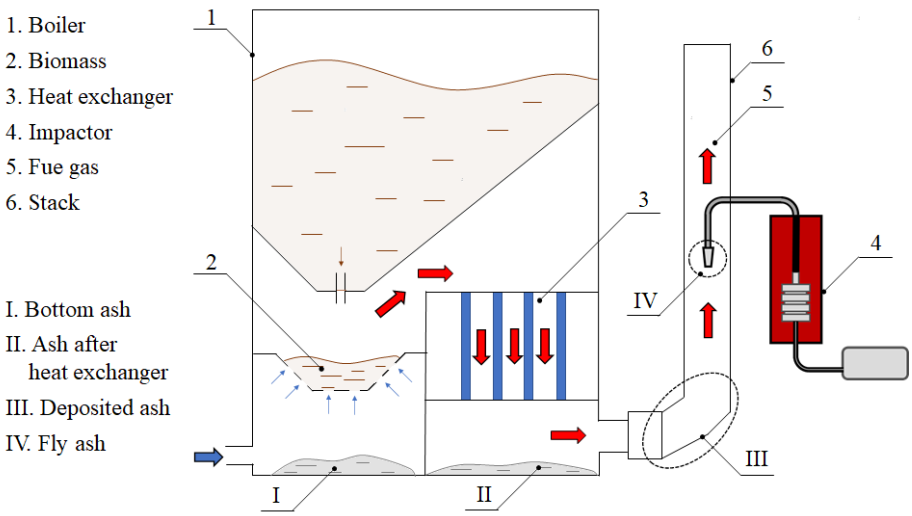

Figure 1. Positions of solid remain collection

To achieve the major purposes of the study, a series of four combustion experiments utilizing contaminated pellets was conducted in a pilot-scale boiler. The experiments were carried out under the same operational circumstances as follows firing rate: Q = 27.6–31.4 kW, fuel feed rate: f = 8.3 kg h^{-1}, typical combustion chamber temperature: T = 882–956 °C. Solid combustion residuals were captured from preselected points as seen in Figure 1. After experiments, bottom ash and after heat exchanger ash were respectively collected from the ashtray and at the position after the heat exchanger. The deposited ash sample was taken from the inside wall of the stack at the end of the combustion process. The capture of fly ash was implemented by an isokinetic fly ash sampling system using a three-stage cascades impactor labeled Dekati® PM10. The collection started after the boiler reached steady-state operational conditions, and the sampling method

DOI: https://doi.org/10.14232/analecta.2022.1.77-82

meets the regulations of the ISO23210 standard. The typical flue gas temperature at the point of fly ash sampling is in the range of 155-158 °C.

The woody biomass (WB) sample used for all the incineration experiments together with combustion ashes are taken for chemical analysis. The combustion ashes include four types of solid remains namely bottom ash (BA), after heat exchanger ash (EA), deposited ash (DA), and fly ash (FA) collected from four combustion experiments. The chemical analysis of the solid samples determined by ICP (Inductively Coupled Plasma) spectrometry was performed by an individual company in Hungary. Perkin Elmer Avio 200 inductively coupled plasma-optical emission spectrometer (ICP-OES) and ICP mass spectrometry (ICP-MS) are employed for the analysis. For the calibration of the measurement, an ICP-OES inner standard solution (Lutecium) was used. The samples were prepared based on the Hungarian standard MSZ EN 13346:2000. The analytical scale was used for taking 5 g samples for analysis. The preparation was carried out by microwave digestion with a Berghof Speedwave4 laboratory equipment, using nitric acid (2 ml, 67% concentrated) and hydrochloric acid (6 ml, 36% concentrated) solvents. The digestion and dissolution time were 30 minutes at 180 °C. The solution was filled up to 50 ml with 5% concentrated nitric acid after the filtration process using MN616 filters. The chemical measurement analyzes the concentrations of most REEs (15 elements namely Ce, Dy, Er, Eu, Gd, Ho, La, Nd, Pr, Sc, Sm, Tb, Tm, Y, Yb) in the solid samples.

3. RESULTS AND DISCUSSION

The analytical outcomes of the solid samples are divided into two metal groups. The first classification consists of Er (erbium), Eu (europium), Ho (holmium), Pr (praseodymium), Tb (terbium), Tm (thulium), Yb (ytterbium) which are below the detection limit (BDL) in all the solid samples. No further investigation nor discussion was made for these elements.

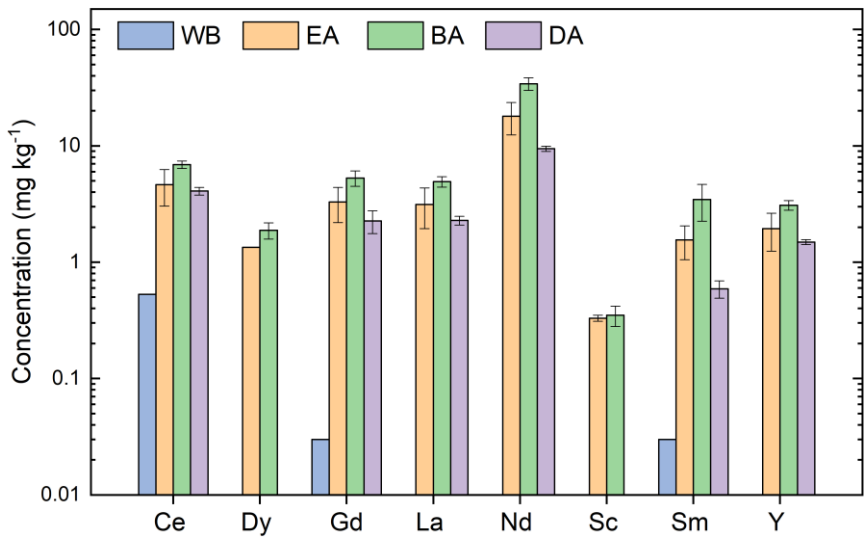

Figure 2. Average concentration of detectable REEs

The second metal group comprises Ce (cerium), Dy (dysprosium), Gd (gadolinium), La (lanthanum), Nd (neodymium), Sc (scandium), Sm (samarium), Y (yttrium) which are detectable in at least one sample. These elements depicted in Table 2 are used for further investigations and calculations. The concentration magnitudes were colorized in the increasing order of green-yellow-red. Intuitively, the elemental concentration results of different experiments in the combustion series largely perform the similarity. In

DOI: https://doi.org/10.14232/analecta.2022.1.77-82

order to deeply assess the reproducibility as well as for further discussion and evaluation, the mean value of the outcomes alongside its standard deviation are calculated and presented in Table 2. Based on the graph, the level of standard deviation is not so high versus its average concentration. It demonstrates that the combustion experiments and their upshots are reproducible.

Several REEs were identified in the solid samples at considerable levels. The most significant results were observed in the case of Nd, such as 34.2 mg kg^{-1} in bottom ash, 18 mg kg^{-1} in after heat exchanger ash, and 9.43 mg kg^{-1} in deposited ash. On the other hand, Sc was scarcely found in the solid remains. The concentration of REEs in fly ash is either below the detection limit or not available. REEs show a consistent trend in the burning system, their levels follow the decreasing order: bottom ash > after heat exchanger ash > deposited ash > woody biomass (Figure 2). The greater concentration in bottom ash versus other ash samples unveils the low volatility of rare earth metal compounds during incineration.

Table 2. Concentration of detectable REEs (mg kg^{-1})

Sample		Element							
		Ce	Dy	Gd	La	Nd	Sc	Sm	Y
Biomass	WB	0.526	<1*	0.026	<0.25*	<0.5*	<0.01*	0.026	<0.25*
Fly ash	FA-1	-	<7.5*	<3*	-	-	-	<3*	-
	FA-2	-	<7.5*	<0.2*	-	-	-	<0.2*	-
	FA-3	-	<10*	<4*	-	-	-	<4*	-
	FA-4	-	<7.5*	<0.2*	-	-	-	<0.2*	-
After heat exchanger ash	EA-1	6.29	<1*	4.03	4.04	18.8	0.344	1.64	2.39
	EA-2	5.71	1.34	4.35	4.16	23.9	0.309	2.18	2.64
	EA-3	3.77	<1*	2.91	2.53	19	<0.25*	1.22	1.60
	EA-4	2.80	<1*	1.87	1.81	10.4	<0.01*	1.15	1.11
Bottom ash	BA-1	6.59	1.50	6.26	4.72	37	0.290	3.49	2.93
	BA-2	7.22	2.16	5.30	5.25	35.8	0.416	5.04	3.35
	BA-3	6.35	1.66	4.30	4.25	27.9	0.304	2.30	2.79
	BA-4	7.44	2.18	5.27	5.47	36.2	0.402	2.97	3.30
Deposited ash	DA-1	4.21	<2*	<10*	2.61	8.73	<0.5*	<5*	1.57
	DA-2	3.81	<2*	2.43	2.20	9.30	<0.01*	0.667	1.45
	DA-3	4.37	<4*	2.62	2.06	9.94	<1*	<2*	1.51
	DA-4	3.91	<2*	1.73	2.26	9.73	<0.01*	0.51	1.41

* The concentration of the metal is BDL (below the detection limit), which is the limit that the concentration can be differentiated from the background noise.
"-" not available

Enrichment factor (EF) is defined as the quotient of metal concentration in solid remains to that in woody biomass. This index is employed to describe the efficiency of the enrichment process in heightening metal levels. Certain elements encompassing Dy, La, Nd, Sc, Y were below the detection limits in the woody biomass. Nonetheless, as a result of the combustion process, their concentrations became high enough to be identified in at least one ash sample. Their enrichment factors were calculated based on the detection limits, which are the minimum values or the worst-case scenario. The minimum enrichment factor of these elements highlighted in red is depicted in Figure 3. In terms of detectable metals in plants including Ce,

DOI: https://doi.org/10.14232/analecta.2022.1.77-82

Gd, Sm, the real values of the enrichment factors are calculated and visualized into the graph (Figure 3). Generally, the enrichment factors vary in a wide range from more than one to over 200. The outstanding results were observed in the case of Gd (EF-BA = 203, EF-EA = 127) and Sm (EF-BA = 133, EF-EA = 60). In similarity to metal concentration, EF of REEs performs the same trend as follows: bottom ash > after heat exchanger ash > deposited ash. The enrichment factor is significant indicating the effectiveness of the combustion process in elevating metal concentrations from biomass into ashes. That is an advantage for the further stage of extraction to reclaim REEs from solid residues.

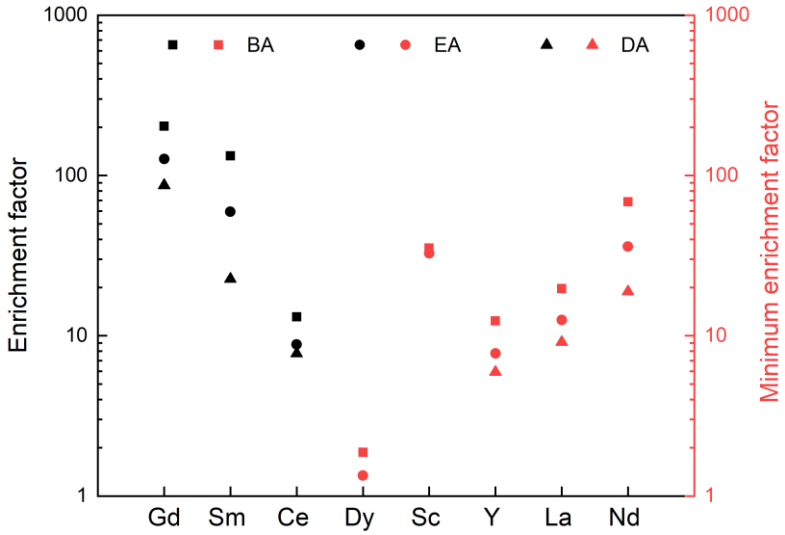

Figure 3. Enrichment factor

4. CONCLUSIONS

A series of combustion experiments utilizing contaminated pellets was conducted aiming to investigate the enrichment of REEs from biomass. Solid samples including woody biomass and solid residues were collected and dissected. The chemical analysis results are reproducible, which are the base of the following statements. The enrichment factor is significant indicating the efficiency of the combustion process in elevating metal concentrations from biomass into solid remains. High levels of REEs in the ash samples have benefits for the further step of extraction to reclaim these valuable elements. The greater concentration in bottom ash versus other ash samples indicates that the volatility of REEs is limited during biomass incineration. In the following study, major parameters having impacts on the distributions of REEs such as combustion temperature or flue gas temperature would be researched. Based on the results, further directions will be defined.

ACKNOWLEDGMENTS

The research was carried out at the University of Miskolc as part of both the “More efficient exploitation and use of subsurface resources” project implemented in the framework of the Thematic Excellence Program funded by the Ministry of Innovation and Technology of Hungary (Grant Contract reg. no.: NKFIH-846-8/2019) and the project titled “Developments aimed at increasing social benefits deriving from more efficient exploitation and utilization of domestic subsurface natural resources” supported by the Ministry of Innovation and Technology of Hungary from the National Research, Development and

Innovation Fund in line with the Grant Contract issued by the National Research, Development and Innovation Office (Grant Contract reg. no.: TKP-17-1/PALY-2020).

REFERENCES

[1] D. Schüler, M. Buchert, R. Liu, S. Dittrich, and C. Merz, "Study on rare earths and their recycling," *Öko-Institut eV Darmstadt*, vol. 49, pp. 30–40, 2011.
[2] V. Balaram, "Rare earth elements: A review of applications, occurrence, exploration, analysis, recycling, and environmental impact," *Geosci. Front.*, vol. 10, no. 4, pp. 1285–1303, Jul. 2019.
[3] S. Massari and M. Ruberti, "Rare earth elements as critical raw materials: Focus on international markets and future strategies," *Resour. Policy*, vol. 38, no. 1, pp. 36–43, Mar. 2013.
[4] G. Gunn, Ed., *Critical Metals Handbook*. Oxford: John Wiley & Sons, 2014.
[5] B. Jally, B. Laubie, Y.-T. Tang, and M.-O. Simonnot, "Processing of Plants to Products: Gold, REEs and Other Elements BT - Agromining: Farming for Metals: Extracting Unconventional Resources Using Plants," A. van der Ent, A. J. M. Baker, G. Echevarria, M.-O. Simonnot, and J. L. Morel, Eds. Cham: Springer International Publishing, 2021, pp. 63–74.
[6] A. van der Ent, A. J. M. Baker, G. Echevarria, M.-O. Simonnot, and J. L. Morel, Eds., *Agromining: Farming for Metals*. Cham: Springer International Publishing, 2021.
[7] Z. Chour *et al.*, "Recovery of rare earth elements from Dicranopteris dichotoma by an enhanced ion exchange leaching process," *Chem. Eng. Process. - Process Intensif.*, vol. 130, pp. 208–213, Aug. 2018.
[8] B. Laubie, Z. Chour, Y.-T. Tang, J.-L. Morel, M.-O. Simonnot, and L. Muhr, "REE Recovery from the Fern D. Dichotoma by Acid Oxalic Precipitation After Direct Leaching with EDTA," 2018, pp. 2659–2667.
[9] Z. Chour, B. Laubie, J. L. Morel, Y.-T. Tang, M.-O. Simonnot, and L. Muhr, "Basis for a new process for producing REE oxides from Dicranopteris linearis," *J. Environ. Chem. Eng.*, vol. 8, no. 4, p. 103961, Aug. 2020.
[10] B. Jally *et al.*, "A new method for recovering rare earth elements from the hyperaccumulating fern Dicranopteris linearis from China," *Miner. Eng.*, vol. 166, p. 106879, Jun. 2021.
[11] H. Kovacs and K. Szemmelveisz, "Disposal options for polluted plants grown on heavy metal contaminated brownfield lands – A review," *Chemosphere*, vol. 166, pp. 8–20, 2017.
[12] T. Dinh, Z. Dobo, and H. Kovacs, "Phytomining of noble metals – A review," *Chemosphere*, vol. 286, p. 131805, Jan. 2022.
[13] C. Liu *et al.*, "Element Case Studies: Rare Earth Elements," 2021, pp. 471–483.
[14] B. Qin *et al.*, "Vacuum pyrolysis method for reclamation of rare earth elements from hyperaccumulator Dicranopteris dichotoma grown in contaminated soil," *J. Clean. Prod.*, vol. 229, pp. 480–488, Aug. 2019.

Analecta Technica Szegedinensia
Vol. 16, No. 01 ISSN 2064-7964 2022

DEVELOPING FATIGUE TEST MACHINE FOR COMPOSITE MATERIAL

Péter Szuchy[1], Tamás Molnár[1], István Bíró[1], Sándor Csikós[2], László Gogolák[2], József Sárosi[2]

[1]Department of Mechanical Engineering, Faculty of Engineering, University of Szeged, Mars tér 7. 6724, Szeged, Hungary,
[2]Department of Mechatronics and Automation, Faculty of Engineering, University of Szeged, Mars tér 7. 6724, Szeged,
e-mail: szpeter@mk.u-szeged.hu

ABSTRACT

This paper's goal is to introduce the third step of the EFOP-3.6.1-16-2016-00014. project on the Faculty of Engineering, University of Szeged. In this period the production technology of composite material was chosen and a fatigue test machine was developed and tested. The paper shortly describes the composite materials and summarizes the theory of fatigue than it presents the process of the development with several prototypes of fatigue test machine, some of which were manufactured and tested. Initially a shaker played the key role in the first two conceptions and finally a crank mechanism became as the best solution. The main solved problems during the development were selection of bearings and solving the partly dynamic balancing of the moving parts.

Keywords: plastic composites, fatigue test machine, dynamic balancing

1. INTRODUCTION (FIRST LEVEL HEADINGS: TNR 10PT, CAPITAL LETTERS, JUSTIFIED)

Only 20% of a presently used cargo aircraft's take-off weight is the payload, approximately half of the rest 80% is the empty weight. Therefore it is evident that the less empty weight, the better for the economy. Due to this fact there is a huge demand in the aircraft industry for light structural materials with advanced parameters. The composite materials are one of the most promising materials from that perspective. Due to the scientific literature the advantages of composites: significant weight reduction, anisotropy, incorrodible, weatherproof, long lifetime, resistance against fatigue, vibration damping, structural severity, formal freedom, aesthetic outfit, retentivity, reasonable heat-expansion, low "tooling" costs, reduced radar wave reflection, low maintenance and operation costs. The disadvantages of the composites: high process costs, low shock and damage resistance (carbon-, graphite-, boron-fibre), tendency to static charge, low lightning-endurance, lower interlayer strength, weak surface press strength, complicated and expensive repair costs, moisture intake, distortion, deformation at overheating, significant differences between tensile and press stress [1-3].
In our opinion the resistance against fatigue needs some more investigations. The composite materials are composed of at least two macroscopically and functionally separable materials in a definite structure. The base materials of the composite technology: reinforcing materials (frame materials, reinforcing fibres), matrix materials (bedding materials), core materials, adhesives, bulking agents, additives. For the purposes of the project the most important ingredients are the reinforcing and the matrix materials. The reinforcing materials are one of the main component parts of the composite materials that ensure the mechanical strength and rigidity of the structure. The matrix materials create the mechanical connection between the separate reinforcing fibres, take the awakening shear stresses, preventing their movement to the others, ensuring the structural integrity. The other parts are not relevant for our investigations [1-3].
In this project the composite material made of woven carbon fibres in epoxy resin produced by vacuum-infusion procession was determined to investigate for fatigue with different number of reinforcing layers. Some of the self-produced specimens were tested only by tensile machine, the others are going to be tested first by fatigue test machine with 10 million loads, and after that comes the tensile test. The difference between the two tensile tests will give details to the resistance against fatigue theory.
Fatigue is one of the most frequent causes for operational failure when the breakage of the material occurs due to fluctuating loads even the occurring stress is far below the yield point. The Wöhler diagram of composite materials is similar to the metal fatigue: it represents the resistance of the tested material to

DOI: https://doi.org/10.14232/analecta.2022.1.83-89

cyclic loads. The diagram shows the fact that the material strength reduces with repeated application of load and inversely proportional to the number of cycles applied. The strength value of the previously determined number of cycles is commonly taken as the fatigue limit. In some cases this is a "true" fatigue limit, when the stress value is below the limit, no fatigue mechanism occurs. But in most cases it is only valid till the operation reaches the selected number of cycles. [4-5].

2. DISCUSSION – DEVELOPING THE FATIGUE TEST MACHINE

Initially an extant Brüel & Kjaer LDS V200 shaker had the key role in the ideas of constructions. The axial loading was the obvious solution (Fig. 1.) where the shaker could prepare repeated normal stress in one direction in the centerline of the sections.

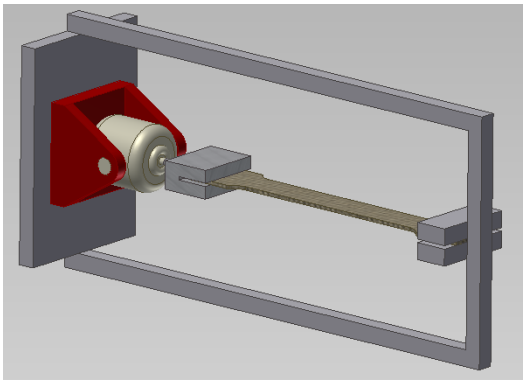

Fig. 1. Model of the tensile fatigue test machine with shaker

As the maximum force of the shaker is only 17,8 N, the tensile stress was not enough high for the specimens which sizes were determined earlier for the tests. So the concept turned to the direction of bending where a smaller force can be compensated with longer arm of force to achieve higher stress. As a specimen with rectangle section with base *b* and height *v* is loaded by a force *F* parallel with *v*, going through the centroid of the section, with a distance *l* from the fixed support, than the maximum bending moment at the fixed support [6]:

$$M = lF \tag{1}$$

The second moment of a cross section *b* x *v* to the main inertia axis *x*:

$$I_{xs} = \frac{bv^3}{12} \tag{2}$$

Accordingly the maximum stress in the section of the fixed support:

$$\sigma_{max} = \frac{M}{I_{xs}}\frac{v}{2} = \frac{12lF}{bv^3}\frac{v}{2} = \frac{6lF}{bv^2} \tag{3}$$

The maximum deflection (where *E* is the Young-modulus):

$$y = \frac{Fl^3}{3I_{xs}E} \tag{4}$$

from which expressing the force *F* and with the substitution of (2):

$$F = \frac{3I_{xs}Ey}{l^3} = \frac{bv^3Ey}{4l^3} \tag{5}$$

DOI: https://doi.org/10.14232/analecta.2022.1.83-89

The maximum stress based on (5) and (3) equations:

$$\sigma_{max} = \frac{6l}{bv^2}\frac{bv^3 Ey}{4l^3} = \frac{3}{2}\frac{vEy}{l^2} \quad (6)$$

As the Young-modulus can be expressed from the previously achieved tensile diagrams, the bending of specimen was really encouraging (Fig. 2.).

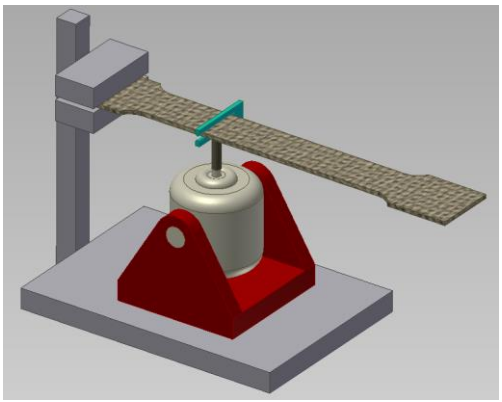

Fig. 2. Model of bending fatigue testing machine

However the maximum amplitude of the shaker is 5 mm that is far than enough to keep the validation of the small deflection equations but not enough to reach the limit stress of fatigue. So the usage of the shaker had to be thrown out and instead of it the rotational movement came into prominence. This was solved easily by a single-phase asynchronous motor controlled by frequency converter. At the first version the horizontally fixed specimen was bended uni-directionally by a pin mounted on a rotating disc (Fig. 3.).

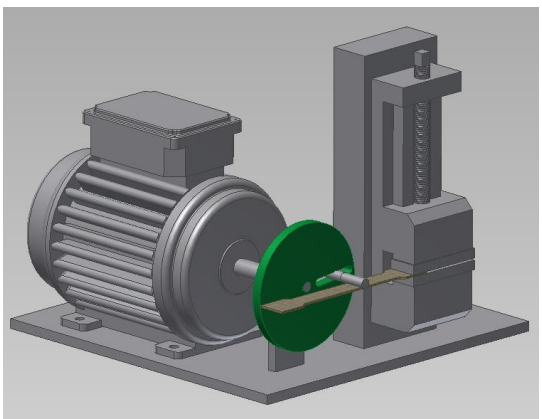

Fig. 3. Uni-directionally bended specimen by rotating disc with pin.

As the construction was extra simple to manufacture the test measures were shortly executed. It was observed that the arrival of the pin to the surface of the specimen is too dynamic, shocking-like, that would probably lead the specimen to go broke earlier than the fatigue would do it. Furthermore the one side bending was not considered effective enough, the symmetric, both directional bending and loading came to the fore.

DOI: https://doi.org/10.14232/analecta.2022.1.83-89

This was the way how the bending fatigue test machine with crank mechanism appeared of which the first model is shown on Fig. 4.

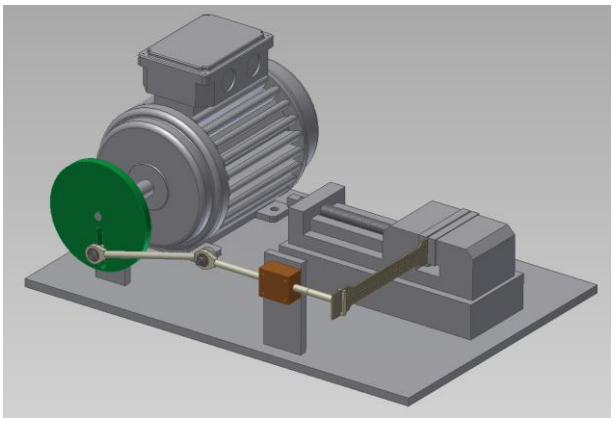

Fig. 4. First model of the bending fatigue test machine with crank mechanism

The main problem in that period of development was choosing the proper, obtainable bearings. Only commercially available bearings, housings and coupling rods were planned to apply. The accelerations due to the relatively high frequency (10 Hz) cause significant bearing forces despite of the small masses. For the self-aligning radial bearings at the rod ends a heavy-duty rod end with integral self-aligning, double row ball bearing, for supporting the horizontally moving coupling rod a sliding bearing with sinterbronze bearing bush was chosen. Due to the lubricant pressed into the porous material during production the maximum sliding speed of this kind of sliding bearing is 10 m/s that is far above our needs. Conversely, two pieces of 08.12.20 (8 mm inner, 12 mm outer diameter, 20 mm length) bush were applied for the horizontal support, and the housing was manufactured at the Faculty. The bushes were controlled against surface pressure by the loading model of Fig.7.

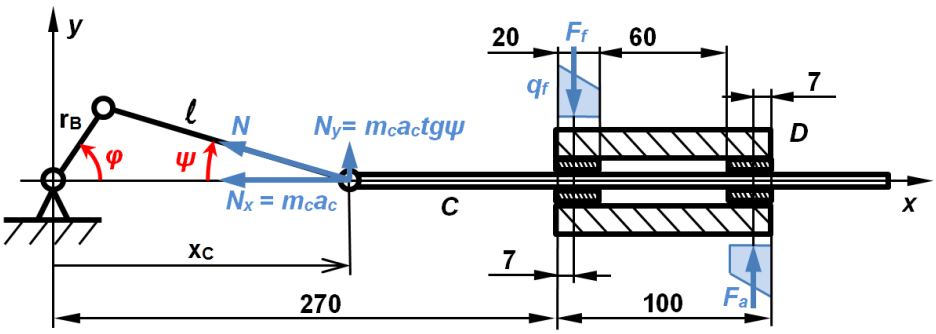

Fig. 7. Loading model of the bushes

At the first model with crank mechanism the previously used disk was taken over, in which there was only one radial slot for setting the bending deflection's size of the specimen. But the accelerations of the crank mechanism were so high that a partly dynamic balancing of the masses [7-8] was neccessary, and the best location of it was on the disc (Fig. 8.).

DOI: https://doi.org/10.14232/analecta.2022.1.83-89

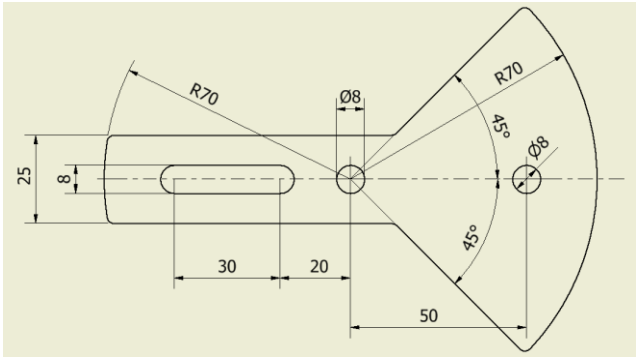

Fig. 8. Disk of the crank mechanism optimized for partly dynamic load [10]

The disk can be divided to two parts (see Fig. 8.): the right one consists of a circular sector with 90° central angle, the other part is the rest of the disc, named stick. The sector's centre of mass measured from the middle point of the circle in case of r=70mm, α=90° (without the hole):

$$r_e = \frac{2}{3}\frac{r\,sin^{\alpha}/_2}{\alpha/_2} = \frac{2}{3}\frac{70mm\frac{\sqrt{2}}{2}}{\frac{\pi}{4}} = \frac{4}{3}\frac{70mm\,\sqrt{2}}{\pi} = 42\ mm \tag{7}$$

The mass of the quarter circle if the width of the disc is v=10 mm:

$$m_e = \frac{r^2\pi}{4}v\rho = \frac{(0{,}07m)^2\pi}{4}0{,}01m\ 7850\frac{kg}{m^3} = 0{,}30\ kg \tag{8}$$

The kinetic model of the crank mechanism with point-like masses without extension is introduced by Fig. 9.:

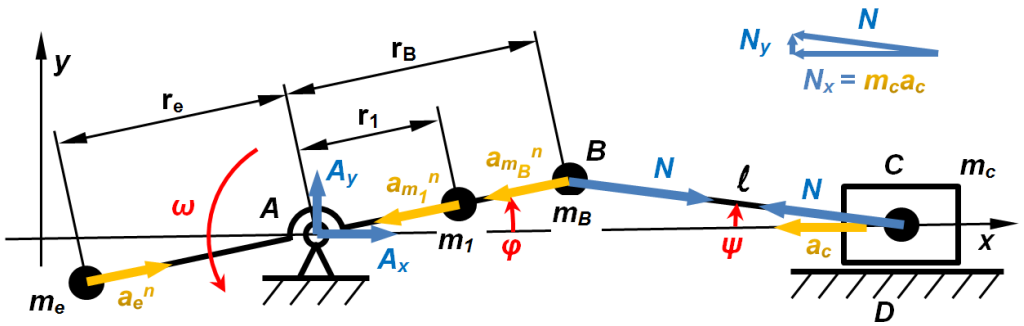

Fig. 9. Kinetic model of crank mechanism [10]

At the kinetic model of crank mechanism the masses are considered without extension: m_e is the mass of the circle section part, m_1 is the mass of the stick, m_B is the mass of pin, bearing and housing connected to the disc, together with the half of the crank, m_C is the mass of the coupling rod with the connected bearing, housing and the other half of the crank. As an engineering approximation the angular velocity of disc ω is considered constant. Accordingly the relationships are the followings:

$$r_B sin\,\varphi = l\,sin\psi \tag{9}$$

$$\psi = arc\,sin\frac{r_B}{l}\,sin\varphi \tag{10}$$

DOI: https://doi.org/10.14232/analecta.2022.1.83-89

$$N = \frac{m_C\, a_C}{\cos\psi} \tag{11}$$

The kinetic equations of movement written to *x* and *y* direction according to D'Alambert:

$$-m_e\, r_e\omega^2 cos\varphi + m_1\, r_1\omega^2 cos\varphi + m_B\, r_B\omega^2 cos\varphi - m_C a_C + A_x = 0 \tag{12}$$

$$-m_e\, r_e\omega^2 sin\varphi + m_1\, r_1\omega^2 sin\varphi + m_B\, r_B\omega^2 sin\varphi - m_C a_C tg\psi + A_y = 0 \tag{13}$$

and so the *x* and *y* directional force components awakening in the point *A*:

$$A_x = m_C a_C + \omega^2\,(m_e\, r_e cos\varphi - m_1\, r_1 cos\varphi - m_B\, r_B cos\varphi) \tag{14}$$

$$A_y = m_C a_C + \omega^2\,(m_e\, r_e sin\varphi - m_1\, r_1 sin\varphi - m_B\, r_B sin\varphi) \tag{15}$$

According to (14) and (15) equations a numerical analysis was executed, on which base an optimization was implemented [9]. The goal of the optimization was bringing to the same level the maximum value of the A_x and A_y bearing force components. Fig. 10. presents the changes of the bearing force components during a whole rotation beside optimized parameters. By increasing the mass m_e of the counterweight, the maximum value of the force component A_x decreases, and the maximum value of A_y increases. As the counterweight decreases, the consequence is converse.

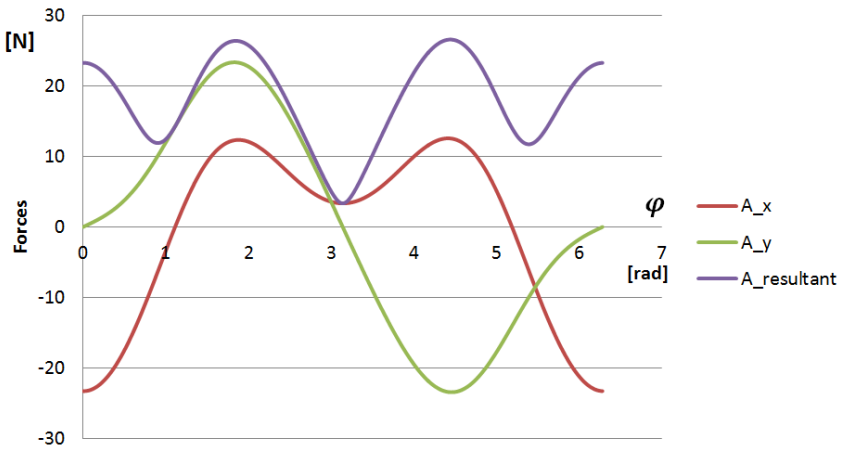

Fig. 10. Changes of force A and x, y components of it during a whole rotation [10]

The test of the fatigue machine with the partly dynamic balanced crank mechanism was successful. For rotation control of the electric motor a frequency converter was applied. For counting the number of bending an optical sensor with a CPU was installed.

3. CONCLUSIONS

One of the main goals of this project was to investigate the fatigue of the previously specialized composite materials and for this purpose a fatigue test machine was developed and manufactured. During the construction initially an extant shaker played the key role, than an electric drive and crank mechanism came to the front. In the course of the development the bearings and the partly dynamic balancing had got special attention. The fatigue machine was completed and was working for more than 20 weeks without any problems. As one specimen's test needed almost two weeks continuous work of the fatigue machine, a new development idea emerged for a multi-gripping and bending system that could be developed in the future.

DOI: https://doi.org/10.14232/analecta.2022.1.83-89

ACKNOWLEDGEMENTS

The project has been supported by the European Union, co-financed by the European Social Fund. EFOP-3.6.1-16-2016-00014. Authors are thankful for it.

REFERENCES

[1] Czvikovszky – Nagy – Gaál: A polimertechnika alapjai, Műegyetemi Kiadó, 2000
[2] Lukács – Csomós – Gácsi - Karcagi – Magyar – Tomolya: Fáradásos repedésterjedés különböző típusú kompozitokban, Anyagvizsgálók Lapja, 2004/4
[3] Koncz – Magyarosi – Pusztai: Kompozitok és szendvicsszerkezetek - Repülőgép kompozit szerkezetjavító szakmai oktatási jegyzet, 2000
[4] Taljera, Ramesh: Fatigue of Composite Materials, In book: Modenr Trends in Composite Laminates Mechanics, Researchgate.net, January 2003. DOI: 10.1007/978-3-7091-2544-1_6 https://www.researchgate.net/publication/312849090_Fatigue_of_Composite_Materials
[5] Zsáry, Árpád: Gépelemek I, Tankönyvkiadó, Budapest, 1989. ISBN 963 18 1453 X
[6] M. Csizmadia, Béla: Statika, Nemzeti Tankönyvkiadó Zrt., Gödöllő-Budapest, 1996. ISBN 978-963-19-2850-1, ISSN 1416-535X
[7] Duffy, J.: Analysis of mechanisms and robot manipulators. Arnold, London, 1980.
[8] Haug, E. J.: Elements and methods computational dynamics, in E. J. HAUG, ed., Computer Aided Analysis and Optimization of Mechanical System Dynamics, Berlin, Springer, 1984. p. 3-21.
[9] Kármán, T. ; Biot, M. A.: Matematikai módszerek műszaki feladatok megoldására. Műszaki Könyvkiadó, Budapest, 1963.
[10] Péter Szuchy, Tamás Molnár, István Bíró, Sándor Csikós, László Gogolák, József Sárosi: Bending fatigue tests of carbon fiber reinforced epoxy resin composite plates, Acta Polytechnica Hungarica Vol. 18, No. 2, 2021

Analecta Technica Szegedinensia
Vol. 16, No. 01 ISSN 2064-7964 2022

CUSTOMER ACQUISITION ACTIVITIES OF WEB STORES

[1]Edina Lendvai, [1]Gábor Tóth

[1]University of Szeged, Faculty of Engineering, Mars tér 7.,6724 Szeged, Hungary,
e-mail: lendvai@mk.u-szeged.hu

ABSTRACT

Based on the domestic and international market trends of the last decades, it can be stated that the number and turnover of web stores, internet commerce is growing dynamically from year to year. The aim of our research is to explore the effective, proven customer acquisition methods of modern web stores. As part of this, the subject of our literature research was to explore the popular advertising platforms for web stores and their basic marketing principles and their optimal structure based on them. In our professional research, on the one hand, we explored through structured interviews what methods and communication are considered effective by the three webshops competing and selling in the different markets based on their experiences. On the other hand, we examined the shopping habits and preferences of consumers in the form of a questionnaire. The information obtained in this way can be crucial in planning the marketing strategy for any existing or new web store. We have found that one of the most important attributes in acquiring customers is reliability. From the beginning, you should strive for positive customer reviews as well as regular value creation proficiency must be demonstrated through content production, with which the business can build a committed community.

Keywords: marketing communication, consumer habits, structured interview, questionnaire

1. INTRODUCTION

E-commerce is an abbreviation for internet/electronic commerce, which is more recently referred to in common parlance as several other synonyms, such as internet commerce, online commerce, e-commerce, online purchase, or online selling. Essentially, every concept embraces the emergence of e-commerce: The sale and purchase of goods take place via the Internet, which includes payment transactions too. E-commerce saves a lot of time and energy for the customer, as the process is much simpler than an average purchase. It is not tied to opening hours, the desired goods or services can be accessed and ordered even from the desk, we can order products or services not only from Hungary but also from the other part of the world. However, customers may find themselves in a vulnerable situation, as they cannot check the authenticity of the seller or the quality and parameters of the ordered product [1.]. On the other hand, the fact that payment transactions take place online is not the only condition for a sale to be considered as e-commerce. Often, payment transactions do not take place online but offline when the e-merchant provides the opportunity to do so. This is the case, for example, with the postpaid or in-store collection. Regardless, the process of the purchase took place in the online space. Drawing from these results, it can be concluded that all sales when the buyer and seller meet online, the buyer selects from the offered goods online and the sale and purchase are also recorded online mean e-commerce [2.]. From a legal point of view, acts relevant to electronic means by distant actors that constitute a civil law relationship between individually identified entities are referred to as e-commerce. An additional condition for this is that the provisions on electronic commerce are not excluded [3.].

In recent decades, digitalization has led to a steady increase in online shopping. In 2019, internet commerce grew by 16%, but restrictions caused by the coronavirus epidemic further increased this number. Research has shown that there is an increase in almost all product categories, but personal interviews have also shown that the limiting factors in people's minds and their reservations about online shopping have not diminished, so the sudden jump is only due to restrictions on offline shopping[4.]. During the coronavirus epidemic, global e-commerce performance has also increased. It increased from 6 percent in 2019 to 19

DOI: https://doi.org/10.14232/analecta.2022.1.90-96

percent per year by 2020, according to a 2021 annual report presented by the United Nations Conference on Trade and Development (UNCTAD) [4.]

1.1 The types of webshops

In order to understand the marketing of different websites, we need to know exactly what kind of webstore we have to deal with. These fundamentally determine the target group of the company, the products it sells to, the methods it uses to reach customers, and its role in the pricing strategy.

Based on several sources, the following categories have been defined:

- From a direction point of view: According to the direction of sales, we distinguish between the B2B and B2C webshop as we discussed above. A feature of business-to-business webstores is that they sell to companies. In contrast, business-to-customer webshops sell their products and services to individuals [2.].

- Quality of the product: According to the quality of the goods, we can speak about 2 large groups, which can also be divided into 2-2 smaller groups. The first large group is the online stores that sell their products. There are online stores that sell physical products, which is practically the application of the model used in offline shopping to online interfaces. In this case, the consumer buys a product that actually exists in the physical reality, who can take it over during personal pick-up or delivery of the product he or she has ordered. There are stores that do not sell physical products. These are typically accessed by the consumer immediately after the processing and confirmation of the payment transaction, so immediately after the purchase is completed, because this product does not need to be delivered. We can talk about products purchased online which can be used in cyberspace. Such a product can be an e-book, a document, or software. The second large group is the webshops which sell services. As in the previous group, it can be divided into two subgroups. In the case of webshops selling physical services, only the order is finalized and recorded in the online space, the service is already performed offline. Among the practical examples, the most common are the various personal trainings, language courses, and wellness services that can be ordered online. In contrast, in the case of those selling non-physical services, similar to those selling non-physical products, the performance also typically begins after the end of the sale. In reality, this group includes online order packages from various mobile operators, online training interfaces, various coaching services, consulting services, etc...

- We can classify webshops according to the number of goods. There are also two extremes here. The first group includes single-product webstores, which, contrary to their name, can even sell a service on their website. In practice, we talk about this when only one product or service can be ordered on a website. This is most often the case with various books, cosmetics, food supplements, or web developers and virtual assistants when we want to speak about services. The other group is the multi-product webshops. This includes a fairly wide range of websites that sell hundreds of products in hundreds of categories, as well as a few product webshops [5.].

- We even differentiate webshops by distributors too. Often, the consumers don't even realize that during the sale and purchase, they didn't buy a product marketed by that particular webshop, but only by a partner. Such interfaces can be the "marketplaces". This means a webplaza, but its common name is even the online flea market or online marketplace. Other companies can place the products they sell on these interfaces, typically for a monthly fee or a commission. The sales, customer acquisition, and payment transactions themselves are not performed by the distributor,

DOI: https://doi.org/10.14232/analecta.2022.1.90-96

but by the intermediary company. Within the same category, a smaller but occasionally larger slice is embraced by so-called "dropshipping" companies. Dropshipping is a newer agreement between a logistics company and a webshop. The logistics company undertakes to procure, store and deliver the products, and the webshop is only responsible for sales. In contrast, there are classic webshops that sell the products they produce themselves, make purchases for themselves, and make payment transactions themselves. In practice, however, the two are often mixed. This means that an online store can sell at the same time through itself and through an intermediary.

- Quantity of categories distributed: In addition, we can group online stores according to the types of goods distributed. According to this, some webshops are only interested in one type of product category, while others are present in several, even independent product categories [5.]

1.2 Marketing channels

In order for an online store to be able to choose the marketing channels that will generate the most of their revenue, two things need to be studied carefully. Firstly, the target group to whom they will sell. This is what the previous unit was about. The other is the knowledge of how possible marketing channels work. This can be divided into two major groups: offline and online channels. The first includes the print press, print magazines, television, radio, poster, and flyer. The second includes Google Ads, social media, comparison sites, and "marketplaces" [6.]. Based on the research of Szántó-Prónay (2013), it can be said that young people say that the presence of companies on social media is not essential, although they have a positive attitude towards the brand, they are willing to follow them and welcome individual communication [7.].

2. MATERIALS AND METHODS

We created a questionnaire, which was available in December of 2021. It was shared on social media and it was filled out by our acquaintances and friends. In our work, we were interested in online shopping frequencies, reasons, most frequently purchased products, average amounts of money spent, the most popular advertising sources, preferences related to online stores, shipping methods and payment systems, and how conscious and impulse buying is typical of the respondents. The data of the completed questionnaires were evaluated using Statistica Trial and Microsoft Office Excel. During processing, for the sake of simplicity, we have given values rounded to one decimal place according to the rules of rounding.

3. RESULTS AND DISCUSSION

Our questionnaire was filled out by approx. 150 people, but only 126 of them were usable. Typically, women (73%) gave answers, mainly between 18 and 25 years (54.8%) and between 26 and 45 years (28.6%). We believe that despite the lack of representativeness of the group of respondents reached, this is the segment that primarily buys in online stores.

Monthly online purchases (64 people, 50.8%) stand out from the answers, half of the respondents indicated this. In addition, there is a significant proportion of purchases every six months (30 people, 23.8%). In contrast, the option „I have never bought online" (2 people, 1.6%) and the „only bought once / twice" (15 people, 11.9%) was indicated by a low proportion of respondents. From these proportions, it can be deduced that online shopping is now an integral part of the majority of people and they regularly take advantage of the opportunities offered by online commerce. However, frequent (daily or weekly) response options have also been marked at a low rate, so it is also clear that the online option does not replace

DOI: https://doi.org/10.14232/analecta.2022.1.90-96

offline shopping, it probably only complements it for certain products. In the following, we looked for the answer to what is the reason why someone chooses to shop online instead of offline. As an answer we have given the following: cheaper, more reliable, faster, more convenient, more choice, I can compare the products. In this case, several outstanding results were achieved. The convenience was the most highlighted (100 people, 79.4%), while the second most popular benefit of online shopping, according to respondents, was the larger amount of products found online (66 people, 52.4%). Almost as many indicated that it was cheaper (44 people, 34.9%), faster (45 people, 35.7%) and the possibility to compare products (46 people, 36.5%). In addition, although it was not one of the options, several people wrote that it is also common for them that what they want to buy is not available near their place of residence or cannot be purchased offline at all. It is clear that for the vast majority of respondents (more than 2/3), convenience is the biggest benefit of shopping online.

In the following, we tried to find out how much they are willing to spend on average online for each purchase. The information obtained in this way can help to shed light on the question of what price range is likely to be sold in the largest volume. The responses can be found in figure 1 in summarizes. It can be stated that the significant majority were those who spend between HUF 5,000 and HUF 20,000, while the answer was at least HUF 20,000+ (9 people, 7%). From the results obtained, it can be seen that consumers are happy to turn to online shopping for products with a value between HUF 5,000 and HUF 20,000.

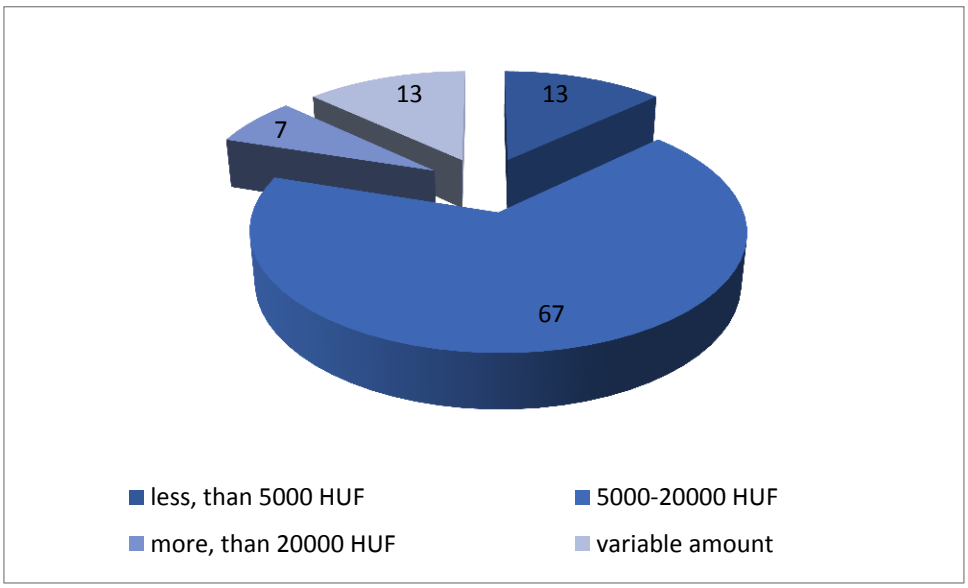

Figure 1.: Distribution of respondents based on the amount spent each time on online shopping (N = 126,%)

When we asked about the product category, we found out that the highest proportion of clothing (61%) is bought, followed by services (55%) - e.g., cinema, theater, followed by technical articles (42%), followed by cosmetics (32%) and books (31%). Food is in 10th place with 18%.
It should be noted that clothing stores can also be found in many places offline, but here it is worth recalling that based on answer 2, consumers like to be able to compare the products of different online stores and sticks in a short time. In the case of clothing, it can be especially helpful for the shopper to find the most appropriate piece of clothing at the best price, relatively quickly, and online. In addition, with the low prices of Chinese and other fast-fashion products, it is difficult for branded garments to compete.

DOI: https://doi.org/10.14232/analecta.2022.1.90-96

Our next question was about what kind of communication affects customers. The answers are shown in Figure 2.

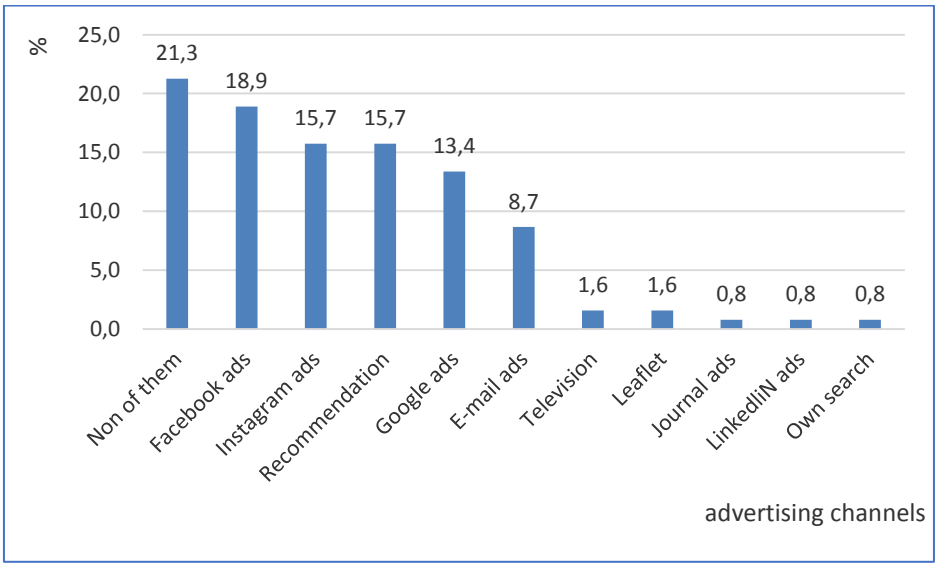

Figure 2. Distribution of questionnaire respondents based on influencing advertisements (N = 126,%)

According to the first category of response, none of the advertisements played a role in the person's choice of the given webshop when shopping online. Among the offers that will be specifically mentioned, we would like to highlight those acquired by acquaintances. In addition, ads on social media have a motivating effect.

Factors most influencing the choice: shipping cost (56.3%), reliable delivery (56.3%), wide product range (53.2%). these factors were important to more than half of the respondents. In addition, almost half of the respondents consider special prices (49.2%), advanced search, filter (57.6%), and various payment methods (47.6%) to be extremely important.
Based on the results, an online store should pay special attention to the following:

- The widest possible choice, even within a product (color, size, etc.),
- Existence of filtering and search criteria,
- Transparent structure,
- Low additional costs (such as transport),
- Reputable transport providers,
- Multiple payment options
- Favorable prices (even advertised with frequent promotions).

Examining the payment options further, we collect the following result: most respondents prefer cash on delivery (47, 6 percent), so almost half of the respondents choose this if possible. Of the card payment providers, Simple Pay stands out from the crowd (23%), PayPal (11.1%), and other card providers (12.7%) performed similarly. In light of this, it is definitely recommended for webshops to provide cash on delivery

DOI: https://doi.org/10.14232/analecta.2022.1.90-96

in the webshop despite the extra costs and logistical problems. The high rate can be explained by a lack of trust in online stores. In the case of cash on delivery, they do not have to deal with the recovery of the purchase amount in case of non-performance or incorrect performance of the webstore or the delivery service provider. Lack of cash on delivery can easily lead to the loss of customers.

Those who fill in the questionnaire - based on their own judgment - typically make a conscious purchase (53%), while 21% have implemented unplanned spending only once and 26% have implemented it more than once. The majority of respondents (49.2%) highlighted the discount prices as a reason for impulse buying, while those who bought based on their emotions accounted for 31.7%. It is worth drawing attention to the contradiction that only 27% of the respondents said that they had never bought like this here, while 53% had previously declared themselves to be conscious consumers. We can resolve this antagonism with the following line of thinking: no matter what promotion appears, the purchase of an item that is not previously planned due to the special prices is not an emotional decision, but an economically correct decision. Many people are aware that they are able to buy a discounted product without planning to buy it in advance, but because they think it is economical, they still feel conscious. Customers can be encouraged to make impulse purchases with various special offers so that the buyer continues to feel conscious afterward. Consistent with this theory are market trends that sales fall sharply in the weeks leading up to well-known promotional periods and then sales jump sharply during promotional periods. (e.g., Black Friday).

Examining the different responses based on demographic characteristics, we found the following:

- The frequency of purchases was not affected by either age group or economic situation
- 18- to 25-year-olds are more likely to pay attention to ads on Instagram (26.1%), while in the circle of 26- to 45-year-olds the ads are equally effective on Google (16.7%) and Facebook (19.4%) and ads received via email (16.7%). For them, Instagram advertisements are not enough effective - according to their own admissions
- In terms of gender, Facebook (20.4%) and Instagram (20.4%) are the most effective for women. In contrast, for men, the „none" responses dominated (35.3%). In addition, recommendations (17.6%) and Facebook ads (14.7%) matter more.
- For payment methods, the breakdown by the group is in line with the frequency findings.

4. CONCLUSIONS

Based on the above mentioned, we make the following suggestions: Before starting a business, every webshop should develop a detailed plan for both marketing and logistics. The necessary information must be obtained either from an external specialist or through in-house training. The primary marketing channels for customer acquisition should be online marketing channels. Depending on the target group, the usage of Instagram and Facebook are recommended for younger women, and Facebook, Google, and newsletters are recommended to use for older people. From the beginning, webshops should strive to gather positive customer feedback and demonstrate proficiency in the product by producing value-creating content on a regular basis, which can also build a committed community. They can be more easily encouraged to buy again later. It is worth providing a clean, transparent interface where those interested can easily find your products and information, as well as choose from a variety of payment and shipping methods. Ensuring cash on delivery is especially important. By maintaining consumer awareness, special offers and upsells can be used to effectively encourage consumers to increase the value of their shopping cart so that it does not appear to be an impulse purchase.

DOI: https://doi.org/10.14232/analecta.2022.1.90-96

REFERENCES

[1] Bányai Júlia – Novák Péter (2016): Online üzlet és marketing. Akadémai Kiadó
[2] Papp-Karkas Kitti (2019): E-kereskedelem: Jelentése, legnagyobb előnyei – és merre tart? https://webshippy.com/blog/e-kereskedelem-jelentese / (2021.04.08)
[3] Kondricz Péter és Tímár András (2000): Az elektronikus kereskedelem jogi kérdései, Complex Kiadó
[4] Németh Péter, Lázár Erika, Szűcs Krisztián, Törőcsik Mária (2020): Vásárlási szokások változása a koronavírus okozta járványhelyzet hatására - az online vásárlási magatartás vizsgálata
[5] Portfólió (2020): A szektor, amely hatalmasat nyert a koronavíruson: e-kereskedelem https://www.portfolio.hu/gazdasag/20200518/a-szektor-amely-hatalmasat-nyert-a-koronaviruson-e-kereskedelem-432490 (2021.04.12)
[6] Gál Péter (2017): Webáruház indítás lépésről lépésre Galocaffe Kft
[7] Horváth Dóra, Nyirő Nóra, Csordás Tamás (szerk.) (2016.): Médiaismeret Reklámeszközök és reklámhordozók. Akadémiai Kiadó
[8] Szántó Szilvia, Prónay Szabolcs (2013): „A Facebook nem a reklámnak lett kitalálva" - A fiatalok viszonyulása a cégek, márkák jelenlétéhez a Facebookon in Dr. Király Éva (szerk.): „Kiterjesztett" marketing. Budapesti Gazdasági Főiskola: Budapest. ISBN: 978 963 715 9 pp. 271–283.

DOI: https://doi.org/10.14232/analecta.2022.1.90-96

Analecta Technica Szegedinensia
Vol. 16, No. 01 ISSN 2064-7964 2022

A MOBILE FIXTURE SYSTEM FOR FRICTION STIR WELDING APPLICATION

[1]Abiodun Akeem Rasheed, [1]Tunde Isaac Ogedengbe, [2]Taiwo Ebenezer Abioye

[1]Industrial and Production Engineering Department, The Federal University of Technology, Akure, Nigeria
[2]Mechanical Engineering Department, The Federal University of Technology, Akure, Nigeria
e-mail: rashkeeeem@gmail.com

ABSTRACT

In an attempt to provide a more flexible means of achieving friction stir welding (FSW) of Aluminum without the use of expensive FSW machine tool, which are not readily available. This study developed a mobile fixture system (MFS) for FSW on a Vertical milling Machine Tool (VMMT). A conceptual design of a fixture system with a moving work table, which provides for transverse feed (movement) of the workpieces during FSW, was generated. The detailed design of the components of the MFS was done using existing mechanical design formulae. Subsequently, the design was fabricated and evaluated. An ATmega 328P Arduino Uno microcontroller was used to design a control system to automate the MFS worktable movement. Results revealed that the MFS worked smoothly during FSW of AA 1100 materials. The efficiency of its motion accuracy was estimated as 87.2%. Also, the trend of the tensile strength and the hardness value as well as the joint efficiencies of the AA 1100 weldments produced using the developed MFS agreed with existing studies. The MFS can be used for FSW of Aluminum materials on VMMT as well as on pillar drilling machine tool.

Keywords: Friction stir welding, mobile fixture, weldments, mechanical design, control system

1. INTRODUCTION

In the world today, the significance of joining engineering components has led to limitless efforts put in place by engineers to bring about new, easy and cost-effective ways of joining metals. During the manufacturing process various metallic materials are joined together at different location depending on the design concepts of the machineries and equipment been manufactured. The joining of these materials during manufacturing is achieved using welding operation which is a manufacturing process used for creating a permanent joint between two or more metallic parts. The joint, technically refers to as weldment, is usually obtained by coalescence induced by a combination of temperature, pressure, and metallurgical conditions. The electric arc welding (EAW) technique commonly used in the manufacturing process is associated with weldment quality issues like porosity, brittleness, corrosion, cracking etc. These together with other unwanted demerits usually found in the weldments of dissimilar metals obtained using EAW, such as brittle intermetallic compound (IMC) reaction phase formation at elevated temperatures, had shifted the attention of researchers to consideration of gas-tungsten arc welding (GTAW) and gas-metal arc welding of similar and dissimilar metals [1; 2]. When the materials are very soft such aluminum, aluminum alloy, copper and zinc the weld defect is usually more pronounced.

In recent times, however, Friction Stir Welding (FSW) is being applied in the manufacturing of products used in our everyday lives due to its strength, versatility and weld quality. This is a relatively new welding process which has been commonly accepted as a promising method for joining light metallic alloys, especially aluminum, having low melting point [3]. It is a continuous, hot shear, autogenous process involving non-consumable rotating tool of harder material than the work piece material. FSW has attracted considerable interest because of its better weld ability of aluminum alloy weld joint. It has a great potential for welding metals as joint quality is exceptionally high, low cost and the process is very repeatable [3]. It is also expected to produce good quality weldments of metals in comparison to EAW, GTAW and GMAW. Unfortunately, dedicated machine (i.e. Friction Stir welding Machine) purposely built for

DOI: https://doi.org/10.14232/analecta.2022.1.97-109

conducting FSW operation is generally not readily available, due to its high cost, which had led researchers to adopt Vertical milling machine tool (VMMT) supported by in-house built fixture for achieving FSW [4].

Basically, the general principle of 3-2-1 location is most commonly used to hold workpieces during the design of fixture. Certain degrees of freedom should necessarily be restricted in the design of FSW fixture, so as to locate and orient the active surfaces of the workpieces with respect to the FSW tool. The main challenge is to curtail the four main forces (see Figure 1) acting on the workpieces during FSW operation.

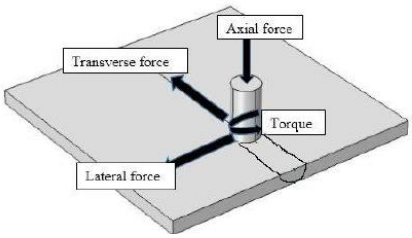

Figure 1: Forces in FSW operation [5]

FSW fixture have been designed, as observed from literatures [6; 7], to comprise (i) base/backing plate (ii) side plates (iii) clamps/clamping plate (iv) bolts/screws as locators and (v) bolts and nuts as holder (vi) Stoppers. A good design of fixture should ensure adequate heat dissipation away from the workpiece to improve the weld quality and performance.

Generally, the existing studies on FSW fixture development can be grouped into two categories. One group involves a situation where the components (backing plate, side plates and clamps) of the fixture are directly held on the milling machine table as a way of assembly [8] while the other group have the elements of the fixture system already assembled together before the assembled fixture is held on the milling machine table for FSW operation [5; 6; 9; 10]. However, while the later approach is preferable for ease of setup both categories are immobile in nature as the workpiece feeding is dependent on the milling machine feed mechanism. This will limit the choice of federate to those available on the milling machine table which oftentimes may not be completely suitable for the investigation at hand as noted from preliminary investigation [4]. If we considered the fact that federate has been established to influence weldment quality during FSW operations [11], this then becomes an important issue which could be handled via the development of a mobile fixture system for use in FSW applications.

Moreover, while some FSW fixture were designed to accommodate only fixed size workpiece width [8; 9] some others were designed to allow a range of workpieces width [5; 6; 10]. The later design allowed flexibility thereby facilitating workpiece preparation for FSW experiments. The design considerations adequate for the development of FSW fixture has been critically examined with some details provided in the direction of systematic design after which a FSW fixture with variable side clamping was developed and utilized for FSW of AA 6101 T6 aluminum alloys successfully [10]. Careful consideration of some of the details provided in line with the basic principle of fixture design will adequately guide FSW fixture design tasks.

Definition of requirement, gathering of necessary information, conceptual design and optimization implementation of the optimum design concept, e t c are some of the processes involved in manufacturing of a machine fixture [12**]**. Generation and analysis of various design concepts with a view to select the most suitable one to achieve FSW on a VMMT were considered would facilitate development of fixture with very good functionality. However, the elements of the product design consideration matrix used for

DOI: https://doi.org/10.14232/analecta.2022.1.97-109

concepts evaluation should focus mainly on functionality. Due consideration of the dimensions of the bed of the milling machine(s) on which fixture is to be used [6] as well as the ability to vary the length, width and thickness of the work pieces [5] has been reportedly used in determining the design parameters of FSW fixtures. Other process parameters like the axial, lateral and transverse load, torque, temperature at the thermo-mechanical heat affected zone (TMHAZ) and feed rates should also be carefully considered for mobile fixture.

Mild steel has been used majorly as the material for manufacturing the various components of FSW fixtures because it has high strength and toughness which is required to withstand unbalanced forces and pressure during FSW operation [6; 7; 9]. However, [8] used aluminum-stainless steel for the backing plate to improve heat dissipation of the TMHAZ while [6] utilized mild steel for base plate and stainless steel for the backing plate to achieve better compressive strength and high wear resistance in comparison to mild steel. [13], reportedly considered Cast Iron (C45), Die Steel (D4), Tool Steel and Hard Alloy (H20) using CAD simulate with C45 steel emerged as the best out the four materials considered.

Though, [10] selected carbon steel for manufacturing all components of its fixture, the study reported that other grades of steel can be used depending on the type of material to be joined and thickness of plates. Therefore, for cost effectiveness, it is important that the materials selected for manufacturing of the fixture must be of low cost, functional and readily available. Based on all the issues raised from literatures, this study developed a mobile-fixture system (MFS) for achieving FSW on a Vertical Milling Machine tool (VMMT) and evaluated its performance.

2. RESEARCH METHODOLOGY

A conceptual design of the MFS was developed and simulated to establish its functionality using Creo 7.0, a computer aided design (CAD) software. The detail dimensions of its components (design parameters) required for its fabrication were determined using existing formulae with consideration to relevant dimensions of bed (worktable) of the VMMT and the maximum load up to which it is to be subjected in operation. The VMMT is available in the central workshop of the School of Engineering and Engineering Technology (SEET) at the Federal University of Technology, Akure (FUTA). Worktable (Backing plate) mobility and automated are the unique features incorporated to the MFS concept. Subsequently, the designed fixture was fabricated

2.1. Design Considerations

The relevant design parameters of the VMMT were obtained from the machine while the loads were established from the literature. These include the length and breadth of the milling machine work table, the work table slot design, the range of the VMMT table feed rate and the range of the spindle speed. Based on the VMMT design parameters obtained, a functional conceptual design (exploded view) of the MFS developed for FSW on the machine and its various components is as shown in Figure 2.

The MFS conceptual design comprises of a worktable with integrated backing plate, clamps, frame, leadscrew, leadscrew nut, support shaft, bearing, stepper motor, control panel, U-channel. The worktable is held on the leadscrew which is in turn connected to the stepper motor. The stepper motor drives the leadscrew whom rotational motion is converted to the translational motion of the MFS worktable, forming a feeding mechanism for feeding the workpieces against the welding tool. The stepper motor wires are connected to an AC main through a controller designed for the system using Arduino Uno microcontroller. The controller was provided with a speed control knob programed to provide the user with the ability to vary the welding speed (mm/min) for the MFS feeding task. To prevent workpieces movement during FSW, provisions were made for securing them to the worktable using two clamps and bolts and nuts. Hence, the feeding of the workpiece on the tool utilizes the MFS feed mechanism and is independent of the VMMT. This increases the flexibility of conducting FSW operation. The MFS is designed to be held on the

DOI: https://doi.org/10.14232/analecta.2022.1.97-109

VMMT work table with the aid of 19-size bolts and nuts to ensure its stability and firmness.

The optimum parameters required for obtaining adequate weldment were established as 2-5 kN [13] 6 kN [14] 3.8 to 9.8 kN [15] 26.58 kN [16] 5.884 kN [17] 122 kN [18] 20 – 60 kN [19], 1-3 ^{o} [20] 11.5 – 24 mm/min [16] 37.5-47.5 mm/min [3] 40 to 140 mm/min [21] 50–300 mm/min [22] 14 – 750 mm/min [23] 50mm/min - 100 mm/min and [14] 2000 rpm [14] 2700 – 5400 rpm [16] 1500 to 2500 rpm [15] 45 – 2000 rpm [23] 900-1400 rpm [3] 600 to 1600 rpm [21] 1000–2500 rpm [22] for the axial force, tool tilt angle, feed rate, and the tool rotational speed respectively. This range of values were considered for the detail design of the MFS. Also, parts standardization, ergonomic, availability of materials and ease of assembly and disassembly were given significant consideration for good maintenance reliability and safety.

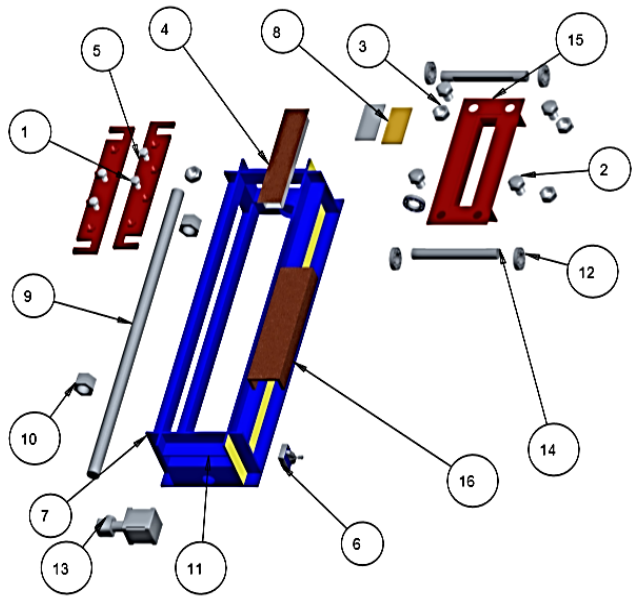

S/N	PART NAME	QTY
1	13BOLT	4
2	22BOLT	4
3	22NUT	4
4	BACKING_PLATE	1
5	CLAMP	2
6	CONTROL_UNIT	1
7	FRAME	1
8	FSW_WORKPIECE	2
9	POWER_SCREW	1
10	POWERSCREW_NUT	2
11	SMALLBEARINGA	2
12	SMALLBEARINGB	4
13	STEPPR_MOTR	1
14	SUPPORTING_SHAFT	2
15	TABLE	1
16	U_CHANNEL	1

Figure 2: Exploded View of the FSW Fixture

2.3 Design Analysis

The components of the MFS whose detailed design, to estimate the design parameters, were discussed in this section include the main frame, clamps, leadscrew, support shafts and their bearings and stepper motor.

2.3.1. Design of the main frame and the clamps

The mainframe of the MFS has the backing plate and worktable as an integral part. Also, rectangular slots are provided at the base for holding the fixture on the VMMT bed. After due consideration of the design parameters of the VMMT bed, the dimensions/design parameters of the main frame, backing plate, worktable, rectangular clamp and slot, in L x B x H mm, were estimated as 810 x 239 x 148 mm, 265 x 60 x 32 mm, 355 x 150 x 45 mm 355 x 60 x 8 mm and 23 x 40 x 8 mm respectively. Mild steel was selected as the material for the manufacturing of the MFS components as established in the literature because of its good tensile strength, low cost and availability locally [24; 25].

DOI: https://doi.org/10.14232/analecta.2022.1.97-109

2.3.2 Design of the supporting shaft and its bearings

The design parameters estimated for the worktable, the backing plate and the clamp, to be supported by the shaft, were utilized to estimate their weights so that the load to which the support shaft is subjected to (Ls) was determined using Equation (1):

$$L_s = W_w + W_b + W_c + F_a \quad (1)$$

Where, W_w, W_b, W_c and F_a represent the weights of the worktable, backing plate, clamp and the axial load respectively. An axial load of 6 kN was considered as the maximum load expected to act on the MFS [13;15].

From Equation (1) it was estimated that the load acting on each of the two supporting shafts is 3430 N. Consequently, according to the procedure given in [26], the diameter of the shaft was determined as 25 mm, using Equation (2).

$$d^3 = \frac{16}{\pi S_S}\sqrt{(K_b M_b)^2 + (K_t M_t)^2} \quad (2)$$

Where d is the diameter of the support shaft; S_S is the allowable shear stress of the shaft material (N/m^2); K_b is the combined shock and fatigue factor applied to bending moment; K_t is the combined shock and fatigue factor applied to torsional moment; M_b is the bending moment (N/m) and M_t is the torsional moment (N/m).
Also, the procedure established in [27] for selecting rolling contact bearing was applied so that NSK 6205 single row radial ball bearings with a bore of 0.25 m and outside diameter of 0.052 m was selected for use on the support shaft.

2.3.3 Design of the leadscrew

The leadscrew carries the worktable, the backing plate, the clamps and the supporting shafts, apart from the axial load. Therefore, the load acting on it was estimated to be 6432.54 N using Equation (3).

$$F = W_w + W_b + W_c + 2W_s + F_a \quad (3)$$

Subsequently, using Equation (4) the Lead Screw diameter was determined to be 25 mm after due consideration of appropriate factor of safety and leadscrew sizes commercially available.

$$D = \sqrt{\frac{8F}{\pi\tau}} \quad (4)$$

Where, F is the total force on the leadscrew, W_s is the weight of each of the shafts, D is diameter of the leadscrew and $\tau = 42\ Mpa$ for mild steel [27].

Following the same method of bearing selection used for the support shaft, NSK 6205 single row radial ball bearings with a bore of 0.025 m and outside diameter of 0.052 m was also selected and used for holding the leadscrew.

2.3.4 Finite Element Analysis of the MFS Structural Concept

FEA (Finite Element Analysis) was applied to the generated design concept to conduct stress analysis after the application of the calculated design parameters. The finite element model of the FSW fixture is

DOI: https://doi.org/10.14232/analecta.2022.1.97-109

subjected to 6 kN axial force. The axial force used was selected within the range of axial force for FSW as established from the literature. The FEA was conducted using Creo 7.0 software.

2.3.5 Design and selection of stepper motor for the drive system

Power to move the worktable is derived from a stepper motor connected to the lead screw. Stepper motors are direct current (DC) motors that move in discrete steps. Stepper motor was selected as it can achieve precise positioning and speed might be controlled with the use of appropriate controller. The power requirement, P, of the stepper motor was calculated using Equation (5).

$$P = \frac{2\pi NT}{60} \quad (5)$$

Where, N is the maximum operational speed of the leadscrew in rpm, and T is the maximum torque required to drive the leadscrew.

Therefore, the power required to produce the maximum torque of 80.41 Nm, obtained using Equation 5 on the leadscrew at a speed of 2.5462 rpm (200 mm/min) was determined as P = 21.44 W. Hence, a 1 hp stepper motor with maximum speed of 3000 rpm and voltage range of 0 -16 V was selected to drive the leadscrew.

An ATmega 328P Arduino Uno microcontroller was selected and used to design a control system MFS motion. It is a high performance, low power controller from Microchip which is easy to program.

2.4 Fabrication and Assembly of the Components of the MFS

The production and joining processes employed in this study include marking out, welding operation and machining operations which include milling, turning, drilling, grinding. The mild steel materials used for the fabrication of the MFS were procured at metals market located around Cathedral area, Akure, Ondo state. Thereafter, the fabrication was done at the SEET central workshop, FUTA, Ondo State, Nigeria. Some bought out parts utilized include roller bearings, stepper motor, washers, bolts and nuts. To form the MFS mainframe, mild steel angle iron was cut into the required sizes, according to the estimated design parameters, and joined together using arc welding process. This type of joining process was chosen due to the heavy-duty nature of the job the MFS was designed for. Similarly, mild steel angle iron and u-channel was used to fabricate the clamps and the worktable respectively. The clamping bolt holes were drilled on pillar drilling machine. The two worktable support shafts were made from hardened mild steel, heat treated to soften it for easy machinability. They were turned on the lathe to Ɵ25 mm and re-hardened later to withstand the load it is being subjected to during friction stir welding process. A power leadscrew of diameter Ɵ25 mm with square thread was sourced and forced fixed into its bearing to avoid any misalignment that may ensue during operation of the FSW fixture as a result of tolerance.

2.5 Evaluation of the MFS

The accuracy of the MFS transverse speed was validated by operating the MFS using selected specific speeds on the controller and then manually timing the movement of the work relative to the welding tool using a stop clock. The actual distance travelled by the work relative to the tool for a given speed were then determined and compared with the expected distance require to be moved for the period of time they were allowed to move. Hence variation between the actual distance covered and the distance the system is expected to cover as a result of the speed used were compared to estimate the accuracy of the drive system.

DOI: https://doi.org/10.14232/analecta.2022.1.97-109

Also, the MFS was engaged on the VMMT to produce weldments of aluminum (AA 1100) plate having a tensile strength of 95.93 MPa and a Hardness of 28 BHN. The workpieces were cut to a dimension of 50 x 100 x 4 mm and welded together using the MFS on VMMT (See Figure 5) for butt type FSW operation.

Three set of experiments with three replicates were conducted using different traverse speeds (i.e. 130 mm/min, 145mm/min and 155 mm/min), a tool speed of 1400 rpm and a tilt angle of 1.8^0. Subsequently, the tensile strength and hardness of the weldments obtained were determined using a computerized Instron Testing Machine model 3369 and a Monsanto Brinell hardness testing machine respectively. An average of three measurements obtained for each weldments sample was recorded as the measured value in all cases to account for possible uncertainty in the measurement procedures. Thereafter, the results obtained were discussed to authenticate the function-ability of the developed MFS.

3. RESULTS AND DISCUSSION

3.1 Finite Element Analysis

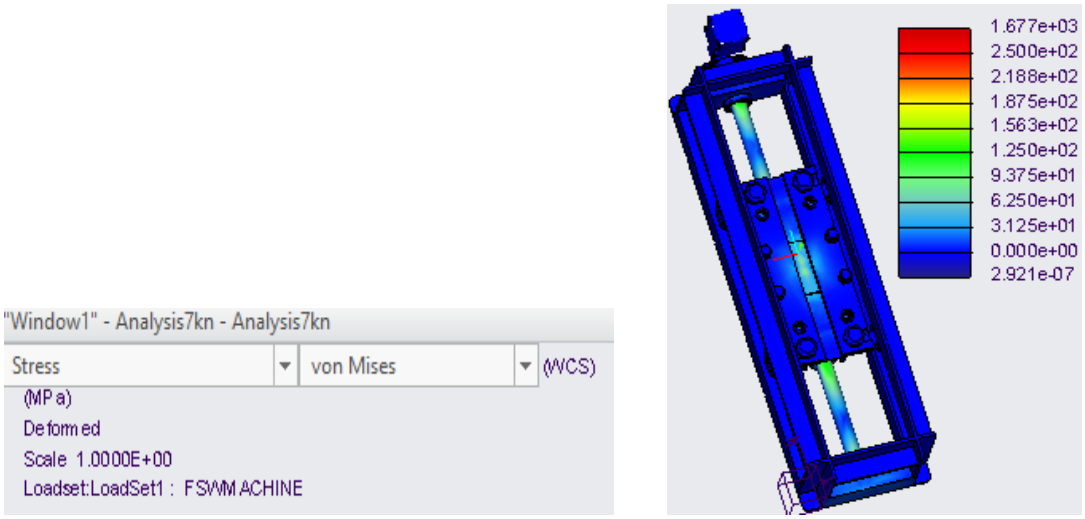

Figure 3: Finite Element Analysis of Friction stir welding fixture

DOI: https://doi.org/10.14232/analecta.2022.1.97-109

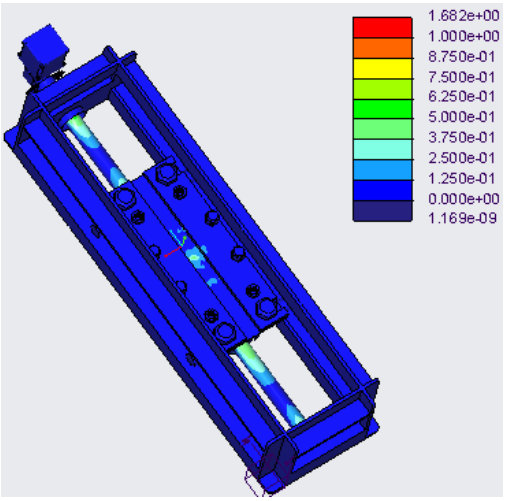

Fixture 4: Failure Index of the Friction Stir Welding Fixture

From Figure 3, the FEA result obtained clearly shows that the developed fixture is saved. The maximum modeling von mises stress is 167 Mpa while yield strength of mild steel used is 250 Mpa meaning that maximum von mises stress is below yield strength of the mild steel material used. For a safety, failure index must not more be greater one. From Figure 4 though the maximum value in the legend is 1.68 but looking at the Figure 4 red colour above one did not appear on the modeling which shows that the failure index is less than one.

3.1 The Developed MFS

The developed MFS is as shown in Figure 5. The system is held on the milling machine bed through the slots provided on the frame using bolts and nuts. Provision is made on the MFS for holding the workpieces to be welded together using the worktable clamps.

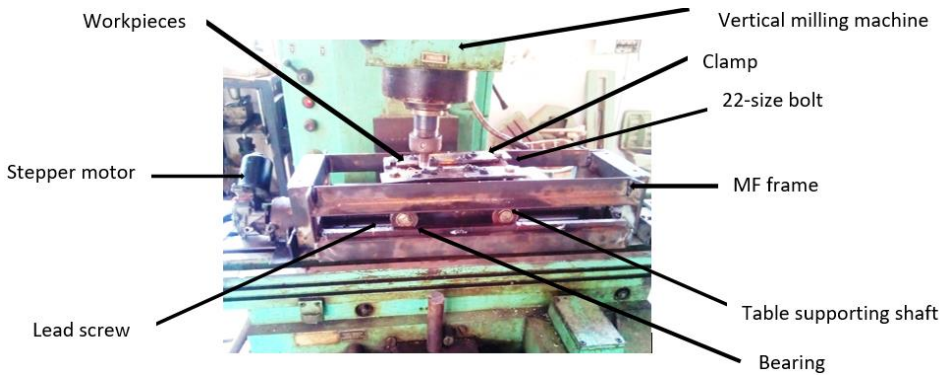

Figure 5: The developed MFS being used for FSW Operation on VMMT

Figure 5 shows the MFS coupled to the milling bed for performance evaluation. The workpieces are held on the worktable with the abutting edges centrally located on the backing plate before being clamped in

DOI: https://doi.org/10.14232/analecta.2022.1.97-109

position. The MFS allows free movement of the FSW tool held on the milling machine spindle as the worktable moves transversely during FSW operation. The system was designed to move along the X axis relative to the VMMT bed when positioned on it. This movement is powered by a stepper motor which drive a lead screw directly attached to the worktable on which the workpieces are clamped. The stepper motor is connected to an AC main through a controller designed for the system. The controller makes use of an AC- DC power module to convert the AC from the mains to the DC required to run the stepper motors. The controller was provided with a speed control knob programmed to provide the user with the ability to set the welding speed (mm/min) for the FSW operation so that the VMMT bed movement is no more necessary for the operation.

3.2 Characteristics of the Developed MFS

Table 1 shows the result obtained during the experiment to validate the adequacy of the welding speed for the worktable of the MFS. The expected distance differs from the welding distance covered. This shows that there is variation between the programmed distance per min in the microcontroller and the distance actually covered by the MFS table. However, the variation is considered to be reasonably accurate. From Table 1, the average efficiency of the motion accuracy of the drive system is estimated as 87.2%. This is considered to be good enough for a start and it can be improved further through more tuning of the control system or modelling of the MFS for speed error compensation.

Table 1: Comparison of the Actual distance covered by the MFS worktable and the expected one for a given transverse speed

S/N	Speed (mm/min)	Distance covered				Expected distance (mm)
		Expt. A (mm)	Expt. B (mm)	Expt. C (mm)	Expt. Ave (mm)	
1	135	109	111	114	111.33	135
2	145	126	128	124	126	145
3	155	141	141	144	142	155

3.3 Characteristics of the Weldment Produced using the MFS on VMMT

Figure 6 shows the Friction stir welded joints while Figure 7 shows the graph of average tensile strength of the weldments produced using the MFS as obtained from the 3 experimental runs with 3 different feed rates.

DOI: https://doi.org/10.14232/analecta.2022.1.97-109

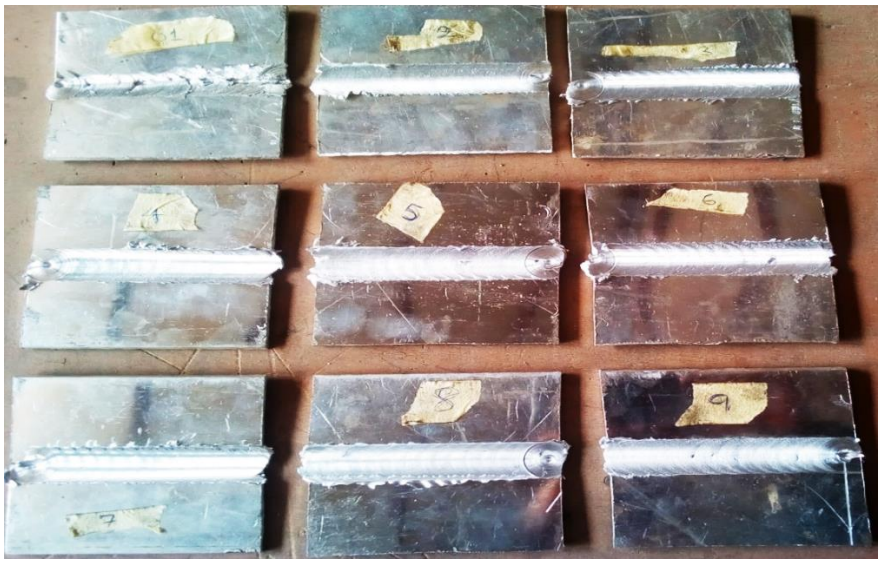

Figure 6: The friction stir welded joints produced using the developed MFS

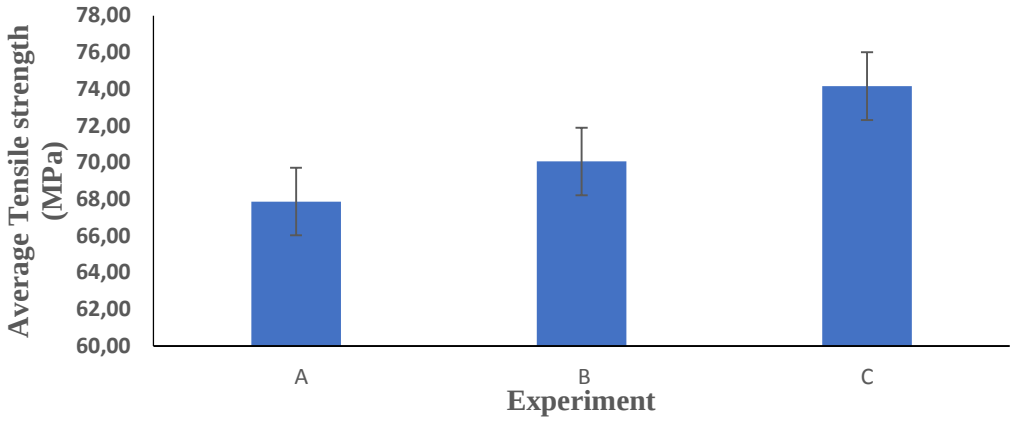

Figure 7: Graph of Tensile Strength (MPa) at the stir zone

From Figure 7, traverse feed rate is directly proportional to the tensile strength of the weldment as Experiment A with 135 mm/min traverse feed rate gave 67.87 MPa tensile strength, 70.06 MPa tensile strength is obtained for experiment B with a federate of 145 mm/min while Experiment C with 155 mm/min gave 74.17 MPa. The tensile strength of the base metal is 95.93 MPa. Hence, the optimum tensile strength of 74.17 MPa is obtained from experiment C with the highest traverse speed of 155 mm/min. This correspond to an average joint efficiency of 73.77 % of the base metal which is suitable when compared with [8; 28; 29; 30].

DOI: https://doi.org/10.14232/analecta.2022.1.97-109

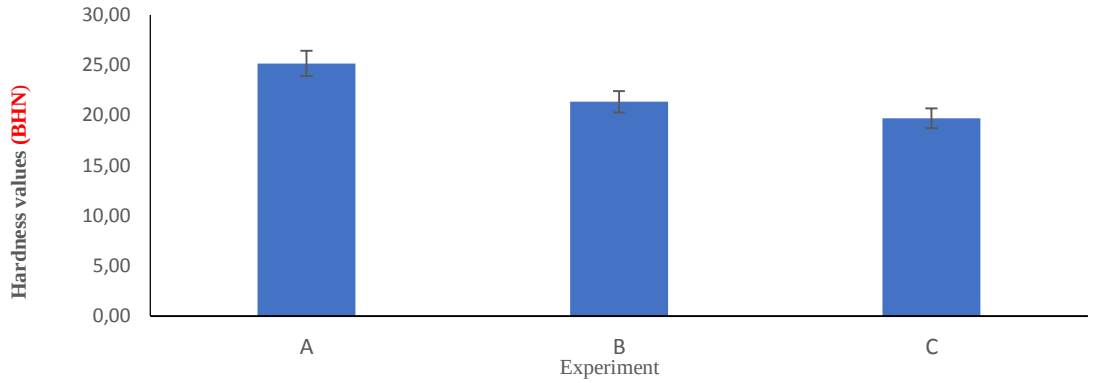

Figure 8: Graph of Hardness (BHN) at the Stir Zone (SZ)

Figure 8 shows the average hardness values of the 3 experimental runs with the three different feed rates. The hardness values of the weldment are inversely proportional to the feed rate within the range of transverse speed used. The base metal (BM) hardness value (as control experiment) was measured to be 28 BHN while the maximum hardness value obtained for the SZ is 25.15 BHN. Compare with the base metal (BM), the lower hardness values exhibited by the SZ and the hardness trend is expected [31; 32]. Based on the hardness values obtained, the average joint efficiency of the weldments produced using the developed MFS was estimated as 78.79%.

4. CONCLUSION

A MFS for FSW of Aluminum materials on a VMMT was developed. The fixture run smoothly in operation and its motion characteristic was found adequate. The mechanical properties of the weldments of AA 1100 produced using the developed MFS agreed with those of other works in literature wherein static fixture were used for FSW. The MFS would provide a more flexible approach to investigation of FSW operations on VMMTs and it is also extendible for use for FSW on pillar drill machine tools.

REFERENCES

[1] Ogedengbe T. I., Abioye T. E. and Ekpemogu I., Investigation of Mechanical Properties and Parametric Optimization of the Dissimilar GTAW of AISI304 Stainless Steel and Low Carbon Steel. World Journal of Engineering, 15(5) (2018), pp. 584-591.

[2] Abioye T.E., Ariwoola O.E., Ogedengbe T.I., Farayibi P.K., Gbadeyan O.O., Effects of Welding Speed on the Microstructure and Corrosion Behavior of Dissimilar Gas Metal Arc Weld Joints of AISI 304 Stainless Steel and Low Carbon Steel, *Materials Today Proceedings*, 17 (2019), pp. 871-877.

[3] Asmare A., Al-Sabur R. and Messele E., Experimental Investigation of Friction Stir Welding on 6061-T6 Aluminum Alloy using Taguchi-Based GRA. (2020), pp. 1-21 doi:10.3390/met10111480.

[4] Rasheed A. A., Development of a FSW Fixture for Joining Materials on a Vertical Milling Machine. Masters Thesis, Federal University of Technology, Akure, Nigeria, (2020), pp. 150.

[5] Alali S. and Injeti N. K., An Innovative Fixture Design in making use of a Milling Machine to Perform the Function of Friction Stir Welding and Eliminate the Exit Hole. International Journal of Innovative Research in Science Engineering and Technology, 5(4) (2016), pp. 5717 – 5723

DOI: https://doi.org/10.14232/analecta.2022.1.97-109

[6] Jadhav G. C. and Dalu R. S., Design and Development of a Fixture for Friction Stir Welding. *International Journal of Mechanical Engineering and Technology (IJMET)*, 8(9) (2017), pp. 132–139.
[7] Shahabuddin, Dwivedi V.K, Fabrication and Design of Fixture with a New Technique for Friction Stir Welding, International Journal of Engineering Technology Science and Research IJETSR, 5(1) 2018, pp. 1540-1544.
[8] Hasan M. M., Ishak M. and Rejab M. R., A simplified design of clamping system and fixtures for friction stir welding of aluminum alloys. *Journal of Mechanical Engineering and Sciences (JMES)*, 9 (2015), pp. 1628-1639.
[9] Baghel P. K., Siddique A. N., Design and development of Fixture for Friction Stir Welding Innovative Systems. *Design and Engineering*, 3(12) (2012), pp. 40-47.
[10] Kamblea L.V., Soman S.N., Brahmankar P.K., Understanding the Fixture Design for Friction stir Welding Research Experiments. *Material Today: Proceeding 4.* 5th *International Conference of Materials Processing and Characterization (ICMPC)*, (2016), pp. 1277 – 1284.
[11] Sreenivas P, Anil Kumar R, Sreejith P. S, Effect of Applied Axial Force on FSW Of AA 6082 - T6 Aluminium Alloys International Journal of Mechanical Engineering and Technology (IJMET) 8(1) 2017, pp. 88–99.
[12] Kaustubh K. A. and Akshaykumar P. K. (2016): Design and Development of Milling Fixture. *International Journal for Research in Engineering Application & Management (IJREAM)* Vol-02, Issue 02; pp 1-3, May 2016.
[13] Ramnath B. Vijaya, Elanchezhian C., Rajesh S., Prakash S. Jaya, Kumaar B. Manoj, Rajeshkannan K., Design and Development of Milling Fixture for Friction Stir Welding. Materials Today: Proceedings 5 (2018) 1832–1838
[14] Awang M. A, Khan S. R., Ghazanfar B., and Latif F. A., Design, Fabrication and Testing of Fixture for Implementation of a New Approach to Incorporate Tool tilting in Friction Stir Welding, 13 annual MTEC Web conference of EDP Science, 2014, pp. 1-6
[15] Gra¨tzel , Hasieber M., Lo¨hn T. and Bergmann JP., Reduction of friction stir welding setup loadability, process forces and weld seam width by tool scaling M Materials: Design and Applications 0(0) 2020, pp. 1–10, DOI: 10.1177/1464420720903331
[16] Singh R., Rizvi S. A. and Tewari S.P Design and Fabrication of Friction Stir Welding Fixture with a New Approach. (Elixir International Journal). (2015), pp. 34844-34846.
[17] Bhavsar K. and Acharya G.D., Design and development of simplified fixture for FSW. International Journal of Creative Research Thoughts (IJCRT), 5(3) (2017).
[18] Akshansh M., Designing and Fabrication of Fixture for Friction Stir Welding of Aluminium AA6061 Alloys *IJSRD - International Journal for Scientific Research & Development*, 5(5) (2017).
[19] Pushp K. B. and Arshad N. S., *Design and Development of Fixture for Friction Stir Welding*, Innovative Systems Design and Engineering, 3(12) (2012), pp. 40 – 47.
[20] Elyasi M., Derazkola H. A., Hosseinzadeh M., Investigations of tool tilt angle on properties friction stir welding of A441 AISI to AA1100 aluminium 230(7), (2016) pp. 1234-1241
[21] Zuluaga-Posada, M., Hoyos, E. and Montoya, Y., Performance evaluation of a novel force measuring device for Friction Stir Welding (FSW) of aluminum alloys. DYNA, 86(210), pp. 150-155, July - September, 2019.
[22] Kavitha M., Manickavasagam V. M., Sathish T., Bhiksha Gugulothu , Sathish Kumar A., Karthikeyan S. and Subbiah R., , Parameters Optimization of Dissimilar Friction Stir Welding for AA7079 and AA8050 through RSM, Hindawi Advances in Materials Science and Engineering Volume (2021), pp. 1-8. https://doi.org/10.1155/2021/9723699
[23] Fratini L., Micari F., Buffa G., Ruisi V.F. (2010): A new fixture for FSW processes of titanium alloys. CIRP Annals – Manufacturing Technology. (59) (2010), pp. 271-274. doi:10.1016/j.cirp.2010.03.003

[24] Ogedengbe T. I., and Abadariki S. O., Development and Performance Evaluation of a Bone Milling Cum Pulverizing Machine. *West Indian Journal of Engineering (WIJE)*, 37(1) (2014), pp. 23-28
[25] Ogedengbe T. I., Development and Performance Evaluation of a Liquid Soap Production Machine for the Local Soap Industry in Nigeria, *Journal of Applied Science and Environmental Management*, 23(6) (2019), pp. 1119 -1125.
[26] Khurmi R.and Gupta J., *Machine Design.* Eurasia Publishing House (PVT.) LTD. New Delhi. 2005.
[27] Ogedengbe T.I and Aderoba A. A., Computer-Aided Selection of Rolling Contact Bearings. Modelling, measurement. Peer Reviewed/International Journal, 74(5) (2005), pp. 1-18.
[28] Goyal A. and Garg R. K., Effect of Tool Rotational and Transverse Speed on Mechanical Properties of Friction Stir Welded AA5086-H32 Aluminium Alloy, *Int. J. Microstructure and Materials Properties*, 12(1/2) (2017), pp. 79-93.
[29] Sevvel Pa ,Jaiganesh Vb Effects of axial force on the mechanical properties of AZ80A Mg alloy during friction stir welding, 5th International Conference of Materials Processing and Characterization (ICMPC 2016), Materials Today: Proceedings 4 (2017), pp.1312–1320
[30] Memon, S.; Murillo-Marrodán, A.; Lankarani, H.M.; Aghajani Derazkola, H. Analysis of Friction Stir Welding Tool Offset on the Bonding and Properties of Al–Mg–Si Alloy T-Joints. Materials 2021, 14, 3604. https://doi.org/ 10.3390/ma14133604
[31] Abioye T. E., Zuhailawati H., Anasyida A. S., Yahaya S. A. and Dhindaw B. K., Investigation of the Microstructure, Mechanical and Wear Properties of AA6061-T6 Friction Stir Weldments with Different Particulate Reinforcements Addition. *Journal of Materials Research and Technology*, (2019), pp. 1-12.
[32] Singh B., Singhal P. and Saxena K.K., Effect of transverse speed on mechanical and microstructural properties of friction stir welded aluminium AA2024-T351, *Advances in Materials and Processing Technologies, (*2020), pp. 1-11.

DOI: https://doi.org/10.14232/analecta.2022.1.97-109

Analecta Technica Szegedinensia
Vol. 16, No. 01 ISSN 2064-7964 2022

CREATING THE CONCEPTUAL AND LOGICAL MODEL OF A JOURNAL DATABASE

György Hampel

Faculty of Engineering, University of Szeged, Mars tér 7, 6724, Szeged, Hungary
e-mail: hampel.gyorgy@szte.hu

ABSTRACT

This article describes the process of creating the conceptual and logical model of a journal database. To efficiently extract the information from the articles published in the journal so far, the idea of creating a database has emerged. To create a database, it is recommended to design a high-level conceptual model and convert that into a logical data model. The benefit of the thoughtful design is that it shows the structure of the database in an easily comprehensible form. The entity-relationship model is a fast and efficient way to create the conceptual model and it can be easily converted to a relational database model, which is a logical model. The initial version of the entity-relationship model of the journal database had one entity type, 25 attributes, and no relationship. The final version contained three entity types, 39 attributes, and three relationships. This final conceptual model was converted to a logical model, the relational model. The result was ten tables to store entity data with 22 different fields and another three tables to ensure the relationships between the tables. The developed model can be created in a relational database manager and is suitable for serving information needs related to the journal.

Keywords: database planning, entity-relationship model, relational model

1. INTRODUCTION

A Hungarian language printed yearbook at the Faculty of Engineering at the University of Szeged containing peer-reviewed scientific publications was first published under the care of the Institute of Economics and Rural Development in 2006 (ISBN: 978-963-482-799-3). The book transformed into a journal in 2009 (ISSN: 1788-7593) and since then, 26 issues of the "Contemporary social and economic processes" (Jelenkori társadalmi és gazdasági folyamatok) – including the first three yearbooks – were published until the end of 2021 under the care of the Institute of Engineering Management and Economics. Since volume 14 (2019) issue 3, the journal is available online as well (ISSN: 2676-9867). Since the first publication there were 489 articles published from 906 authors in a variety of disciplines.
Seeing the unbroken development, the idea arose to create a database which could make it easier to extract relevant information from issues of the journal. Based on this idea, the task was to (step one) design the database in a high-level model, (step two) to create a logical data model based on the previous step, and (step three) to physically create the database with a relational database manager.
This article describes the first two steps: the creation of the high-level concept with the use of the entity-relationship model, and the conversion to the logical model using the relational data model.
The benefits of this thoughtful design are:

- It shows the structure of the database, the entities, and their relationships in an easy-to-understand format.
- As it is easy to understand, it facilitates the dialogue between the user and the programmer.
- It gives new ideas to both users and programmers.
- It is a plan or description that does not need to be changed by selecting or modifying the database management system.

Fig. 1 shows the process of database modelling and implementation. This article deals with the first three steps. All four steps appear in [1] and [2].

DOI: https://doi.org/10.14232/analecta.2022.1.110-121

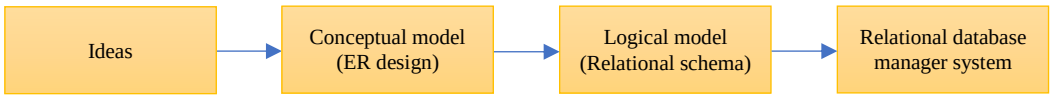

Figure 1. Database modelling and implementation process. Modified from [3].

2. MATERIALS AND METHODS

2.1. Database and data modelling

A database can be described several ways as there is no uniformly agreed definition for this concept. A few examples to define database: It consists of field-specific data, metadata describing the type of data and relationships, and a data management system [4]; It is a set of finite number of entity occurrences, their finite number of property values and relationship occurrences, organized according to a data model [5]; It is an integrated data structure that stores the occurrence data of several different objects in an organized manner according to a data model with auxiliary information called metadata, to ensure efficiency, integrity and data protection [6].
The data must be grouped to be retrievable according to some sorting principles and other aspects [5]. There are several benefits to creating and using a database, such as:

- it is a uniform, logically clear data structure,
- data can be queried in a flexible way,
- the data and the managing programs are independent of each other, so both can be modified without changing the other [7][8].

The database is always linked to a data model, in fact, it is an implemented data model [9]. On the one hand, the data model must be robust enough to grab the user's attention and meet his or her expectations, but it must also be simple and understandable for the user [7].
During the design of the database, one must first create the conceptual model, and then the logical model. Only after that should the physical implementation (the real, physical creation of the database) follow [10].
The creation of a conceptual (high-level) data model plays a significant role in the database design process, both in theory and in practice [11]. A conceptual data model is a collection of tools designed to describe reality in such a way that the created model is able to answer questions about reality [12]. This model does not address data structure or physical storage issues. Conceptual schemas include the set of entities, their characteristics, relationships, and constraints. In addition, the structure of the database is illustrated with diagrams. The database is illustrated in a way that is comprehensible even to those who are not experts in this field [4].
Of course – like everything – this can be ruined as well: improper use of modelling tools, limitations in the imagination of users and database designers, different visions and approach to the problem of users and database developers may contribute to poor design [13]. Although creating a conceptual model seems simple, it is essential that modeler has the ability to correctly identify the required objects and their relationships [12]. According to Watson [12], those not yet familiar with data modelling (e.g., university students learning database design) make these common mistakes:

- failure to recognize that something thought to be an attribute is, in fact, an entity,
- inability to generalize and assign entities to entity sets,
- failure to check relationships between entity sets from all directions, so the cardinality (number of connected entities) is incorrect,
- exceptions may be ignored.

DOI: https://doi.org/10.14232/analecta.2022.1.110-121

Based on [3], there are some useful principles to consider when designing a database:

1. Create a realistic model: Entity sets, attributes, and relationships must reflect reality. For example, the workplace should not be the attribute of the ARTICLE, but rather the AUTHOR entity set.
2. Keep it simple: Do not add more entity sets, attributes, and relationships than necessary. For example, in the case of AUTHOR, it is probably unnecessary to include the eye colour.
3. Choose the right type of objects: There are several ways to describe reality, for example, we can describe a piece of reality with an entity set, attribute, or relationship. In general, attributes are easier to put into the model than an entity set or relationship, but solving everything with attributes is not always practical, because it can make it difficult to manage the database (see Fig. 2 for an example).
4. Avoid (or at least try to prevent) unnecessary data redundancy: Every effort should be made to include all data only once. For example, do not store the author's name as an attribute in the ARTICLE and in the AUTHOR entity set as well. This avoids anomalies that make it difficult to use and maintain the database [14][15]. At the same time, there may be cases when, for reasons of expediency, we may still be forced to store data redundantly. This may depend on the situation, the needs, and the database management system.
5. Choose the right relationships: Entity sets can be related in many ways, especially if there are many of them. It is usually not advisable to create all relationships, as this can lead to anomalies which make it difficult (or even impossible) to manage the database. It is advisable to indicate only relationships necessary for the given problem to be solved and for this we need to know in advance what we expect from the database. For example, it is advisable to establish a many-to-many relationship between the AUTHOR and the ARTICLE entity sets, as an author may write more than one article and an article may have several co-authors; or there can be only one-to-many relationship between the JOURNAL and the ARTICLE entity sets, since an article can be published (normally) only once in a journal, and a journal issue can contain several articles.

2.2. The conceptual model: Entity-relationship model

Chen laid the foundations for the Entity-Relationship model (ER model) [16] and thus had a lasting effect on data modelling. It is the most popular tool for conceptual data modelling [17]; In addition to its simplicity, its popularity is due to its theoretical validity and the fact that it is excellent for preparing the relational data model used by today's database management systems. As a result, the ER model is taught in many higher education institutions, which also contributes to its popularity and prevalence [18]. On the one hand the entity-relationship model (ER model) is expressive, simple (even for non-professionals relatively easy to understand), uses few concepts (so it can be learned quickly), works with illustrative diagrams. On the other hand, due to the representation method used, it can be difficult to describe very complex databases [19].

The elements of the entity-relationship diagrams (ERD) are:

1. An entity can be any (abstract) object or concept which can be described with a name and has attributes. Similar entities form a set (for example: JOURNAL, ARTICLE, AUTHOR) [3]. It is represented in a rectangle.
2. The attribute belongs to an entity set or relationship, it describes its features, properties [3][4] (for example: in the case of an AUTHOR: name, academic degree, job, gender). An entity set must have at least one attribute, while it is not mandatory to assign attribute to a relationship. Like in the case of entities, a noun is commonly used to name an attribute [4]. An attribute can be simple (ellipse with single line), composite (can be divided into sub attributes, denoted in ellipses connected to the composite attribute), multivalued (ellipse drawn with a double line), or derived (can be calculated from other values, ellipse with a dashed line) [9].
3. A relationship – described with a verb – connects entity sets. The most common type is the binary relationship connecting two entity sets, but the model allows connecting any number of sets [3][4].

DOI: https://doi.org/10.14232/analecta.2022.1.110-121

According to the studies of Dey [11], the understanding of entity sets, and their attributes usually does not cause problem for the users, however, this cannot be said for the interpretation of relationships. The types can be [3][4]: recursive (relationship between two entities within the same entity set), one-to-one or 1:1 (relationship between one entity of an entity set with one and only one entity in another entity set), one-to-many (1:N) or many-to-many (N:M). The degree of relationship is determined by the connected entity sets. In addition, the participation in the relationship can be total (mandatory) when all entities form a relationship or partial (optional) when there are entities with no connection to other entities [20].

The key attribute plays an important role. It is marked by underlining the attribute [3]. A key is an attribute that is suitable to uniquely identify an entity. If there is more than one attribute suitable for the purpose, we have to select one, and this will be the primary key, while the others will be alternative keys. It is possible that an attribute cannot be identified by one attribute alone, but by combining the minimum number of required attributes, we can obtain a composite key suitable for unambiguous identification. The model also allows so called weak entities, which have no key attributes, where the entity is in a double line rectangle. (While keys are not compulsory in the ER model, they are required in the relational model. Relational database management programs allow the creation of keyless tables which is fine when creating simple databases with only one table.)

It should also be noted that several variants of the representation of ER diagrams coexist [17], which differ mainly in the representation of relationships [21] or add additional possibilities to the model's ability to describe reality, such as introducing main and subclasses, generalization, and specialization concepts [3][4], but they do not play a significant role in the current database to be implemented. According to Watson, it is not the mode of representation that matters primarily, but the ability to model correctly [12].

2.3. The logical model: relational model

Several types of logical data models have emerged since the beginning of computer database management, such as the hierarchical, mesh, object-oriented and relational data models [4] [22][23][24]. The relational model first described by Codd is the most widespread due to its simplicity and mathematical validity [25]. A data model must have a database manager based on it, so relational database managers are based on the relational data model [4].

The relational model is made up of a system of tables. A logical connection between tables can be created using fields whose contents can be found in both related tables. The structure of the tables in the relational model is as follows: The table must have a unique name that distinguishes it from other tables. The table header contains the unique column names; these column names are the identifiers of the attributes. A column is called a field (and the header is the field name). A row (or tuple) other than the header is a record. The number of columns is the degree of the table, the number of rows is called cardinality. The order of the columns or rows (except for the header) is indifferent, they can be interchanged. The attribute by which each record in the table can be clearly distinguished from another is called the primary key. If there are several suitable fields, we select one as the primary key and the others are alternative keys. If a set of several fields form a primary key, that is called composite key. The number of fields in the key must be minimal. The foreign key can be used to refer to another table that is logically related to the reference table [3][4].

There are a lot of cases when data cannot be stored and managed efficiently in a single table, because that can result in unnecessary repetitions (redundancy), which can cause various insertion, modification and deletion difficulties, problems (anomalies) [4][14][15]. To avoid anomalies, the table should be broken down into several interrelated tables using normalization rules [13][14]. Relational database managers have been devised to efficiently manage the resulting tables. Note: some spreadsheet programs – for example Microsoft Excel with Microsoft Power Pivot add-in – can handle databases and create result tables form joined tables with queries [26], but they are less effective than relational database managers.

DOI: https://doi.org/10.14232/analecta.2022.1.110-121

Relational and other additional operations can be used to extract the desired information from the relational tables [25][27].
If conceptual modelling is done using the ER model, it is necessary to transform it into a relational model. This is because although the ER model is an easy-to-learn and easy-to-use tool, there is no database manager based on it. The main rules that can be used during the transformation are the following [3][4][6][11]:

- Entity set: Each entity set is converted to a relation, i. e. a table.
- Attribute: Simple attributes of the ER model will be the fields in the tables and the fields are named after the attribute names. In case of composite attributes, only the sub attributes are added to the table as simple attributes. Since each cell of the relational schema can contain only one elementary value, multivalued attributes are put in a separate table linked to the original table using a foreign key. Derived attributes are calculated from data from other attributes, so they are not included as fields in the tables.
- Relationship: The transformation is determined by the type of relationship. The options are as follows: (1) One-to-one relationship (1:1): The primary key of table A is embedded into table B as a foreign key (or vice versa, it does not matter). (2) One-to-many relationship (1:N): The primary key of the table in the one-side of the relationship is embedded in the many-side table as a foreign key. (3) Many-to-many relationship (N:M): A separate table provides the connection between the two tables to be connected, which contains the primary key of the linked tables. This solution can be used in any type of relations (one-to-one and one-to-many) as well.

3. RESULTS AND DISCUSSION

3.1. The description of the created conceptual model with ER diagram

After collecting and overviewing the needs, the first version of the ER model was born (Fig. 2). It contains a single entity set and its associated attributes. Since this model contains aggregated data per journal issue, it is not suitable for storing detailed data of the articles (such as the names of authors, article titles etc.).
Name of the entity set: JOURNAL. The attributes, their type, and associated metadata are listed below in the following format: *attribute name; attribute type; metadata*. For ease of reference, multi-word expressions were used to name the attributes. Remember that the attribute data refers to an entire journal issue!

1. ID; Composite attribute; Used to identify each journal issue.
2. Volume; Simple attribute, a sub attribute of ID; The volume number of the journal.
3. Issue; Simple attribute, a sub attribute of ID; The issue number within a volume number.

The Volume and Issue together form a composite key (underlined) that uniquely identifies a particular journal.

4. Year; Simple attribute; The year the journal was published.
5. Isbn Issn; Multivalued attribute; ISBN and ISSN numbers of the journal. The print and online versions have separate numbers, so it can have multiple values at the same time.
6. Publisher; Simple attribute; Name (and other details if applicable) of the responsible publisher. This attribute can even be a combined attribute (broken down to name, scientific grade, position, etc. sub-attributes) if there is a need to store these data separately for information retrieval.
7. Editor-in-Chief; Multivalued attribute; The position of editor-in-chief can be filled by several people at the same time.
8. Responsible Editor; Simple attribute; Name (and other details if required) of the editor.
9. Technical Editor; Multivalued attribute; An issue can have multiple technical editors at once.
10. Page; Simple attribute; The total number of pages in a journal issue (not just page number of the articles).

DOI: https://doi.org/10.14232/analecta.2022.1.110-121

11. Topic; Simple attribute; Number of topics in a journal issue.
12. Article; Simple attribute; Number of scientific articles.
13. One Author; Simple attribute; Number of articles with one author.
14. Two Authors; Simple attribute; Number of articles with two co-authors.
15. Multiple Authors; Simple attribute; Number of articles with more than two co-authors.
16. Hungarian Article; Simple attribute; Number of Hungarian articles in an issue.
17. Foreign Article; Simple attribute; Number of foreign language articles.
18. Author; Simple attribute; Number of authors per journal issue.
19. Faculty Author; Simple attribute; The number of authors who are employees of the Faculty of Engineering.
20. Not Faculty Author; Simple attribute; The number of authors who are not employees of the Faculty of Engineering.
21. Degree; Simple attribute; Number of authors with an academic degree.
22. Hungarian Author; Simple attribute; Number of Hungarian authors (identified by name since citizenship data are not available).
23. Foreign Author; Simple attribute; Number of non-Hungarian authors.
24. Male; Simple attribute; Number of male authors.
25. Female; Simple attribute; Number of female authors.

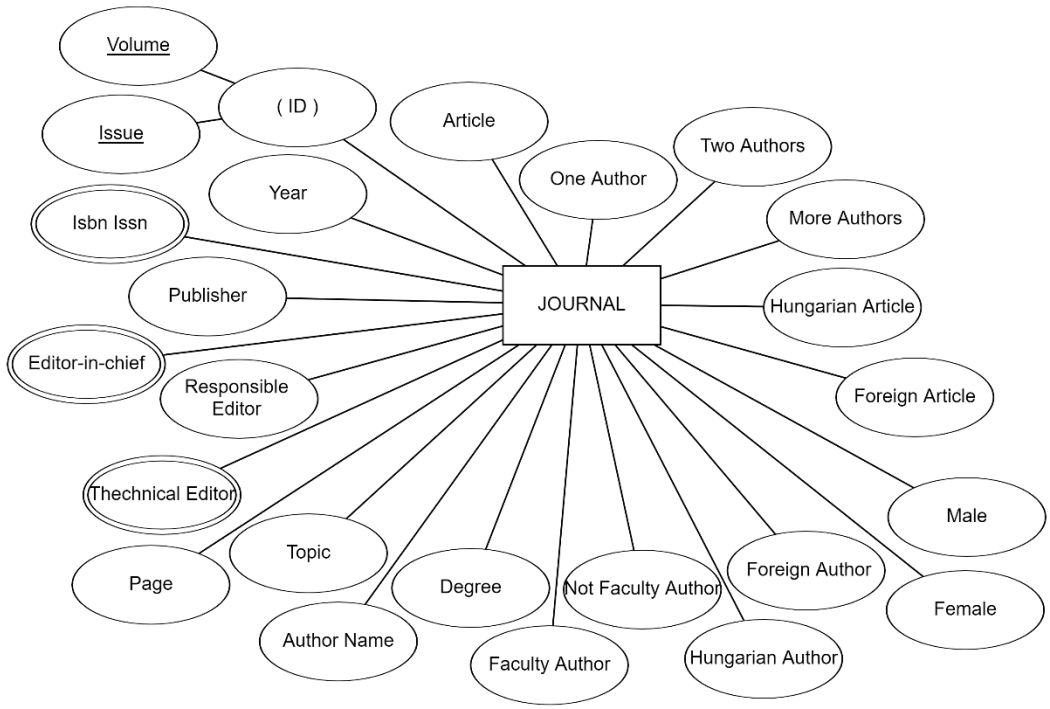

Figure 2. The ER diagram of the journal database (version 1) created with erdplus.com data modelling website.

This ER model which consists of a single entity set and twenty-five attributes is suitable to store a lot of information. But if it would be implemented this way, data entry would require a lot of preparation and preliminary manual aggregation, and the database would not contain important basic, detailed data.

DOI: https://doi.org/10.14232/analecta.2022.1.110-121

After reviewing the first version of the ER model, a few modifications were made and eventually a final version was developed. This model contains three entity sets (JOURNAL, ARTICLE, AUTHOR) with several attributes, and three relationships (Writes, Publishes, Contains). The description of the model, the attributes, their type, and their associated metadata are listed in *attribute name; attribute type; metadata* format.

Attributes of JOURNAL:

1. Volume; Simple attribute; The volume number of the journal (a serial number).
2. Issue; Simple attribute; The issue in a volume.

The Volume and Issue together is a composite key (underlined).

3. Year; Simple attribute; The publication year of the volume issue.
4. Isbn Issn; Multivalued attribute; ISBN and ISSN numbers of the journal.
5. Responsible Publisher; Simple attribute; Name (and other details if applicable) of the responsible publisher.
6. Editor-in-Chief; Multivalued attribute; Name (and other details) of editor-in-chiefs.
7. Responsible Editor; Simple attribute; Name (and other details) of the editor.
8. Technical Editor; Multivalued attribute; Name (and other details) of the technical editors of an issue.
9. Page; Simple attribute; The number of pages of the journal.
10. Total pages; Derived attribute; The sum of pages in a journal (the sum of Page attribute).

Attributes of ARTICLE:

1. Article Title; Simple attribute and primary key; Number of scientific articles. There can be no articles with the same title in the database.
2. Topic; Simple attribute; The name of the scientific topic where the article belongs.
3. First Page; Simple attribute; The first page of the article in the journal issue.
4. Last Page; Simple attribute; The last page of the article.
5. Language; Simple attribute; The language of the article.
6. Keyword Hungarian; Multivalued attribute; Hungarian keywords of the article.
7. Keyword English; Multivalued attribute; English keywords of the article.
8. No of Sources; Simple attribute; Number of sources in the article.
9. Article Pages No; Derived attribute; The total number of pages of the article.
10. Article No; Derived attribute; Number of articles.
11. Topic No; Derived attribute; Number of topics.
12. Foreign Article No; Derived attribute; Number of articles written in foreign language (so far only English).
13. Hungarian Article No; Derived attribute; Number of Hungarian language articles.
14. N Author No; Derived attribute; Number of articles written by N number of authors.
15. Faculty Article No; Derived attribute; Number of articles written by faculty members.
16. Not Faculty Article No; Derived attribute; Number of articles written by not faculty members.

Attributes of AUTHOR:

The attribute(s) to identify each author should be carefully selected. The name alone is not enough, as different authors may have the same name, or if someone changes name between writing articles, he/she will have two different names and will therefore count as two different people. Combining the attributes of name, degree (and workplace) doesn't get us any further: if an author who publishes multiple times gets a (new) academic degree or changes workplace, he/she will again count as two (or more) different people. The problem can be handled with an arbitrarily created unique ID that can be used as a key attribute.

1. Author ID; Simple attribute and primary key; Serves as a unique identifier to distinguish authors.
2. Author Name; Simple attribute; The first name(s) and family name of the author
3. Degree; Multivalued attribute; The (scientific) degree(s) of the author when writing the article.
4. Workplace; Multivalued attribute; Details of the author's workplace(s).

DOI: https://doi.org/10.14232/analecta.2022.1.110-121

5. Gender; Simple attribute; The gender of the author by name (since we do not ask the author's gender this data is based on the first name).
6. Author No; Derived attribute; Total number of authors.
7. Degree No; Derived attribute; Number of authors with academic degree.
8. Hungarian Author No; Derived attribute; Number of Hungarian authors (based on the author's name).
9. Foreign Author No; Derived attribute; Number of foreign (not Hungarian) authors (based on the author's name).
10. Faculty Author No; Derived attribute; Number of authors of the Faculty of Engineering.
11. Not Faculty Author No; Derived attribute; Number of authors not working at the Faculty of Engineering.
12. Female No; Derived attribute; The number of female authors (based on the author's name).
13. Male No; Derived attribute; The number of male authors (based on the author's name).

The features of the relationships:

- 1 issue can contain articles from several authors, 1 author can publish in several issues, 1 article can be published in only 1 issue.
- Each author must publish in one of the issues: an author must have at least 1 relationship with an article and can have relationships with multiple articles; an author must have at least 1 relationship with a journal issue and can have multiple ones with journal issues.
- All articles must be published in one issue: one article must have 1 and only 1 relationship with the journal; an article must have at least 1 relationship with one author and can have relationships with multiple authors.
- All journal issues must have an author: one journal issue must have at least 1 relationship with 1 author and can have relationships with more than one author.
- Each journal issue must have an article: a journal issue must have at least 1 relationship with an article.
- As a result of the above, all relationships are total. A many-to-many relationship must be created between the JOURNAL and the AUTHOR and between the AUTHOR and the ARTICLE, and a one-to-many relationship must be established between the ARTICLE and the JOURNAL.

Fig. 3 shows the ER diagram of the completed conception model.

DOI: https://doi.org/10.14232/analecta.2022.1.110-121

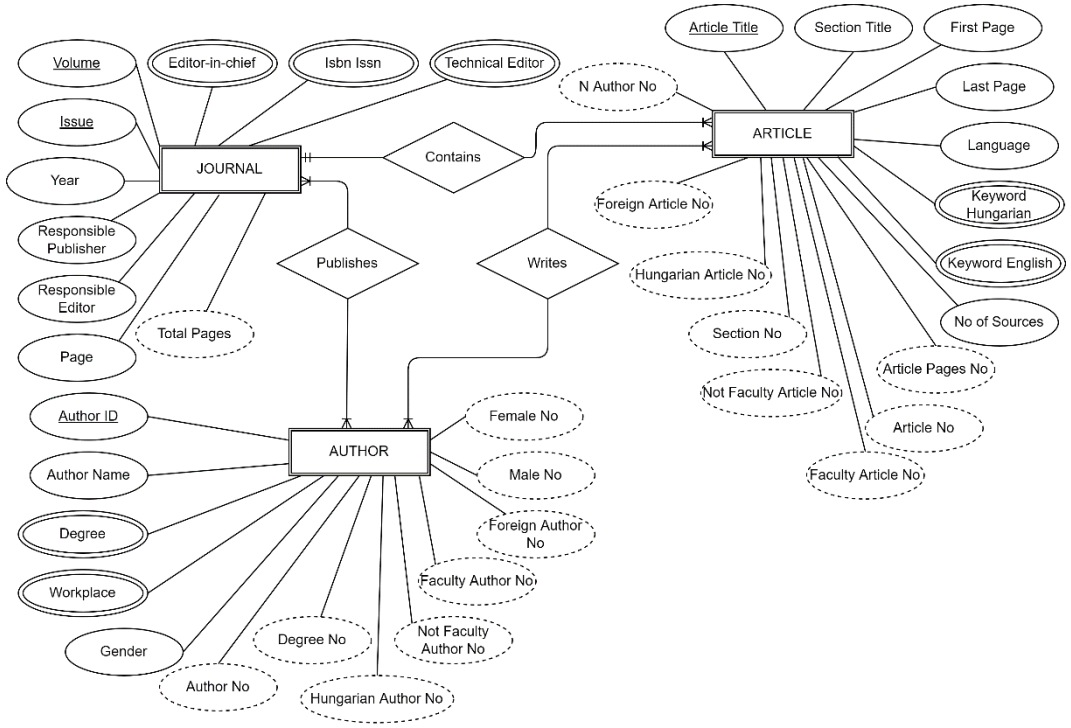

Figure 3. The ER-diagram of the journal database (final version) created with app.diagrams.net website.

3.2. The description of the logical model with relational schema

In this description of the relational schema – which is the converted ER model –, the *names of the tables* are capitalized and followed by the *field names* (attributes) in parentheses, with the *primary keys* underlined:

1. Journal entity set and its attributes: It can be divided into the following four tables:

- JOURNAL (Volume, Issue, Year, ResponsiblePublisher, ResponsibleEditor, NumberOfPages);
- EDITORINCHIEF (Volume, Issue, NameOfEditorInChief);
- ISBNISSN (Volume, Issue, IsbnIssnNumber);
- TECHNICALEDITOR (Volume, Issue, NameofTechnicalEditor);

The ER model includes a derived attribute (Total Pages) in the JOURNAL entity set which is not included in any of the tables because it can be calculated from the page data.

2. Author entity set and attributes: This set can be converted to the following tables:

- AUTHOR (AuthorID, AuthorName, Gender);
- DEGREE (AuthorID, DegreeName);
- WORKPLACE (AuthorID, WorkPlaceName);

The ER model denotes eight derived attributes in Author entity set, but since these are calculated from other attributes, they are not included in the scheme of the tables (the number of Hungarian and foreign authors, number of different degrees, males, females, etc.)

3. Article entity set and attributes: The following tables can be created in the relational model from this entity set:

- ARTICLE (ArticleTitle, TopicName, FirstPage, LastPage, Language, NumberOfSources);
- KEYWORDHUN (ArticleTitle, KeywordHungarian);

DOI: https://doi.org/10.14232/analecta.2022.1.110-121

- KEYWORDENG (ArticleTitle, KeywordEnglish);

The ER model also contains eight derived attributes in the ARTICLE entity type that will not be included in the tables in the relational model (Number of articles with N authors, Number of foreign and Hungarian language articles, etc.).

4. Relationships: Based on the ER model, all relationships are total. There is many- to-many relationship between the JOURNAL and the AUTHOR and between the AUTHOR and the ARTICLE tables. The name of the tables providing the relationships are PUBLISHES and WRITES. A one-to-many relationship must be created between the ARTICLE and the JOURNAL; the name of the connection table is CONTAINS. The schemas of the tables are:

- PUBLISHES (Volume, Issue, AuthorID);
- WRITES (AuthorID, ArticleTitle);
- CONTAINS (ArticleTitle, Volume, Issue);

Fig. 4 created in MySQL Workbench shows the relational model of the journal database.

4. CONCLUSION

Systematic reflection on what seemed to be a simple (and quick to do) task at first (what to include as an entity set, what attributes to add, what kind of relationship is needed between the entity sets) helped to create a correct database concept.

The created relational model is suitable for the implementation, but it is advisable to check – even with test data – whether (1) it contains anomalies, (2) whether it is worthwhile to further reduce the redundancy in the data, (3) whether is it at least in the 3rd normal form. Depending on these, further refinement or modification may be necessary.

After checking the created relational model, the next phase of database design, the physical implementation can follow. This would be an SQL-based implementation of the relational schema in the selected relational database management system.

Should the need arise in the future, the implemented database can be further developed to be suitable for text mining. In this case, it can contribute even more effectively to the exploitation of the knowledge inherent in the Journal of Contemporary Social and Economic Processes.

DOI: https://doi.org/10.14232/analecta.2022.1.110-121

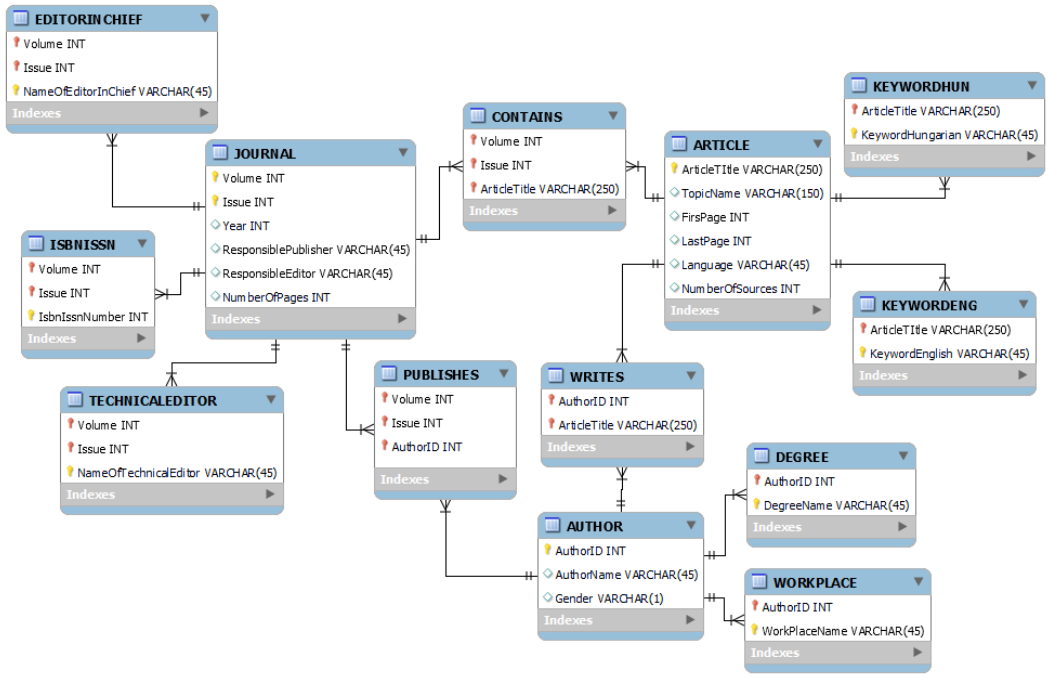

Figure 4. The relational model of the journal database created with MySQL Workbench.

REFERENCES

[1] Z. Fabulya, Access alkalmazás kialakítása ügyfélközpontú szolgáltatások nyilvántartására, Jelenkori Társadalmi és Gazdasági Folyamatok, 13 (1-2) (2018), pp. 67-76. http://acta.bibl.u-szeged.hu/55838/1/jelenkori_013_001_002_067-076.pdf

[2] Z. Fabulya, Access alkalmazás kialakítása dolgozói jelenlét nyilvántartására, Jelenkori Társadalmi és Gazdasági Folyamatok, 13 (1-2) (2018), pp. 151-160.
http://acta.bibl.u-szeged.hu/62062/1/jelenkori_013_003_004_151-160.pdf

[3] H. Garcia-Milina, J. D. Ullman, J. Widom, Database Systems: The Complete Book, 2nd Edition, Prentice Hall, Upper Saddle River, New Jersey, 2008

[4] L. Tímár, K. Vígh, J. Tátrai, J. Szigeti, Á. Vathy, É. Telekesi, I. Vass, T. Kocsis, R. Zs. Priskinné, M. Erdélyiné, Építsünk könnyen és lassan adatmodellt! Veszprémi Egyetem & Műszertechnika-Veszprém Kft., Veszprém, 19997

[5] B. Halassy, Az adatbázis-tervezés alapjai és titkai, IDG Magyarországi Lapkiadó Kft., Budapest, 1994

[6] L. Kovács, Adatbázisok tervezésének és kezelésének módszertana, Computer Books, Budapest, 2004

[7] D. M. Kroenke, C. D. Gray, Toward a Next Generation Data Modeling Facility: Neither the Entity-Relationship Model nor UML Meet the Need, Journal of Information Systems Education, 17 (1) (2006), pp. 29-38.

[8] B. L. Kacsukné, T. Kiss, Bevezetés az üzleti informatikába, Akadémiai Kiadó, Budapest, 2019 http://www.doi.org/10.1556/9789634544852

[9] Gy. Hampel, Cs. Heves, Informatika alapjai mérnököknek, alapszakos hallgatók számára, Szegedi Tudományegyetem, Szeged, 2019

DOI: https://doi.org/10.14232/analecta.2022.1.110-121

[10] V. T. N. Chau, S. Chittayasothorn, "A Bitemporal SQL Database Design Method from the Enhanced Entity-Relationship Model," 2021 7th International Conference on Engineering, Applied Sciences and Technology (ICEAST), 2021, pp. 85-90, http://www.doi.org/10.1109/ICEAST52143.2021.9426270
[11] D. Dey, V. Storey, B. Terence, Improving Database Design Through the Analysis of Relationships, ACM Transactions on Database Systems, 24 (4) (1999), pp. 453-486.
https://doi.org/10.1145/331983.331984
[12] R. T. Watson, The Essential Skills of Data Modeling, Journal of Information Systems Education, 17 (1) (2006), pp. 39-41. https://aisel.aisnet.org/jise/vol17/iss1/7/
[13] A. Badia, D. Lemire, A Call to Arms: Revisiting Database Design, Sigmod Record, 40 (3) (2011), pp. 61-69. https://doi.org/10.1145/2070736.2070750
[14] B. Halassy, Adatmodellezés. Elmélet és gyakorlat, Budapest, 2000, https://mek.oszk.hu/11100/11144
[15] R. Foorthuis, On the nature and types of anomalies: a review of deviations in data, International Journal of Data Science and Analytics, 12 (2021), pp. 297-331. https://doi.org/10.1007/s41060-021-00265-1
[16] P. P.-Sh. Chen, The Entity-Relationship Model – Toward a Unified View of Data, ACM Transactions on Database Systems, 1 (1) (1976), pp. 9-36. https://doi.org/10.1145/320434.320440
[17] S. Hartmann, Reasoning about participation constraints and Chen's constraints, Database Technologies 2003, Proceedings of the 14th Australasian Database Conference, ADC 2003, Adelaide, South Australia, February 2003, pp. 105-113.
https://www.researchgate.net/publication/221152543_Reasoning_about_participation_constraints_and_Chen%27s_constraints
[18] T. A. Carte, J. Jasperson, M. E. Cornelius, Integrating ERD and UML Concepts When Teaching Data Modeling, Journal of Information Systems Education, 17 (1) (2006), pp. 55-63.
https://aisel.aisnet.org/jise/vol17/iss1/9/
[19] Ch. L. Dunn, G. J. Gerard, S. V. Grabski, Critical Evaluation of Conceptual Data Models, International Journal of Accounting Information Systems, 6 (2) (2005), pp. 83-106.
https://doi.org/10.1016/j.accinf.2004.03.002
[20] J. Dullea, Il-Y. Song, I. Lamprou, An Analysis of Structural Validity in Entity-Relationship modeling, Data & Knowledge Engineering, 47 (2) (2003), pp. 167-205.
https://doi.org/10.1016/S0169-023X(03)00049-1
[21] C. E. H. Chua, V. C. Storey, Issues and Guidelines in Modeling Decomposition of Minimum Participation in Entity-Relationship Diagrams, Communications of the Association for Information Systems, 29 (9) (2011), pp. 159-184. https://doi.org/10.17705/1CAIS.02909
[22] Nyerges T., Logical Data Models, The Geographic Information Science & Technology Body of Knowledge (1st Quarter 2017 Edition), John P. Wilson (ed.). 2017.
https://doi.org/10.22224/gistbok/2017.1.2
[23] A. Silberschatz, H. F. Korth, S. Sudarshan, Data Models, ACM Computing Surveys, 28 (1) (1996) pp. 105-108. https://doi.org/10.1145/234313.234360
[24] B. Szabó, Adatbázis fejlesztés és üzemeltetés I., Eszterházy Károly Főiskola, Eger, 2013
[25] E. F. Codd, Derivability, Redundancy, and Consistency of Relations Stored in Large Data Banks, Research Report RJ599, IBM, San Jose, California, 1969
[26] M. Russo, A. Ferrari, Analyzing Data with Power BI and Power Pivot for Excel, Microsoft Press, Redmond, Washington, 2017
[27] A. Silberschatz, H. F. Korth, S. Sudarshan, Database System Concepts, 7th editon, McGraw-Hill Education, New York, 2020

DOI: https://doi.org/10.14232/analecta.2022.1.110-121

Analecta Technica Szegedinensia
Vol. 16, No. 01 ISSN 2064-7964 2022

DETECTION OF TRANSVERSE CRACKS IN PRISMATIC CANTILEVER BEAMS AFFECTED BY WEAK CLAMPING USING A MACHINE LEARNING METHOD

[1]David Lupu, [1]Cristian Tufisi, [1]Gilbert-Rainer Gillich, [1] Mario Ardeljan

[1]Department of Engineering Science, Babeș-Bolyai University, Str. M. Kogălniceanu 1, 400084 Cluj-Napoca, România
e-mail: cristian.tufisi@ubbcluj.ro

ABSTRACT

Because our infrastructure is aging and approaching the end of its intended functioning time, the detection of damage or loosening of joints is a topic of high importance in structural health monitoring. The most desired way to assess the health of engineering structures during operation is to use non-destructive vibration-based methods that can offer a global evaluation of the structure's integrity. A comparison of using different modal data for training feedforward backpropagation neural networks for detecting transverse damages in beam-like structures that can also be affected by imperfect boundary conditions is presented in the current paper. The different RFS, RFS_{min}, and DLC training datasets are generated by applying an analytical method, previously developed by our research team, that uses a known relation, based on the modal curvature, severity estimation of the transverse crack, and the estimated severity for the weak clamping. The obtained dataset values are employed for training three feedforward backpropagation neural networks that will be used to locate transverse cracks in cantilever beams and detect if the structure is affected by weak clamping. The output from the three ANN models is compared by plotting the calculated error for each case.

Keywords: damage detection, machine learning, natural frequency, structural health monitoring, weak clamping

1. INTRODUCTION

Different types of damages can occur in structures and can be caused by a multitude of factors, such as exceeding the expected operating demands, degradation caused by environmental conditions, material fatigue, loosening of joints due to shocks and excessive vibrations, and improper manufacturing conditions. For a structural monitoring method to be efficient, it is desired to detect invisible damage in the incipient state, preferably by non-invasive methods. Traditional non-destructive detection techniques present the disadvantage that they are limited to an accessible area and require having prior knowledge of the possible location of damage by considering the areas with the highest risk, which in most cases can be erroneous [1]. To increase the operational safety of equipment, installations, and structures, new methods have been developed to monitor structural integrity; these methods can be an integral part of the structure from the design phase or can be mounted retroactively, to assess the condition of the equipment [2].
Promising methods of structural assessment have been developed in recent decades that are based on the use of modal parameters of the structure. Although damage assessment using modal parameters is still under development, over time, many methods of evaluating the integrity of structures, by using the natural frequencies have proven to be reliable [3, 4, 5].
The fundamental starting point of vibration-based damage detection methods starts from the known fact that damages occurring in structures, significantly affect the stiffness and the energy dissipation properties of a system, which in turn will change its dynamic response [6].
The biggest challenge in using detection methods based on modal parameters is the use of a large amount of data, as well as certain disturbances that may occur during signal acquisition caused by environmental conditions and by the improper clamping of structural elements.
To address the shortcomings of current methods of vibro-diagnosis, new techniques have been developed over time, by using artificial intelligent networks which present promising results [7, 8].
In the current paper, we present a mathematical relation used for predicting the natural frequencies of beams affected by transverse breathing cracks and by improper boundary conditions developed in the paper

DOI: https://doi.org/10.14232/analecta.2022.1.122-128

[9]. By employing this algorithm, we can easily create different datasets, namely relative frequency shifts (RFS), normalized relative frequency shifts (RFS_{min}), and damage location indicators (DLC) that are later used for training six machine learning models, three models are trained for generating 3 outputs (transverse crack location, transverse crack severity and weak clamping severity if present) and the remaining 3 models are trained to detect only the position of the transverse crack also if the beam is affected by weak clamping.
To evaluate the quality of the developed computational intelligent methods used for damage identification, a set of FEM-generated tests are produced for different damage scenarios. The test natural frequencies are generated by employing the simulation software, ANSYS.

2. MATERIALS AND METHODS

The paper presents the use of a feedforward backpropagation neural network, which is developed in the MATLAB deep learning environment, to detect transverse cracks and also weak clamping in cantilever beams, by using different sets of generated training data.

2.1. Training dataset

The training datasets are generated by using a previously developed method [9] for predicting the natural frequencies for beam-like models affected by cracks, starting from Equations (1):

$$f_{i-D}(x,a) = f_{i-U}\left\{1-\gamma(a)\left[\bar{\phi}_i''(x)\right]^2\right\} \tag{1}$$

In Equation (1), the terms $\gamma(0,a)$ and $\bar{\phi}_i''(x)$ represent the crack severity and the modal curvature, respectively. The transverse crack severity is determined with the model presented in paper [10], using the following Equation (2):

$$\gamma(a) = \frac{\sqrt{\delta_D(a)} - \sqrt{\delta_U}}{\sqrt{\delta_D(a)}} \tag{2}$$

In Equation (2), the terms $\delta_D(a)$ and δ_U represent the deflection of the beam with damage, respectively in an undamaged state.
The modal curvature caused by the crack, with a known position x, is given by Equation (3) [11]:

$$\phi''(x) = \cosh(\lambda\frac{x}{L}) + \cos(\lambda\frac{x}{L}) - \frac{\cos\lambda+\cosh\lambda}{\sin\lambda+\sinh\lambda}\cdot\left[\sinh(\lambda\frac{x}{L}) + \sin(\lambda\frac{x}{L})\right] \tag{3}$$

To generate the training data, for several scenarios of the damaged beam, the relative frequency shift (RFS) values are used, according to Equation (4) [12, 13]:

$$\Delta\bar{f}_i(x,a) = \frac{f_{i-U} - f_{i-D}(x,a)}{f_{i-U}} = \gamma(0,a)\cdot\left[\bar{\phi}_i''(x)\right]^2 \tag{4}$$

The model shown in equations (1-4) is valid for generating the training data set for the perfect boundary conditions.

DOI: https://doi.org/10.14232/analecta.2022.1.122-128

In paper [10] a model that uses the superposition principle is described and the resulting Equation (5) is developed for generating the RFS values for a beam that is affected both by a transverse crack and weak clamping, of known severities.

$$\Delta\bar{f}_{i-D}(0,a_1,x_2,a_2)=\gamma_1(a_1)+\gamma_2(a_2)\left[\bar{\phi}_i''(x_2)\right]^2 \tag{5}$$

where $\gamma_1(a_1)$ is the severity for the weak clamping and $\gamma_2(a_2)$ the severity of the transverse crack.

By using Equation (5), for the research presented in the current paper, we have generated the RFS values, which is the first training dataset used for the ANN models. The RFS values are generated for the first eight weak axis bending vibration modes for several damage scenarios, by considering transverse cracks located on several positions along the beam when the cantilevers clamping is considered to be both in perfect condition and also weak condition. The considered crack position for each set of values is considered starting from *x=2* mm and continuing to *x=998* mm with a step of *s=2*mm. The datasets are generated for a transverse crack depth of *a=1* mm, and for simulating the weak clamping cases a transverse crack at the fixed end of depth *a=1* mm is considered. For both cracks, the severity is calculated using Equation (4).

Furthermore, from the calculated RFS values, we generate a second type of dataset by reducing each value of the RFS series with the minimum value of the series for each damage position, as described in Equation (6):

$$RFS_{\min}=\Delta\bar{f}_{i-D}(0,a_1,x_2,a_2)-\min\Delta\bar{f}_{i-D} \tag{6}$$

In Tab. 1, we present a partial dataset series obtained for a damage scenario where the crack is positioned at x= 510 mm using Equation (5)

The third training dataset is also generated starting from the obtained RFS values by normalizing the dataset according to Equation (7):

$$DLC=\frac{\Delta\bar{f}_{i-D}(0,a_1,x_2,a_2)}{\max\Delta\bar{f}_{i-D}} \tag{7}$$

Table 1. Calculated training values for a cantilever with a crack depth 20% affected by a 10% weak clamping

Damage position x [mm]	Transverse crack severity	Weak clamping severity	Mode no.	Dataset type		
				RFS	RFS_{min}	DLC
510	0.003345971	0.000866543	1	0.001226	0.000341	0.473765
			2	0.002589	0.001703	1
			3	0.000885	0	0.342059
			4	0.002517	0.001632	0.972443
			5	0.000899	1.37E-05	0.347357
			6	0.00249	0.001605	0.961976
			7	0.000935	4.99E-05	0.361338

DOI: https://doi.org/10.14232/analecta.2022.1.122-128

			8	0.002448	0.001563	0.945801

The generated data is used for training six ANN models, two for each training dataset, resulting in three models for predicting 3 outputs (transverse crack location, transverse crack severity, and weak clamping severity if present), and the remaining 3 models are trained to detect only the position of the transverse crack also if the beam is affected by weak clamping.
The precision of the developed ANN models is evaluated by comparing the outputs obtained from the considered measured test data generated using the described FEM method.

2.2. Neural network models

The three generated datasets, i.e., RFS, RFS_{min}, and DLC are used for training the six ANN models by using the integrated Deep Learning module of the MatLab software. The training function used is Bayesian regularization, with the parameter sets presented in Fig. 1.

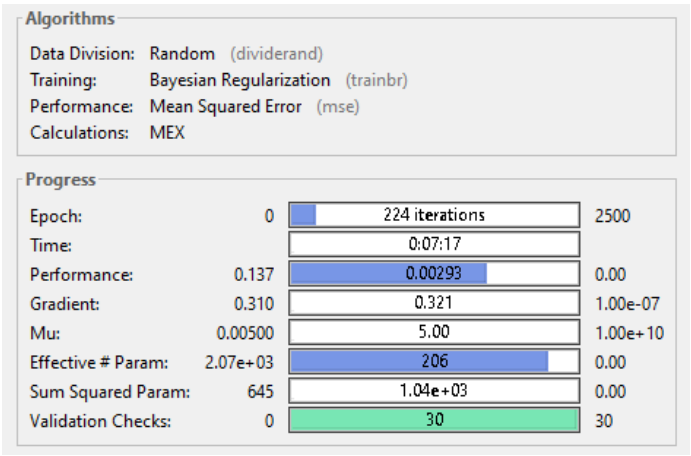

Figure 1. Neural network parameters

Each ANN model is denoted by the name of the dataset type and the number of outputs, resulting in six network names: RFS_1_output, RFS_3_output, RFS_{min}_1_output, RFS_{min}_3_output, DLC_1_output, DLC_3_output.
The Backpropagation algorithm used in the current study learns (finds) the optimal values of the interconnection weights between learning units in a multi-level network with a fixed number of learning units. It uses a gradient slope to try to minimize the error between the value of the network output and the value that is wanted to be obtained for that entry. The problem with learning in this network is to look for the optimal values of the weights in the large space of the hypotheses given by all learning units in the network. The algorithm is described here for a feed-forward network containing three hidden neuron layers, each containing 30 neurons, as shown in Fig.2.

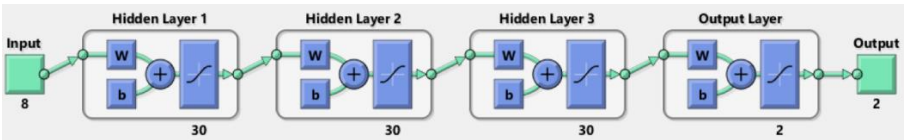

Figure 2. Developed network configuration

DOI: https://doi.org/10.14232/analecta.2022.1.122-128

2.3. Test data

The structure considered for the current research is a steel cantilever beam, presented in Fig. 3, with its main dimensions *L=1000* mm, *B=50* mm, and thickness *H=5mm*. The first step for generating the training data was to determine using FEM simulations the natural frequencies for the cantilever in an undamaged state.

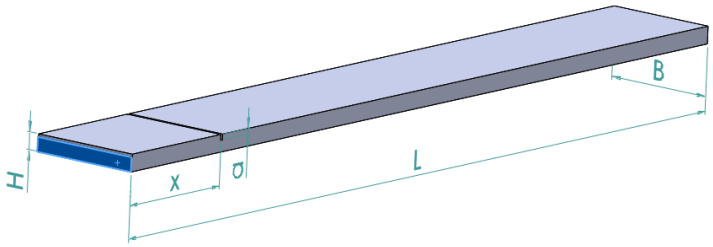

Figure 3. Cantilever beam affected by a transverse crack and weak clamping

The considered beam material, Structural Steel is applied from the ANSYS database with its physical-mechanical properties presented in Tab.2.

Table 2. Physical-mechanical properties of the cantilever beam

Yield strength [MPa]	Ultimate strength [MPa]	Mass density ρ [kg/mm^3]	Young modulus E [N/m^2]	Poisson ratio v [-]
250	460	7850	$2 \cdot 10^{11}$	0.3

The test data consists of the first eight natural frequencies for the out-of-plain vibration modes, for the healthy beam and the beam with different damage scenarios containing both ideal clamping and non-ideal clamping. The 1 mm depth crack is applied by cutting the 3D model using a rectangle of $1 \cdot 0.04$ mm.
To simulate the weak clamping behaviour, we considered also a 1 mm depth cut on the fixed end of the beam, and by applying the boundary condition only on the remaining surface, as shown in Fig. 3. The severity value for the transverse crack as well as for the weak clamping is determined by performing static simulations under own weight for the beam in undamaged state, damaged state, and with weak clamping. The deflections obtained are used for calculating the severity values using Equation (2).
For the FEM test data, we have considered several damage scenarios, all crack depth (transverse crack and the crack simulating the weak clamping) are considered at depth *a=1* mm. The first 32 scenarios take into consideration the cases where the beam is perfectly clamped, and the only variable considered is the crack location, which is considered one by one at *x*= 56, 73, 81, 120, 165, 173, 210, 233, 255, 290, 325, 347, 360, 414, 466, 489, 516, 560, 563, 590, 660, 687, 690, 760, 796, 810, 820, 876, 896, 906, 946, 980. The next 32 damage scenarios take into consideration the same crack positions but also consider the weak-clamping scenario at the fixed end.

3. RESULTS AND DISCUSSION

The frequencies obtained from the FEM simulations for the undamaged and the 64 damaged beam cases are used for calculating the test data, meaning the RFS, $RFS_{min,}$ and DLC measured values, which are later introduced correspondingly in each of the 6 developed ANN models, depending on the data type.

DOI: https://doi.org/10.14232/analecta.2022.1.122-128

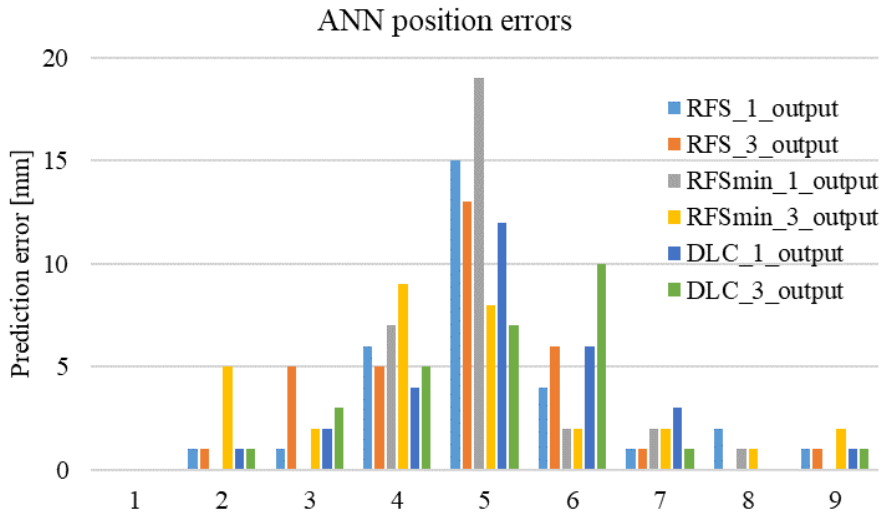

Figure 4. Graphical representation of the obtained errors for the 6 ANN models

The precision of predicting the position of a transverse crack present in cantilever beams by using the developed neural networks trained with different data types is assessed by comparing the prediction of each ANN model. The obtained errors are graphically plotted and illustrated in Fig. 4.

4. CONCLUSIONS

In the current study, six feedforward backpropagation neural networks are trained, using different datasets, for predicting the damage location for several scenarios, including the case where the cantilever is affected by weak clamping.

After analyzing the obtained differences, it results that the largest error achieved for predicting the location of the crack is 19 mm for the network that is trained using the RFSmin_1_output dataset. The largest prediction error is obtained for the scenario where the crack is closer to the free end, i.e., x=980 mm.

The ANN models with the best performance considering the crack position between x=2 mm and x=906 mm is the RFS_1_output and DLC_1_output models, the first being the more precise one.

The ANN models with the best performance considering the crack position starting from x=906 are DLC_3_output and RFS_{min}_3_output models.

From the obtained prediction values, we can conclude that the method used could offer reliable data for evaluating the location of transversal cracks, even if the crack is located near the free end of the beam where the frequency drop due to the presence of damage is very small. The described algorithm can easily be applied for generating any of the three presented dataset types for training ANN models.

ACKNOWLEDGMENTS

This paper received financial support through the project "Entrepreneurship for innovation through doctoral and postdoctoral research": POCU/380/ 6/13/123866, a project co-financed by the European Social Fund through the Operational Program Human Capital 2014-2020.

REFERENCES

[1] A. Khajeh, A. Y. Koma, Suitable Frequency of Structural Health Monitoring, 7th International Conference on Mechanical Engineering, Dhaka, Bangladesh, December 29-31 2007.
[2] J. R. Casas, J. J. Moughty, Bridge Damage Detection Based on Vibration Data: Past and New Developments, Frontiers in Built Environment 3, DOI:10.3389/fbuil.2017.00004, February 2017.
[3] Y. Yang, Y. Zhang, X. Tan, Review on Vibration-Based Structural Health Monitoring Techniques and Technical Codes, Symmetry 13(11):1998, DOI:10.3390/sym13111998, October 2021.
[4] C. P. Fritzen, Vibration-Based Structural Health Monitoring-Concepts, and Applications, Key Engineering Materials 293, DOI:10.4029/www.scientific.net/KEM.293-294.3, September 2005.
[5] A. Guechaichia, I. Trendafilova, A simple method for enhanced vibration-based structural health monitoring, Journal of Physics Conference Series 305(1):012073, DOI:10.1088/1742-6596/305/1/012073, July 2011.
[6] M. I. Friswell, Damage identification using inverse methods, Phil. Trans. R. Soc. A. 2007, 365 (1851), (2007), pp. 393-410.
[7] L. Nguyen-Ngoc, H. Tran-Ngoc, T. Bui-Tien, A. Mai-Duc, M. A. Wahab, H. X. Nguyen, G. De Roeck, Damage detection in structures using Particle Swarm Optimization combined with Artificial Neural Network 28(1), (2021), pp.1-12.
[8] N. Gillich, C. Tufisi, C. Sacarea, C. V. Rusu, G. R. Gillich, Z. I. Praisach, M. Ardeljan, Beam Damage Assessment Using Natural Frequency Shift and Machine Learning, Sensors 22(1118), 2022.
[9] G. R. Gillich, D. Frunzaverde, Z. I. Praisach, F. P. Minda, A new method to detect, locate and evaluate the severity of damages using natural frequencies, SISOM 2011 and Session of the Commission of Acoustics, Bucharest, May 25-26 2011.
[10] G. R. Gillich, N. M. Maia, M. A. Wahab, C. Tufisi, Z. I. Korka, N. Gillich, M. V. Pop, Damage Detection on a Beam with Multiple Cracks: A Simplified Method Based on Relative Frequency Shifts, Multidisciplinary Digital Publishing Institute, 2021.
[11] G. R. Gillich, C. Tufisi, M. A. Wahab, C. O. Hamat, Crack Assessment Based on the Use of Severity-Adjusted Modal Curvatures of the Healthy Beam. Proceedings of the 15th AVMS, Timisoara, 2019.
[12] G. R. Gillich, J. L. Ntakpe, M. A. Wahab, Z. I. Praisach, M. C. Mimis, Damage detection in multi-span beams based on the analysis of frequency changes. Journal of Physics: Conference Series 842(1):012033, May 2017.
[13] G. R. Gillich, C. Tufisi, Z. I. Korka, C.O. Hamat, N. Gillich, Automatic detection of L and T shaped cracks in semifinished casting products, IOP Conference Series: Materials Science and Engineering 393(1):012016, 2018.

DOI: https://doi.org/10.14232/analecta.2022.1.122-128

Analecta Technica Szegedinensia
Vol. 16, No. 01 ISSN 2064-7964 2022

INVESTIGATION OF ULTRAFILTRATION PARAMETERS OF DIFFERENT ORGANIC LOAD WASTEWATER TYPES

*[1]Emilija Fodor, [1]Zita Šereš, [2]Gréta Gergely, [2]Cecilia Hodúr, [2]Szabolcs Kertész**

[1]Faculty of Technology, University of Novi Sad, Bulevar cara Lazara 1, 21102, Novi Sad, Serbia
[2]Department of Biosystems Engineering, Faculty of Engineering, University of Szeged, Moszkvai krt. 9., H-6725, Szeged, Hungary
e-mail:kertesz@mk.u-szeged.hu

ABSTRACT

Almost a third of Earth's freshwater resources are used by municipalities, agriculture and industries and therefore very large quantities of wastewater are generated and discharged into surface water or groundwater. If discharged inadequately and without previous treatment, wastewater can cause chemical pollution, affect aquatic life as well as human health and have a negative impact on the environment. An emerging technology for wastewater treatment is the membrane separation process due to the low cost, the use of ambient temperature, the low energy consumption compared to other traditional techniques, and the high selectivity of different separation mechanisms with compact design.
In this study, ultrafiltration (*UF*) technique was investigated to treat wastewater with different organic loads. The effects of the stirring and a three-dimensional (3D) printed spacer, integrated into the *UF* cell were analyzed on the permeate fluxes, membrane rejections of turbidity, conductivity and chemical oxygen demand (*COD*).

Keywords: ultrafiltration, food wastewater, membrane separation processes, 3D printed spacers

1. INTRODUCTION

Wastewater effluents are becoming an environmental and societal concern and can cause serious human concern because of the unknown effects on aquatic life, human health and the environment [1-2]. The use of water, especially by the food industry is much greater than other industry sectors since water is used as a raw material or for cooling, heating, cleaning, cooking, transportation and other various purposes [3]. Although food industry wastewater is difficult to characterize because its content varies according to used products, processes and the season, the main contaminants are microorganisms, biodegradable organic materials, fertilizers, pesticides, metals, nutrients, organic and inorganic materials [4]. Unlike municipal wastewater, wastewater generated by the food industry is biodegradable, nontoxic and is characterized by a high concentration of suspended solids. In Europe and the United States, the bakery industry is one of the greatest water users and more than half of the used water is later released as wastewater [5]. Bakery industry wastewater contains a substantial amount of organic materials, organic carbon, sugars, proteins, and enzymes [6]. In addition to high values of biochemical oxygen demand (*BOD), COD* and a high concentration of suspended solids, bakery wastewater is also characterized by a high value of total nitrogen and a dark color [5]. The dairy industry generates large amounts of wastewater as well. Water is used in all steps of production in the dairy industry such as sanitization, heating, cooling, milk processing, packaging and cleaning of milk tankers [7]. Most of the wastewater generated by the dairy industry results from cleaning of tank trucks, milk silos, the transport lines and equipment during production. Wastewater from the dairy industry typically contains a high concentration of proteins, lipids and carbohydrates. Additionally, it has a high concentration of suspended solids, chlorides, and high *BOD* and *COD* values [3]. Some studies presented that food, bakery wastewater is an acidic wastewater rich in oil, grease and suspended solids with a high *COD* value that is generally in the range of 1-10 g/L [5, 8, 9].
Membrane separation processes are applied in a wide range of industries – food, chemical, medicine, pharmaceutical and many other fields. Membrane techniques have found their application in wastewater treatment because of their potential to remove particles, improve the aesthetic of the water and inactivate

DOI: https://doi.org/10.14232/analecta.2022.1.129-135

pathogens. On the other hand, the main disadvantage of them is the membrane fouling which causes flux decrease and a decrease in productivity. Recent studies have indicated that the changing of the hydrodynamic conditions into the membrane module can result in enhanced mixing efficiency and improved flow conditions. The use of three-dimensional (3D) printed spacers into the module can result in enhanced mixing efficiency and improved flow conditions. The use of 3D printed spacers into the module can enhance mass transfer through the *UF* membrane by reducing concentration polarization and fouling tendency. 3D printing can enable a promising new class of efficient laboratory devices for filtration processes [10-11]. On the other hand, higher mechanical stirring into the module can alleviate membrane fouling with increasing the shear rate on the surface of the membrane.

The main aim to use plastic spacers into the membrane module is the improving of the hydrodynamics of the fluid flow. They can serve as obstacles in the flow with disrupting the laminar flow profile in the boundary layer and initiate vortices. This type of mixing intensification also results in higher velocities and shear rates at the membrane surface, which can mitigate membrane fouling. The spacers can be in a form of 2D structures such as squares, triangles and circles, but the potential application of 3D printed technology has been gaining attention. Nowadays, the significant development of 3D printing has also broken into the field of wastewater treatment. The 3D printing is becoming more efficient and cheaper to design 3D printed spacers that can be integrated into membrane filter modules, which became unimaginably fine and detailed using complex geometries [12-13].

In this article, we have demonstrated the role of 3D printed spacers, promoters in performance enhancement of the ultrafiltration cell in low- and high-loaded model dairy wastewater and real bakery and dairy wastewater types. Ultrafiltration permeate fluxes, permeate flux decline, resistances and chemical oxygen demand (COD) rejections with and without spacer and stirring were studied and compared testing the different organic load wastewater types.

2. MATERIALS AND METHODS

2.1. The tested food wastewater types

The real bakery wastewater (*Real bakery ww.*) sample was collected from a bakery in Serbia, which offers a variety of products, but specializes in the production of filled puff pastry that is frozen and stored at -18°C. This sample came from the production of pastry filled with soft white cheese. After collection, the sample was stored in sterile freezer container. The real dairy wastewater (*Real dairy ww.*) sample was collected from a dairy company in Szeged, Hungary and was frozen and stored at -18°C. Additionally, two different concentration model dairy wastewater solutions were prepared using tap water and milk powder. These solutions were prepared to represent a minimum, relatively low organic loaded dairy synthetic wastewater (*Low-loaded ww.*) and a maximum, relatively high organic loaded dairy synthetic wastewater (*High-loaded ww.*) types with *COD* value of 1000 and 10 000 mg/L respectively. The initial *COD* values were 1000, 10000, 2800 and 1400 mg/L for Low-loaded dairy, High-loaded dairy, Real bakery and Real dairy wastewater samples respectively.

2.2. The laboratory membrane separation apparatus

Ultrafiltration experiments were carried out with a *Millipore Solvent Resistant Stirred Micro- and Ultrafiltration Cell* shown on Fig. 1. (Merckmillipore, Germany). The special device is constructed from stainless steel and borosilicate glass, which offers a rapid and efficient method for concentration of smaller, laboratory samples volume up to 300 mL at low and medium pressure (max. 5 bar). In this device the solutes, molecules and particles, less than the membrane's molecular weight cut-off (*MWCO)* can pass through the membrane as filtrate while solutes bigger than the *MWCO* are retained and concentrated within the retentate side into the cell after the membrane separation process.

DOI: https://doi.org/10.14232/analecta.2022.1.129-135

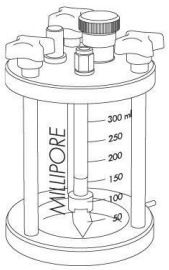

Figure 1. Millipore Solvent Resistant Stirred Cell (from device book)

2.3. The polymer membranes

Polyethersulfone (*PES*) membrane with 30 kDa *MWCO* were used for the experiments, which was chosen based on literature that indicate that it had the lowest permeate flux decline and lowest fouling degree, as well as fouling resistances using *UF* of whey model solutions compared to 5 kDa and 15 kDa [4]. The active membrane surface area was about 40 cm^2.

2.4. The laboratory *UF* experiments

Four different wastewater types were tested with the following measuring order: Firstly, distilled water was used as feed on raw, clean membrane to determine the membrane water flux before the filtration. Then, the concentration experiment was started with the *UF* of the tested wastewater at 25℃ and using *TMP* (Transmembrane Pressure) of 4 bar. Every type of wastewater was filtered with three different experiments: (1) Control *UF* experiments without stirring and the use of the 3D printed spacer;
(2) experiments with stirring at the rate of 400 rpm (it was determined earlier to be the optimal speed) without spacer; and
(3) experiments with stirring of 400 rpm and the use of a 3D printed spacer.
The membrane rejections were calculated using the measured turbidity, conductivity and *COD* values of feed and permeate samples after every type of wastewater membrane separation experiment.

2.5. The 3D printing characteristics

The spacer was designed by Cura software (Ultimaker Cure 5.0.0), printed by a Creality CR-10S Pro V2 3D printer (China). This particular design was chosen as optimal based on our Department previous results and it is shown in Fig. 02. The spacer was made from PLA (Polylactic Acid) material, printed by FDM (Fused Deposition Modelling) technique using 0.2 mm layer thickness with 100 % infill density, cubic infill pattern at 215℃ printing and 60℃ bed temperature.

Figure 2. 3D printed spacer used in experiments

3. RESULTS AND DISCUSSION

3.1. Permeate flux results, as the ultrafiltration process velocity

DOI: https://doi.org/10.14232/analecta.2022.1.129-135

In Fig. 3. it can be seen that the time of the *UF* experiments of different organic load wastewater types significantly different, and the most emphasized flux decline tendencies were observed in the first part of the membrane separation processes. The initial fluxes of the control *UF* experiments were significantly lower (360 and 85 $Lm^{-2}h^{-1}$ for *Low-loaded* and *High-loaded* dairy ww. respectively) than the *UF* experiments with spacer and stirring (487 and 183 $Lm^{-2}h^{-1}$ for *Low-loaded* and *High-loaded* dairy ww. respectively). On one hand, in the model dairy wastewater ultrafiltration experiments (Fig. 3/a.), the shortest *UF* time of less than 400 s was observed with the sample of *Low-loaded* dairy ww. with spacer and 400 rpm stirring. The longest *UF* time was about 5320 s for the control *UF* of *High-loaded* dairy ww. without stirring and spacer. In general, the wastewater types with higher organic loads had lower initial and average flux values. On the other hand, in the real wastewater ultrafiltration experiments (Fig. 3/b.), the shortest *UF* time of 1000 s was observed with the sample of bakery ww. also with spacer and stirring. The longest *UF* time was about 3875 s for the control *UF* of bakery ww.. From these results it can be concluded that the module integrated 3D printed spacer together with a high stirring velocity resulted the highest flux values in all wastewater ultrafiltration experiments.

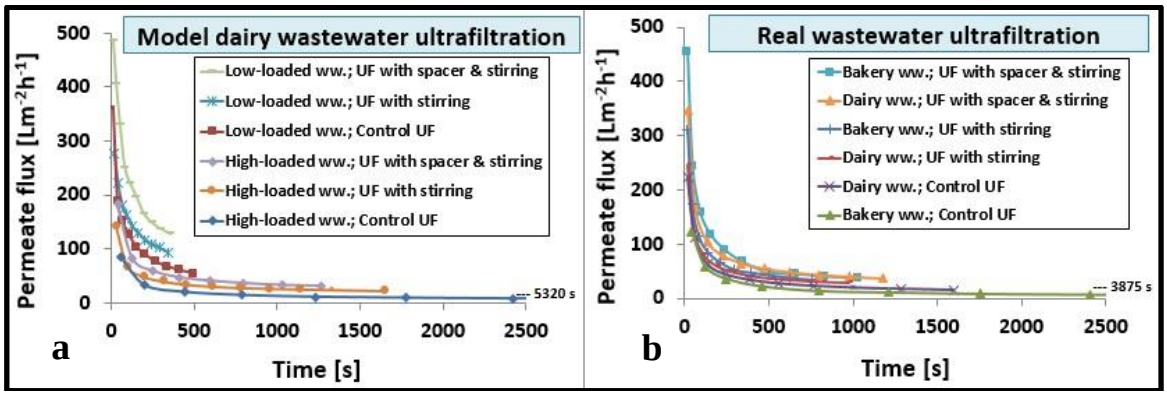

Figure 3. The permeate flux changing during ultrafiltration of model (a) and real (b) wastewater types

Next to the real permeate flux values (J), it is also important to know the permeate flux decline or the flux decreasing ratio which can be calculated from the certain flux (J) and the initial, first measured flux (J_0) value during *UF*. If we analyze this flux decline tendency (J/J_0) results of the different experiments as a function of *VRR* (Volume Reduction Ratio), it can be seen that, from the same initial flux, the flux decline was more emphasized in the control *UF* experiments. In Fig. 4. it can be also seen that the *High-loaded* model dairy wastewater types had higher permeate flux decline ratio, so the membrane fouling tendency was higher in their cases. In the case of control, where the flux decline tendency was most emphasized, it dropped to 0.15 with *Low-loaded* and 0.0575 with *High-loaded* model dairy wastewater types. It can be also observed that the *UF* experiments with spacer and stirring had lower results than the *UF* experiments with only stirring, however they had higher flux values in general.

DOI: https://doi.org/10.14232/analecta.2022.1.129-135

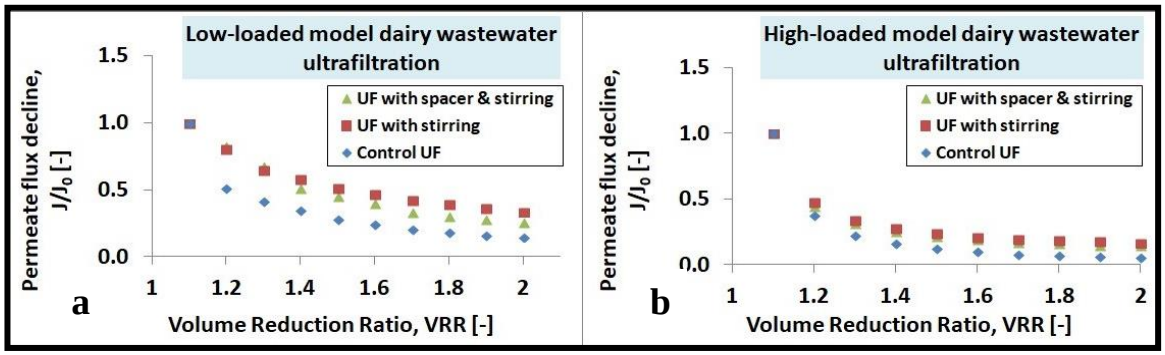

Figure 4. The permeate flux declines during ultrafiltration of low-loaded (a) and high-loaded (b) model dairy wastewater types

3.2. Resistance results, as the membrane fouling tendency

In Fig. 5. it can be seen that the different resistance values of the *UF* experiments of different wastewater types significantly different. The clean membrane own resistances were negligible and the reversible resistances were the most emphasized ones in all cases. The control *UF* experiments had the highest and the *UF* experiments with spacer and stirring resulted the lowest total resistance values. On one hand, in the model dairy wastewater ultrafiltration experiments (Fig. 5/a.), the *High-loaded* dairy ww. had much higher resistance values than the *Low-loaded* dairy ww.. On the other hand, in the real wastewater ultrafiltration experiments (Fig. 5/b.), the Control *UF* with bakery ww. resulted higher total resistance than dairy ww.. However, the reversible resistances were higher in dairy ww. *UF* experiments. From these results, it can be concluded that the module integrated 3D printed spacer together with a high stirring velocity resulted the lowest resistance values in all wastewater ultrafiltration experiments.

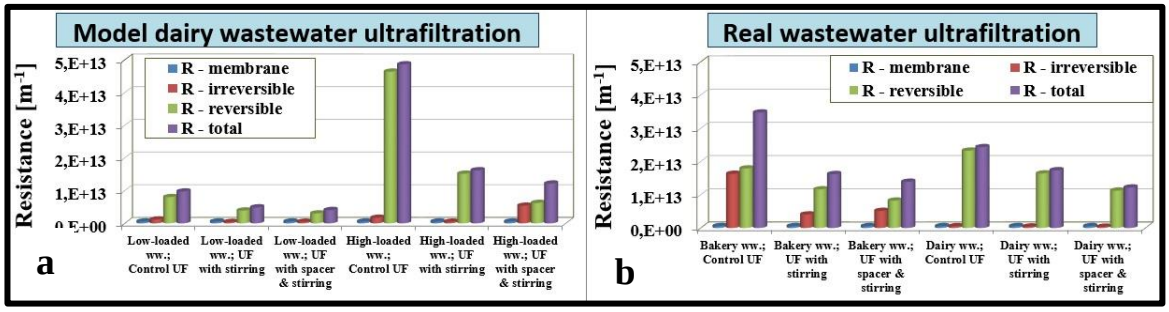

Figure 5. The resistance values of ultrafiltration of model (a) and real (b) wastewater types

3.3. The ultrafiltration membrane rejection results, as the process quality

The membrane percentage removal of *COD* is shown in Fig. 05. It can be seen that the rejection varied in a wide range from 13 to 74 %. On one hand, in the model dairy wastewater ultrafiltration experiments (Fig. 5/a.), the lowest rejection of 13 % was observed with the control *UF* experiment of *Low-loaded* dairy ww. without spacer and stirring, while the highest rejection of 32 % for the *High-loaded* dairy ww. *UF* with stirring. On the other hand, in the real wastewater ultrafiltration experiments (Fig. 5/b.), the lowest rejection of 14 % shortest was observed with the sample of dairy control *UF* experiments, while the highest rejection of 74 % for the bakery *UF* with stirring case. In general, the stirring increased the rejection values, but the spacer and stirring together decreased compare to stirring cases.

DOI: https://doi.org/10.14232/analecta.2022.1.129-135

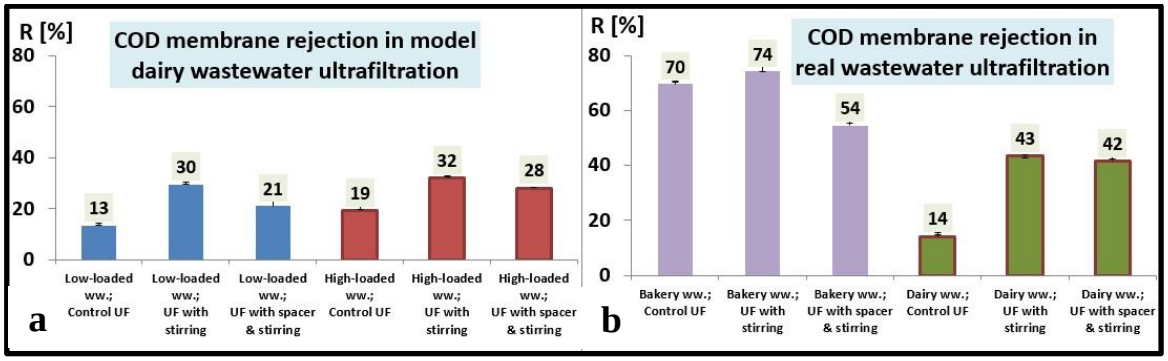

Figure 6. The organic content, chemical oxygen demand (COD) percentage membrane rejection of the model dairy wastewater (a) and real wastewater ultrafiltration (b) experiments.

It can be observed that the real, industrial wastewater samples had significantly higher membrane rejection values than the model wastewater samples, because their content were more heterogeneous. Furthermore, the real bakery wastewater had much higher rejection of control *UF* experiment of about 70 % than the dairy wastewater sample control with 14 %, even it had two times higher initial *COD* value, 2800 compare to 1400 mg/L. All samples had very similar changes in total salt rejection measured by conductivity measurements. It can be observed that the experiment with stirring lowered the conductivity values the most in all types of wastewater. But turbidity values were lowered approximately 99 % and there was not a significant difference between experiments or different types of wastewater.

4. CONCLUSIONS

The results of this research have shown that the use of a 3D printed spacer and stirring at a high velocity have increased the efficiency of membrane separation of all types of wastewater and resulted in the highest flux values and the lowest resistance values in all wastewater ultrafiltration experiments. The high-loaded model dairy wastewater type had a higher permeate flux decline ratio compared to the low-loaded model dairy wastewater and therefore tendency for membrane fouling was higher in those experiments. Which was proven by the resistance results also.
According to the membrane percentage removal of *COD*, the samples of industrial wastewater types had significantly higher membrane rejection values than the model wastewater samples. Moreover, the industrial bakery wastewater samples had much higher rejection values than industrial dairy wastewater samples. The experiments with stirring had the highest rejection values in all the wastewater types, but the experiments with spacer and stirring together had comparable rejection values.

Acknowledgments: Thanks the support of the János Bolyai Research Scholarship of the Hungarian Academy of Sciences (BO/00576/20/4) and the New National Excellence Program of the Ministry of Human Capacities (UNKP-21-5-SZTE-550). Additionally, many thanks to the project "Building Entrepreneurial Ecosystem – Student entrepreneurship beyond borders" acronym BEE-Student of the Interreg IPA CBC Programme (project no. HUSRB/1903/43/0012) for the support.

REFERENCES

[1] Bagatin, R., Klemeš, J.J., Reverberi, A.P. and Huisingh, D., 2014. Conservation and improvements in water resource management: a global challenge. *Journal of Cleaner Production*, 77, pp. 1-9. https://doi.org/10.1016/j.jclepro.2014.04.027

[2] Schwarzenbach, R.P., Escher, B.I., Fenner, K., Hofstetter, T.B., Johnson, C.A., Von Gunten, U. and Wehrli, B., 2006. The challenge of micropollutants in aquatic systems. *Science*, 313(5790), pp. 1072-1077. DOI: 10.1126/science.1127291
[3] Cristian, O., 2010. Characteristics of the untreated wastewater produced by food industry. *Analele Universităţii din Oradea, Fascicula: Protecţia Mediului*, 15, pp. 709-714.
[4] Heponiemi, A. and Lassi, U., 2012. Advanced oxidation processes in food industry wastewater treatment–A review. *Food Industrial Processes-Methods and Equipment*, pp. 313-338.
[5] Struk-Sokolowska, J. and Tkaczuk, J., 2018. Analysis of bakery sewage treatment process options based on COD fraction changes. *Journal of Ecological Engineering*, 19(4). https://doi.org/10.12911/22998993/89653
[6] Yadav, A. and Garg, V.K., 2019. Biotransformation of bakery industry sludge into valuable product using vermicomposting. *Bioresource Technology*, 274, pp. 512-517. https://doi.org/10.1016/j.biortech.2018.12.023
[7] Sreedhar, N., Thomas, N., Al-Ketan, O., Rowshan, R., Hernandez, H., Al-Rub, R.K.A. and Arafat, H.A., 2018. 3D printed feed spacers based on triply periodic minimal surfaces for flux enhancement and biofouling mitigation in RO and UF. *Desalination*, *425*, pp. 12-21. https://doi.org/10.1016/j.desal.2017.10.010
[8] Vistanti, H., Malik, R.A. and Mukimin, A., 2020. Performance of a Full-Scale Anaerobic Digestion on Bakery Wastewater Treatment: Effect of Modified Distribution System. *Jurnal Riset Teknologi Pencegahan Pencemaran Industri*, 11(1), pp. 12-18., DOI: 10.21771/jrtppi.2020.v11.no1.p12-18
[9] Chakraborty, B., Kundu, P., Mukherjee, J. and Mukherjee, S., 2021. Kinetics Study of a Suspended Growth System for Biological Treatment of Bakery and Confectionery Wastewater. In *Advances in Bioprocess Engineering and Technology* (pp. 339-348). Springer, Singapore. https://doi.org/10.1007/978-981-15-7409-2_34
[10] Dang, B.V., Charlton, A.J., Li, Q,. Kim, Y.C., Taylor, R.A., Le-Clech, P., Barber, T., 2021. Can 3D-printed spacers improve filtration at the microscale? *Separation and Purification Technology*, 256, 117776. https://doi.org/10.1016/j.seppur.2020.117776
[11] Abouther Al-Shimmery, Saeed Mazinani, Jing Ji, Y.M. John Chew, Davide Mattia; 3D printed composite membranes with enhanced anti-fouling behaviour; Journal of Membrane Science, 574 (2019) 76-85. https://doi.org/10.1016/j.memsci.2018.12.058
[12] Jing Wee Koo, Jia Shin Ho, Jia An, Yi Zhang, Chee Kai Chua, Tzyy Haur Chong; A review on spacers and membranes: Conventional or hybrid additive manufacturing?; Water Research, 188 (2021) 116497. https://doi.org/10.1016/j.watres.2020.116497
[13] Xin Qian, Mayur Ostwal, Ayse Asatekin, Geoffrey M. Geise, Zachary P. Smith, William A. Phillip, Ryan P. Lively, Jeffrey R. McCutcheon; A critical review and commentary on recent progress of additive manufacturing and its impact on membrane technology; Journal of Membrane Science, 645 (2022) 120041. https://doi.org/10.1016/j.memsci.2021.120041